



Durham E-Theses

Dynamic analysis of a small weaving loom

Gülen, Serdar

How to cite:

Gülen, Serdar (1976) *Dynamic analysis of a small weaving loom*, Durham theses, Durham University. Available at Durham E-Theses Online: <http://etheses.dur.ac.uk/9561/>

Use policy

The full-text may be used and/or reproduced, and given to third parties in any format or medium, without prior permission or charge, for personal research or study, educational, or not-for-profit purposes provided that:

- a full bibliographic reference is made to the original source
- a [link](#) is made to the metadata record in Durham E-Theses
- the full-text is not changed in any way

The full-text must not be sold in any format or medium without the formal permission of the copyright holders.

Please consult the [full Durham E-Theses policy](#) for further details.

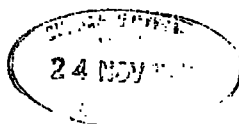
Dynamic Analysis of a
Small Weaving Loom

by

Serdar Gülen B.Sc.

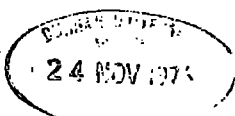
Thesis submitted for the degree of Master of Science
in the University of Durham.

August, 1976



ABSTRACT

The project deals with an investigation to determine experimentally the axial and bending strains (normal to the plane of the mechanism) in the two connecting rods of the weaving mechanism of a small textile loom. A complete theoretical, kinematic, force and stress analysis has been made on the six-bar chain constituting the mechanism. The peak to peak strain values have been measured at various different crank speeds. The nature of the bending strains in a direction normal to the plane of the mechanism have been further examined by static tests which have been performed on the mechanism. Measured dynamic strain data for the connecting rods is presented and comparison is made between calculated and measured values. Experimental results for axial peak to peak and cyclic strain variation showed good agreement with the calculated values.



ACKNOWLEDGMENTS

I wish to express my sincere gratitude to Professor G.R. Higginson and Dr. P.A.T. Gill for their guidance, advice and continuous encouragement during the preparation of this work.

I would also like to express my thanks to Mr. T. Sweeting for his constant help during the experimental stage of the project and to Miss J. Campbell for typing this thesis.

I am indebted to my parents for providing me with financial support.

CONTENTS

	Page
Abstract	i
Acknowledgements	ii
Contents	iii
Nomenclature	
Introduction	
1 Stages encountered during the development of the project	1
2 Historical background to the investigation	2
3 Plane mechanisms in general, current research and short bibliographical review	3
 <u>Chapter 1</u>	
Description of the machine	6
1.1 Power transmission system	6
1.2 Mechanism Unit box	8
 <u>Chapter 2</u>	
Kinematic analysis of the mechanism	
2.1 Introduction to kinematic analysis of the mechanism	22
2.2 Geometry of the mechanism	22
2.3 Velocity and acceleration Analysis - Analytic method	24
2.4 Algebraic approach	36
2.5 Application of Raven's Analysis	48

2.6	Graphical Approach	54
2.7	Energy variation of the system	55
<u>Chapter 3</u>					
Force and Stress Analysis					
3.1	Kinetostatic Approach	58
3.2	Application of virtual work				
	method to the mechanism	65
3.3	The Power equation	66
3.4	Graphical approach	70
3.5	Simplified Force Analysis	73
3.6	Stress Analysis	75
<u>Chapter 4</u>					
Instrumentation, Experiments and					
experimental Results					
4.1	Instrumentation	86
4.2	Elements of the experimental				
	set up	90
4.3	Strain gauges and gauge				
	installations	91
4.4	Experiments				
	1 Dynamic strain measurements	94
	2 Static bending-strain				
	measurements	95
	3 Stress distribution in				
	links 3 and 5	95
	4 Tensile Test	99
4.5	Dynamic strain measurement				
	results	103

4.6	Speed Fluctuation	103
	Table 4.1	105
	Table 4.2	116
	Table 4.3	128
 <u>Chapter 5</u>					
	Discussion of Results	
5.1	Determination of Axial working stress for link 5 - A theoretical approach	145
5.2	Theoretical and experimental stress range variation with the crank speed in link 5	151
5.3	Calculation of eccentricity from experimental data, for links 5 and 3	154
5.4	Eccentricity - dynamic case	156
5.5	Determination of Axial working stress for link 3 - a theor- etical approach	157
5.6	Theoretical and experimental axial stress range variation with the crank speed in link 3	158
5.7	Bending stresses in a direction normal to the plane of the mechanism	159
5.8	Stress distribution in the links Table 5.4 to 5.7	160 161 - 164
5.9	General Considerations	168

Chapter 6

Conclusion	169
Appendix (A1)	171
Appendix (A2)	185
Appendix (A3)	186
References	187

List of Figures, Tables and Plates

	Page
Fig. 1.1	7
Table 1.1 specification of links	8
Fig. 1.2 Mechanism	9
Plate 1.1 Power transmission system	10
Plate 1.2 Mechanism unit box left end	10
Fig. 1.3 Mechanism shown as pin jointed rods	11
Plate 1.3 Mechanism box right end	12
Plate 1.4 Mechanism complete with connecting rods	12
Plate 1.5 Connecting rods, rigid triangular link 4 and link 6	13
Plate 1.6 Main drive shaft	13
Table 1.2 specification of shafts	14
Fig. 1.4 Main drive shaft crank arm end detailed drawing	15
Fig. 1.5 Link 6 and shaft O_3 with the comb	16
Fig. 1.6 rigid triangular link 4	17
Fig. 1.7 Simplified weaving mechanism. Horizontal positioning of shafts O_1 , O_2 and O_3	18
Plate 1.7 Top view - mechanism unit box	20
Plate 1.8 shaft O_2 , shaft bearings and the bevel gears	20
Plate 1.9 Needle arms	21
Plate 1.10 shaft O_3 , comb and bearings	21
Fig. 2.1	23
Fig. 2.2 Variation of angle γ with the crank angle	25

Fig. 2.3	Variation of angle beta with the crank angle	26
Fig. 2.4	Variation of angle α with the crank angle	27
Fig. 2.5	Variation of angle λ with the crank angle	28
Fig. 2.6	Variation of transmission angles α and β with the crank angle	29
Fig. 2.7	Analytical velocity and acceleration analysis	35
Fig. 2.8	Variation of angular acceleration of link 3 with the crank angle	37
Fig. 2.9	Variation of angular acceleration of link 4 with the crank angle	38
Fig. 2.10	Variation of angular acceleration of link 5 with the crank angle	39
Fig. 2.11	Variation of angular acceleration of link 6 with the crank angle	40
Fig. 2.12	Angular velocity curves	41
Fig. 2.13	Variation of angular velocity ratio with the crank angle	42
Fig. 2.14 (a-b)	44
Fig. 2.15	Dead-centre positions for links 4 and 6	45
Fig. 2.16	49
Fig. 2.17	Variation of kinetic energies of shafts O_3 , O_2' and links 3 and 4 with the crank angle	56
Fig. 2.18	Variation of the kinetic energy with the crank angle	57

Plate 4.1	88
Plate 4.2	88
Plate 4.3	Electric motor and speed variator unit	89
Fig. 4.3	Static bending-strain measurement	96
Fig. 4.4	Static bending-strain test for link 5	97
Fig. 4.5	Static bending-strain test for link 3	98
Fig. 4.6	100
Fig. 4.7	101
Fig. 4.8	Tensile test for links 3 and 5	102
Table 4.1	Speed fluctuation	105
Fig. 4.9	Theoretical and experimental variation of axial stress range in link 5 with the crank speed	106
Fig. 4.10	Experimental variation of bending stress range in link 3 with the crank speed	107
Fig. 4.11	Experimental variation of bending stress range in link 5 with the crank speed	108
Fig. 4.12	Theoretical and experimental variation of axial stress range in link 3 with the crank speed	109
Fig. 4.13	Variation of peak to peak stresses in links 3 and 5 with the square of the crank speed	110
Fig. 4.14	Experimental strain patterns	111
Fig. 4.15	Experimental and theoretical variation of axial stress in link 3 with the crank angle	114
Fig. 4.16	Theoretical and experimental variation of axial stress in link 5 with the crank angle	115

Fig. 3.1	62
Fig. 3.2	Free body diagrams	63
Fig. 3.3	Variation of torque transmitted by link 4 with the crank angle	67
Fig. 3.4	Variation of torque transmitted by link 6 with the crank angle	68
Fig. 3.5	Variation of Power transmitted by links 4 and 6 with the crank angle	69
Fig. 3.6	Graphical force analysis by instantaneous centres method	71
Fig. 3.7a	74
Fig. 3.7b	Variation of axial stresses in links 3 and 5 with the crank angle	76
Fig. 3.8	Theoretical variation of axial stress range with the square of the crank speed	77
Fig. 3.9	Connecting rod - link 3	79
Fig. 3.10	Link 5	80
Fig. 3.11	Variation of the external torque T_2 required to drive the mechanism with the crank angle	81
Fig. 3.12	Variation of axial force - link 5 with the crank angle	82
Fig. 3.13	Variation of axial force - link 3 with the crank angle	83
Fig. 3.14	Variation of theoretical maximum axial tensile and compressive stresses in links 3 and 5 with the crank speed	84
Fig. 4.1	Experimental set-up Block diagram	86
Fig. 4.2	87

Table 4.2	Dynamic strain measurement results	116
Table 4.3	Static bending-strain measurement results	128
Fig. 5.1	146
Fig. 5.2	147
Fig. 5.3	150
Table 5.1	152
Table 5.2a and 5.2b	156
Table 5.3	159
Table 5.4	161
Table 5.5	162
Table 5.6	163
Table 5.7	164
Fig. 5.4	165
Fig. 5.5	166
Fig. 5.6	167
Fig. 5.7	167
Appendix A3	186

Nomenclature

$\psi = \text{psi}$	crank angle in degrees - in a direction counterclockwise from the horizontal
$\beta = \text{Beta}$	angle in degrees between link 3 and the horizontal, in a counterclockwise direction from the horizontal
$\gamma = \text{gama}$	angle in degrees between the side O_2C of the rigid triangular link 4 and the horizontal in a direction counterclockwise from the horizontal
$x\lambda = \text{xlambda}$	angle in degrees between link 5 and the horizontal in a direction counterclockwise from the horizontal
upa	angle in degrees between link 6 and the horizontal in a direction clockwise from the horizontal
$A_A^t = \text{AAT}$	Tangential acceleration component of $A\text{-m/s}^2$
$A_A^r = \text{AAR}$	Radial acceleration component of $A\text{-m/s}^2$
$A_B^t = \text{ABT}$	Tangential acceleration component of $B\text{-m/s}^2$
$A_B^r = \text{ABR}$	Radial acceleration component of $B\text{-m/s}^2$
$A_{BA}^t = \text{ABAT}$	Tangential acceleration component of B with respect to $A\text{-m/s}^2$
$A_{BA}^r = \text{ABAR}$	Radial acceleration component of B with respect to $A\text{-m/s}^2$
$A_D^r = \text{ADR}$	Radial acceleration component of $D\text{-m/s}^2$
$A_D^t = \text{ADT}$	Tangential acceleration component of $D\text{-m/s}^2$
$A_{DC}^r = \text{ADCR}$	Radial acceleration component of D with respect to $C\text{-m/s}^2$
$A_{DC}^t = \text{ADCT}$	Tangential acceleration component of D with respect to $C\text{-m/s}^2$
α_2	Angular acceleration of link 2 - rad/s^2
$\alpha_3 = \text{ANGC3}$	Angular acceleration of link 3 - rad/s^2
$\alpha_4 = \text{ANGC4}$	Angular acceleration of link 4 - rad/s^2
$\alpha_5 = \text{ANGC5}$	Angular acceleration of link 5 - rad/s^2
$\alpha_6 = \text{ANGC6}$	Angular acceleration of link 6 - rad/s^2

V_A	velocity of A-m/s ²
$V_B = VB$	velocity of B-m/s
$V_{BA} = VBA$	velocity of B with respect to A-m/s
$V_D = VD$	velocity of D-m/s
$V_{DC} = VDC$	velocity of D with respect to C-m/s
$\omega_2 = \text{OMEGA}2$	angular velocity of link 2-rad/s
$\omega_3 = \text{OMEGA}3$	angular velocity of link 3-rad/s
$\omega_4 = \text{OMEGA}4$	angular velocity of rigid triangular link 4-rad/s
$\omega_5 = \text{OMEGA}5$	angular velocity of link 5-rad/s
$\omega_6 = \text{OMEGA}6$	angular velocity of link 6-rad/s
I_n	Mass moment of inertia of the corresponding links about their mass centres - kg - m ²
where $n =$	2,3,4,5,6
I_{on}	Mass moment of inertia of the corresponding shafts - kg - m ²
where $n =$	1,2,3
EN1	Kinetic energy due to rotation - link 4 - kgm ² /s ²
EN2	Kinetic energy due to rotation - shaft O ₃ - kgm ² /s ²
EN3	Kinetic energy due to rotation - shaft O ₂ - kgm ² /s ²
EN4	Kinetic energy due to rotation - link 3 - kgm ² /s ²
EN5	Kinetic energy due to rotation - link 5 - kgm ² /s ²
EN6	Kinetic energy due to rotation - link 6 - kgm ² /s ²
RT1	(Angular velocity of link 3)/(angular velocity of crank arm)
RT2	(Angular velocity of link 4)/(angular velocity of crank arm)
RT3	(Angular velocity of link 5)/(angular velocity of crank arm)
RT4	(Angular velocity of link 6)/(angular velocity of crank arm)
CAL	Angle of transmission in degrees - angle ABO ₂
YUM	Angle of transmission in degrees - angle CDO ₃

Introduction

1 Stages encountered during the development of the Project

The primary objective was to determine both theoretically and experimentally the axial forces and the corresponding stresses in two of the linkage members of the mechanism. For this purpose pairs of strain gauges were placed on opposing faces of the rods in a configuration capable of measuring axial strains as well as bending strains in a direction normal to the plane of the links. Bending strains in the plane of the linkage could not be measured because of space limitations and the complex shape of the connecting rods which prohibited alternative placing of the gauges. Two different $\frac{1}{2}$ bridge 120 Ω strain-gauge circuits were available to measure axial and bending strains independently. The bending strains were expected to be zero. However in the course of the measurements it became apparent that substantial bending stresses were present in these members. To confirm the dynamic strain measurement results and to determine the nature and cause of the bending strains a set of static tests was carried out on the mechanism.

The steps taken to achieve these objectives were:

- 1 - A detailed examination and description of the machine
- 2 - A complete theoretical kinematic, force and stress analysis
- 3 - Preparation of the experimental set-up
- 4 - Determination of basic material properties for the two connecting rods
- 5 - Measurement of dynamic strains
- 6 - Static tests on the mechanism aiming to find out the nature and cause of bending strains in a direction normal to the plane of the mechanism
- 7 - Comparison and discussion of experimental and calculated results.

2 Historical background to the Investigation

Bonas Machine Company Ltd., of Sunderland, England, have started to manufacture a high-speed weaving loom that weaves ribbon or tape. The loom was hoped to operate at 4000 r.p.m. but it was found that some of the moving parts fractured below this speed. By the increase of speed stoppages due to component fracture occurred more frequently. At the time of the initiation of this project the loom ran commercially at just over 2000 r.p.m. The basic problem was the short term fatigue failures of weft needle arms and the reeds. There were also failures of the connecting rods and links. Although dynamic stresses in the needle arms and reeds have been measured experimentally and calculated analytically in a previous study (24), no investigation had been made on the link mechanism driving the components. To improve the operating characteristics of the machine, the designer suggested that the following major points should be considered in further projects;

- a Measuring the strain of the components under investigation under various conditions
- b Interpreting the results
- c Suggesting possible design changes which would increase the maximum speed of the loom

In order to be able to suggest solid changes in design, the driving mechanism, weaving components, lubrication system and power transmission mechanism should be studied in great detail analytically and experimentally involving fatigue, material, structural, dynamic and economical analyses with different models.

3 Plane Mechanisms in General, current research and short bibliographical review

If all points of the curves of motion of all the links of a mechanism lie in one and on the same plane, the mechanism is called a plane mechanism. A mechanism can simply be defined as a combination of machine elements arranged to achieve a certain motion. Since it deals with the composition of members of a machine into an assemblage to perform a task, to produce a new and unusual result, mechanisms are one of the most fascinating topics in the field of mechanical engineering. Machine design is a creative art involving the possession of careful analytical ability, good judgement and a broad experience. The basic factors which must be taken into consideration in general machine design are: utility, safety, cost, strength, rigidity, deflection, friction, lubrication, wear, heat, noise, flexibility, control and appearance. A tremendous amount of work has been published on various aspects of mechanisms especially in the last two decades. The introduction of computers into design work has accelerated the research a great deal. Numerous new methods have been developed. Today the techniques for studying the dynamics of mechanisms can be classified as kineto-static or time response approaches (4). Current research topics in the field are concentrated on:

- (a) Optimum mechanism design combining kinematic and dynamic force considerations.
- (b) Synthesis of linkage function generators by means of mathematical methods, models and computers.
- (c) Shaking and bearing force optimization.
- (d) Experimental and theoretical study of connection forces and frequency response characteristics.

Dynamic effects in mechanisms become important as operating speeds increase and as light low power consuming economical designs are sought. In the design and experimental examination of the strength of mechanism links the state of stress and strain has to be investigated. Strength may be checked both theoretically and experimentally, however it is usually impossible to calculate stresses theoretically. Theoretical calculations are sometimes too inaccurate because a number of premises and assumptions have to be made. Most components and members are stressed three-dimensionally but with the existing methods of measurement only stresses at the surface can be determined and these do not give an overall picture of the stress distribution. The most expedient way of studying strength problems for mechanism links is to supplement theoretical calculation by experimental data and coefficients.

The efficiency of linkages is greater than that of any gear or cam due to their small frictional losses and high power transmitting ability. The four-bar linkage due to its simplicity has been used for transmission of motion in general. Although it is the simplest possible lower-paired mechanism, since more complex mechanisms have four-bar linkages as elements, the theory of the four-bar linkage is useful in designing of these mechanisms. The recent major contribution in this field can be found in (1), (25) and (4). Mechanism dynamics deals with the motion of a mechanism in response to actuating forces, torques and also the forces and torques produced by a given mechanism motion. Controlling force and torque levels is an important concern in avoiding problems of fatigue, vibration and noise. Most of the present dynamic design procedures start with a mechanism skeleton, distribute the mass of the members, and add springs or dampers to meet dynamic performance criteria associated with shaking moment, input torque balancing, and dynamic time response synthesis (25), (10). Elasticity in the links of mechanisms has a substantial effect on the dynamic behaviour of the mechanisms. The

introduction of clearances in mechanisms causes a substantial increase in the connection forces resulting in degradation of life and performance (16). In mechanisms axial loads are induced in the links by impacts at bearing surfaces and by operating loads. Impact-induced axial loads are highly transient in nature (16). Kineto-elastodynamic analysis, which is the kinematic and dynamic study of mechanisms in motion including the effects of elasticity and mass distribution has recently been given increased attention(25). Imam and Sandor divide the complete mechanism design process into the following three steps:

- (1) Selection of the type of mechanism
- (2) Selection of the design parameters to satisfy kinematic requirements
- (3) Selection of the design parameters to satisfy dynamic and kineto-elastodynamic requirements - mass distribution, inertia and reaction forces at the joints and bearings, transient and steady state vibrations, frequency and time response, elastic deformation of the components, dynamic stress in the links, impact, dynamic stability and balancing.

The basic criteria in designing and optimizing the areas of cross section of mechanism links are (4)

- 1 - The deviation (elastic deflections) from the ideal performance (rigid body motion) must be within the prescribed tolerances
- 2 - The mass of the linkage is to be minimized
- 3 - The stresses in any of the links are not be exceed the endurance limits
- 4 - Various combinations of the criteria such as mass, deformation and stress are to be minimized

A new method of kineto-elastodynamic design of high-speed mechanisms, which is general for all planar linkages including multi-loop and multi-degree-of-freedom mechanisms has recently been presented (25). Of special interest to this work is (15) which is considered and discussed in Chapter 5.

Chapter 1.

Description of the Machine.

The machine is a small variable high-speed weaving loom designed to manufacture ribbon or tape. The main body consists of a rigid steel case enclosing the sump and lubricating mechanism above which is mounted an H-shaped mechanism unit box. The whole complex is mounted on a π - shaped, box section steel platform. The main control box is mounted on the right side of the body while the opposing face is reserved for the power transmission. An inspection cover is fitted to the front of the main body. The important weaving components are mounted externally to the rear and top of the mechanism unit box. The main body and basic features are shown in Fig. (1.1) and Plate (1.1)

1.1 Power Transmission System

Originally an "Elektrim 1410 r.p.m., 1.1 kw, 1.5 HP, 415 V. 2.5 amp" constant speed electric motor was fitted to the rear of the main body. The replacement was a 3 phase, 2 HP variable speed (480-4320 output r.p.m.) electric motor. The motor was mounted on the rear end of the π -shaped platform, complete with an adjustable carriage which enabled belt adjustment to be carried out. AC current is taken directly from the floor by an insulated cable fed into the switch box. A "Fenner B 1800 B69" V-belt was used to transmit the power to the intermediate shaft. Fitted to the intermediate shaft was a 40 tooth pulley driving via a timing belt the 20 tooth pulley fitted to the main drive shaft. The timing belt used was "Fenner 240 L 100". The V-belt also drove the oil-pump shaft end disc. (Fig. 1.1). A handwheel/flywheel was attached to the main drive shaft. The intermediate V-belt pulley was manufactured to suit the available belt. All pulleys were fitted to their respective shafts using "taper-lock" drive device. The two intermediate pulleys were first screwed together before fitting to the shaft.

At speeds in excess of 2500 r.p.m. (main drive shaft speed) slip was detected between "taper-lock" device and the main drive shaft. Due to vertical eccentricity in the axes of the motor pulley, intermediate shaft and main drive shaft excess wear was observed on the v-belt and on the timing belt.

1.2 Mechanism Unit box.

The left(drive) and right (output) end sections of the mechanism unit box, with covers removed, are shown in Plates (1.2) and (1.3). Plate (1.4) shows the right end section complete with connecting rods. In figures (1.2) and (1.3) the mechanism is shown as actual shafts and links and as pin jointed rods respectively. The main drive shaft goes through O_1 causing the crank arm O_1A to rotate with constant angular velocity. The rotary motion of the crank arm is transmitted to the rigid triangular link 4 via the coupler (link 3). The crank arm, coupler and rigid link 4 represent an offset crank-rocker mechanism. The oscillatory motion of link 4 is transmitted to shaft O_3 via the connecting rod link 5 and link 6. The connecting rods, rigid link 4 and link 6 are shown in Plate (1.5). The specification of the links are given in the following table:

Table 1.1

Link No.	Material	Experimental Location of Mass centres	Experimental Moment of inertia about mass centre kg - m ²	Experimental BHN
3	Phosphor Bronze alloy	12 mm from A	5.84×10^{-5}	117
4	Carbon Steel	7.5 mm from O_2 30° from O_2C	4.35×10^{-5}	-
5	Phosphor Bronze alloy	1.45 mm from C	7.5×10^{-6}	142
6	Carbon steel	1 mm from O_3	2.26×10^{-5}	-

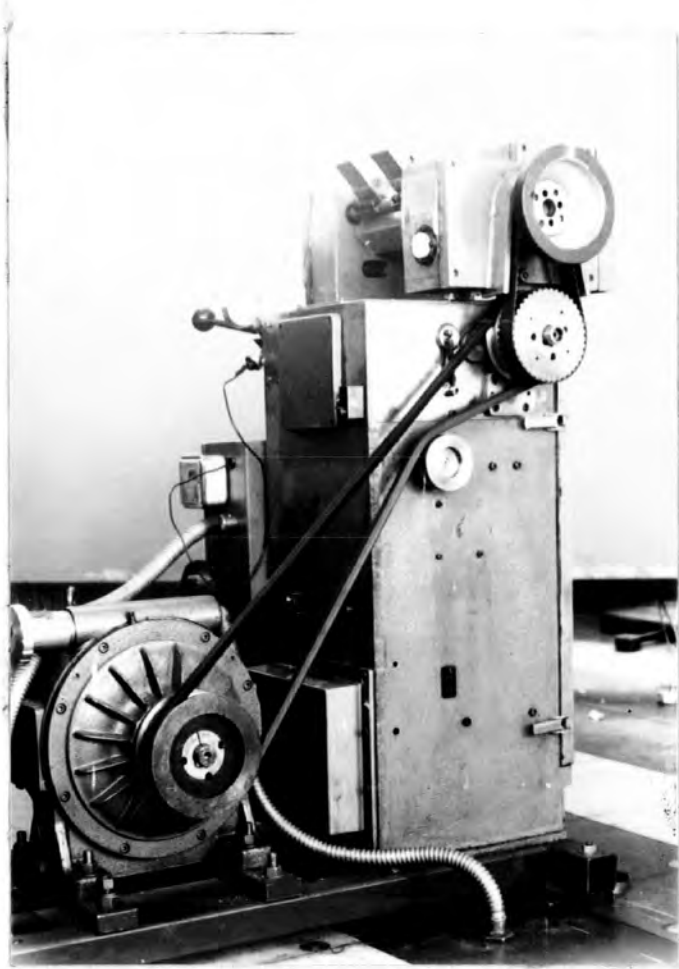


Plate (1.1) Power transmission system

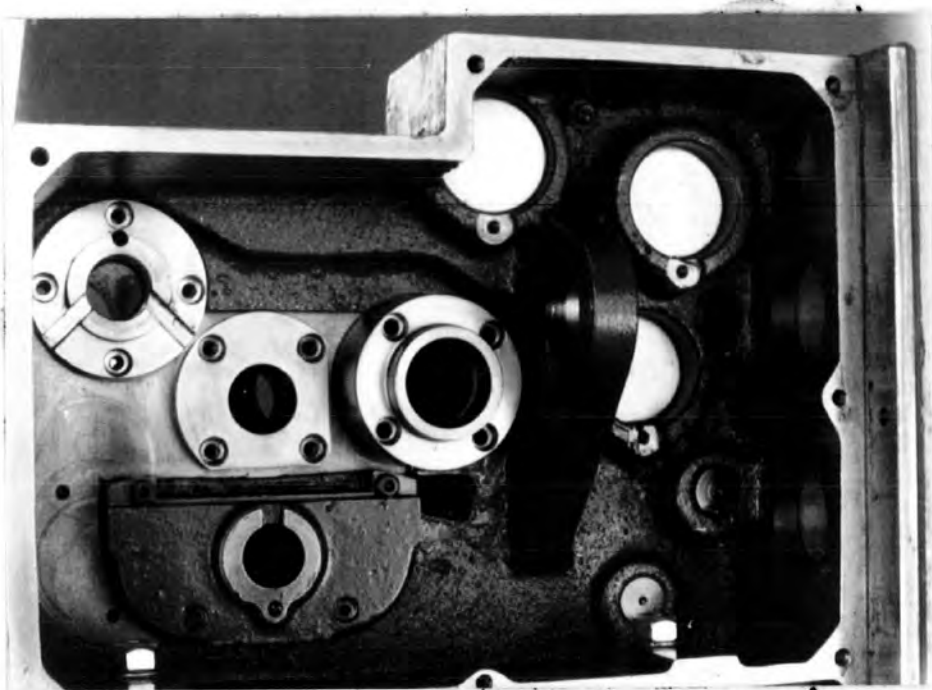


Plate 1.2 Mechanism box left end. From left to right. Bearings for shafts O_3 , O_2 and O_1

mechanism shown as pin jointed rods

$O_1A = 11\text{ mm}$.

$AB = 42\text{ mm}$.

$BO_2 = O_2C = 22\text{ mm}$.

$CD = 29\text{ mm}$.

$DO_3 = 20\text{ mm}$.

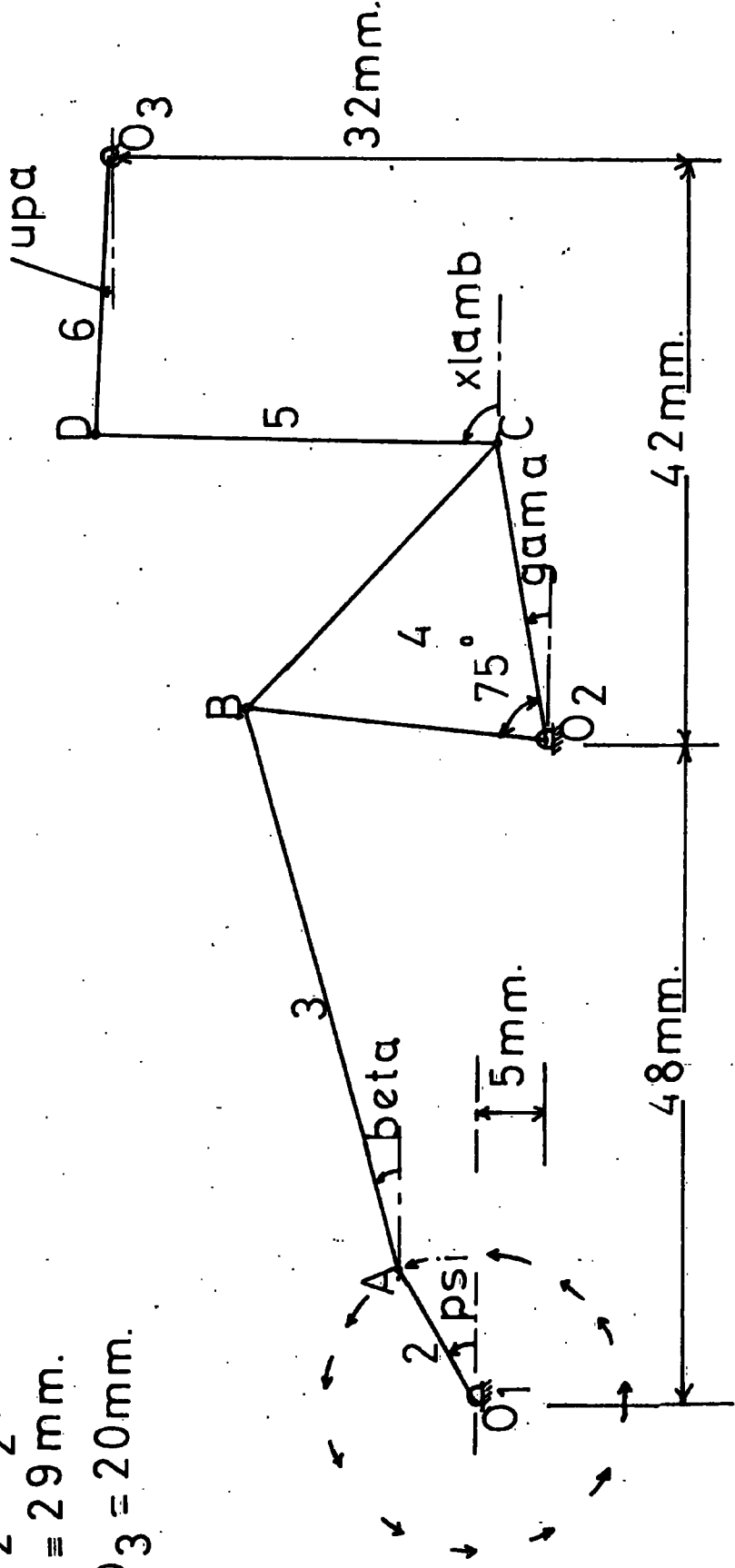


Fig. (1.3)

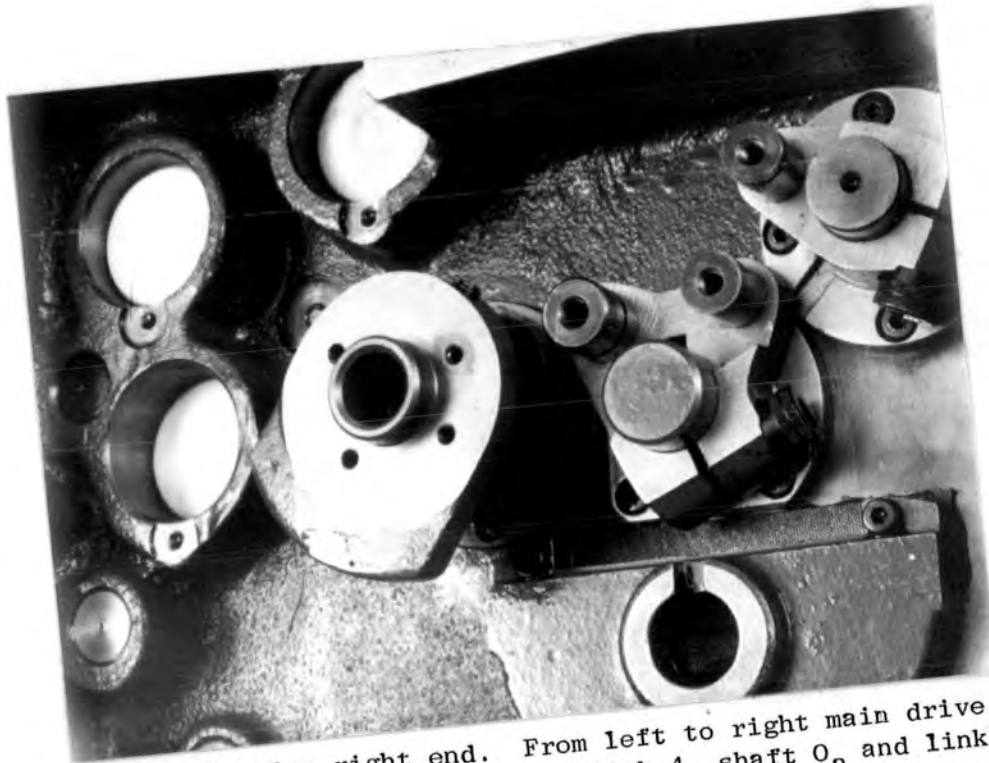


Plate 1.3 Mechanism Box right end. From left to right main drive shaft (O_1) crank arm, shaft O_2 and rigid link 4, shaft O_3 and link 6

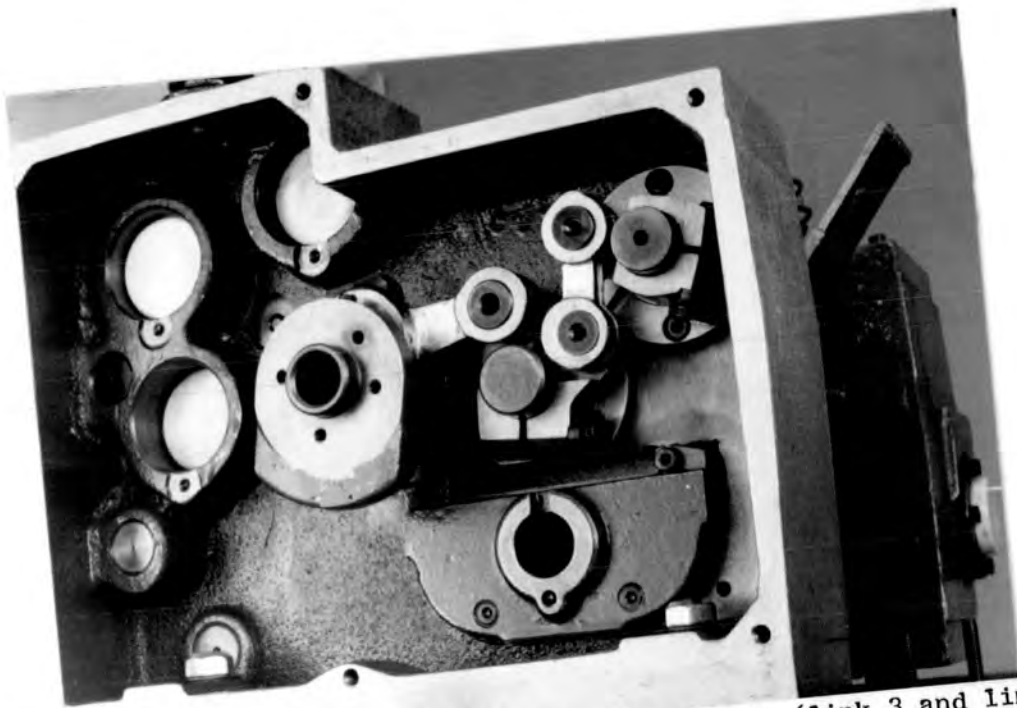


Plate 1.4 Mechanism, complete with connecting rods (link 3 and link 5)

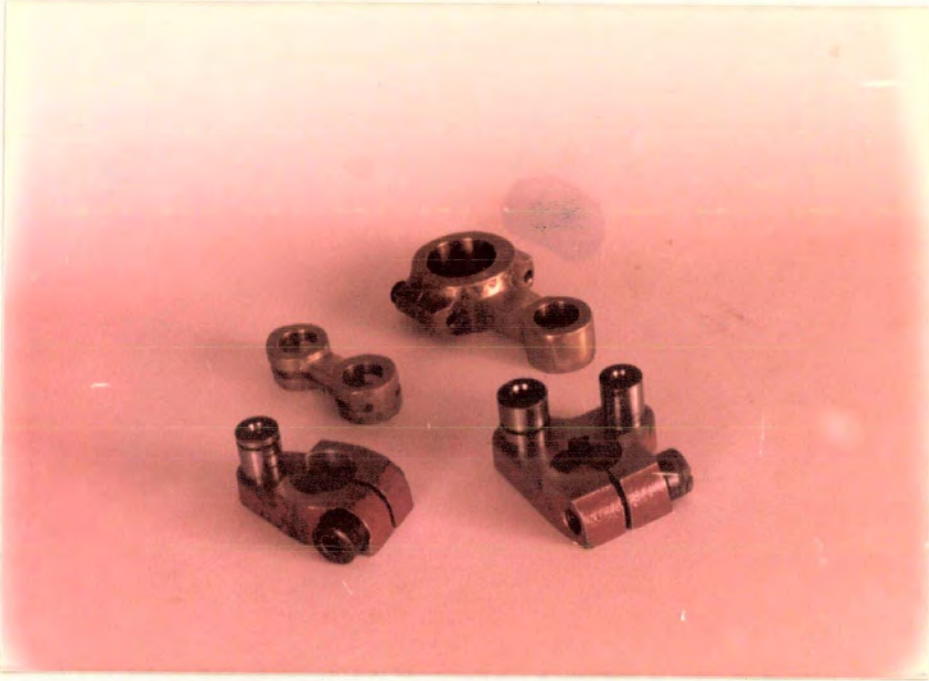


Plate 1.5 Connecting rods (links 3 and 5), rigid triangular link 4 and link 6

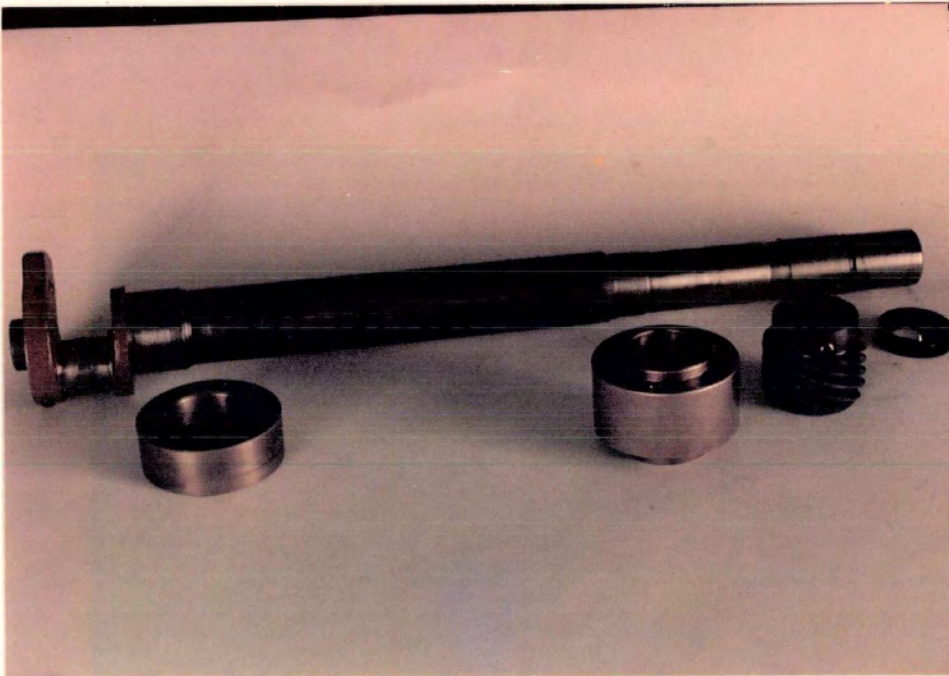


Plate 1.6 Main drive shaft (shaft O₁)

The main drive shaft, which was manufactured hollow to allow for lubrication, is shown in Plate (1.6). The diameter varies from point to point. A detailed crank-arm end drawing is shown in Fig. (1.4). The rigid triangular link 4 is attached to shaft O_2 by a clamp mechanism and secured with a key, while link 6 is attached by a similar clamp mechanism but without a key. At high crank arm speeds (approaching to 2500 r.p.m.) slip between link 6 and shaft O_3 caused stoppages and mechanical damage. Lubrication was hydrodynamic in the shaft bearings. Lubricant enters the bearings via converging channels to support the shafts without shaft to bearing contact. Hollow head cap screws were used to fit the bearings to the frame. The shafts were not secured against movement in a direction perpendicular to the plane of the mechanism. At right angles to the axis of the shaft O_2 is the rotation of the needle arms produced by pairs of bevel gears on the needle arm base and shaft O_2 .

Detailed drawings of link 6 and shaft O_3 with the comb, are shown in Fig. (1.5) and (1.6). The horizontal positioning of the shafts are shown in Fig. (1.7) The specification of shafts O_1 , O_2 and O_3 are presented in Table 1.2.

Table 1.2

shaft no.	mass kg.	Exp. moment of inertia about mass centres kg-m^2	Function
O_1	1.409	8.72×10^{-4} (with the hand wheel)	Main drive shaft delivers power to the system
O_2	0.699	9.22×10^{-5} (with the bevel gears)	Carries a pair of partial bevel gears to rotate the needle arms
O_3	0.805	3.06×10^{-4} (with the combs)	Carries a pair of combs for weaving

SHAFT O₁ — crank

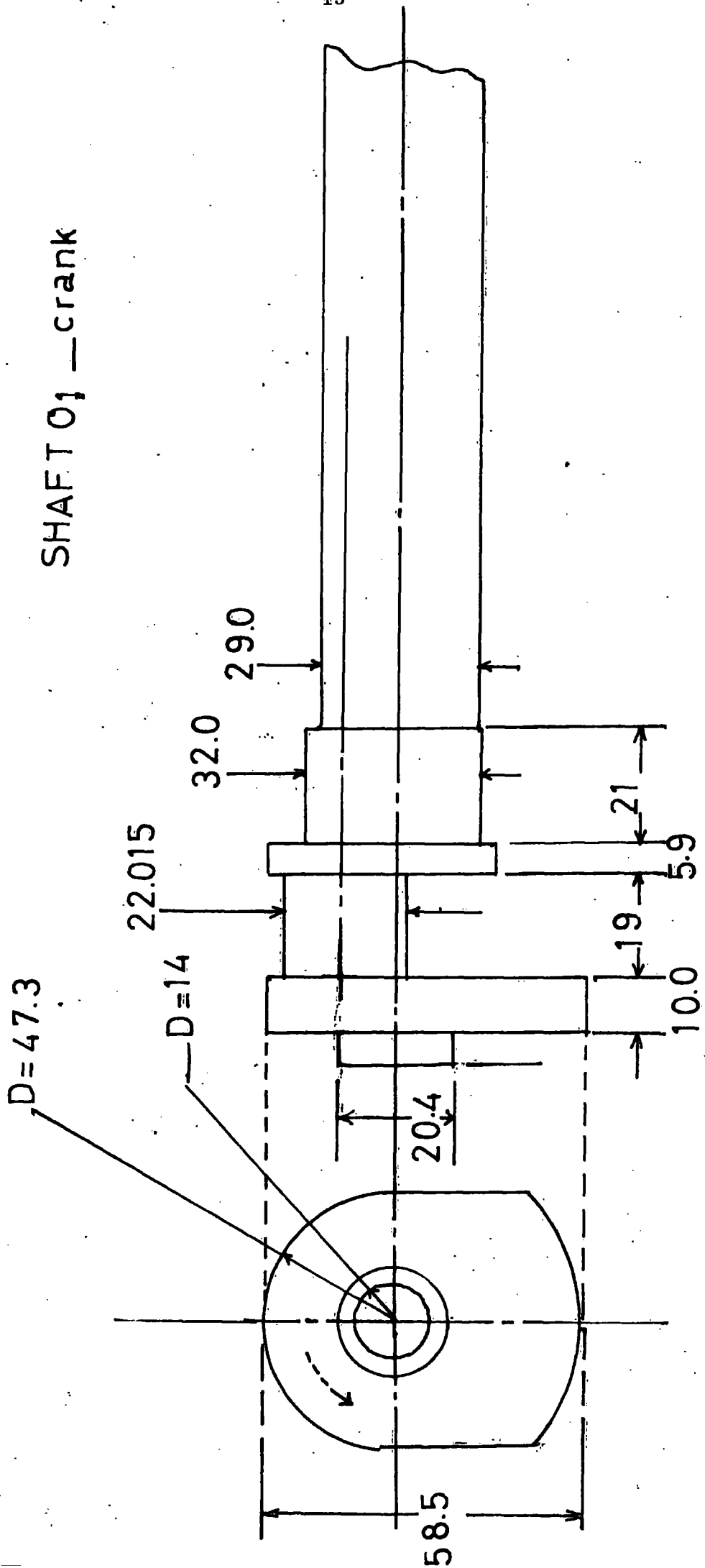


Fig. 1.4 Main drive shaft crank arm end detailed drawing

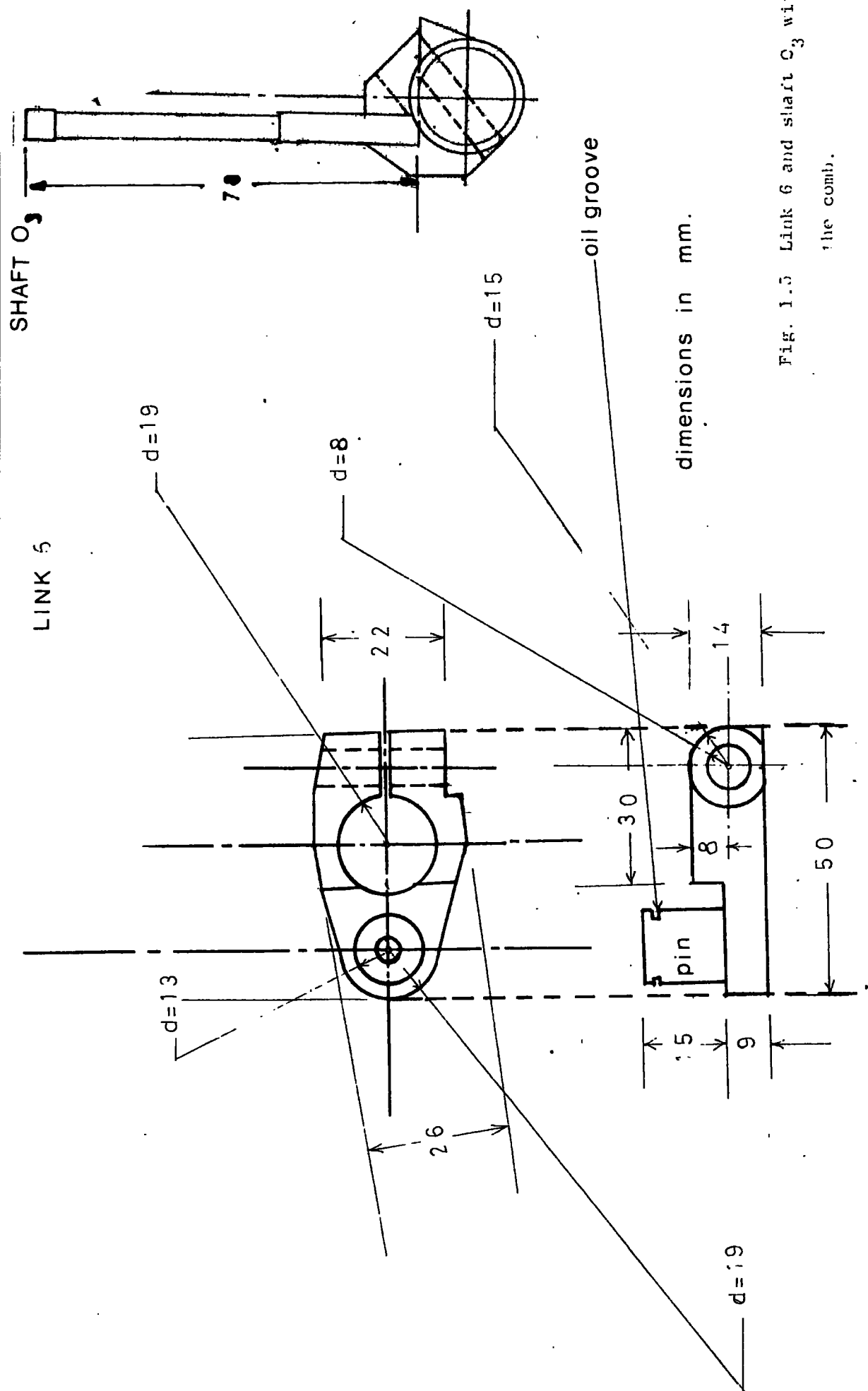
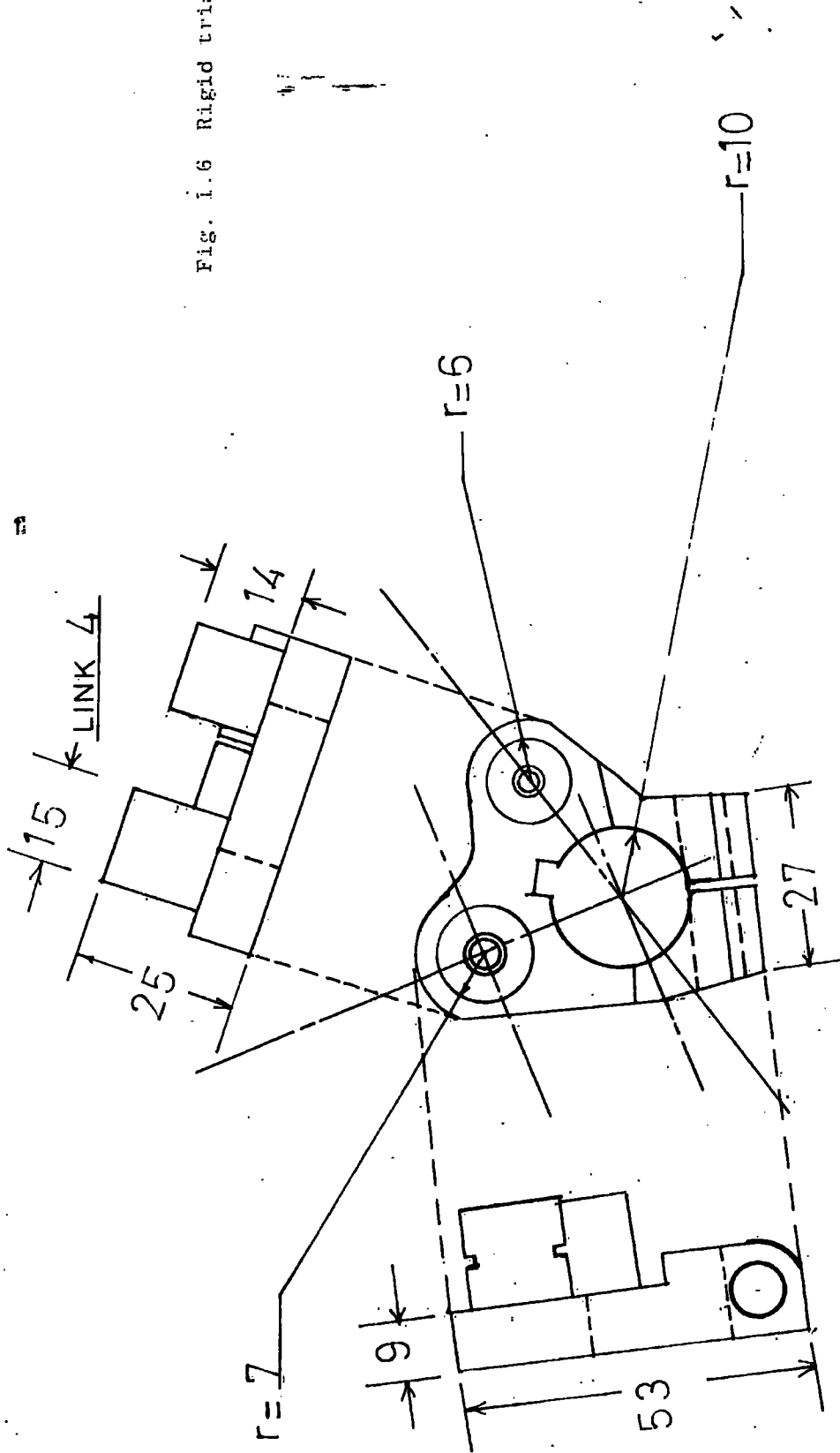


Fig. 1.5 Link 6 and shaft O₃ with the comb.

Fig. i.6 Rigid triangular link 4



dimensions in mm

INTERLOCKING GEARS DRIVING NEEDLE ARMS

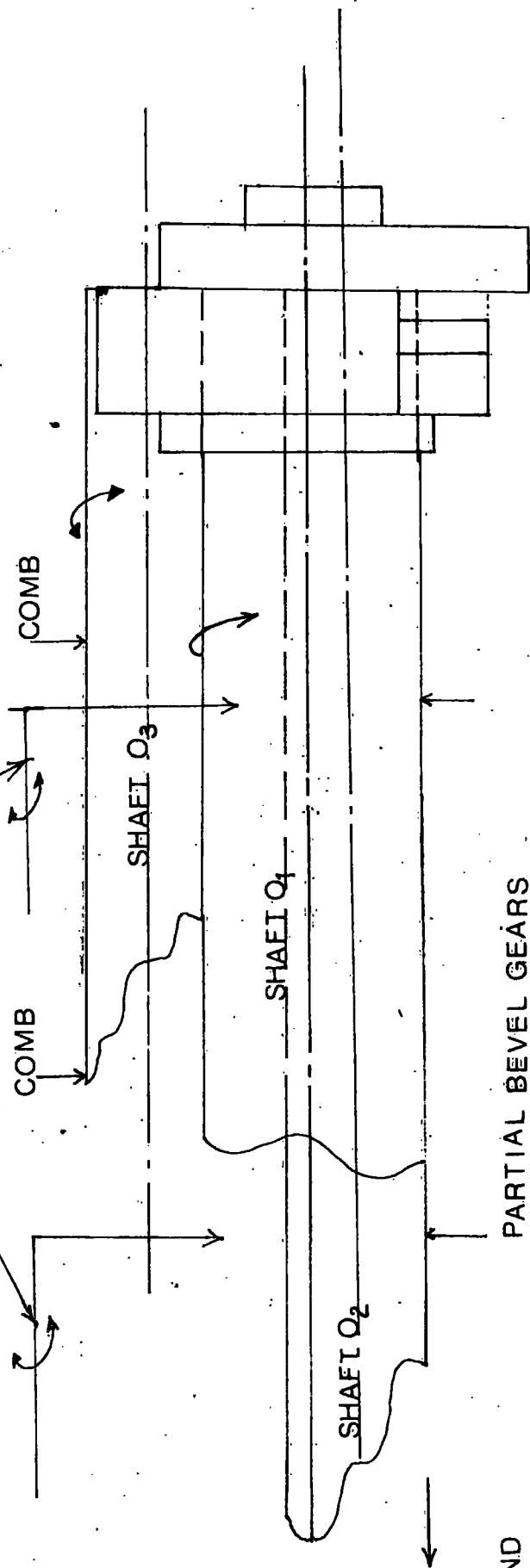


Fig. 1.7 Simplified weaving mechanism. Horizontal positioning of shafts O_1 , O_2 and O_3

The experimental moment of inertia values presented in Tables 1.1 and 1.2 are determined by a trifilar suspension. The needle arms and shaft O_3 with the comb and bearings are shown in Plates 1.9 and 1.10. The masses of links 3, 4, 5 and 6 are: 0.116 kg, 0.116 kg, 0.0283 kg and 0.0749 kg respectively. The mass centres of the links are determined by using a knife edge. The top view of the mechanism unit box and shaft O_2 are shown in plates 1.7 and 1.8 respectively.

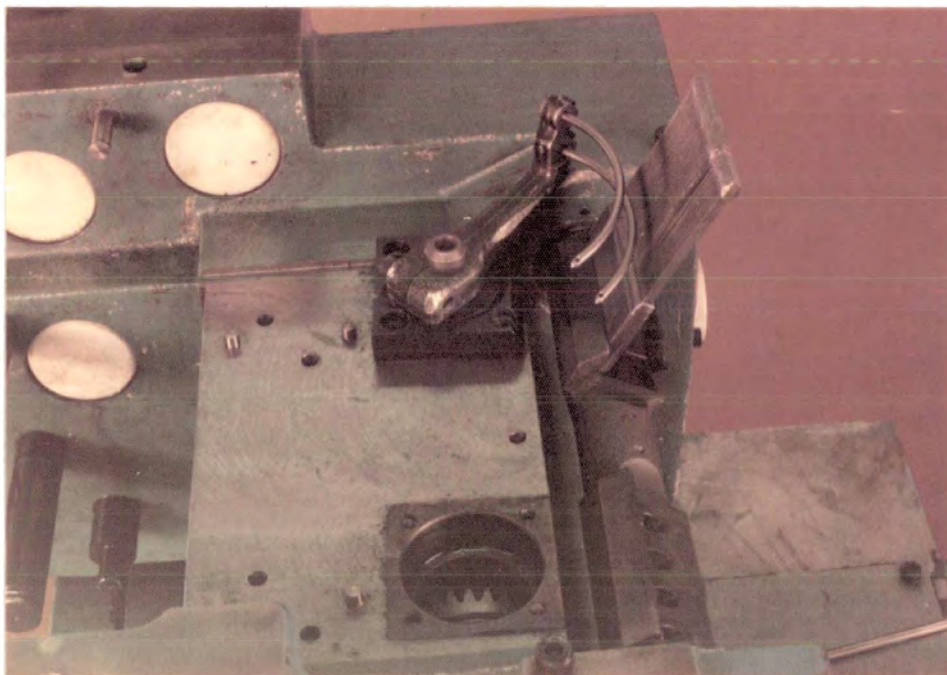


Plate 1.7 Top view - Mechanism unit box. Bevel gears carried by link O_2 , weft needle arm, shaft O_3 and the reed.



Plate 1.8 Shaft O_2 , shaft bearings, and the bevel gears.

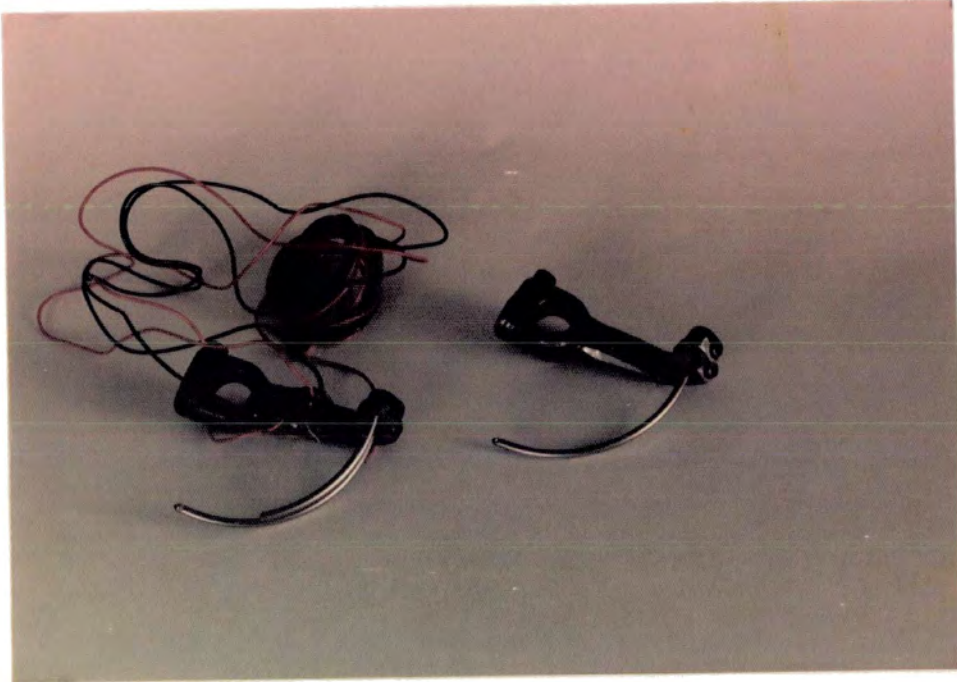


Plate 1.9 Needle arms



Plate 1.10. Shaft O_3 , comb and bearings

Chapter 2

Kinematic Analysis of the Mechanism

2.1. Introduction to Kinematic Analysis of the Mechanism

Recently a variety of methods have been developed for dynamic and kinematic analysis of mechanisms such as methods based on kinematic constraints, motor algebra, matrix methods, quaternion and dual-number methods, relative motion and incremental equations utilizing numerical methods, in addition to the classical methods. Other basic methods are; Quinn's energy distribution method, Lagrangian method, solutions employing complex polar notation and complex numbers, kineto-elastodynamic analysis, Raven's analysis, velocity analysis by instantaneous centres, velocity analysis by components, velocity and acceleration image method, graphical and analytical velocity and acceleration analysis and various algebraic methods. In the following sections a complete kinematic analysis of the mechanism is presented to specify the motion of the mechanism and to determine the kinematic values. It is assumed that all the links of the mechanism move in the same plane and the crank speed is constant.

2.2 Geometry of the Mechanism

From Fig. (2.1); for ψ $0^\circ \longrightarrow 360^\circ$

$$O_1E = \cos(\psi) (0.011)$$

$$AE = \sin(\psi) (0.011)$$

$$AF = AE + 0.005$$

$$O_2F = 0.048 - O_1E$$

$$AO_2 = (AF)^2 + (O_2F)^2$$

$$\eta = \tan^{-1} \left(\frac{AF}{O_2F} \right)$$

$$zek = \cos^{-1} \frac{0.00128 - (AO_2)^2}{(-0.044) (AO_2)^2}$$

$$cal = \cos^{-1} \frac{0.002248 - (AO_2)^2}{(0.001848)}$$

$$\alpha = 180^\circ - (zek + cal)$$

$$\beta = \alpha - \eta$$

$$\gamma = 180^\circ - (\eta + zek + 75^\circ)$$

$$\theta = \tan^{-1} \frac{0.032 - \sin(\gamma) (0.022)}{0.042 - \cos(\gamma) (0.022)}$$

$$CO_3 = \frac{0.032 - \sin(\gamma) (0.022)}{\sin(\dots)}$$

$$van = \cos^{-1} \frac{(0.029)^2 + (CO_3)^2 - (0.02)^2}{(0.029)^2 (CO_3)}$$

$$x\lambda = van + \theta$$

$$\phi = \cos^{-1} \frac{(0.02)^2 + (CO_3)^2 - (0.029)^2}{(0.04) (CO_3)}$$

$$upa = \phi - \theta$$

$$yum = 180^\circ - (x\lambda + upa)$$

all the angles are in degrees. Relationships between ψ , γ , $x\lambda$ and upa depend upon the link lengths. Numerical variation of γ , β , $x\lambda$ and upa with ψ are given in (A1) and are shown graphically in Figures (2.2), (2.3) (2.4) and (2.5). Variation of the transmission angles, cal and yum with ψ are shown in Fig. (2.6)

2.3 Velocity and Acceleration Analysis - Analytic method

Angular positions of links 3,4,5 and 6 are determined relative to the x axis

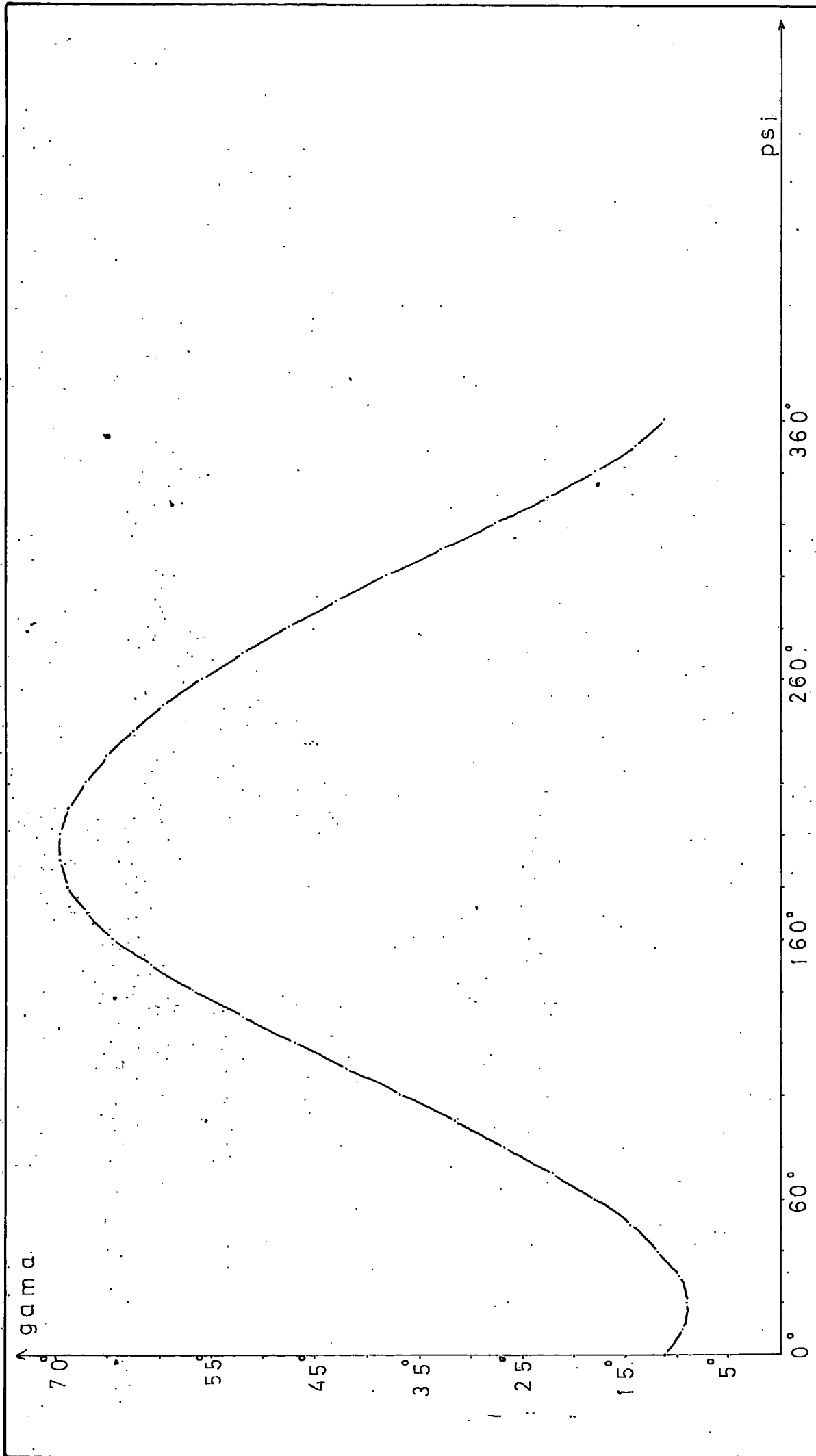


Fig. 2.2 Variation of angle γ by the crank angle ψ (angles measured from horizontal in counter clockwise direction)

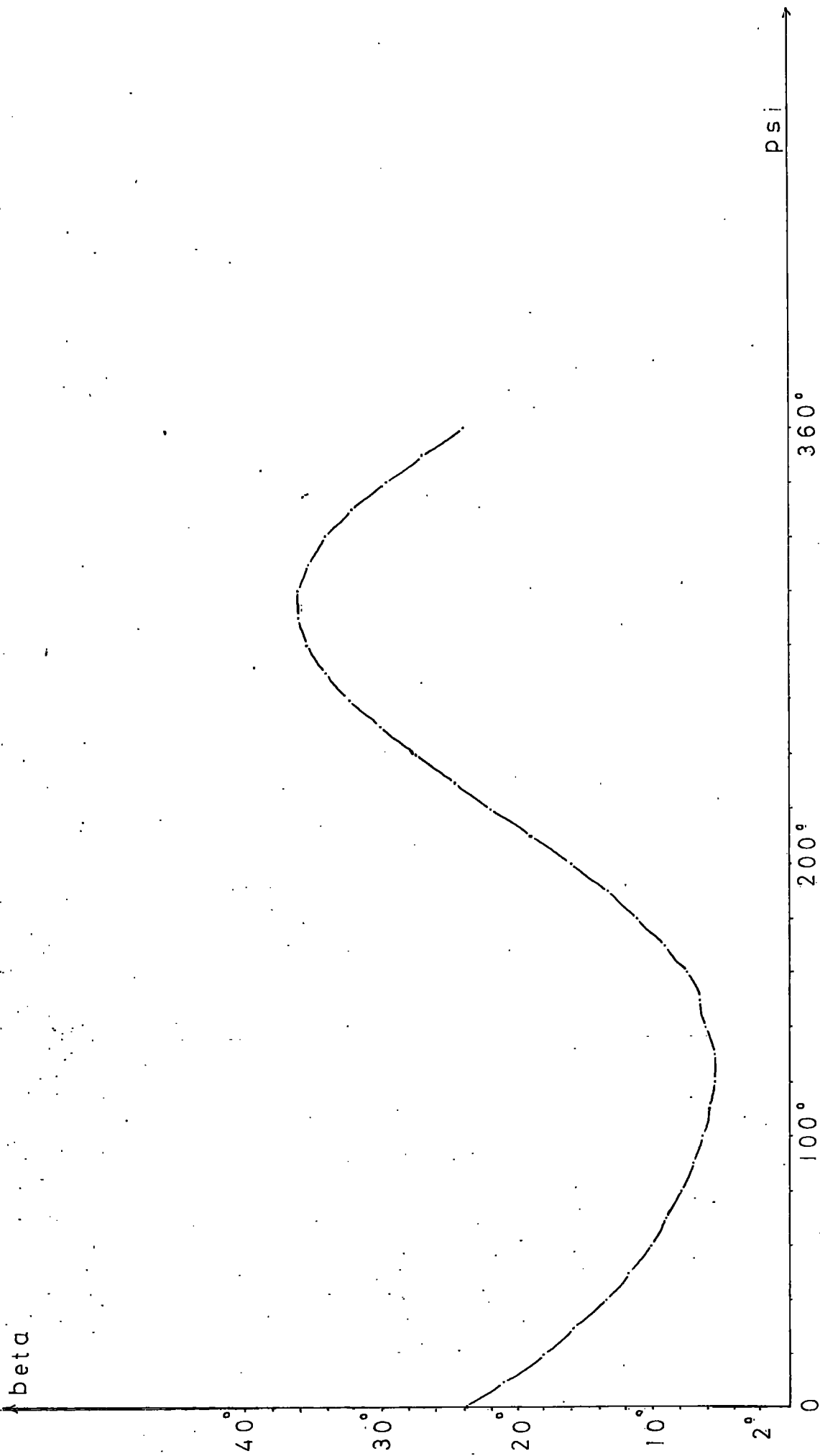


Fig. 2.3 Variation of angle beta by the crank angle psi (angles measured from horizontal in counter clockwise direction)

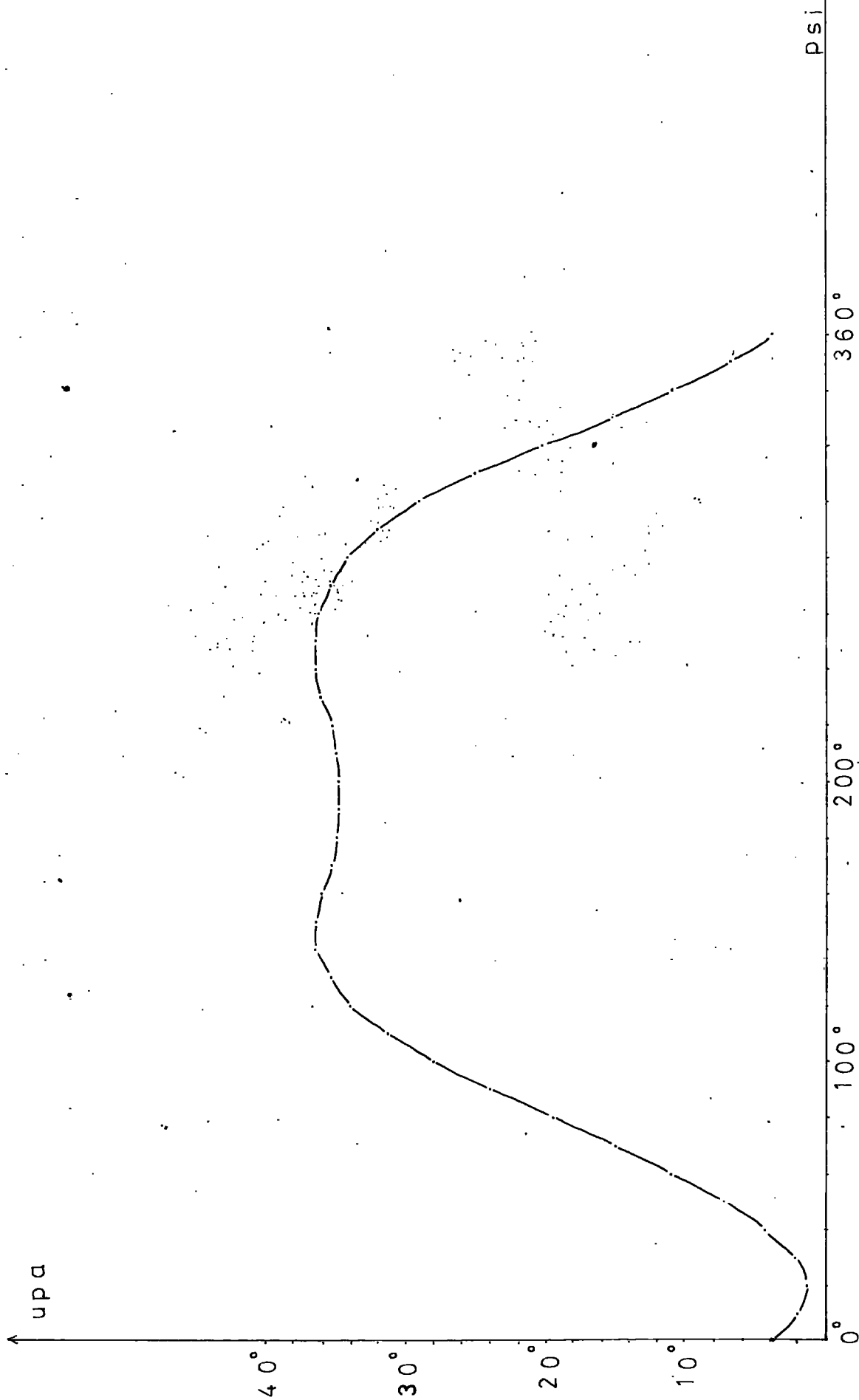


Fig. 2.4 Variation of angle upa with the crank angle ψ (crank angle measured from horizontal in counter clockwise direction and upa measured from horizontal in clockwise direction)

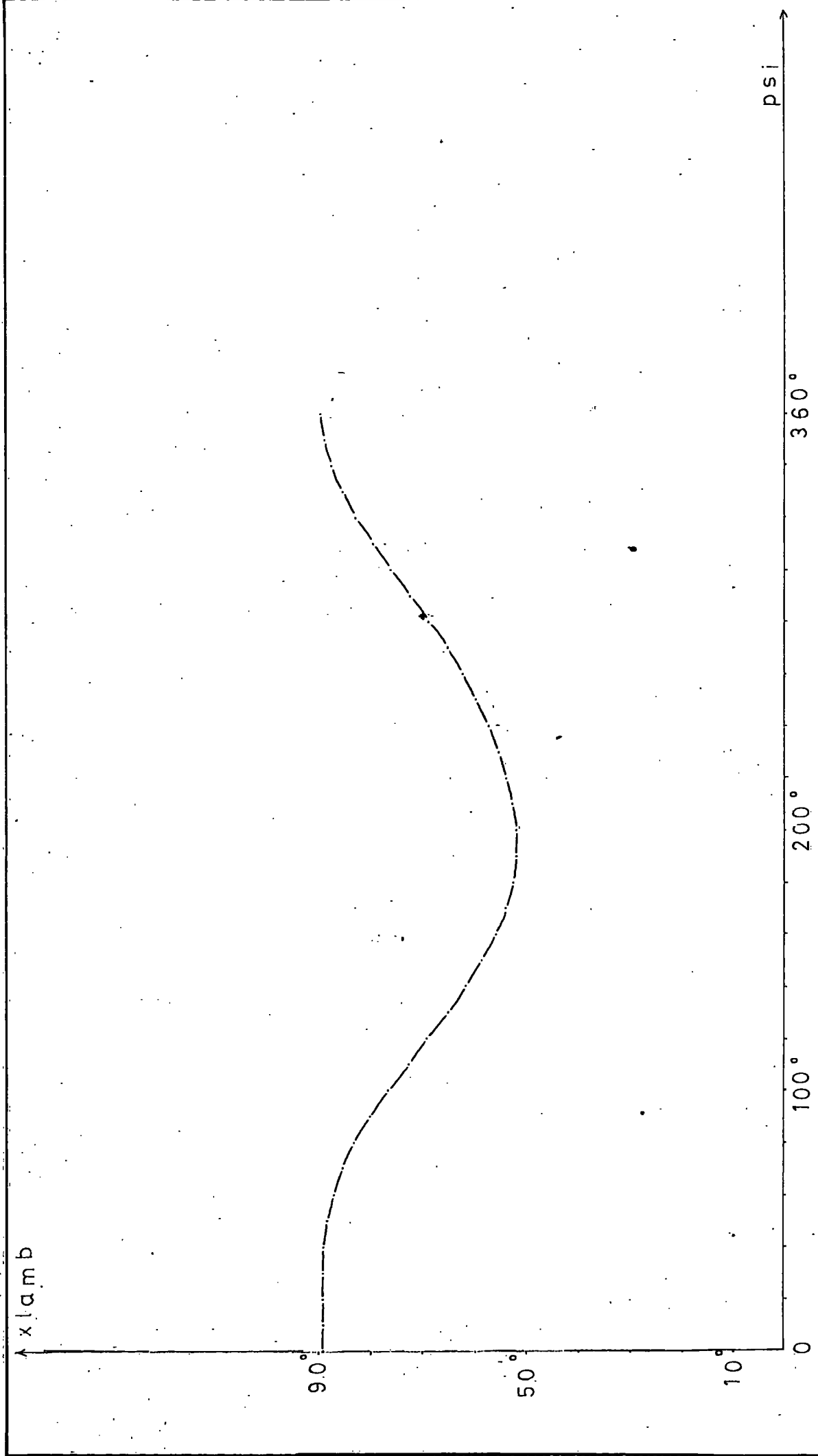


Fig. 2.5 Variation of angle x_{λ} with the crank angle ψ (angles measured from horizontal in counter clockwise direction)

The velocity of A is;

$$V_A = O_1 A \cdot \omega_2 \quad \theta \quad (\text{where } \theta \text{ shows angular position})$$

$$\text{where } \theta = \psi + 90^\circ$$

ω_2 = angular velocity of the crank arm in rad/s

The velocity of B is:

$$V_B = v_B \angle \theta$$

$$\text{where } \theta = \gamma + 165^\circ$$

The velocity of B with respect of A is

$$V_{BA} = v_{BA} \angle \theta$$

$$\text{where } \theta = \beta + 90^\circ$$

the directions are assumed for V_B and V_{BA} may be incorrect. Subsequent calculations will indicate whether this is true or not.

The relative velocity equation is;

$$V_B = V_A + V_{BA}$$

transforming V_B , V_A and V_{BA} into complex rectangular notation;

$$(\dot{x}_B + jy_B) = (\dot{x}_A + jy_A) + (\dot{x}_{BA} + jy_{BA}) \quad (2.1)$$

where \dot{x}_A and \dot{y}_A are known

Knowing the directions of V_B and V_{BA} ;

$$\frac{\dot{y}_B}{\dot{x}_B} = \tan(\gamma + 165^\circ) \quad (2.2)$$

$$\frac{\dot{y}_{BA}}{\dot{x}_{BA}} = \tan(\beta + 90^\circ) \quad (2.3)$$

solving equations (2.1), (2.2) and (2.3) simultaneously, \dot{x}_{BA} , \dot{y}_{BA} , \dot{x}_B and \dot{y}_B can be determined.

The angular velocity of links 3 and 4 may be calculated as;

$$\omega_3 = \frac{v_{BA}}{AB} \quad \text{and} \quad \omega_4 = \frac{v_B}{O_2 B}$$

from the geometry of the mechanism;

$$v_B = v_C \quad (\text{in magnitude})$$

$$v_C = v_C \angle \theta$$

where

$$\theta = \gamma + 90^\circ$$

the velocity of D is;

$$v_D = v_D \angle \theta$$

where

$$\theta = 90^\circ - \text{upa}$$

the velocity of D with respect of C is;

$$v_{DC} = v_{DC} \angle \theta$$

where

$$\theta = x \lambda + 90^\circ$$

the relative velocity equation is;

$$v_D = v_C + v_{DC}$$

transforming into complex rectangular notation;

$$(\dot{x}_D + j\dot{y}_D) = (\dot{x}_C + j\dot{y}_C) + (\dot{x}_{DC} + j\dot{y}_{DC}) \quad (2.4)$$

knowing the directions of v_D and v_{DC}

$$\frac{\dot{y}_D}{\dot{x}_D} = \tan(90^\circ - \text{upa}) \quad (2.5)$$

$$\frac{\dot{y}_{DC}}{\dot{x}_{DC}} = \tan(x\lambda + 90^\circ) \quad (2.6)$$

solving equations (2.4), (2.5) and (2.6) simultaneously,

$$\dot{x}_{DC}, \dot{y}_{DC}, \dot{x}_D \text{ and } \dot{y}_D \text{ can be determined}$$

thus, the angular velocity of links 5 and 6 are;

$$\omega_5 = \frac{v_{DC}}{DC} \quad \text{and} \quad \omega_6 = \frac{v_D}{DO_3}$$

the components of acceleration can be obtained as follows;

$$A_A^t = O_1A \alpha_2 \angle \theta$$

where

$$\theta = \psi + 90^\circ$$

$$A_A^t = 0, \text{ since } \alpha_2 = 0$$

$$A_A^r = O_1A \cdot \omega_2^2 \angle \theta$$

where

$$\theta = -(180^\circ - \psi)$$

$$A_{BA}^r = AB \cdot \omega_3^2 \angle \theta$$

where

$$\theta = -(180^\circ - \beta)$$

$$A_B^r = O_2B \cdot \omega_4^2 \angle \theta$$

where

$$\theta = -[180^\circ - (75^\circ + \gamma)]$$

from the geometry of the mechanism;

$$A_B^r = A_C^r \text{ (in magnitude)}$$

$$A_B^t = A_C^t \text{ (in magnitude)}$$

both A_{BA}^t and A_B^t are unknown and are to be determined

The relative acceleration equation is;

$$A_B^t + A_B^r = A_A^t + A_A^r + A_{BA}^t + A_{BA}^r \quad (2.7)$$

transforming the acceleration components into complex rectangular notation

and substituting into equation (2.7) produces

$$(\ddot{x}_B^t + jy_B^t) + (\ddot{x}_B^r + jy_B^r) = (\ddot{x}_A^r + jy_A^r) + (\ddot{x}_{BA}^t + jy_{BA}^t) + (\ddot{x}_{BA}^r + jy_{BA}^r) \quad (2.8)$$

the required slopes of these components are such that;

$$\frac{\ddot{y}_B^t}{\ddot{x}_B^r} = \tan(\gamma + 165^\circ) \quad (2.9)$$

$$\frac{\ddot{y}_{BA}^t}{\ddot{x}_{BA}^t} = \tan(90^\circ + \beta) \quad (2.10)$$

by equating the real and imaginary parts of equation (2.8) and solving simultaneously with equations (2.9) and (2.10) gives \ddot{x}_B^t , \ddot{y}_B^t , \ddot{x}_{BA}^t and \ddot{y}_{BA}^t

The acceleration of B is;

$$A_B = A_B^t + A_B^r$$

where

$$A_B^t = \ddot{x}_B^t + jy_B^t$$

acceleration of link 3 is;

$$A_{BA} = A_{BA}^t + A_{BA}^r$$

where

$$A_{BA}^t = \ddot{x}_{BA}^t + jy_{BA}^t$$

the angular acceleration of links 3 and 4 are;

$$\alpha_3 = \frac{a_{BA}^t}{AB} \quad \alpha_4 = \frac{a_B^t}{O_2B}$$

similarly, the relative acceleration equation for links 4, 5 and 6 can be

written as

$$A_D^t + A_D^r = A_C^r + A_C^t + A_{DC}^t + A_{DC}^r \quad (2.11)$$

where

$$A_D^r = DO_3 \omega_6^2 \angle \theta ; \theta = 360^\circ - \text{upa}$$

$$A_{DC}^r = DC \omega_5^2 \angle \theta ; \theta = 180^\circ + x\lambda$$

$$A_C^r = a_C^r \angle \theta ; \theta = 180^\circ + \gamma$$

$$A_C^t = a_C^t \angle \theta ; \theta = \gamma + 90^\circ$$

\ddot{x}_C^t and \ddot{y}_C^t are therefore known as well as \ddot{x}_C^r and \ddot{y}_C^r . Again by transforming equation (2.11) into complex rectangular notation;

$$\begin{aligned} (\ddot{x}_D^t + jy_D^t) + (\ddot{x}_D^r + jy_D^r) &= (\ddot{x}_C^r + jy_C^r) + (\ddot{x}_C^t + jy_C^t) + (\ddot{x}_{DC}^t + jy_{DC}^t) \\ &+ (\ddot{x}_{DC}^r + jy_{DC}^r) \end{aligned} \quad (2.12)$$

the required slopes are;

$$\frac{\ddot{y}_D^t}{\ddot{x}_D^t} = \tan (90^\circ - \text{upa}) \quad (2.13)$$

and

$$\frac{\ddot{y}_{DC}^t}{\ddot{x}_{DC}^t} = \tan (x\lambda + 90^\circ) \quad (2.14)$$

from equations (2.12), (2.13) and (2.14), \ddot{x}_D^t , \ddot{y}_D^t , \ddot{x}_{DC}^t and \ddot{y}_{DC}^t can be obtained.

$$A_D^t = \ddot{x}_D^t + jy_D^t$$

the acceleration of D is;

$$A_D = A_D^t + A_D^r$$

angular acceleration of links 5 and 6 are;

$$\alpha_5 = \frac{a_{DC}^t}{DC}$$

$$\alpha_6 = \frac{a_D^t}{DO_3}$$

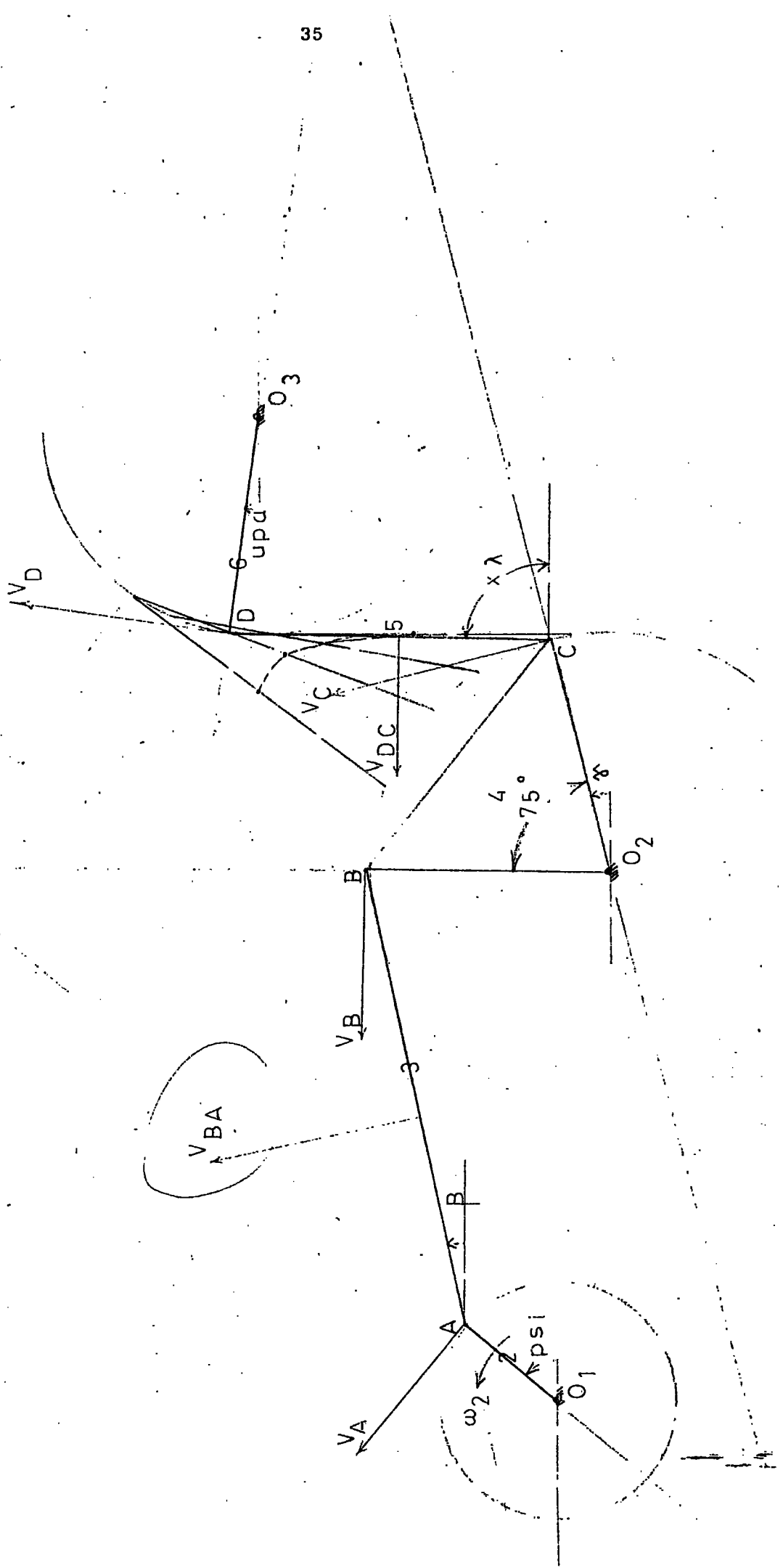


Fig 2.7 Analytical velocity and acceleration analysis

Variation of the angular acceleration of links 3,4,5 and 6 with crank angle ψ are shown in Fig. (2.8). Fig. (2.9), Fig. (2.10) and in Fig. (2.11). Variation of angular velocities of links 3,4,5 and 6 with the crank angle ψ are given in Fig. (2.12) for a crank speed of 2500 r.p.m. Ratio of angular velocity of the individual links to crank arm angular velocity is shown in Fig. (2.13), for a complete revolution of the crank arm. All the kinematic values calculated above, are presented in (A1) for a crank speed of 2500 r.p.m.

2.4 Algebraic Approach

The system is separated into two loops, Fig. (2.14, a and b) Fig. (2.15) The first loop represents a crank-rocker mechanism, also known as a crank-lever mechanism, which is a popular type of the well known four-bar linkage for converting continuous rotary motion to oscillation. The second loop is a four-bar chain attached to the rigid link 4 of the first loop at point C. The two extreme positions of the output lever (link 4) of the first loop are expected to occur when crank arm (link 2) is in line with the coupler. Proportions of the mechanism satisfy Grashoff's criterion as in the following:

$$\text{Base link} < \text{coupler} + (\text{output lever} - \text{driving crank})$$

$$4.8 < 5.3$$

$$\text{Base link} > \text{coupler} - (\text{output lever} - \text{driving crank})$$

$$4.8 > 3.1$$

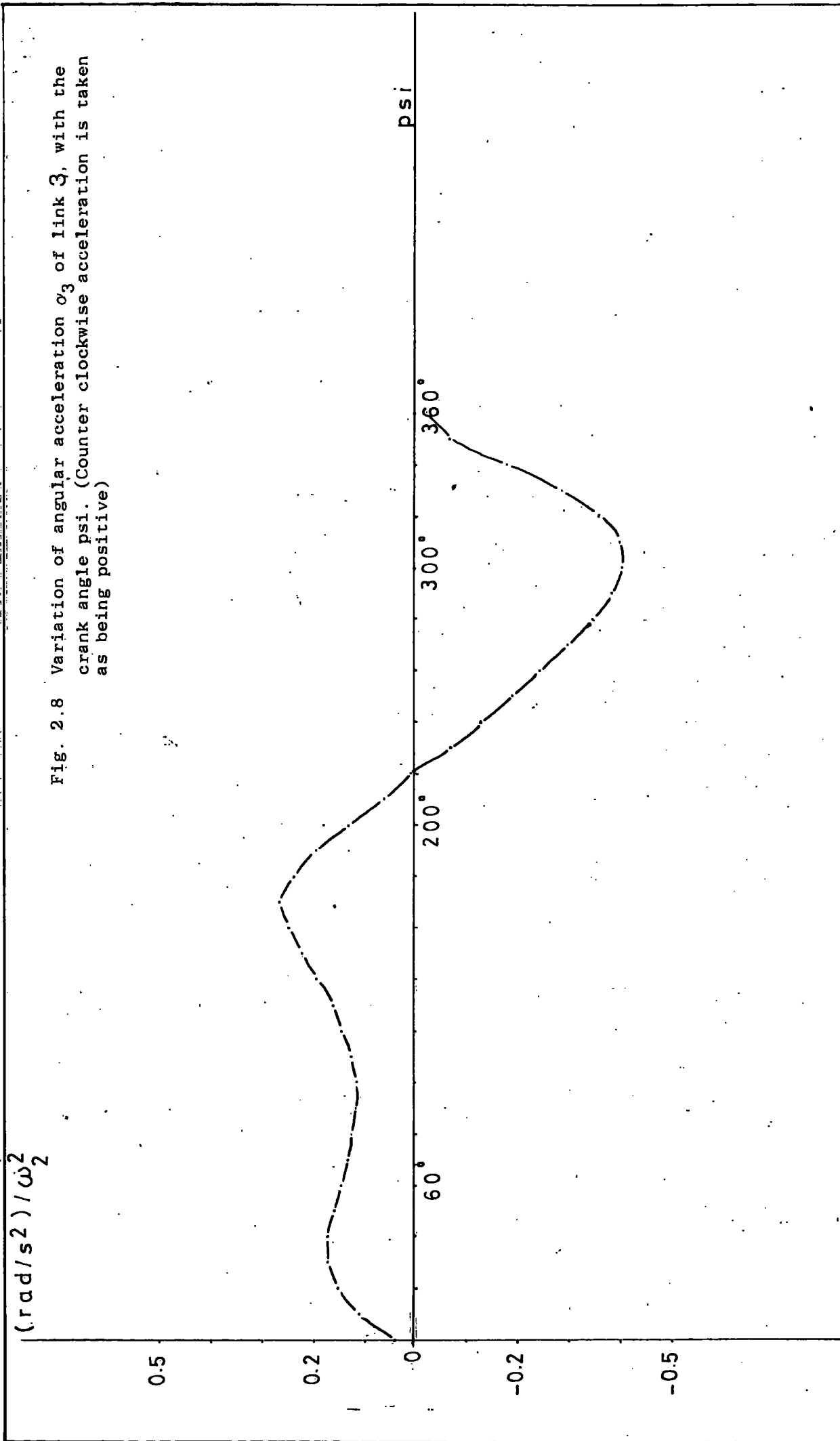
Let A,B,C and D be lengths of input crank, coupler link, output lever, and base link of the first loop, Fig. (2.14a)

$$\alpha_1, \alpha_2 = \text{angles showing dead-centre positions of output link}$$

$$\Delta \alpha = \alpha_2 - \alpha_1$$

$$\Delta \beta = \beta_2 - \beta_1 - \pi$$

the unit of angles being in degrees.



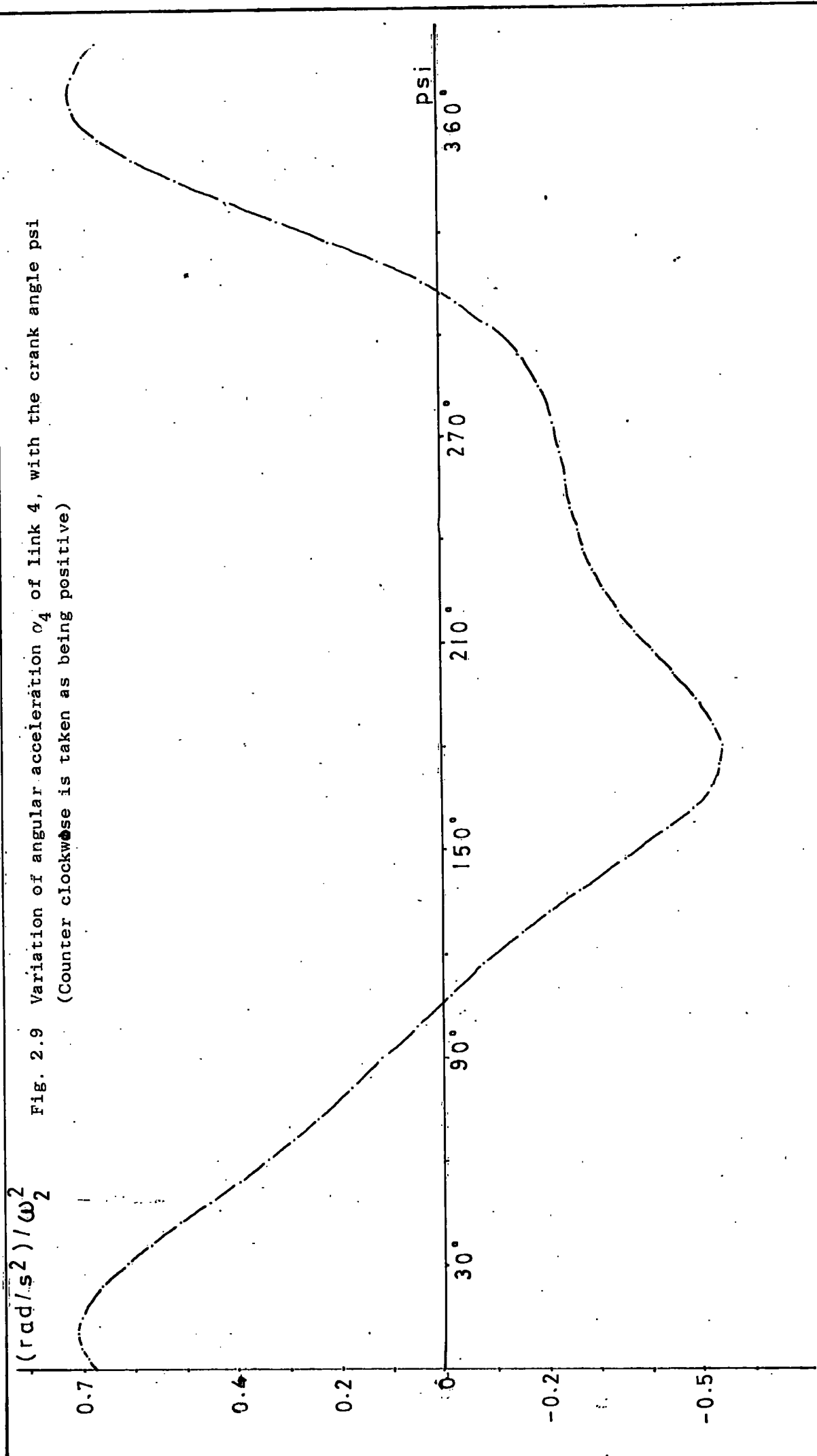


Fig. 2.9 Variation of angular acceleration α_4 of link 4, with the crank angle ψ (Counter clockwise is taken as being positive)

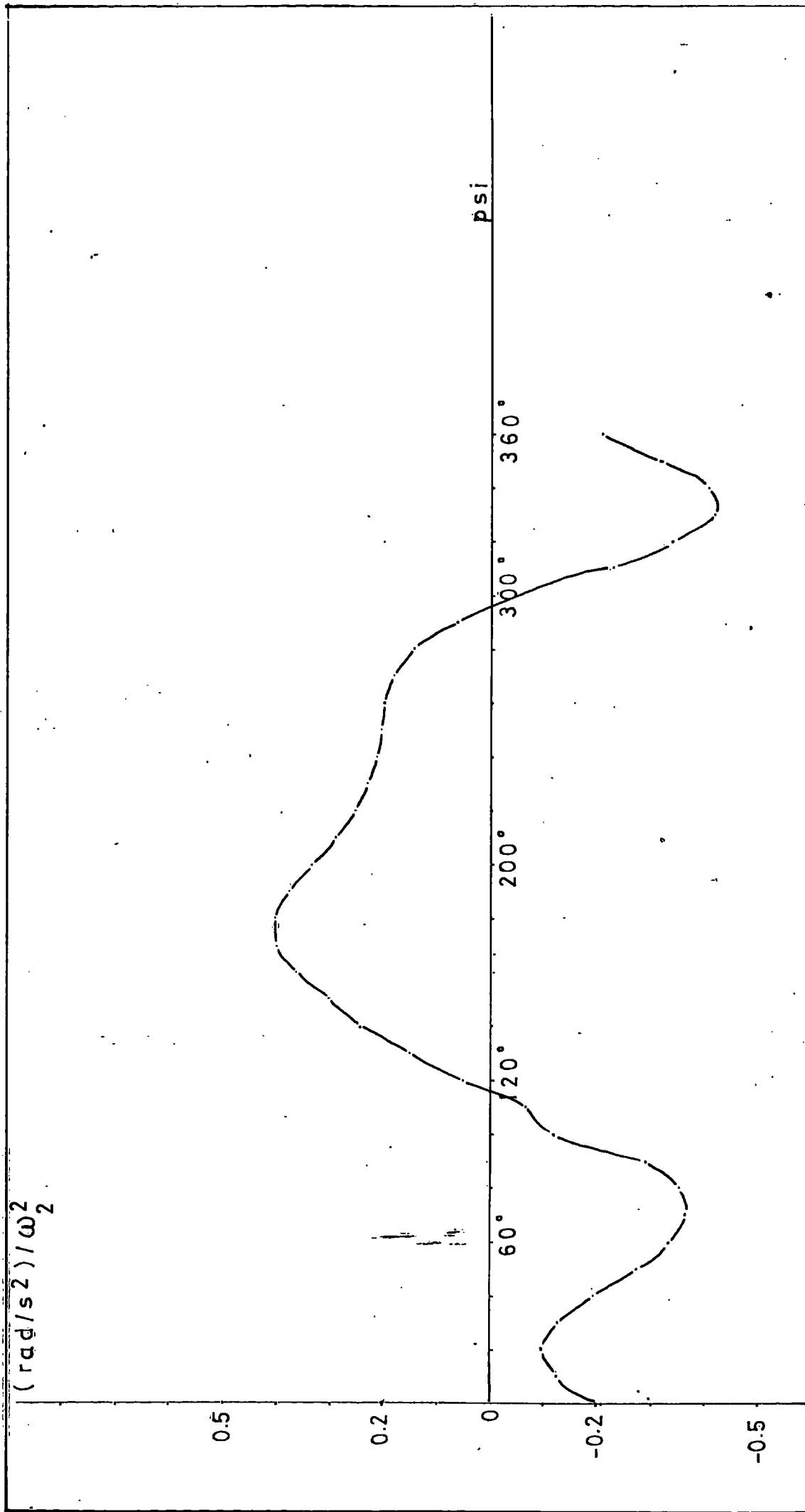


Fig. 2.10 Variation of angular acceleration α_5 of link 5 with the crank angle ψ (counter clockwise acceleration is taken as being positive)

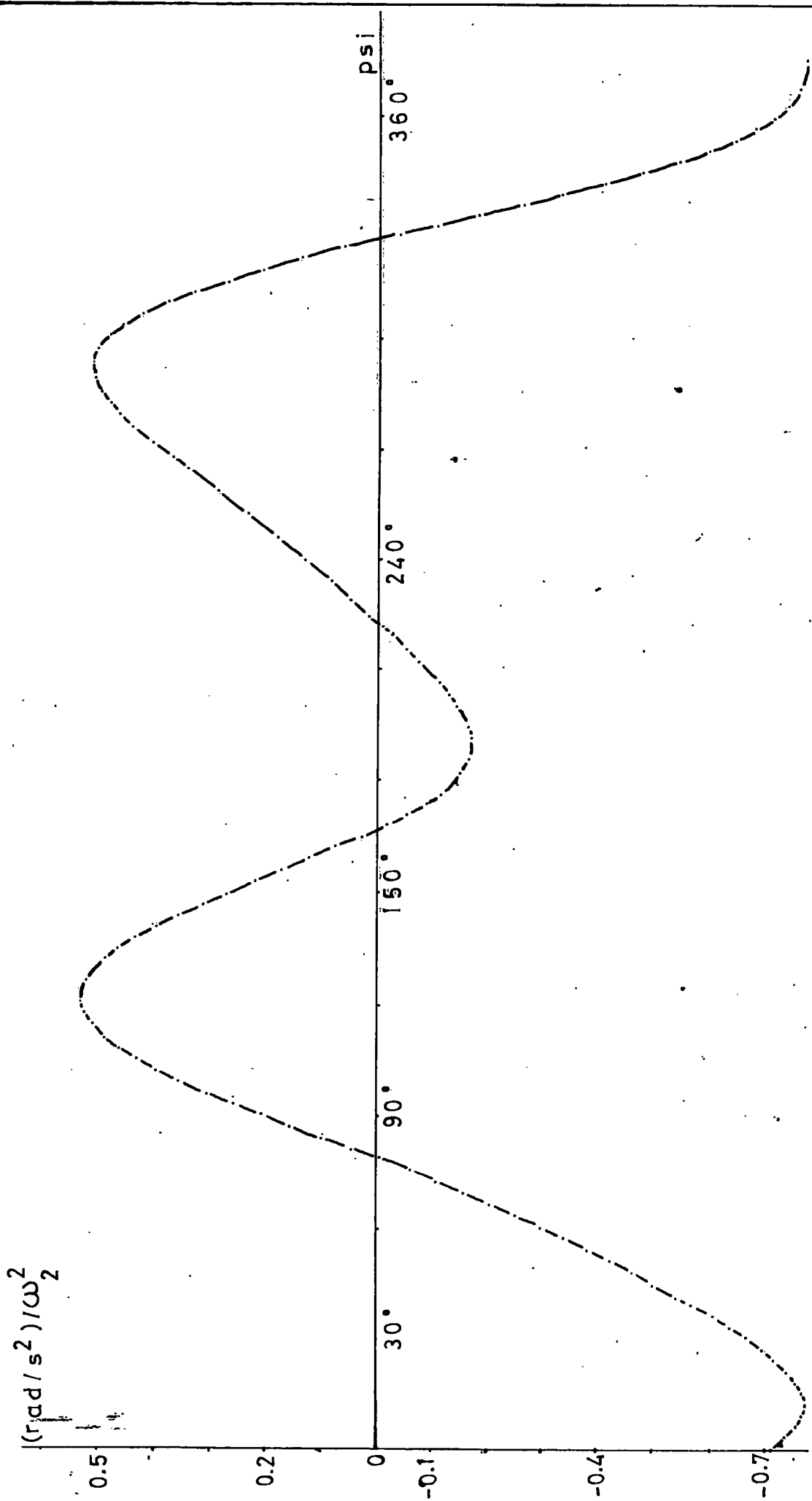
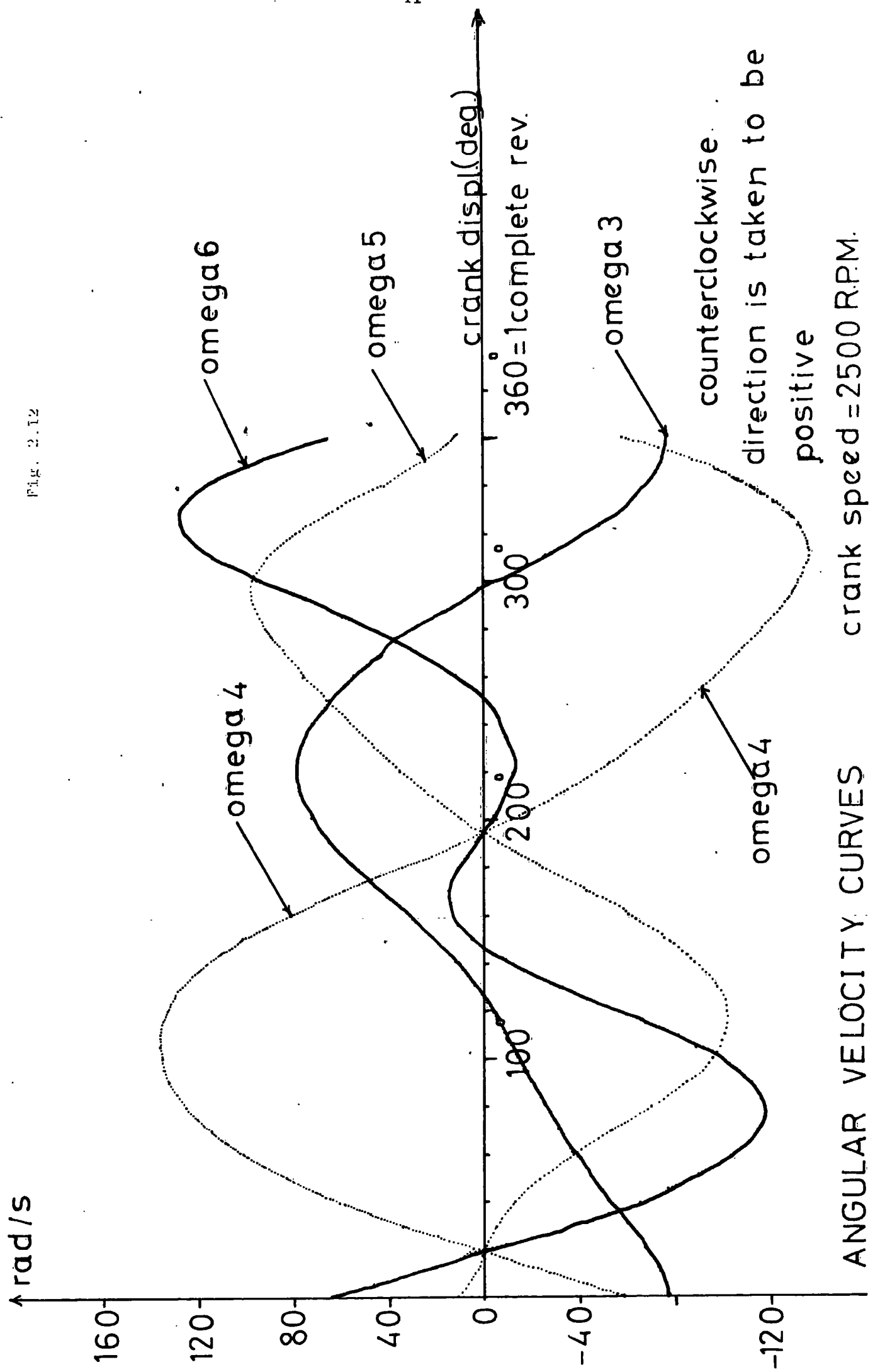


Fig. 2.11 Variation of angular acceleration α_6 of link 6 with the crank angle ψ
 (counter clockwise acceleration is taken as being positive)

Fig. 2.12

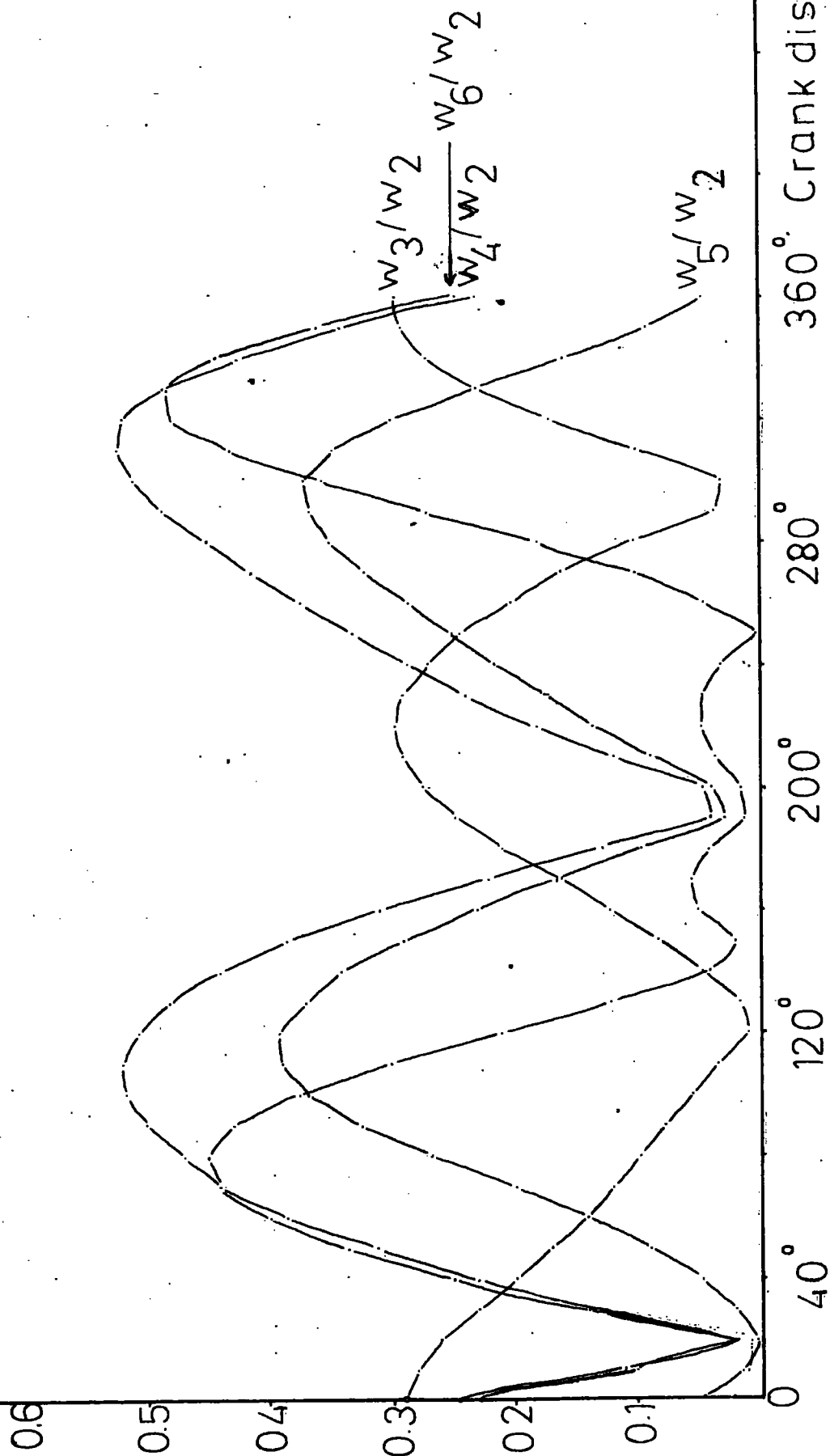


ANGULAR VELOCITY CURVES

crank speed = 2500 R.P.M.

Ω_n / Ω_2

Fig. 2.13 Variation of Angular velocity ratio with crank angle psi



By using complex algebraic notation, the displacement equations can be expressed as;

$$(A + B) e^{i\beta_1} = D + C e^{i\alpha_1} \quad (2.15)$$

$$Ae^{i\beta_2} + Be^{i(\beta_2 - \pi)} = D + Ce^{i\alpha_2} \quad (2.16)$$

equating real and imaginary parts of equations (2.15) and (2.16) respectively;

$$(A + B) \cos\beta_1 - C \cos\alpha_1 = D \quad (2.17)$$

$$(A + B) \sin\beta_1 - C \sin\alpha_1 = 0 \quad (2.18)$$

$$(A - B) \cos\beta_2 - C \cos\alpha_2 = D \quad (2.19)$$

$$(A - B) \sin\beta_2 - C \sin\alpha_2 = 0 \quad (2.20)$$

from equations (2.17) and (2.18);

$$A + B = \frac{C \sin\alpha_1}{\sin\beta_1} = \frac{D + C \cos\alpha_1}{\cos\beta_1} \quad (2.21)$$

from equations (2.19) and (2.20)

$$A - B = \frac{C \sin\alpha_2}{\sin\beta_2} = \frac{D + C \cos\alpha_2}{\cos\beta_2} \quad (2.22)$$

from equation (2.21)

$$\frac{C}{D} = \frac{\sin\beta_1}{\sin(\alpha_1 - \beta_1)} \quad (2.23)$$

from equation (2.22)

$$\frac{C}{D} = \frac{\sin\beta_2}{\sin(\alpha_2 - \beta_2)} \quad (2.24)$$

equations (2.23) and (2.24) are combined to give;

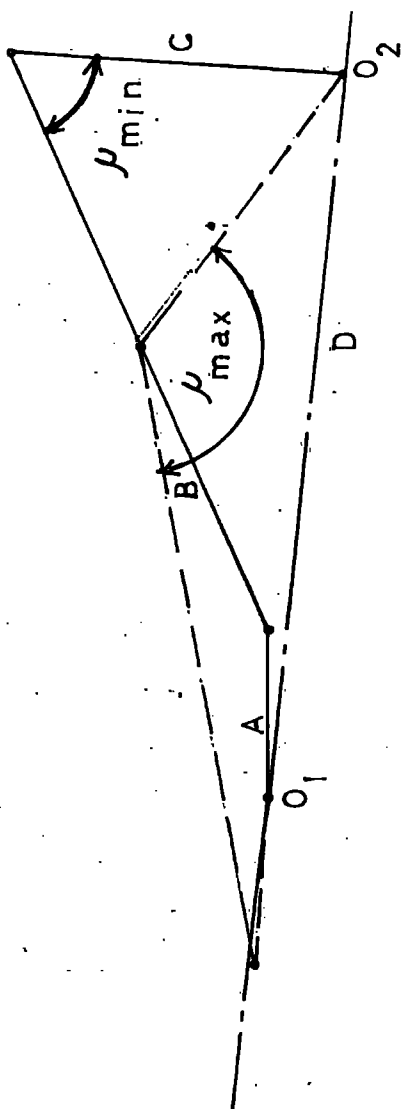


Fig. 2.14 a

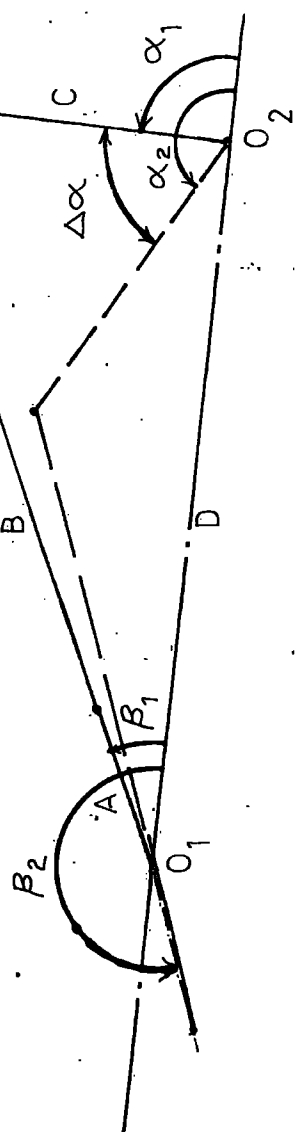


Fig. 2.14 b

LOOP-1

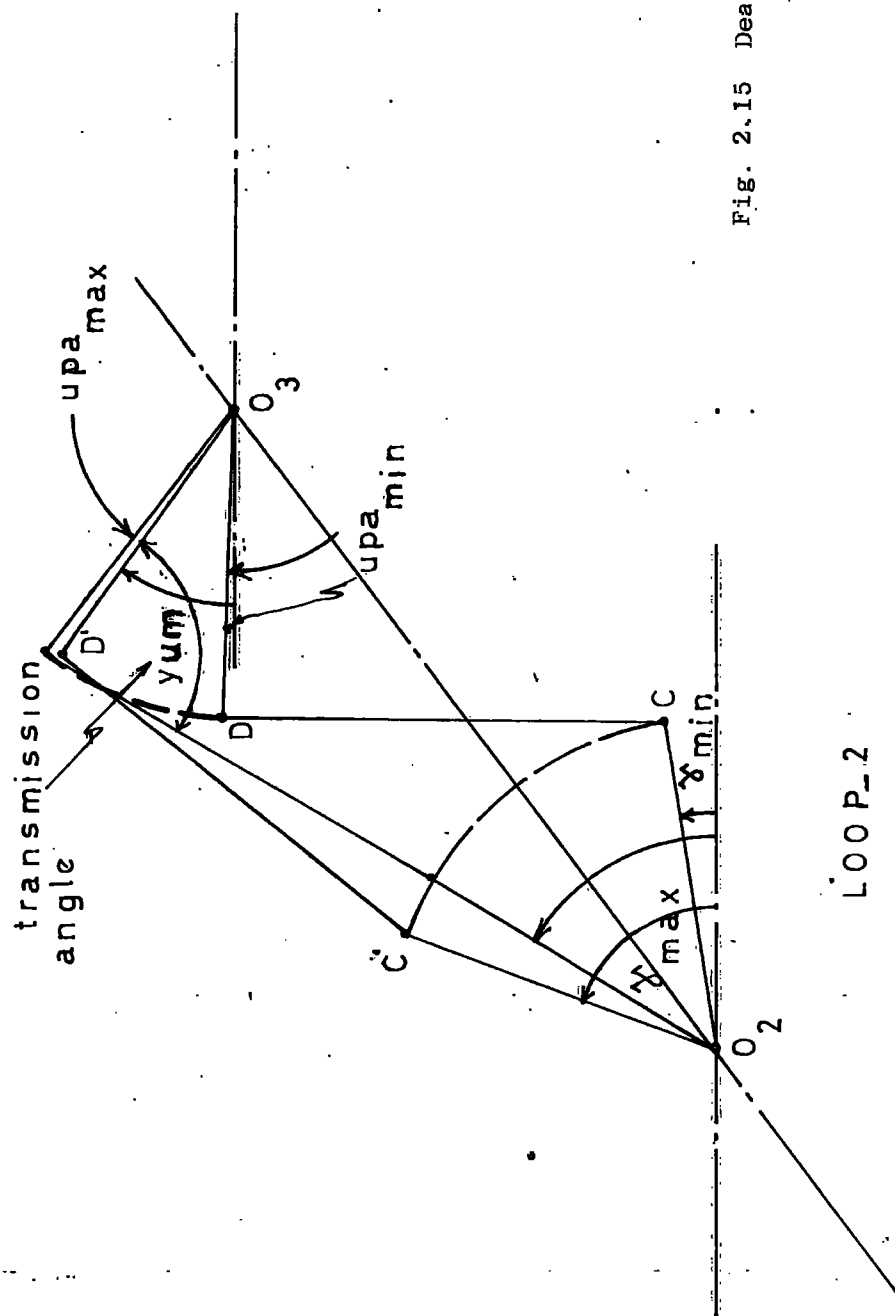


Fig. 2.15 Dead-center positions for links 4 and 6

LOOP_2

$$\frac{\sin \beta_1}{\sin (\beta_1 + \Delta\beta)} = \frac{\sin (\alpha_1 - \beta_1)}{\sin (\alpha_1 + \Delta\alpha - \beta_1 - \Delta\beta)} \quad (2.25)$$

by expanding equation (2.25) and making the following substitutions;

$$\gamma = \alpha_1 + \Delta\alpha - \Delta\beta$$

$$\delta = \alpha_1$$

$$\lambda = \Delta\beta$$

$$p = \cos \delta \cos \lambda - \cos \gamma$$

$$q = \sin \gamma + \cos \delta \sin \lambda - \sin \delta \cos \lambda$$

$$r = -\sin \delta \sin \lambda$$

$$p \tan^2 \beta_1 + q \tan \beta_1 + r = 0 \quad (2.26)$$

$$\text{where } x = \tan \beta_1$$

yield the quadratic equation;

$$p x^2 + qx + r = 0 \quad (2.27)$$

where the initial angle of the input crank is;

$$\beta_1 = \arctan (\pm x)$$

($\pm x$) being the two roots.

There exists only one real root which gives the solution of β_1 . The initial angle of the output lever arm can be calculated from;

$$\alpha_1 = \arctan \left[\frac{a(k+b)}{bf - ah} \right] \quad (2.28)$$

where

$$\xi = -\beta_1 + \Delta\alpha - \Delta\beta$$

$$a = \sin \beta_1$$

$$b = \sin \beta_2$$

$$f = \cos \beta_1$$

$$h = \cos \xi$$

$$k = \sin \xi$$

from equations (2.15) to (2.28), the following values have been calculated for loop 1;

$$\beta_2 \approx 201^\circ$$

$$\beta_1 \approx 25^\circ$$

$$\alpha_1 \approx 90^\circ$$

$$\alpha_2 \approx 151^\circ$$

It is desirable to have the transmission angle deviation as small as possible throughout the range of operation. The minimum permissible transmission angle depends on the magnitude of the transmitted forces, joint friction and manufacturing tolerances. The extreme values of the transmission angles are shown in Fig. (2.14 b). From the cosine law;

$$\mu_{\min} = \arccos \left[\frac{B^2 + C^2 - (D - A)^2}{2 BC} \right] \quad (2.29)$$

$$\mu_{\max} = \arccos \left[\frac{B^2 + C^2 - (D + A)^2}{2 BC} \right] \quad (2.30)$$

and

$$A^2 + D^2 = B^2 + C^2$$

while;

$$C = \frac{\sin \beta_1}{s_1} D \quad \text{or} \quad C = \frac{\sin \beta_2}{s_2} D$$

$$A = \left(\frac{r_1 + r_2}{2} \right) C \quad B = \left(\frac{r_1 - r_2}{2} \right) C$$

where;

$$r_1 = \frac{\sin \alpha_1}{\sin \beta_1} \quad r_2 = \frac{\sin \alpha_2}{\sin \beta_2}$$

$$s_1 = \sin (\alpha_1 - \beta_1)$$

$$s_2 = \sin (\alpha_2 - \beta_2)$$

substituting numerical values into equations (2.29) and (2.30)

$$\mu_{\min} \approx 62^\circ$$

$$\mu_{\min} \approx 134^\circ$$

$$\Delta\mu \approx \mu_{\max} - \mu_{\min} = 72^\circ$$

In order to have a smooth motion throughout the whole range of operation, transmission angle is of the utmost importance. Freudenstein (1) has shown that a good choice of transmission angle also coincides with minimum overtones of the output lever, although a large transmission angle does not necessarily guarantee low fluctuation of torques. The force transmission from the coupler to the output lever is ideally effective when the transmission angle is nearly 90° or deviates as little as possible from 90° . A good discussion of the equations and procedure applied above are given in (1). Dead-centre positions of link 6 and link 4 are shown in Fig. (2.15). Variation of the transmission angle, γ , with crank angle ψ has been presented in Fig. (2.6). Oscillating motion exercised by link 4 is transferred to link 6 via the intermediate link 5.

2.5 Application of Raven's Analysis

As shown in Fig. (2.16) each link is replaced by its position vector. Two separate reference frames have been taken, x - y and x^1 - y^1 corresponding to two separate but dependent loops, loop 1 and loop 2. Writing the summation law for the first loop, gives

$$R_1 + R_2 + R_3 + R_4 = 0 \quad (2.31)$$

Transforming to complex notation,

$$r_1 e^{j\theta_1} + r_2 e^{j\theta_2} + r_3 e^{j\theta_3} + r_4 e^{j\theta_4} = 0 \quad (2.31a)$$

In differentiating eq. (3.31a)

$$j r_2 \dot{\theta}_2 e^{j\theta_2} + j r_3 \dot{\theta}_3 e^{j\theta_3} + j r_4 \dot{\theta}_4 e^{j\theta_4} = 0 \quad (2.32)$$

r_1, r_2, r_3, r_4 and θ_1 are constants.

Letting $\dot{\theta}_2 = \omega_2$, $\dot{\theta}_3 = \omega_3$ and $\dot{\theta}_4 = \omega_4$, gives

$$j r_2 \omega_2 e^{j\theta_2} + j r_3 \omega_3 e^{j\theta_3} + j r_4 \omega_4 e^{j\theta_4} = 0 \quad (2.32a)$$

Equation (2.32a) contains the following quantities;

$$V_A = r_2 \omega_2, \quad V_{BA} = r_3 \omega_3, \quad V_B = r_4 \omega_4,$$

and is the solution of the equation

$$V_B = V_A + V_{BA}$$

After a transformation to complex rectangular notation and a separation of the real and imaginary terms eq. (2.32a) becomes;

$$r_2 \omega_2 \cos\theta_2 + r_3 \omega_3 \cos\theta_3 + r_4 \omega_4 \cos\theta_4 = 0 \quad (2.33a)$$

$$- r_2 \omega_2 \sin\theta_2 - r_3 \omega_3 \sin\theta_3 - r_4 \omega_4 \sin\theta_4 = 0 \quad (2.33b)$$

The unknown quantities in equations (2.33a) and 2.33b) are ω_3 and ω_4 .

Since there are two equations and two unknowns, ω_3 and ω_4 can be determined.

By differentiating equation (2.32a), using a uniform angular velocity of 2, gives

$$j^2 r_2 \omega_2 \dot{\theta}_2 e^{j\theta_2} + j r_3 \dot{\omega}_3 e^{j\theta_3} + j^2 r_3 \omega_3 \dot{\theta}_3 e^{j\theta_3} + j r_4 \dot{\omega}_4 e^{j\theta_4} + j^2 r_4 \omega_4 \dot{\theta}_4 e^{j\theta_4} = 0 \quad (2.34)$$

where $j^2 = -1$ and $\dot{\omega}_n = \alpha_n$

$$-r_2\omega_2^2 e^{j\theta_2} + jr_3\alpha_3 e^{j\theta_3} - r_3\omega_3^2 e^{j\theta_3} + r_4\alpha_4 e^{j\theta_4} - r_4\omega_4^2 e^{j\theta_4} = 0 \quad (2.34a)$$

the terms are identified as;

$$a_a^r = r_2\omega_2^2$$

$$a_{BA}^r = r_3\omega_3^2$$

$$a_B^r = r_4\omega_4^2$$

$$a_{BA}^t = r_3\alpha_3$$

$$a_B^t = r_4\alpha_4$$

$$a_a^t = 0$$

equation 2.34a corresponds to the vector equation,

$$A_B^t + A_B^r = A_A^t + A_A^r + A_{BA}^t + A_{BA}^r$$

corresponding to the acceleration polygon.

using the equation

$$e^{j\theta} = \cos\theta + j \sin\theta$$

equation (2.34a) can be transformed into complex rectangular notation.

Separating the real and imaginary terms gives;

$$-r_2\omega_2^2 \cos\theta_2 - r_3\alpha_3 \sin\theta_3 - r_3\omega_3^2 \cos\theta_3 - r_4\alpha_4 \sin\theta_4 - r_4\omega_4^2 \cos\theta_4 = 0 \quad (2.35a)$$

$$-r_2\omega_2^2 \sin\theta_2 + r_3\alpha_3 \cos\theta_3 - r_3\omega_3^2 \sin\theta_3 + r_4\alpha_4 \cos\theta_4 - r_4\omega_4^2 \sin\theta_4 = 0 \quad (2.35b)$$

the only unknowns in equations (2.35a) and (2.35b) are α_3 and α_4 . The simultaneous solution of these equations utilising determinants yield values of α_3 and α_4 .

Writing the summation law for the second loop gives,

$$R_1^1 + R_2^1 + R_3^1 + R_4^1 = 0$$

Transforming to complex notation

$$r_1^1 e^{j\theta_1^1} + r_2^1 e^{j\theta_2^1} + r_3^1 e^{j\theta_3^1} + r_4^1 e^{j\theta_4^1} = 0 \quad (2.36)$$

where r_1^1 , r_2^1 , r_3^1 , r_4^1 and θ_1^1 are constant

differentiating equation (2.36) gives

$$jr_2^1 \theta_2^1 e^{j\theta_2^1} + jr_3^1 \theta_3^1 e^{j\theta_3^1} + jr_4^1 \theta_4^1 e^{j\theta_4^1} = 0 \quad (2.37)$$

Letting $\theta_2^1 = \omega_4$

$$\theta_3^1 = \omega_5$$

$$\theta_4^1 = \omega_6$$

$$jr_2^1 \omega_4 e^{j\theta_2^1} + jr_3^1 \omega_5 e^{j\theta_3^1} + jr_4^1 \omega_6 e^{j\theta_4^1} = 0 \quad (2.37a)$$

equation (2.37a) contains the following quantities;

$$V_C = r_2^1 \omega_4$$

$$V_{DC} = r_3^1 \omega_5$$

$$V_D = r_4^1 \omega_6$$

and is the solution of the equation

$$V_D = V_C + V_{DC}$$

After a transformation to complex rectangular notation and a separation of the real and imaginary terms eq. (2.37a) becomes;

$$r_2^1 \omega_4 \cos \theta_2^1 + r_3^1 \omega_5 \cos \theta_3^1 + r_4^1 \omega_6 \cos \theta_4^1 = 0 \quad (2.38a)$$

$$- r_2^1 \omega_4 \sin \theta_2^1 - r_3^1 \omega_5 \sin \theta_3^1 - r_4^1 \omega_6 \sin \theta_4^1 = 0 \quad (2.38b)$$

The unknown quantities in equations (2.38a) and (2.38b) are ω_5 and ω_6 .

Solving them simultaneously gives ω_5 and ω_6 . Differentiating equation

(2.37) gives;

$$\begin{aligned} jr_2^1 \theta_2^1 e^{j\theta_2^1} - r_2^1 \theta_2^1 e^{j\theta_2^1} + jr_3^1 \theta_3^1 e^{j\theta_3^1} - r_3^1 \theta_3^1 e^{j\theta_3^1} + jr_4^1 \theta_4^1 e^{j\theta_4^1} \\ - r_4^1 \theta_4^1 e^{j\theta_4^1} = 0 \end{aligned} \quad (2.39)$$

where

$$\theta_2^1 = \alpha_4 \quad \theta_2^1 = \omega_4^2$$

$$\theta_3^1 = \alpha_5 \quad \theta_3^1 = \omega_5^2$$

$$\theta_4^1 = \alpha_6 \quad \theta_4^1 = \omega_6^2$$

$$\begin{aligned} jr_2^1 \alpha_4 e^{j\theta_2^1} - r_2^1 \omega_4^2 e^{j\theta_2^1} + jr_3^1 \alpha_5 e^{j\theta_3^1} - r_3^1 \omega_5^2 e^{j\theta_3^1} + jr_4^1 \alpha_6 e^{j\theta_4^1} \\ - r_4^1 \omega_6^2 e^{j\theta_4^1} = 0 \end{aligned} \quad (2.40)$$

the terms are identified as;

$$a_c^r = r_2^1 \omega_4^2$$

$$a_c^t = r_2^1 \alpha_4$$

$$a_{Dc}^r = r_3^1 \omega_5^2$$

$$a_{Dc}^t = r_3^1 \alpha_5$$

$$a_D^r = r_4^1 \omega_6^2$$

$$a_D^t = r_4^1 \alpha_6$$

equation (2.40) corresponds to the vector equation,

$$A_D^t + A_D^r = A_C^t + A_C^r + A_{DC}^t + A_{DC}^r$$

corresponding to the acceleration polygon using the equation

$$e^{j\theta} = \cos \theta + j \sin \theta$$

equation (2.40) can be transformed into complex rectangular notation.

Separating the real and imaginary terms gives;

$$\begin{aligned} -r_2^1 \alpha_4 \sin \theta_2^1 - r_2^1 \omega_4^2 \cos \theta_2^1 - r_3^1 \alpha_5 \sin \theta_3^1 - r_3^1 \omega_5^2 \cos \theta_3^1 \\ - r_4^1 \alpha_6 \sin \theta_4^1 - r_4^1 \omega_6^2 \cos \theta_4^1 = 0 \end{aligned} \quad (2.41a)$$

$$\begin{aligned} r_2^1 \alpha_4 \cos \theta_2^1 - r_2^1 \omega_4^2 \sin \theta_2^1 + r_3^1 \alpha_5 \cos \theta_3^1 - r_3^1 \omega_5^2 \sin \theta_3^1 \\ + r_4^1 \alpha_6 \cos \theta_4^1 - r_4^1 \omega_6^2 \sin \theta_4^1 = 0 \end{aligned} \quad (2.41b)$$

The only unknowns in equations (2.41a) and (2.41b) are α_5 and α_6 . A simultaneous solution of these equations yield values of α_5 and α_6 .

2.6 Graphical Approach

The velocity and acceleration polygons have been solved graphically for a set of different crank positions and are presented in(A2).

2.7 Energy variation of the system

The total kinetic energy of the system at any instant is composed of the kinetic energy of translation about the mass centres of the links and the kinetic energy of rotation about the mass centres of the links and shafts. This can be expressed as in the following form;

$$\begin{aligned} \text{Total kinetic energy} &= \frac{1}{2} [I_{O1}\omega_2^2 + I_3\omega_3^2 + I_{O2}\omega_4^2 + I_4\omega_4^2 + I_5\omega_5^2 + I_6\omega_6^2 + I_{O3}\omega_6^2] \\ &+ \frac{1}{2} [m_2V_{g2}^2 + m_3V_{g3}^2 + m_4V_{g4}^2 + m_5V_{g5}^2 + m_6V_{g6}^2] \end{aligned} \quad (2.42)$$

where $V_{g1 \rightarrow 6}$ = linear velocities of the mass centres of the corresponding links

in equation (2.42) $I_{O1}\omega_2^2$ and $m_2V_{g2}^2$ are constants (since $\alpha_2 = 0$). The variation of the kinetic energies due to rotation of shafts O_2 , O_3 , link 4 and link 3 with the crank angle as shown in Fig. 2.17. The total kinetic energy due to translation is negligible in comparison with the kinetic energy due to rotation. Therefore equation 2.42 can be reduced to;

$$\text{Total kinetic energy} \approx \frac{1}{2} [I_3\omega_3^2 + I_{O2}\omega_4^2 + I_4\omega_4^2 + I_5\omega_5^2 + I_6\omega_6^2 + I_{O3}\omega_6^2] + C \quad (2.43)$$

where $C = \frac{1}{2} I_{O1}\omega_2^2$

variation of the total kinetic energy (excluding C) with the crank angle is shown in Fig. 2.18

↑ N m $(1/2)I\omega^2$
kinetic energy variation

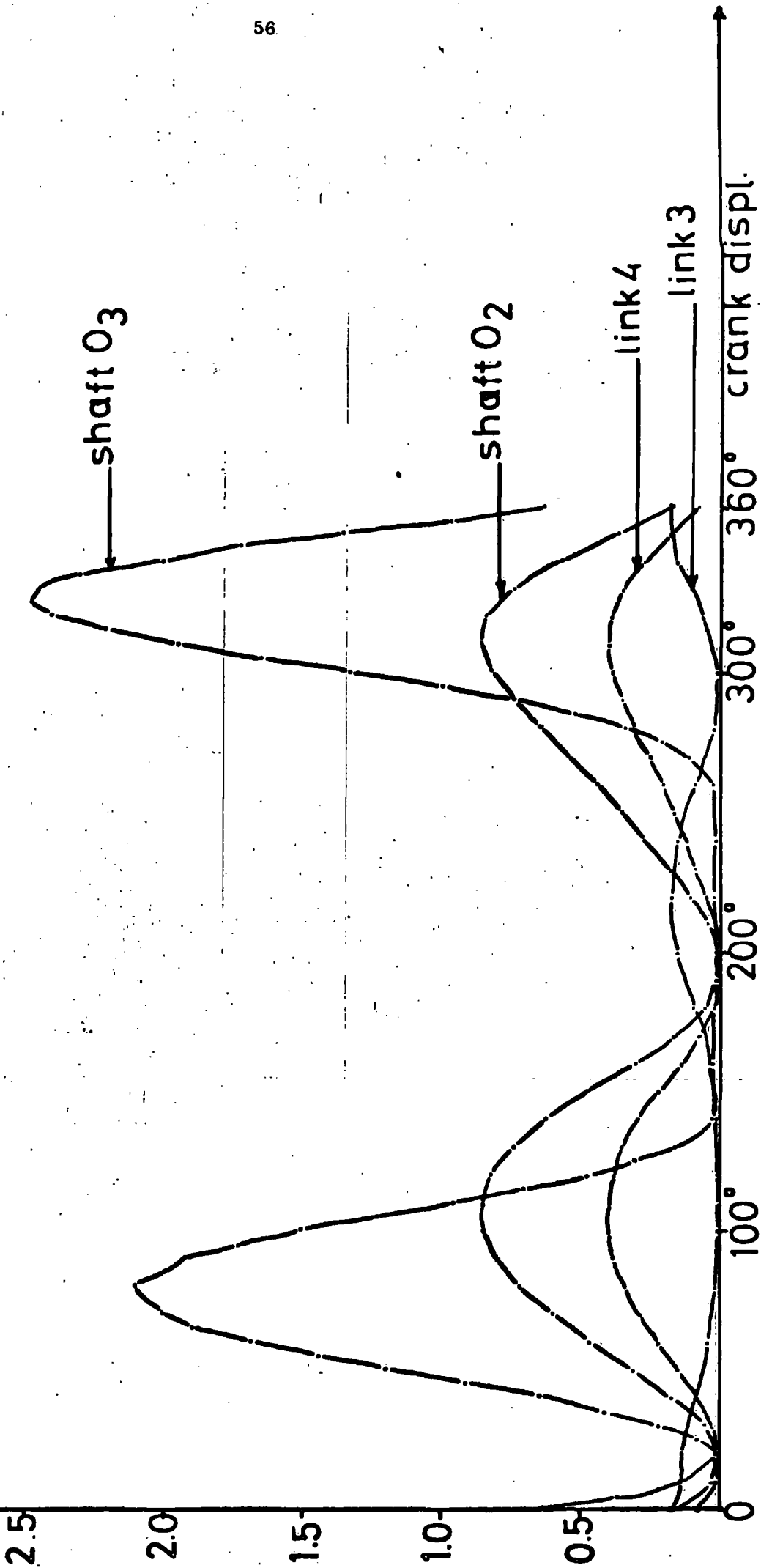
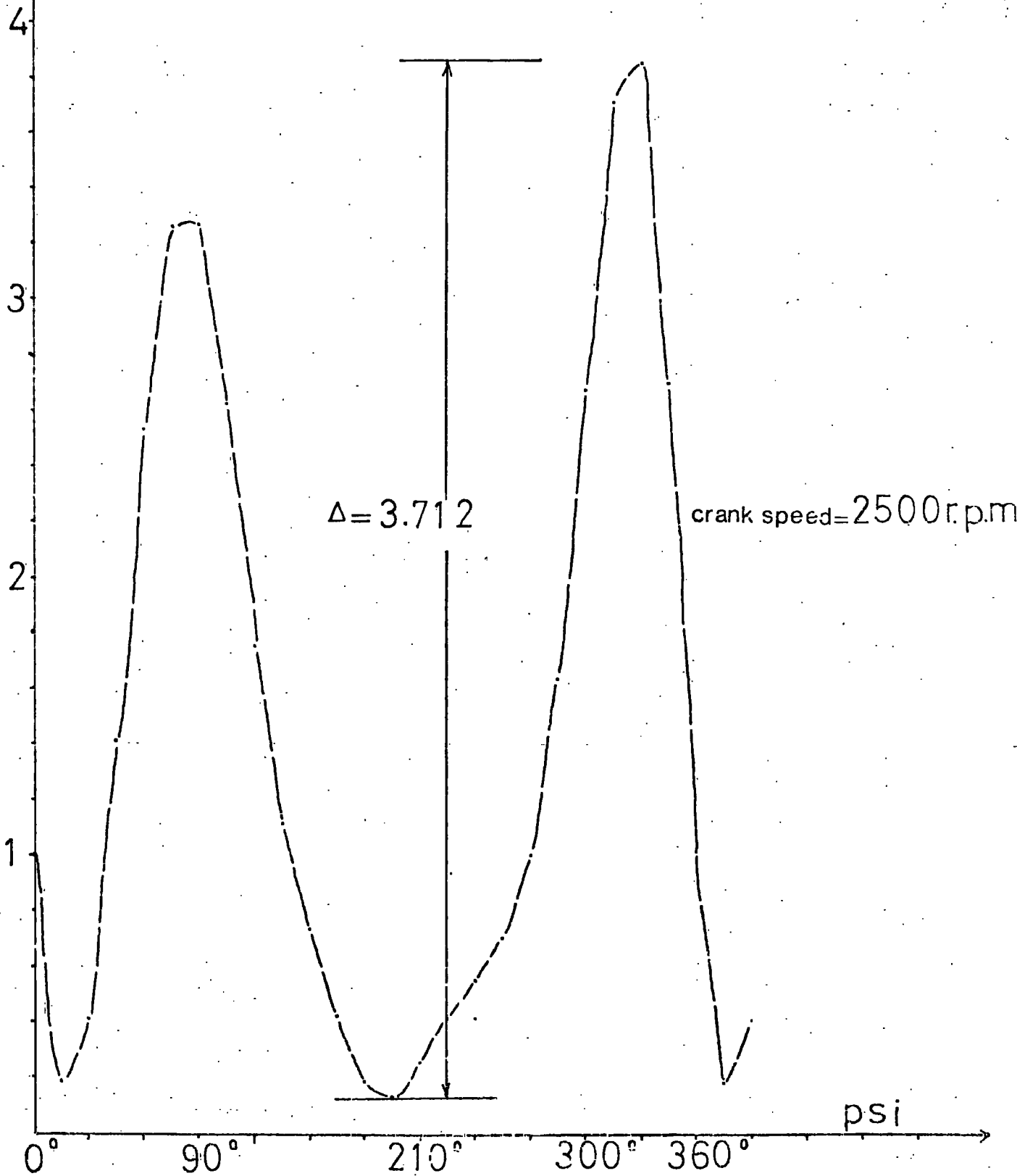


Fig. 2.17 Variation of kinetic energies of shafts O₃, O₂ and links 3 and 4 with the crank angle. Crank speed = 2500 r.p.m.

N.m

Fig. 2.18 Variation of the kinetic energy with the crank angle



Chapter 3 Force and Stress Analysis

3.1 Kinetostatic Approach

The motion of the mechanism is completely specified and the purpose is to compute the bearing reactions, shaking forces, shaking moments as well as the forces and the torque required to produce the motion. The size, shape and material of each link are known. The inertia forces are taken as if they acted at a point on the links, although they are distributed along the links and are not concentrated at one point. In the following analysis the concern is only with the forces at points where the links are paired with other links. These forces are treated as external forces on the links. The shapes of the links are assumed to be rigid and the pin joints are considered to be frictionless. The inertia effects of the individual links, in comparison with the inertia effects of the shafts through O_2 and O_3 are reasonably negligible and this aspect of the dynamic analysis has been shown in further steps. However for a detailed dynamic analysis of the system, which is beyond the scope of the objective, the distribution of the inertia forces along the link can be important. In most advanced engineering cases the stresses due to inertia forces are determined by breaking the link into equal length sections. The inertia force for each section is determined from the mass of the section and the acceleration of the midpoint of the section which represents the distribution of the inertia forces along the link (21). In cases where the links are not of uniform cross section the accuracy of this approximation depends upon the number of sections that the link is broken into. By increasing the number of sections a greater accuracy can be achieved.

A solution to the dynamic force analysis of a four-bar planar mechanism has recently been presented (4), as a set of algebraic equations. The forces along the links 3 and 5 cause pure normal stresses, and the normal forces cause bending stresses. In the actual case the normal stresses vary along the links because of the inertia forces. The system has a single degree of freedom, the angular positions of links 3, 4, 5 and 6, given by $\phi_3(t) = \beta$, $\phi_4(t) = \gamma + 75^\circ$, $\phi_5(t) = x\lambda$, and $\phi_6(t) = 360^\circ - \text{upa}$, are functions of the angular position $\phi_2(t) = \psi$, and the length of the links. The link lengths are denoted by l_i , $i = 2, 3, 4, 5$ and 6 , and each of the moving links has mass m_i , $i = 2, 3, 4, 5, 6$ and a moment of inertia I_i with respect to the centre of mass. The locations of the centres of mass of the members are defined by parameters l_i and θ_i . The bearing reaction F_{ij} is the force of member i on member j . The D'Alembert couple on link i is;

$$C_i = - I_i \ddot{\phi}_i$$

The x and y components of the D'Alembert force being;

$$D_{ix} = - m_i a_{ix}$$

and

$$D_{iy} = - m_i a_{iy}$$

where a_{ix} and a_{iy} are the corresponding acceleration components of the centre of mass of member i . The motion of the mechanism is known and the inertia loading on the system is defined. T_2 is the external torque on the input link 2, required to produce the prescribed motion. The dynamic

equilibrium equations for the five moving links yield the following system of fifteen linear algebraic equations:

$$D_{2x} + F_{12x} - F_{23x} = 0 \dots\dots\dots (3.1)$$

$$D_{2y} + F_{12y} - F_{23y} = 0 \dots\dots\dots (3.2)$$

$$D_{3x} + F_{23x} - F_{34x} = 0 \dots\dots\dots (3.3)$$

$$D_{3y} + F_{23y} - F_{34y} = 0 \dots\dots\dots (3.4)$$

$$D_{4x} + F_{34x} + F_{14x} - F_{45x} = 0 \dots\dots\dots (3.5)$$

$$D_{4y} + F_{34y} + F_{14y} - F_{45y} = 0 \dots\dots\dots (3.6)$$

$$D_{5x} + F_{45x} - F_{56x} = 0 \dots\dots\dots (3.7)$$

$$D_{5y} + F_{45y} - F_{56y} = 0 \dots\dots\dots (3.8)$$

$$D_{6x} + F_{56x} - F_{67x} = 0 \dots\dots\dots (3.9)$$

$$D_{6y} + F_{56y} - F_{67y} = 0 \dots\dots\dots (3.10)$$

$$C_2 = - I_2 \ddot{\theta}_2$$

$$C'_2 = - I_{O1} \ddot{\theta}_2$$

$$C''_2 = - (I_2 + m_2 r_2^2 + I_{O1}) \ddot{\theta}_2$$

where

I_{O1} = Moment of inertia of the driving shaft through O_1

$$C_2'' - D_{2x} r_2 \sin \theta_2 + D_{2y} r_2 \cos \theta_2 + T_2 + F_{23x} l_2 \sin \theta_2 - F_{23y} l_2 \cos \theta_2 = 0 \dots\dots (3.11)$$

$$C_3 = - I_3 \ddot{\theta}_3$$

$$C_3 - D_{3x} r_3 \sin \theta_3 + D_{3y} r_3 \cos \theta_3 + F_{34x} l_3 \sin \theta_3 - F_{34y} l_3 \cos \theta_3 = 0 \dots\dots\dots (3.12)$$

$$C_4 = - I_4 \ddot{\theta}_4$$

$$C'_4 = - I_{O2} \ddot{\theta}_4$$

where

I_{O2} = Moment of inertia of the shaft through O_2

$$C_4'' = - (I_4 + m_4 r_4^2 + I_{O2}) \ddot{\theta}_4$$

$$\begin{aligned}
C_4'' &= D_{4x} r_4 \sin(\phi_4 + \theta_4) + D_{4y} r_4 \cos(\phi_4 + \theta_4) \\
&\quad - F_{34x} l_4 \sin \phi_4 + F_{34y} l_4 \cos \phi_4 - F_{45x} l_4 \sin \phi_4^1 \\
&\quad + F_{45y} l_4 \cos \phi_4^1 = 0 \dots \dots \dots (3.13)
\end{aligned}$$

$$C_5 = -I_5 \ddot{\phi}_5$$

$$\begin{aligned}
C_5 &= D_{5x} r_5 \sin \phi_5 + D_{5y} r_5 \cos \phi_5 + F_{56x} l_5 \sin \phi_5 \\
&\quad - F_{56y} l_5 \cos \phi_5 = 0 \dots \dots \dots (3.14)
\end{aligned}$$

$$C_6 = -I_6 \ddot{\phi}_6$$

$$C_6' = -I_{O3} \ddot{\phi}_6$$

where

I_{O3} = Moment of inertia of the shaft through O_3

$$C_6'' = -(I_6 + m_6 r_6^2 + I_{O3}) \ddot{\phi}_6$$

$$\begin{aligned}
C_6'' &= D_{6x} r_6 \sin \phi_6 - D_{6y} r_6 \cos \phi_6 - F_{65x} l_6 \sin \phi_6 \\
&\quad + F_{65y} l_6 \cos \phi_6 = 0 \dots \dots \dots
\end{aligned}$$

(dot denotes differentiation with respect to time t)

The configuration of the mechanism and the free-body diagrams are shown in Fig.(3.1-3.2) for $\phi_2(t) = \psi = 50^\circ$. Relations of the form

$F_{43x} = -F_{34x}$, etc., have been employed in the formulation of these

equations. The shaking force F_s , is the resultant force on the frame.

The x and y components of the shaking force are;

$$\begin{aligned}
F_{sx} &= F_{21x} + F_{41x} + F_{67x} = -F_{12x} - F_{14x} - F_{76x} \\
&= D_{2x} + D_{3x} + D_{4x} + D_{5x} + D_{6x} \dots \dots \dots (3.16)
\end{aligned}$$

and

$$\begin{aligned}
F_{sy} &= F_{21y} + F_{41y} + F_{67y} = -F_{12y} - F_{14y} - F_{76y} = \\
&= D_{2y} + D_{3y} + D_{4y} + D_{5y} + D_{6y} \dots \dots \dots (3.17)
\end{aligned}$$

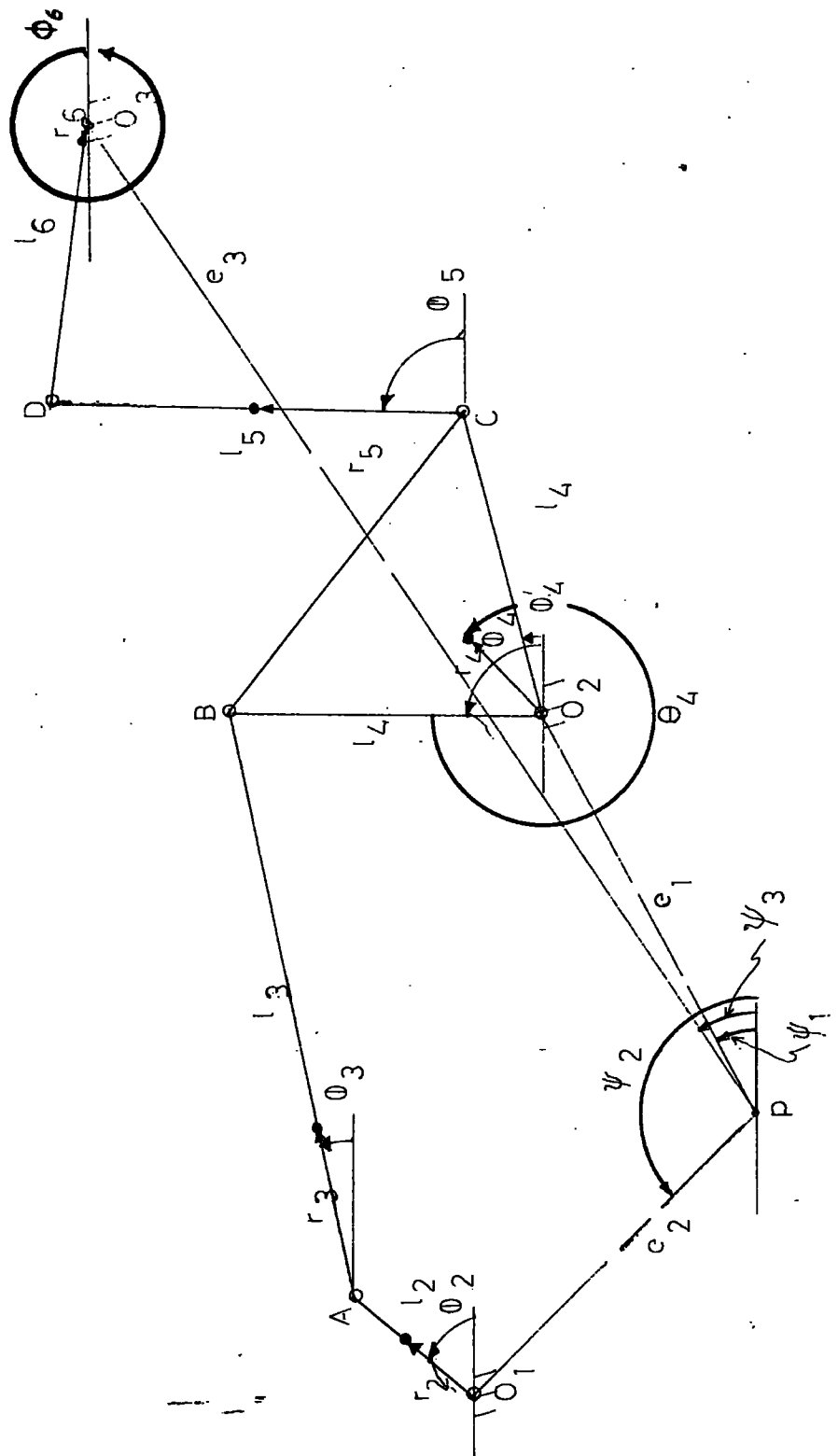


FIG. (3.1)

The shaking moment M_{sp} about an arbitrary point 'p' on the frame Fig. is

$$\begin{aligned}
 M_{sp} = & -T_2 - F_{41x} e_1 \sin \psi_1 + F_{41y} e_1 \cos \psi_1 \\
 & - F_{21x} e_2 \sin \psi_2 + F_{21y} e_2 \cos \psi_2 - F_{67x} e_3 \sin \psi_3 \\
 & + F_{67y} e_3 \cos \psi_3 \dots\dots\dots (3.18)
 \end{aligned}$$

The effect of gravitational pull on the links has been neglected. The compressive and/or tensile forces acting on the links can be determined by resolving the forces acting on the links along themselves.

3.2 - Application of Virtual Work Method to the Mechanism

Energy methods can be used to short-cut the previous kinetostatic approach. The following solution, utilising the method of virtual work introduces greatest timesaving to the analysis. The main advantage of the method is that, it eliminates the link-to-link treatment, and permits an examination of the whole system at one time. A good discussion of this method is given in (8), and (9).

For any mechanism composed of n members, the method of virtual work is written:

$$T_n \cdot \Omega_n + F_n \cdot V_n + (-m_n A_{Gn} \cdot V_{Gn}) + (-I_n \alpha_n \Omega_n) = 0 \dots \dots \dots (3.19)$$

which can normally be solved for one quantity. Since the terms are vector quantities, the solution includes both the magnitude and direction of the unknown. Its major disadvantage is that since eq 3.19 contains only the applied forces and torques, it can not be used to solve for internal forces or the reactions between members of the mechanism. Formulation of eq. 3.19 utilizes an imaginary small displacement of the mechanism, being consistent with the constraints of the mechanism. The work done by the virtual displacements is referred to as virtual work and if the system is in static equilibrium under the action of the applied forces and torques then the work done with a virtual displacement is zero. Application of eq. 3.19 to the mechanism yields.

$$T_2 \Omega_2 + (-m_2 a_2 \cdot v_2) + (-m_3 a_3 \cdot v_3) + (-m_4 a_4 \cdot v_4) + (-m_5 a_5 \cdot v_5) + (-m_6 a_6 \cdot v_6) + (-I_3 \alpha_3 \Omega_3) + (-I_5 \alpha_5 \Omega_5) + [-(I_4 + m_4 r_4^2) \alpha_4 \Omega_4] + [-(I_6 + m_6 r_6^2) + I_{O3}] \alpha_6 \Omega_6] = 0 \dots\dots\dots (3.20)$$

$$F_n V_n = 0$$

Substituting the appropriate values for 'ψ' equation (3.20) is used to calculate the external torque T₂. In the formulation of equation (3.19) the gravitational effects are neglected. A modified form of this equation taking account of gravitational effects is given in (8)

3.3 The Power equation

The power equation for the system can be written as;

$$T_2 \omega_2 - T_6 \omega_6 = T\omega \dots\dots\dots (3.21)$$

where

T₂ = external torque applied on input link 2

T₆ = the torque transmitted by DO₃

Tω = power necessary to accelerate or to decelerate the system

ω = angular velocity of the shaft to which torque T is referred

Equation (3.21) corresponds to the dynamical relation:

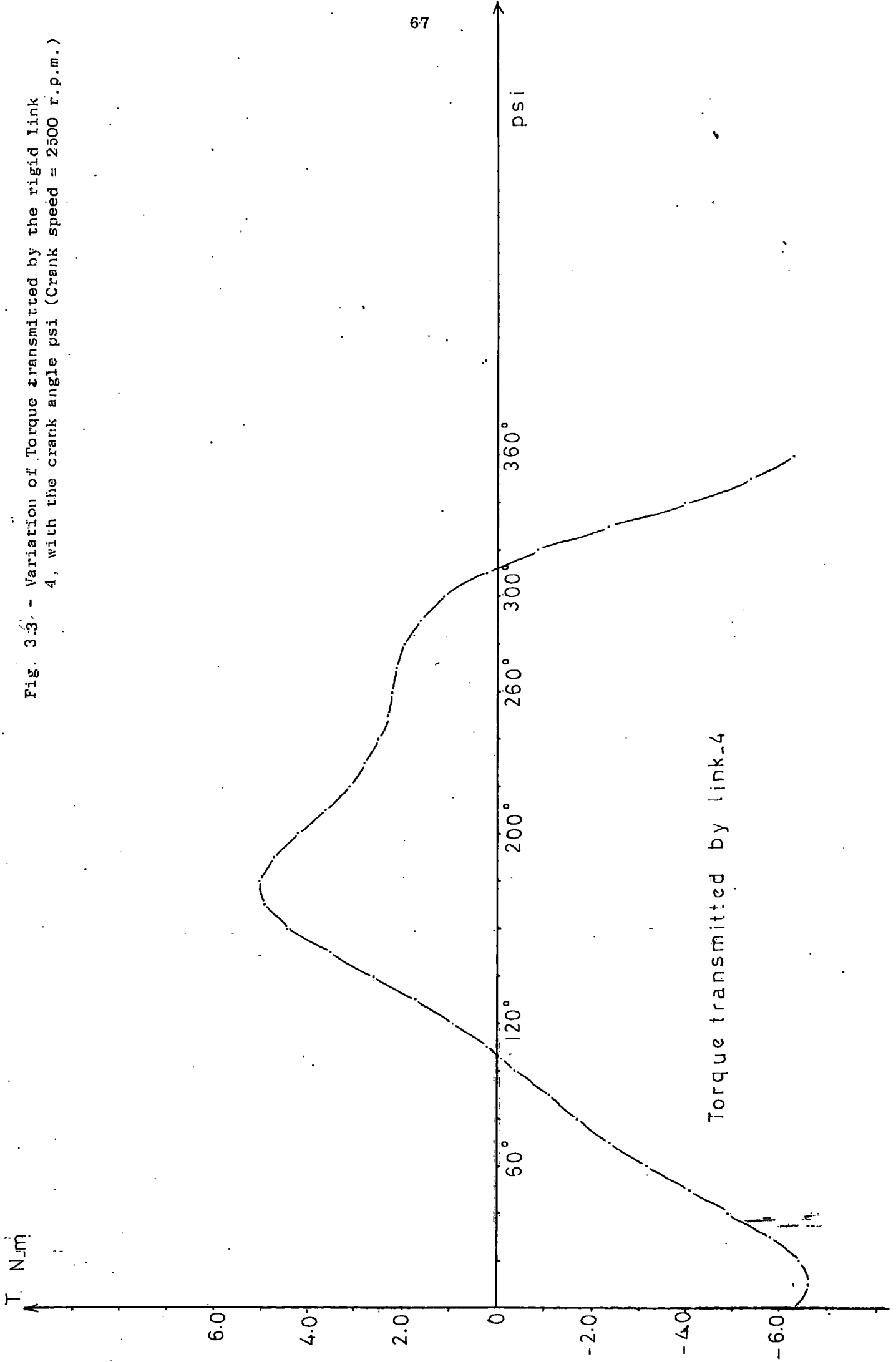
Rate of work done by external forces = Rate of change of kinetic energy of the system

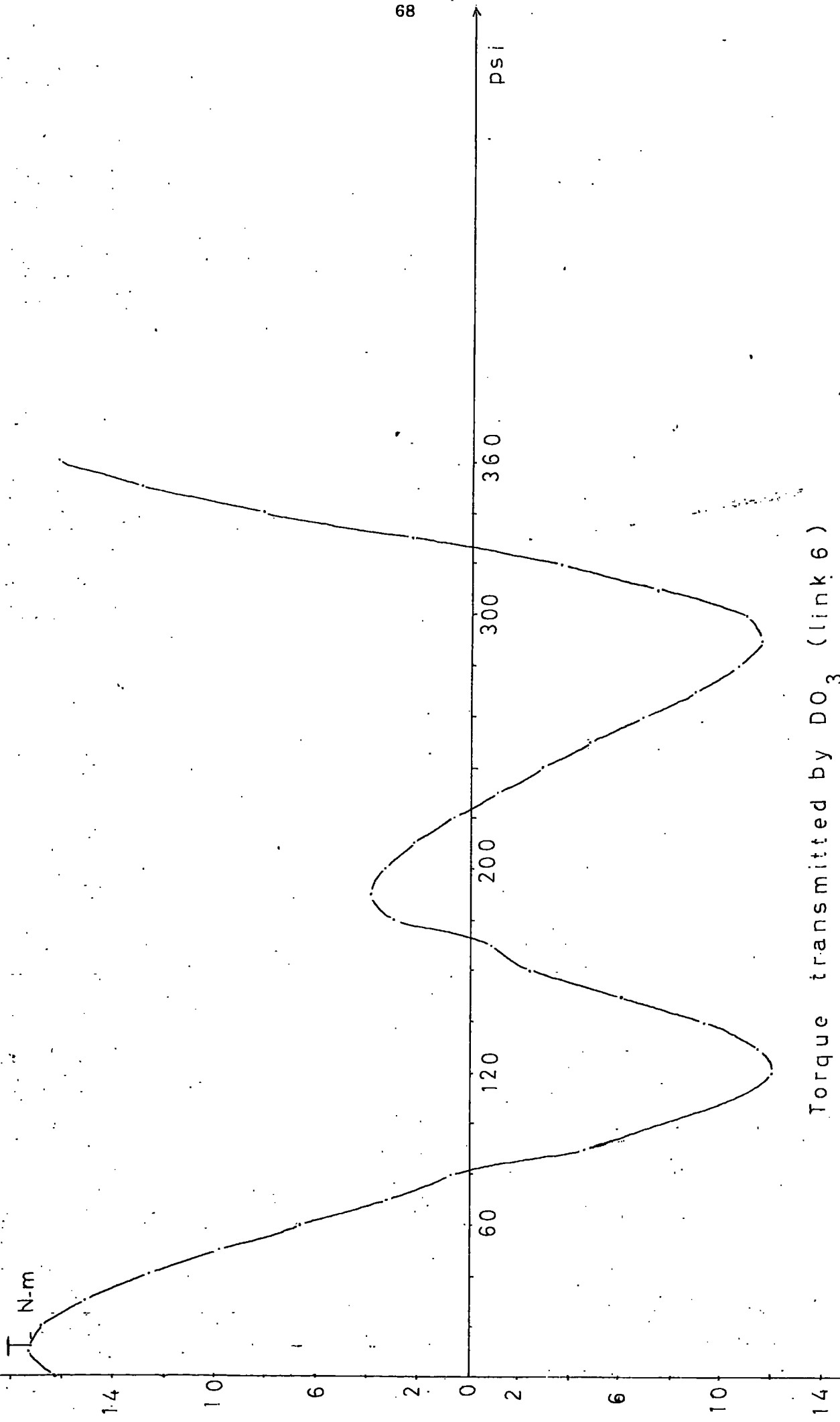
or alternatively:

Rate of work done by external forces = Rate of work done by effective forces

The variation of the torques transmitted by rigid link 4 and DO₃ are shown in Fig.(3.3) and in Fig.(3.4). The corresponding transmitted power is shown in Fig (3.5)

Fig. 3.3 - Variation of Torque transmitted by the rigid link 4, with the crank angle psi (Crank speed = 2500 r.p.m.)





Torque transmitted by DO₃ (link 6)

Fig. 3.4 - Variation of the Torque transmitted by link 6 (DO₃) with the crank angle psi (Crank speed = 2500 r.p.m.)

3.4 Graphical Approach

At any instant the motion of any individual link is equivalent to the rotation of the link as a whole about a fixed point in space. By determining instantaneous centres of rotation, (as shown in Figure (3.6) graphical force analysis), it is possible to determine the dynamic forces acting on the mechanism. A detailed analysis of this procedure is presented in (21), (14), (12), (13) and (3).

Referring to Fig.(3.6), $O_1ab O_2$ and $O_2 cd O_3$ can be treated as two separate but dependent four-bar chains, I_1 and I_2 are the locations of the instantaneous centres of rotation. Both the linear velocity of the mass centres and the angular velocity of rotation vary from instant to instant. The line of action of the force applied to the links does not pass through their mass centres. The individual links are constrained to move in a definite way by the adjacent links to which they are connected, and the resultant of all the forces applied through those connections is equal to the force required to accelerate the link, the effective force R_1 . The magnitude of the effective force is replaced by another force equal to $-m_1 a_{cgl}$, displaced from the mass centre a distance h_1 . This fictitious force replaces the combined effects of the inertia torque and the inertia force. ab is a link with pins at A and B, constrained to move along the paths shown. Since the weight of the links is small in comparison to the other forces which act on the link, the effect of gravity is ignored as previously. The magnitude and lines of action of R_3 is determined. A similar procedure is applied to link cd . The force F_A which is applied to the link AB at pin A, by the crank arm O_1A will have a component F_a^1 , tangential to the path of A and also a component F_a^{11} , perpendicular to the path of A. F_a^1 does the useful work on the link, F_a^{11} constrains the pin A to follow the given path. This assumption is similarly valid for the forces acting at b, c and d. By calculating the

graphical force analysis

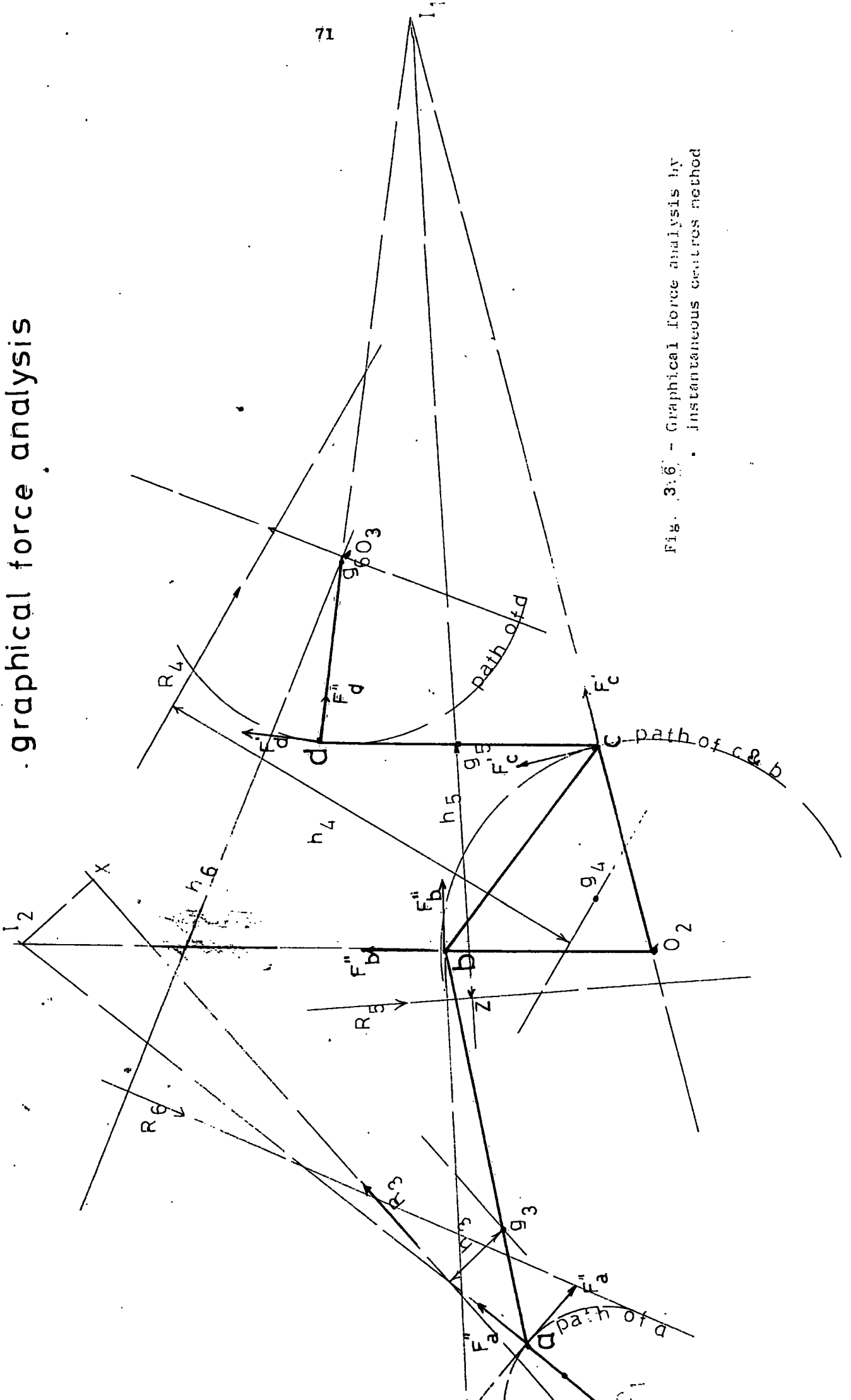


Fig. 3:6 - Graphical force analysis by instantaneous centres method

component in the tangential direction, the component in the normal direction and the two other components acting on the next pin are found from the equilibrium conditions of the link, namely, the vector sum of all the forces which act on the link being zero, and the algebraic sum of the moments of the forces about any point in their plane being zero. Components of F_a , F_b , F_c and F_d , normal to the paths of a, b, c and d are known. For link ab, the moments are taken about I_2 , the point of intersection of the lines of action of F_b^{11} and F_a^{11} , and for link cd, about I_1 , the intersection of the lines of action of F_c^{11} and F_d^{11} . The equations for F_b^1 and F_d^1 are then

$$F_b^1 = \frac{-F_a^{11}(ax) - R_3(I_2x)}{(bI_2)} \dots\dots\dots (3.22)$$

$$F_d^1 = \frac{R_5(zI) - F_c^{11}(cI_1)}{(dI_1)} \dots\dots\dots (3.23)$$

where

$$R_3 = m_3 a_{g3} \qquad h_3 = \frac{I_3 \alpha_3}{-R_3}$$

$$R_4 = -m_4 a_{g4} \qquad h_4 = \frac{I_4 \alpha_4}{-R_4}$$

$$R_5 = -m_5 a_{g5} \qquad h_5 = \frac{I_5 \alpha_5}{-R_5}$$

$$R_6 = -m_6 a_{g6} \qquad h_6 = \frac{I_6 \alpha_6}{-R_6}$$

The moment of inertia values for the shafts are included in the above expressions as appropriately. After the magnitudes of F_a^{11} , F_b^{11} , F_c^{11} and F_d^{11} are obtained by drawing the force polygon. The torque which must be applied by the crank arm O_1a , to the whole system, in order to overcome the combined effects of inertia is given by the product $F_a^1 \cdot O_1a$.

As in the earlier sections, the crank is assumed to rotate at constant angular velocity ω_2 .

3.5 Simplified Force Analysis

As mentioned in section 3.1 neglecting the inertia effects of links 3, 4, 5 and 6, which are relatively small in comparison with the inertia effects of shafts through O_2 and O_3 , the force analysis can be simplified to a large extent. From Fig.(3.7), the force applied to link 5 by link 6, F_5 , is determined by taking moment about O_3

$$T_6 = -I_{O3}\alpha_6 = F_5 k_1 \dots\dots\dots (3.24)$$

where k_1 = Moment arm

from equation (3.24)

$$F_5 = \frac{-I_{O3}\alpha_6}{k_1}$$

Repeating the same procedure for O_2

$$-I_{O2}\alpha_4 + F_5 k_2 + F_3 k_3 = 0 \dots\dots\dots (3.25)$$

$$F_5 k_2 = -F_3 k_3$$

$$F_3 = \frac{F_5 k_2}{k_3}$$

from equation (3.25)

$$F_3 = \frac{I_{O2}\alpha_4 - F_5 k_2}{k_3}$$

Torque required to drive the mechanism is then,

$$T_2 = F_3 k_4$$

Although the analysis presented above does not give very accurate results, it offers a quick and reasonable method to determine the axial loading range on links 3 and 5.

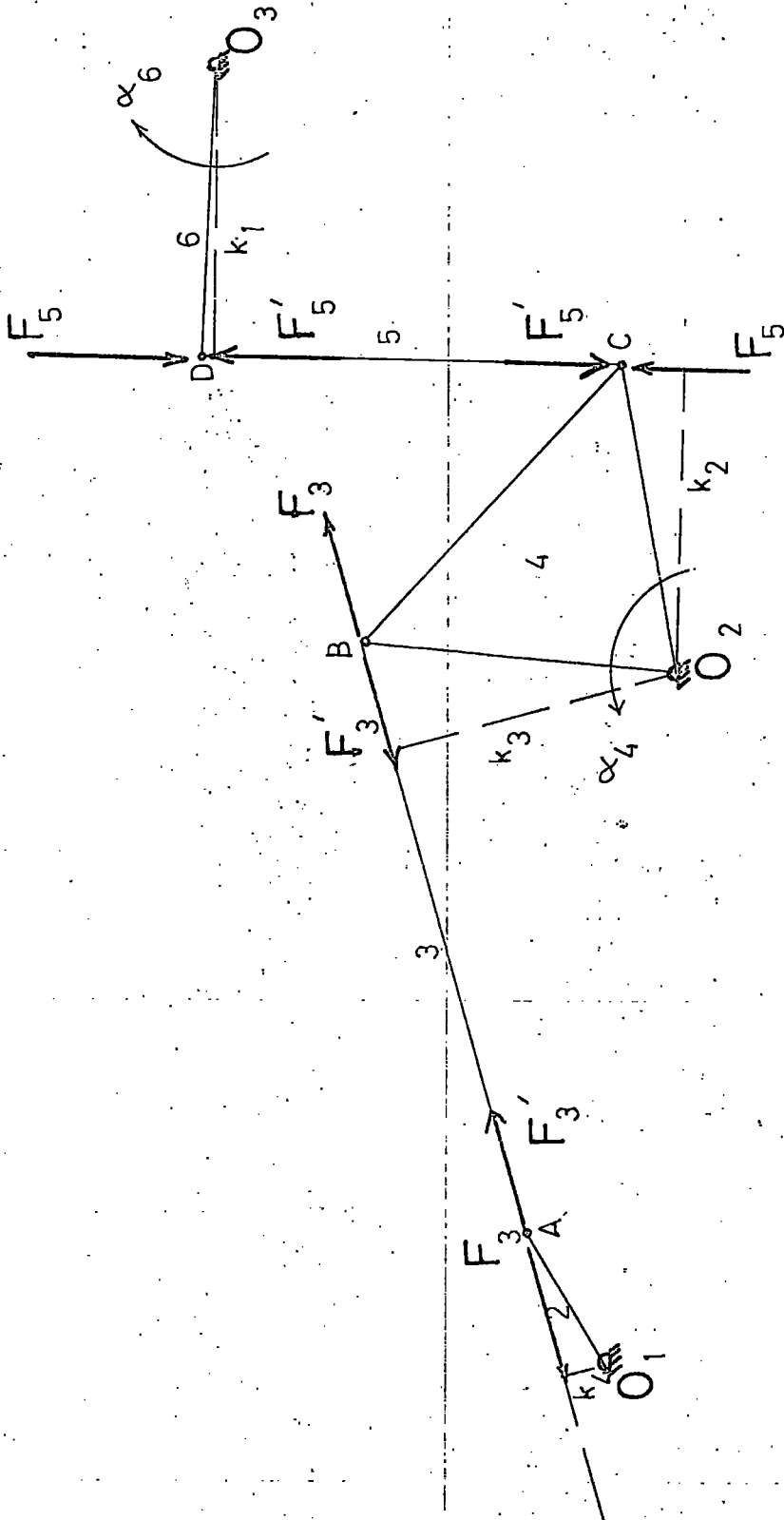


Fig. 3.7

3.6 Stress Analysis

The axial stress variation for links 3 and 5 are determined from;

$$\sigma_{5AX} = \frac{F_{5AX}}{A_1} \text{ and } \sigma_{3AX} = \frac{F_{3AX}}{A_2}$$

From Fig. (3.9) and (3.10)

$$A_1 = \text{cross sectional area - link 3 - BB} = 10^{-5} \times 14.95 \text{ m}^2$$

$$A_2 = \text{cross sectional area - link 5 - CC} = 10^{-5} \times 6.32 \text{ m}^2$$

The links do not have a uniform cross-sectional area thus axial stress varies accordingly. Stresses are proportional with the square of the crank speed. Variation of axial stresses for A_1 and A_2 are shown in Fig. (3.7) for a complete cycle, at a crank speed of 2500 r.p.m.

The peak to peak (maximum to minimum) stress values are referred to as stress range, and the variation of this range with respect to the square of the crank-arm angular velocity is given in Fig. (3.8). Plane bending stress values for the same cross-sections of links 3 and 5 can be calculated from

$$\sigma_{5b} = \frac{M_5 y_{c5}}{I_{c5}} = \frac{F_{5b} (l_5/2) y_{c5}}{I_{c5}} \dots\dots\dots (3.26)$$

where y_{c5} = distance from the neutral axial-cross-section CC

I_{c5} = Moment of inertia of the cross-section CC

and

$$\sigma_{3b} = \frac{M_3 y_{b3}}{I_{B3}} = \frac{F_{3b} (l_3/2) y_{b3}}{I_{B3}} \dots\dots\dots (3.27)$$

where y_{b3} = distance from the neutral axis-cross-section BB

I_{B3} = Moment of inertia of the cross-section BB

and F_{5b} = force component acting normal to link 5

F_{3b} = force component acting normal to link 3

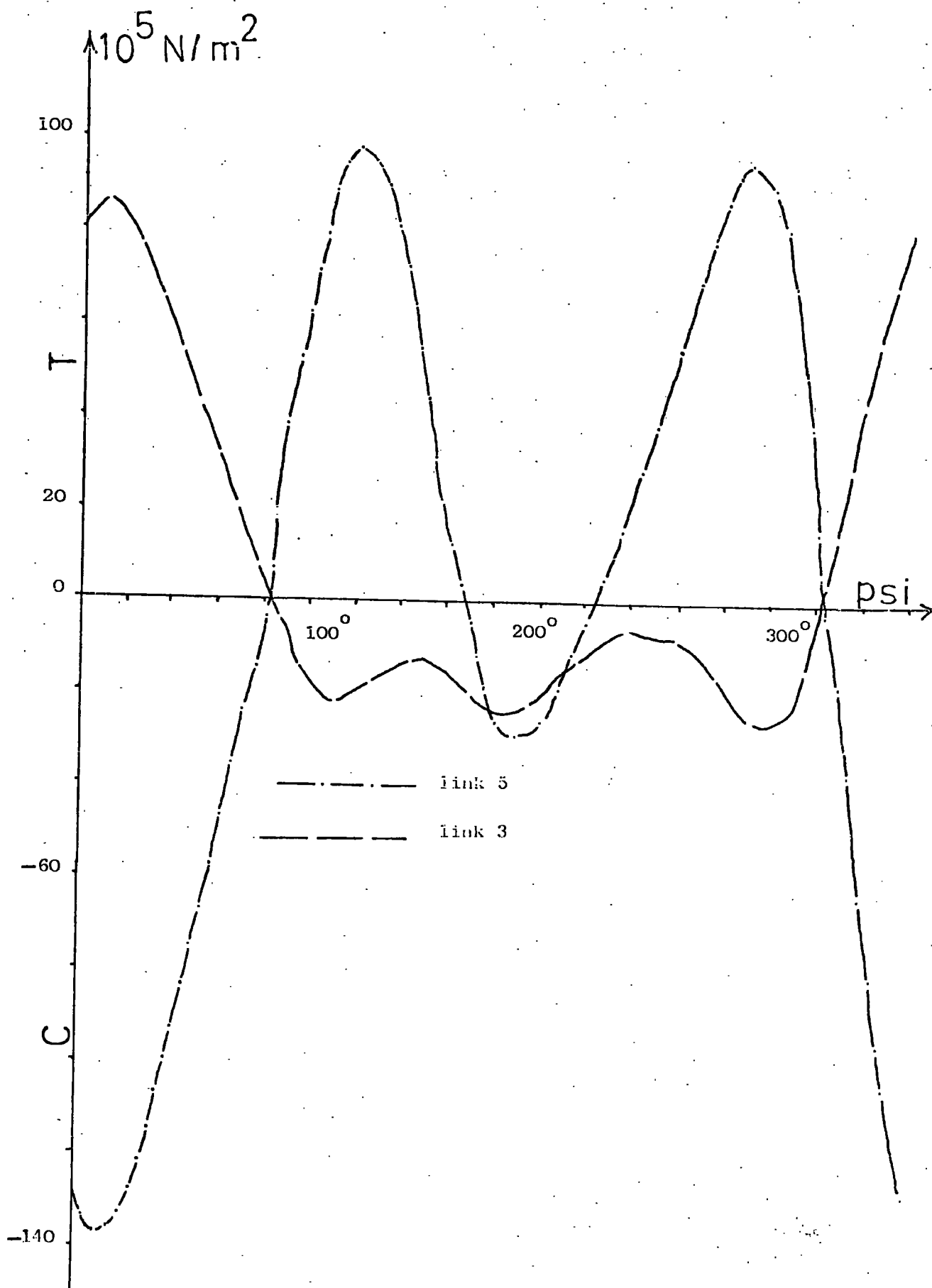


Fig. 3.7. Variation of axial stresses in links 3 and 5 with the crank angle (crank speed = 2500 r.p.m.)

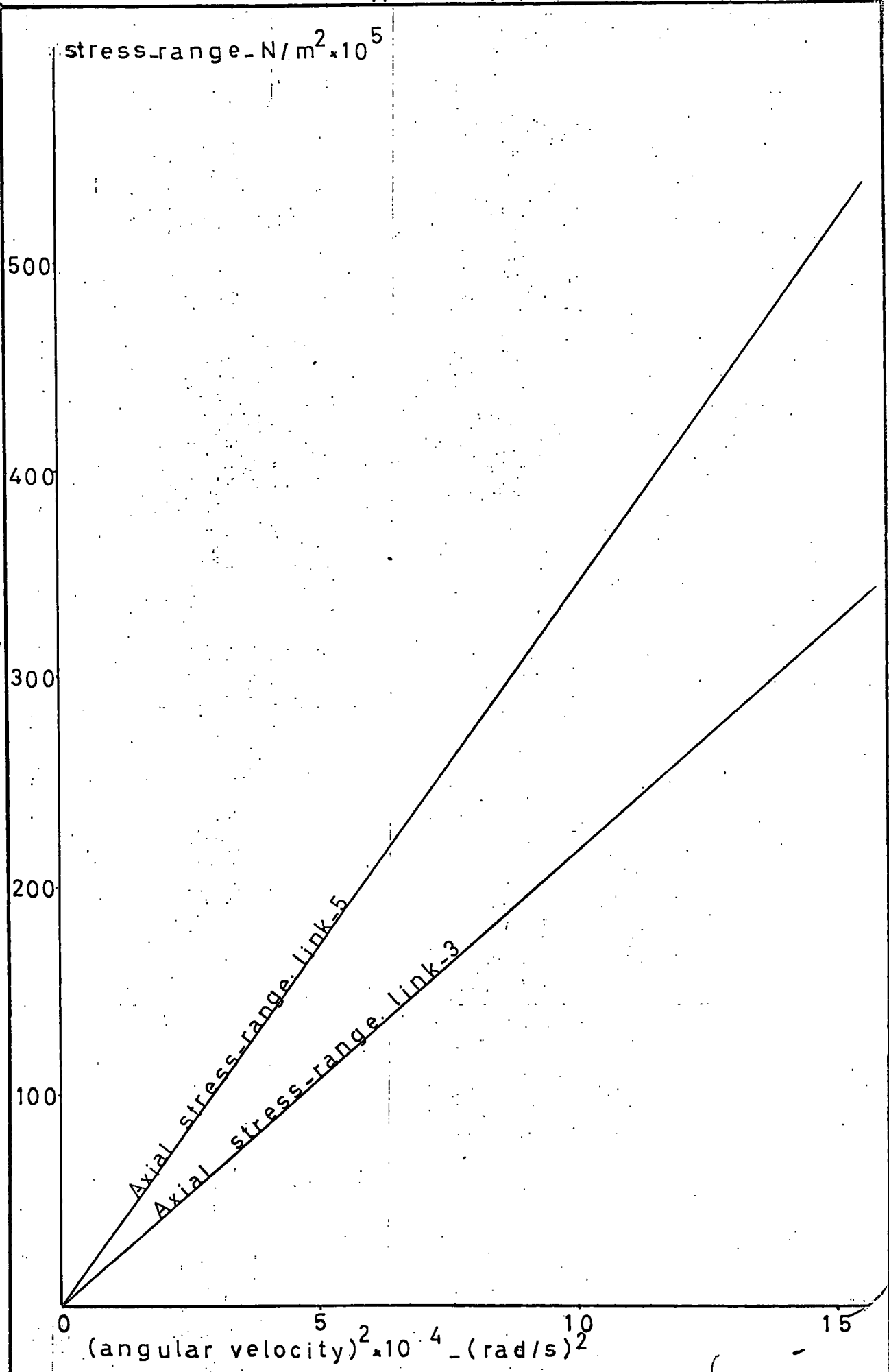


Fig. 3.8 - Theoretical variation of axial stress - range by the square of crank-speed

The links are treated to be beams of non-uniform cross-section, and magnitude of stress and deflection is assumed to be directly proportional to the load.

Resultant stress over a cross-section is then given by:

$$\sigma = \frac{F_{nax}}{A_n} \pm \frac{My_{cn}}{I_{cn}} \dots\dots\dots (3.28)$$

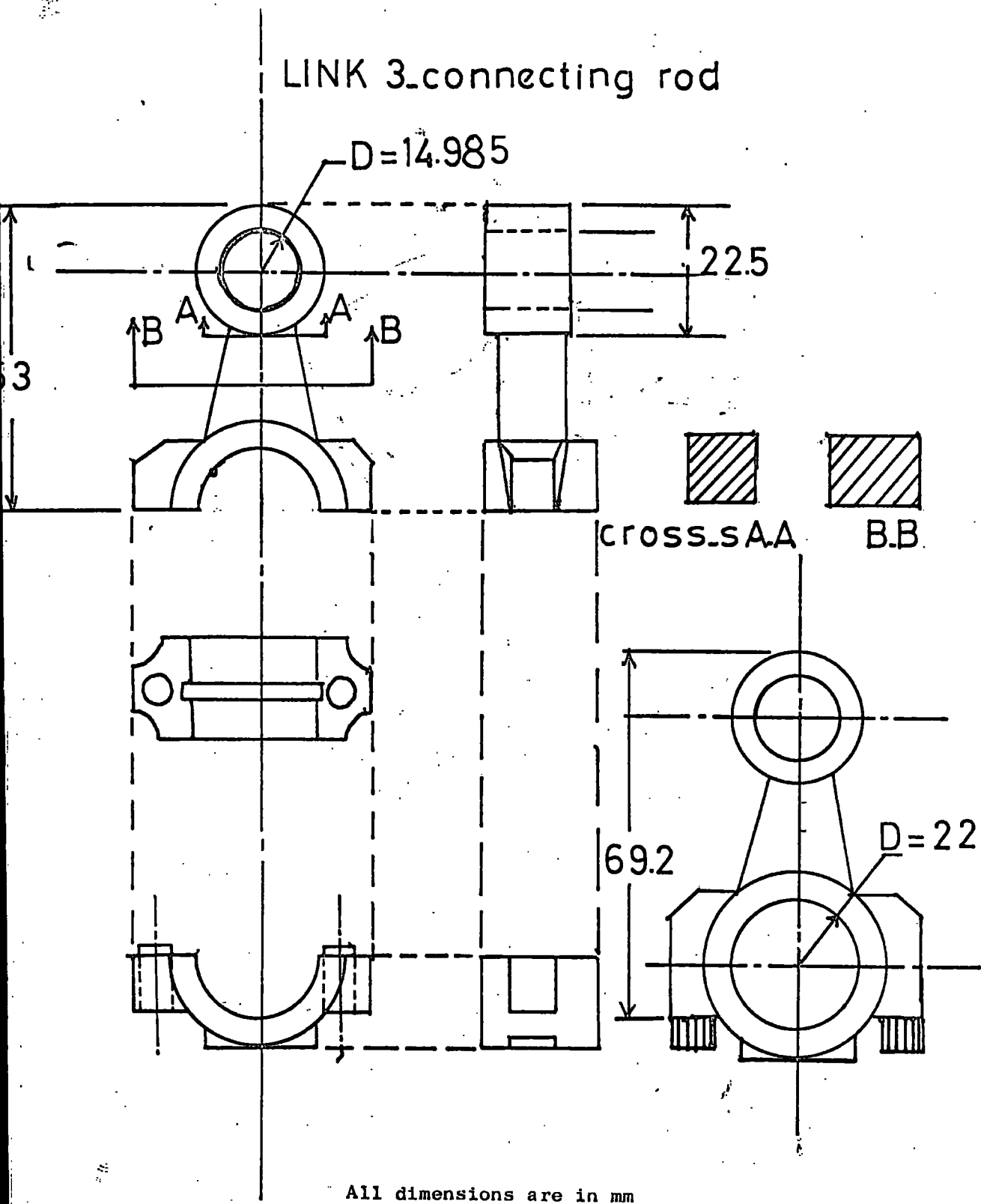
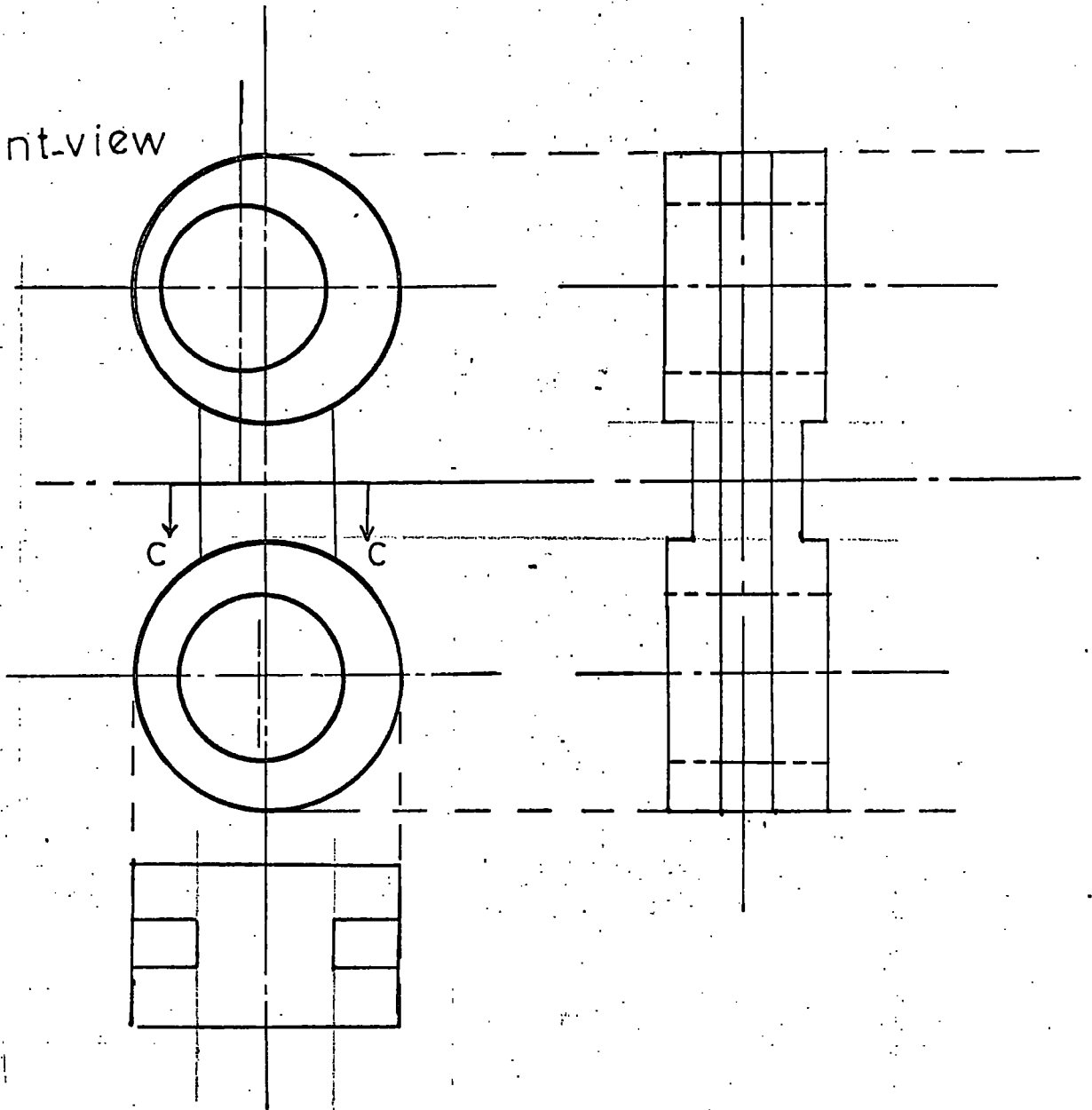


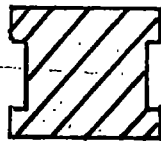
Fig. 3.9 Link 3

LINK_5

front-view



CROSS SEC_CC

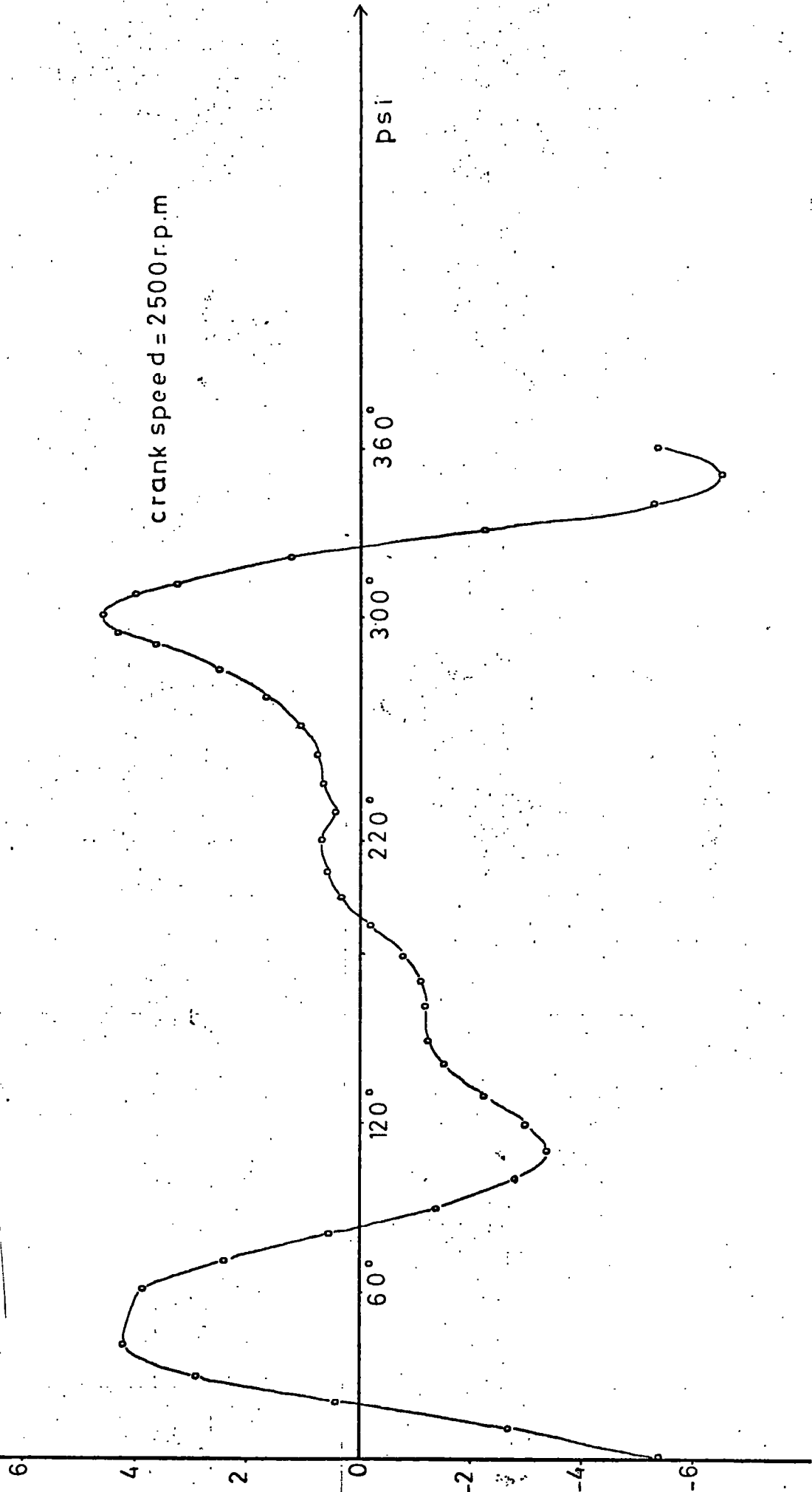


scale. x 2

Fig. 3.10

$T_2 - \text{kg m}^2 / \text{s}^2$

Fig. 3 11 - Variation of the external Torque T_2 required to drive the mechanism, with the crank angle psi



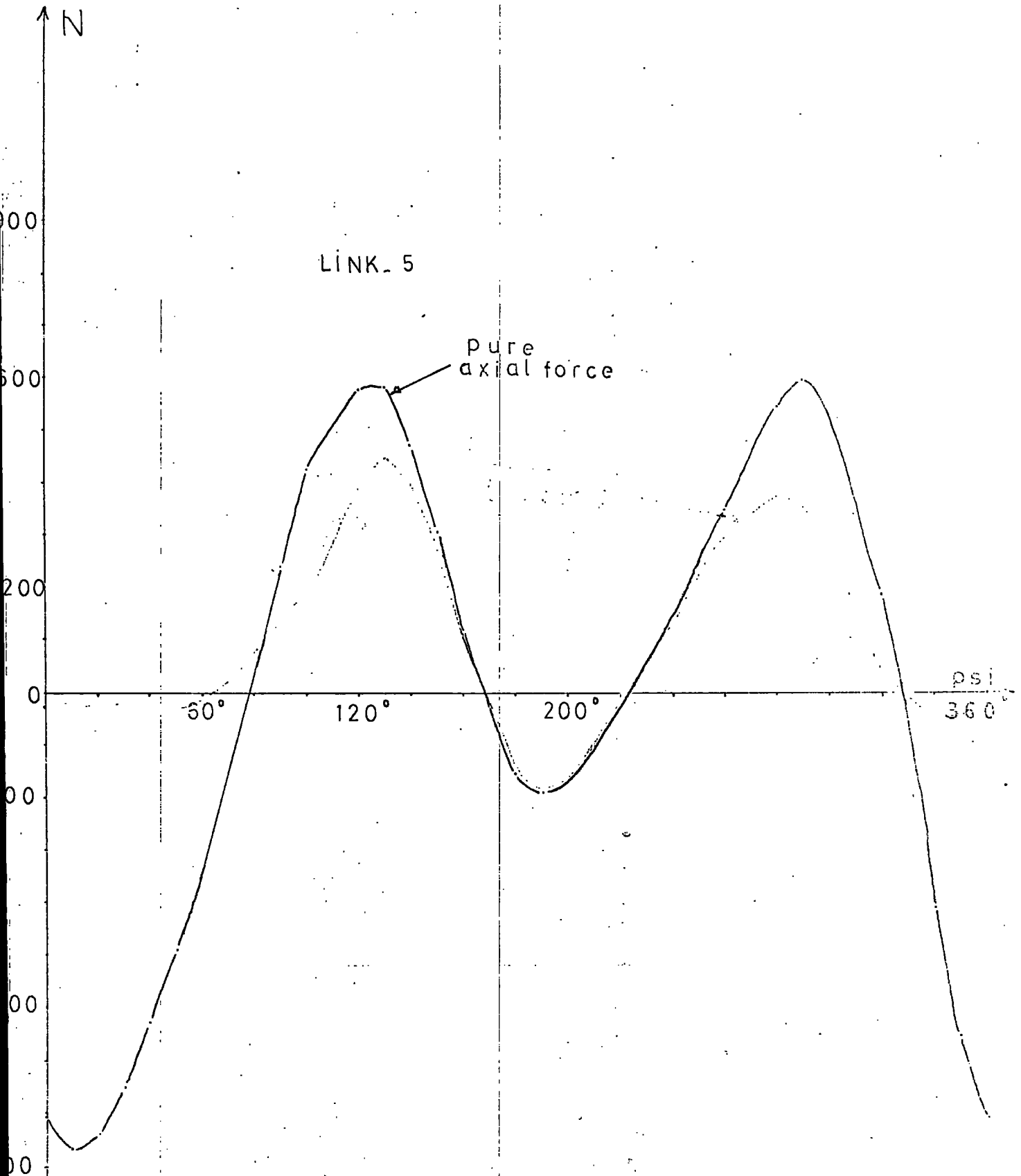


Figure 3.12 Variation of axial force with the crank angle 2500 r.p.m.

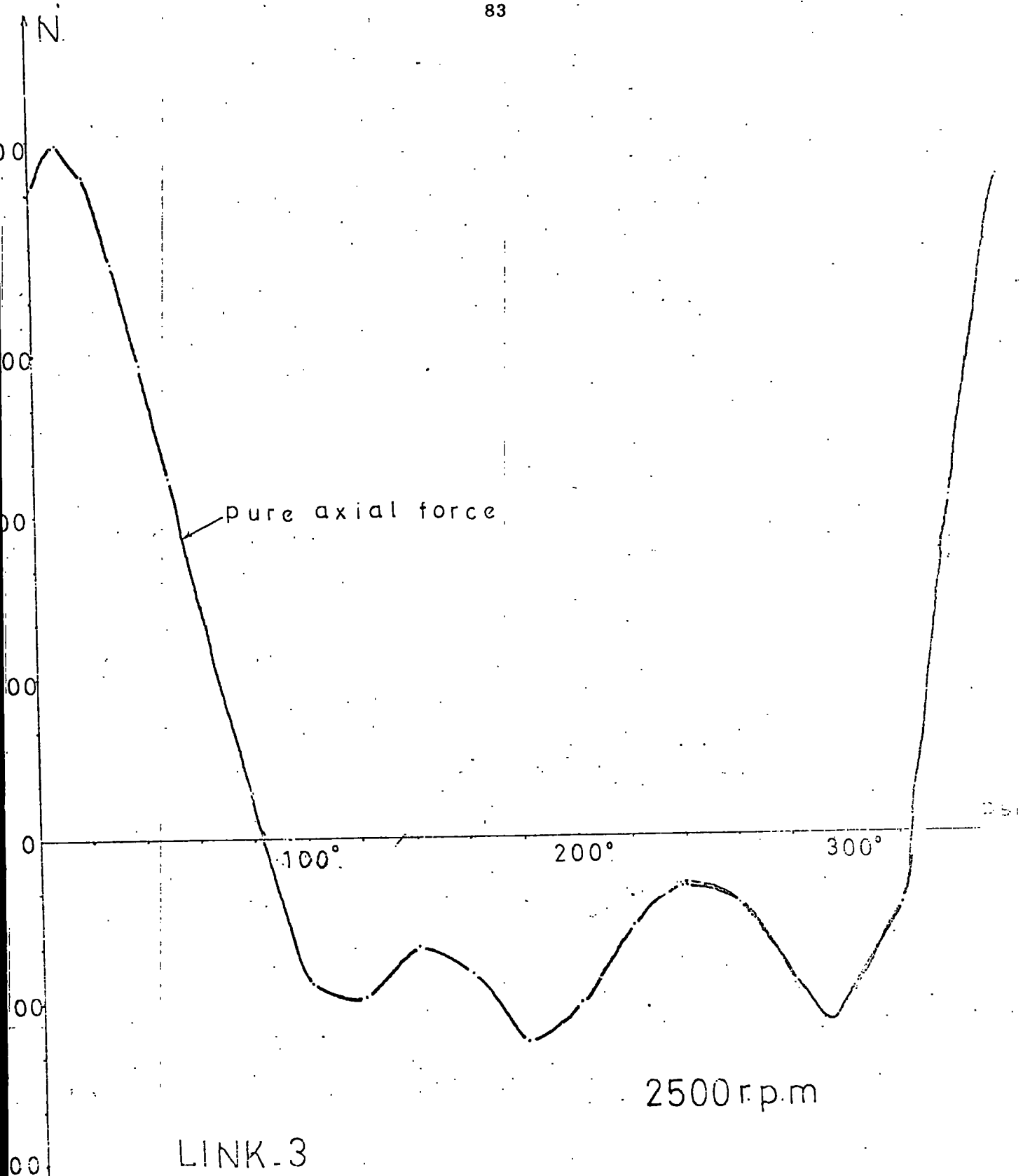
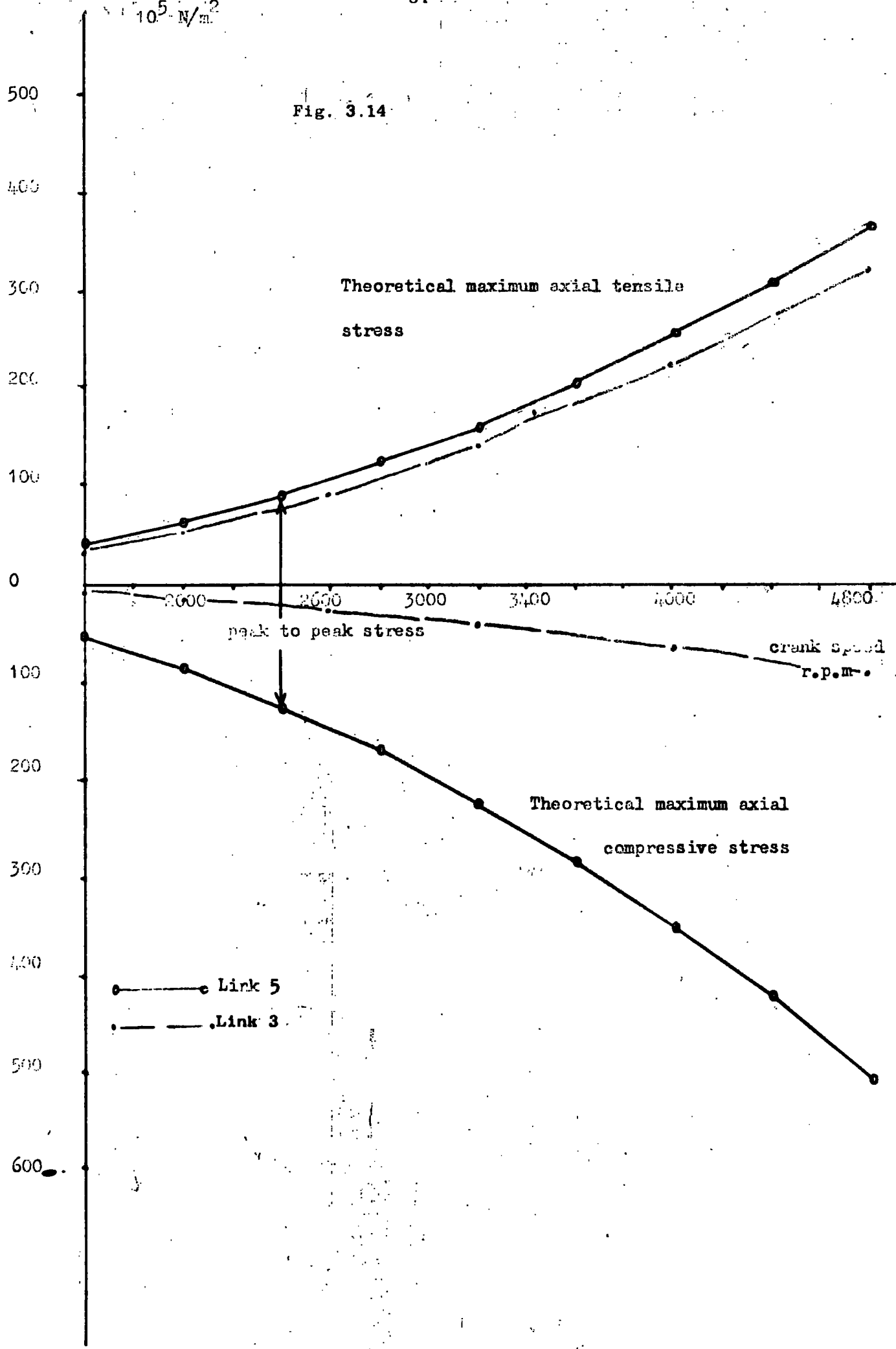


Figure 3.13 Variation of axial force at crank angle

10^5 N/m^2

Fig. 3.14



Theoretical maximum axial tensile stress

peak to peak stress

crank speed r.p.m.

Theoretical maximum axial compressive stress

○ — Link 5
● — Link 3

Chapter 4

Instrumentation, Experiments and Experimental Results

4.1 Instrumentation

The strain gauge installation and ancillary equipment is shown in Figs. (4.1), (4.2), Plate (4.1) and Plate (4.2). Each pair of gauges is wired in various configurations on the extension box to measure only axial and only bending (z direction) strains. The output from the extension box is fed into the carrier-amplifier where a metre is used in conjunction with the balance knobs on the extension box to balance the bridge circuit. The output from the amplifier is fed through a lead to an ultra-violet recorder where dynamic records are produced on photo-sensitive paper. To prevent failure due to overloading resistors and a fuse are connected in the leads to the u.v. recorder. If a record was not required it was convenient to display the response of the strain gauges on the oscilloscope to examine the strain pattern. A slotted metal disc is attached to the drive shaft and an electro-magnetic pick-up unit is placed close to the disc to produce a variable voltage. This variable voltage showed one blip for each revolution of the shaft which is recorded by the u.v. recorder at the same time as the trace from the strain gauges was recorded, which enabled the speed of the shaft to be determined for each recording. A variable-speed 2HP electric motor is used to drive the loom Plate (4.2). The wires leading from the tag strips on the specimens to the extension box were partially protected by plastic tubes against fatigue failure. In order to prevent damage due to fracture at high operating speeds, a sheet steel cover is used over the combs. The basic principle applied in the design of the dynamic measuring system is that the whole set-up will faithfully measure the strain no matter how it varies with time. Since the signal from the strain-gauge circuits is small a carrier amplifier is engaged, which is capable of receiving signals in the millivolt range and

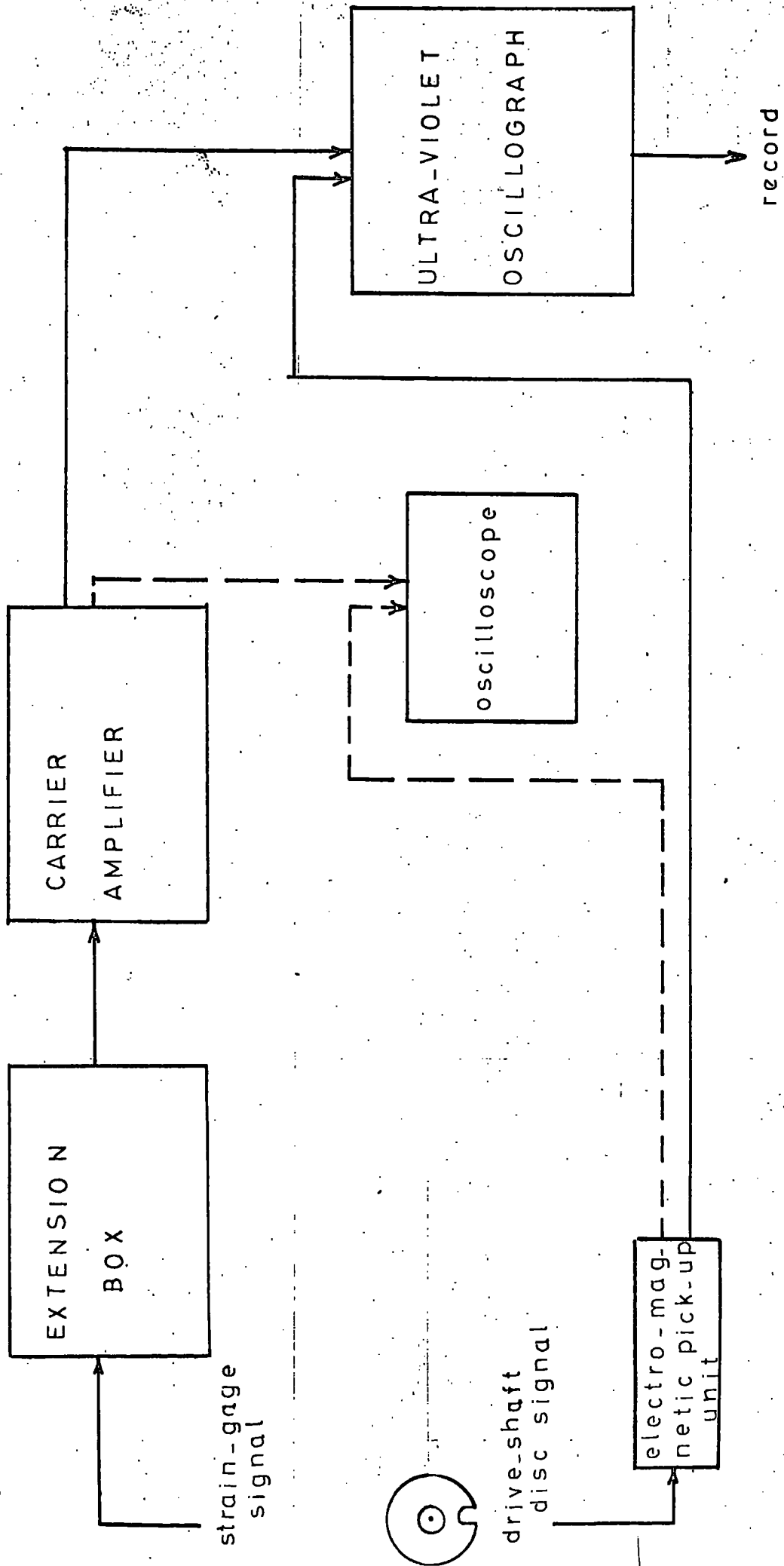


Fig. 4.1 Experimental set-up. Block diagram

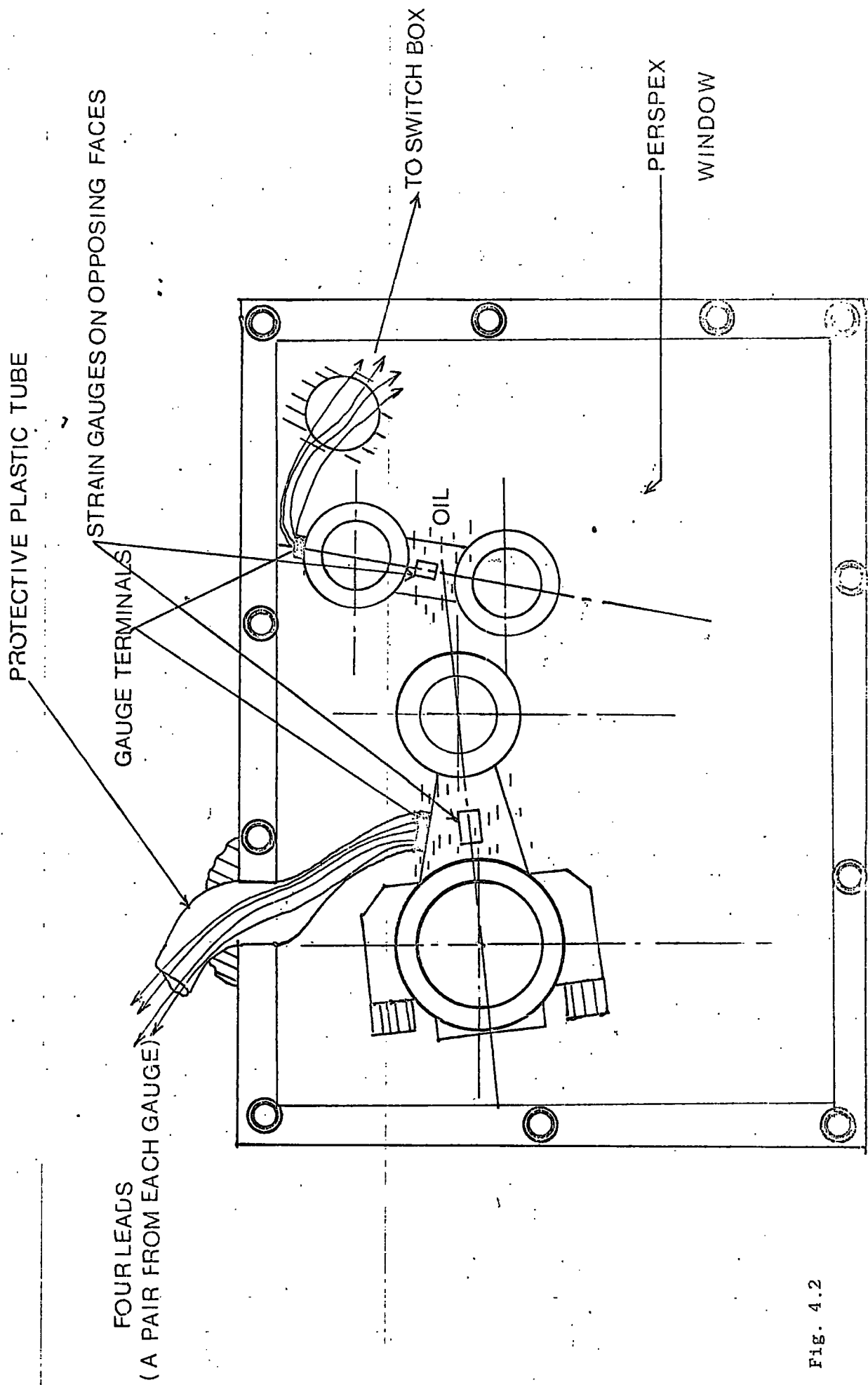


FIG. 4.2



Plate 4.1 Oscilloscope, amplifier, switch box, u.v. recorder
(with speed pick-up connection)



Plate 4.2 Featuring the viewing window modified to accept the
strain gauge leads

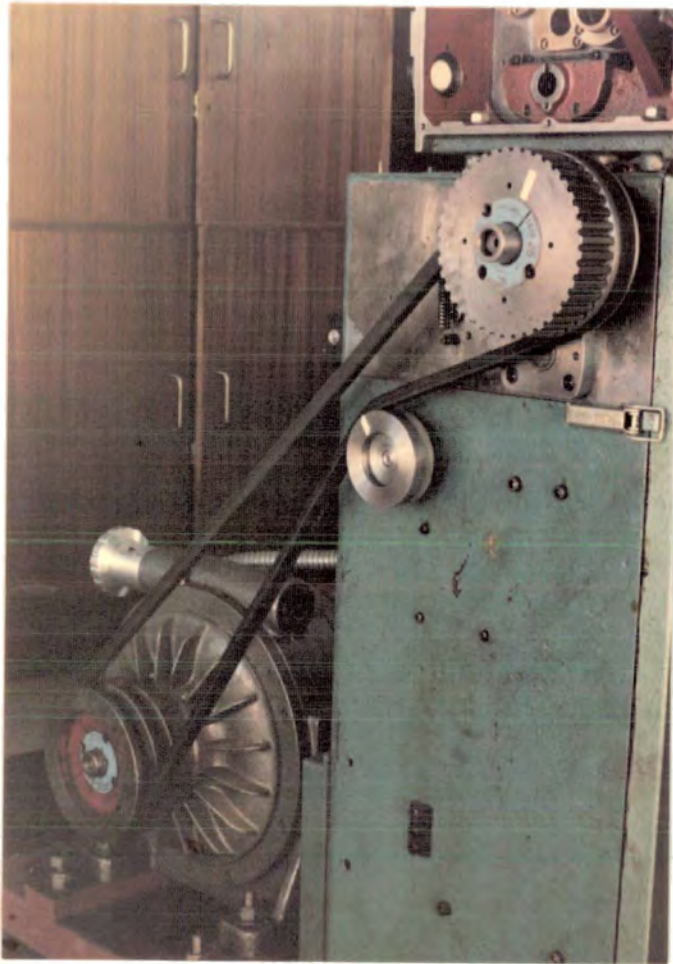


Plate 4.3 2 HP Electric motor and speed variator unit

of supplying a signal in the volt range. The record is on sensitized paper which requires no developing. A polaroid land-type camera is fitted to the oscilloscope to photograph the experimental strain pattern. The results are all taken from records produced by the u.v. recorder. It is assumed that the only resistive elements in the strain-gauge circuit are the gauges themselves (the presence of leads which affect sensitivity and calibration are negligible).

4.2 Elements of the Experimental Set-up.

1. Carrier-Amplifier; A Universal carrier-amplifier, type 581 DNH-Peekel, is used. Eleven gauge factors were available, ranging from 1.75 to 2.25, with an accuracy of 0.5%. Half and quarter-bridge (120 Ω) circuits are employed. There are six internal calibration values, 30, 100, 300, 1000, 3000 and 10000 microstrain. Bridge voltage is 5 volts, on the most sensitive range (3 μ s, full-scale deflection) for one active strain-gauge. The output gives 1 volt for full scale of the metre and remains linear for dynamic measurements even up to 10 volts. The specified accuracy of the equipment for dynamic measurements is $\pm 0.75\%$ for all ranges. Time delay is 0.5 ms for 5000 Hz. Linearity of the recorder output is $\pm 0.05\%$ for 2 volts peak-to-peak output and $\pm 0.1\%$ for 20 volts peak-to-peak output, provided that the input is balanced for capacity. Drift is approximately 1 μ strain/day
2. Ultra-Violet Recorder; A "Southern Instruments" ultraviolet oscillograph 10-100 series is used for continuous direct recording of input signals. Signal is fed to a miniature tubular galvanometer which reflects a spot of intense ultraviolet light onto the photosensitive record paper. The deflection of the galvanometer is a function of the amplitude of the input-signal current. A choice of eight paper speeds is available. Two of the input sockets are used. First one for the carrier-amplifier output-signal and the second one for the electromagnetic pick-up unit output-signal. A

paper speed of 37 mm/s is used for calibration while paper speeds of 111 and 333 m/s are alternatively used during actual measurements. Four fixed time intervals are available, 0.01, 0.1, 1 and 10 seconds, and the specified accuracy of the printed lines is within $\pm 2\%$. Paper speed stability is $\pm 3\%$. Since, instead of pen-aim, an ultraviolet light beam of zero mass is introduced, direct recording of frequencies up to 10 KHz can be performed. SMI, Type SMI/N, Ser. No. 1480-2 galvanometer is employed for recording.

3. Extension Box: A "Peekel 4-channel 4 UD" type switch box is used. There are four input channels, for full-bridge, half-bridge or quarter-bridge, 120 Ω configurations. Each channel has four balancing controls, three for resistive balancing and one for capacitive balancing of the bridge circuit. The specified typical error of switch contacts is 1 - 2 microstrain. Ranges of resistive and capacitive balancing are $\pm 6000 \mu s$ and ± 1000 pf respectively.

4. Oscilloscope: A cathode ray oscilloscope is employed to display the rapidly varying strain waveform. Since the output of the strain gauge circuit is connected to vertical amplifiers, vertical deflection is related to strain. The internal sweep circuit allows the trace to be driven horizontally at a preselected rate.

4.3 Strain gauges and gauge installations

Since strain gauges are used to measure varying and repeated strains, special care is exercised in gauge selection, in gauge bonding and in lead attachment. "Timsley, Telcon" elements type 7/120/EC, of different batch numbers, gauge factor = 2.18 Range = 120 $\Omega \pm 1\%$, electrical strain gauges are employed. The resistive element is fixed to a transparent plastic base, and is bonded to the point at which strain is measured. The gauges are placed on the specimens as shown in Fig. (4.2). Although it was felt that helically wound wire gauges and "Isoelastic" wire gauges offer a superior

fatigue life, recent research has shown that other standard gauges have as great or even greater fatigue life (6). Flat-grid, wire and foil metal gauges on paper back and bonded with cellulose nitrate cement have been strain cycled ($\pm 1000 \mu\text{s}$ / in for 1,250,000 cycles without failure (6)). Epoxy-backed foil metal gauges bonded with epoxy cements are capable of more than 300,000 cycles at $\pm 1500 \mu\text{s}$. However it is generally agreed that as the magnitude of cyclic strain increases from $1500 \mu\text{s}$, the fatigue life is reduced very rapidly (6). A well established fact is that the connection of the lead wires is one of the most critical steps in the installation of a gauge for cyclic strain service.

Cyanoacrylate (Loctite, IS - 12 adhesive) is used to bond the base to the specimen. However since it is a poor gap filler the surface of the specimen is filed to obtain a smooth area and is cleaned with carbon tetrachloride and/or acetone. Dove and Adams (6) have used cyanoacrylate to measure dynamic strains (rise time 1 millisecond) as high as $2000 \mu\text{s}$. Cyanoacrylate cement bonds under the action of modest contact pressure, and works satisfactorily up to temperatures of 120°C . Cement cures by chemical polymerization, and obtains its optimum adhesive strength after about 48 hours. In vibration environments the weak point of the gauge is the point at which the filament is connected to the gauge lead. The gauges are checked for correct bonding, gauge resistance and gauge-to-specimen resistance by using a low-voltage type of mega ohm metre. The transverse sensitivity of the gauge is negligible, and it is assumed that, since the specimens have a relatively high modulus of elasticity, the strain is uniform, through the cross-sections at which the gauges are applied. The minor effect of localised stiffening on the surface, producing distortion of the strain pattern is neglected. The gauge factor is taken to be constant. since practically it is unchanged even in the plastic region. Unless, thermal or mechanical shock is expected, cyanoacrylate cement is regarded as superior

to other gauge bonding materials for dynamic strain measurements. The oil temperature does not vary in short term operations and is assumed to stay constant.

The bonded gauges were first protected with Araldite against oil. However ordinary Araldite coating is attacked by the oil (Mobil Vactra oil) and failed to hold the installation. This major installation problem is solved by using "Micro Measurement Inc. M-Coat G Compound". In order to be able to measure the strains accurately, gauge instability and mechanical damage are minimized. Basic mechanical damages were due to vibration, high operating speed and limited available space. During measurements strain-gauge installations have been replaced several times because of mechanical damage and instability. Oil act to reduce the gauge-to-surface resistance or partially to short-circuit sections of the gauge itself. The effect of oil is to place a resistance path in parallel with the strain gauge, producing a change in resistance equivalent to strain. This effect is very important since the change associated with strain is very small. The coating material employed is a two-part 100% solids polysulphide modified epoxy compound, which provides a tough flexible layer, offering good protection against commercial oils, greases, gasoline, most acids, alkalis and most solvents. It cures to a firm, tack free condition in six hours at 24°C. Full cure in 24 hours again at 24°C. It can be safely used up to an oil temperature of 82°C. An incomplete protection around leadwires was very frequent and a common cause of oil penetration into the gauge installations. By introducing practical solutions, and getting familiar with the vital problems created by hostile environment, the number of installation failures are reduced, and longer terms of stability and accuracy in readings are achieved. Coatings are applied to cleaned surfaces, since coatings extending into unclean areas will loosen with time. Generally a thick coating offers a more difficult path for oil penetration than a thin one. M-Coat G forms a flexible rubbery coating, and its chemical resistance may

be further improved by a one hour bake at 93° C. The solder joints and wiring terminals are covered with a thin layer of M-Coat D (an air-drying solvent thinned acrylic coating) before applying M-Coat G in order to prevent any electrical leakage under adverse conditions. The prime coat dries in 15 minutes under normal ambient conditions. In applying M-Coat G care is taken to avoid air pockets and the coating is extended out as far as possible on all sides beyond the edges of the M-Coat D layer. Oil, most often, enters coated strain-gauge installations along insulated lead wires producing signals which are unrelated to, but hardly distinguishable from strain. For this reason wires are completely coated as far back from the installation as practical, which is usually not more than one cm, due to space limitations. However, most of the time insulated wire does not bond well to the coating.

4.4. Experiments

1. Dynamic Strain Measurements

As shown in Plate (4.3), a variable speed (480-4320 output r.p.m.), 2 HP, 3 phase 50 cycles electric motor is used to run the loom, replaced by the original 1.1 Kw, 1410 r.p.m., 1.5 HP, 3 phase 50 cycles motor. A tachometer is used to check drive shaft speed in addition to the u.v. recorder. The motor is calibrated against the drive shaft speed by using the variac speed selector unit. The bending strains measured are in the z direction, perpendicular to the x-y plane of the mechanism. The strains due to plane bending are not measured, (as explained in the introduction; see Section I). The results of the dynamic strain measurements are given in Table (4.2). Measurement periods, usually did not exceed 15 minutes. The drive shaft speed is gradually increased from approximately 1050 r.p.m to 2550 r.p.m. The circuit is rebalanced for resistance and capacitance before each run, and a calibration trace has been recorded. The basic problems encountered during dynamic-measurements are:

- a - Gauge installation failures
- b - Excess noise and vibration due to improper contact of bevel gears at high operating speeds
- c - Mechanical failure due to slip between link 6 and shaft O_3
- d - stretching and bending of the lead wires

2 Static Bending-strain measurement

To examine the nature of bending strains, a static bending strain test is performed on the mechanism. Fig. (4.3) shows the simple set up. A 0.3 m lever arm is attached to the drive shaft to apply torques of known magnitude to the system. The test results are given in table (4.3). The shaft O_3 is locked by a clamp mechanism to allow the forces to be transmitted throughout the links. Both axial and bending strains (z direction) are measured under the same loading conditions.

The variation of axial and bending (z direction) stresses with the applied torque in each link are shown in Figs. (4.4) and (4.5). Applied torque is increased up to 74 N.m. Half-bridge (120 Ω) circuits are employed during measurements. The crank angle 'psi' is kept 90° (from the horizontal in counter-clockwise direction).

3 Stress distribution in links 3 and 5

Using the same experimental set-up, strain variation within the links themselves are measured. Strain-gauges on opposing faces of link 5 are identified as gauges m and k. Quarter-bridge (120 Ω) circuit is employed to measure the combined axial and bending strain on each face separately by feeding the two lead-wires directly into the carrier amplifier. The procedure is repeated for both gauges by reversing the link. During the measurements crank angle 'psi' is kept at 90° . A maximum torque of 35.3 N.m is applied to the main drive shaft via the lever-arm. The pure axial compressive strain is then

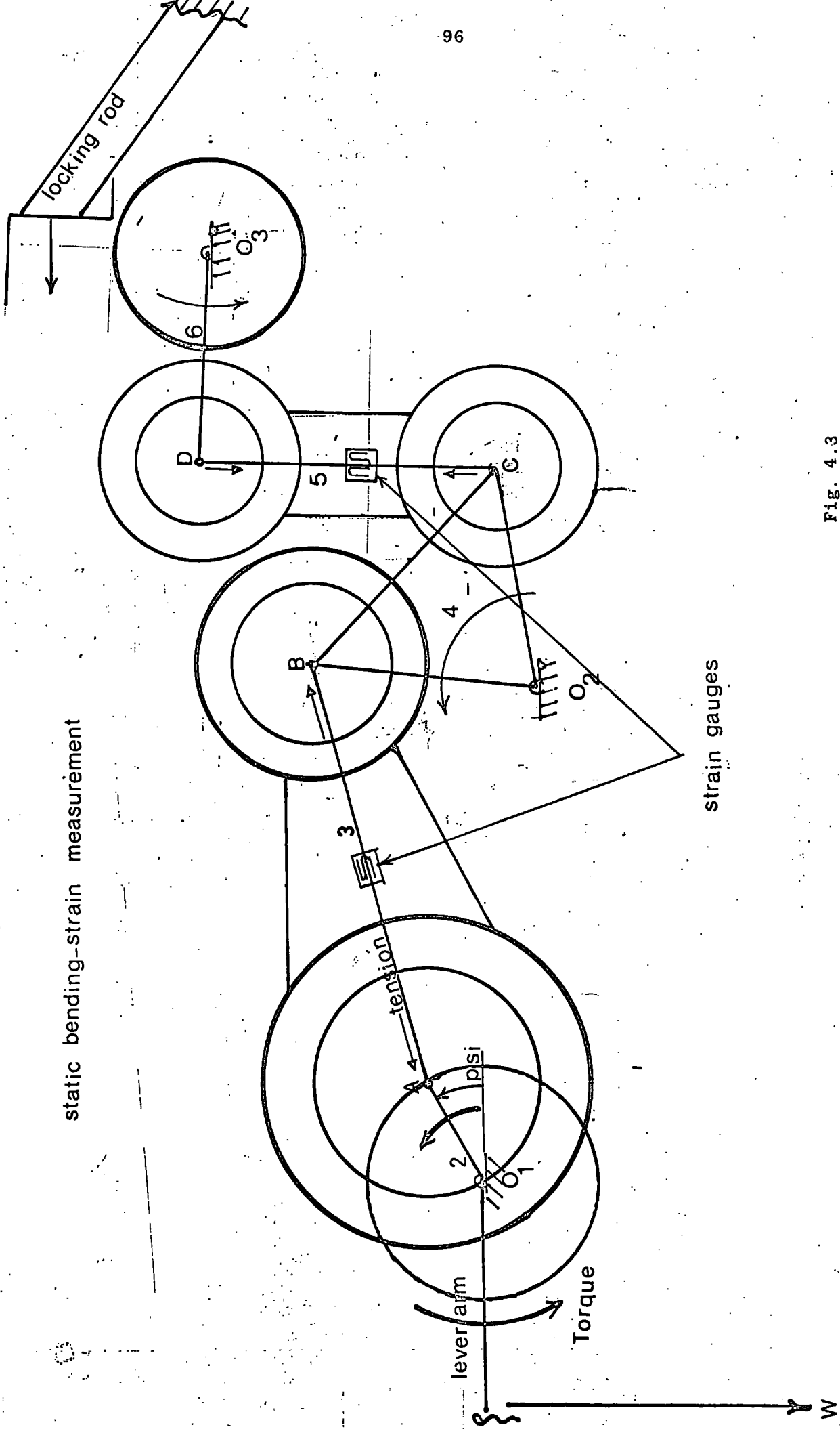


Fig. 4.3

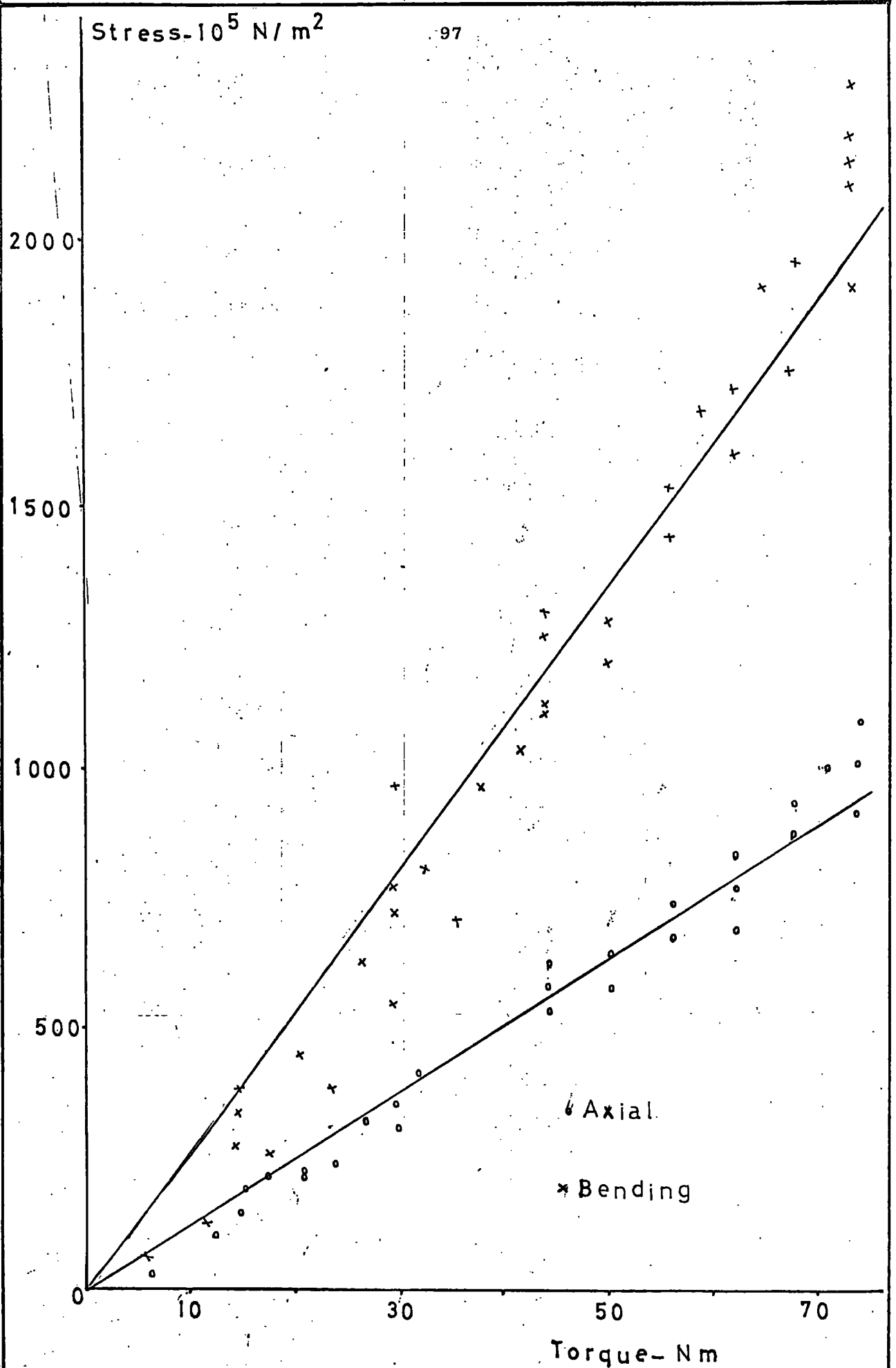


Fig. 4.4 Static Bending - strain test for link 5. Variation of axial and bending (z-direction) stresses with the applied torque.

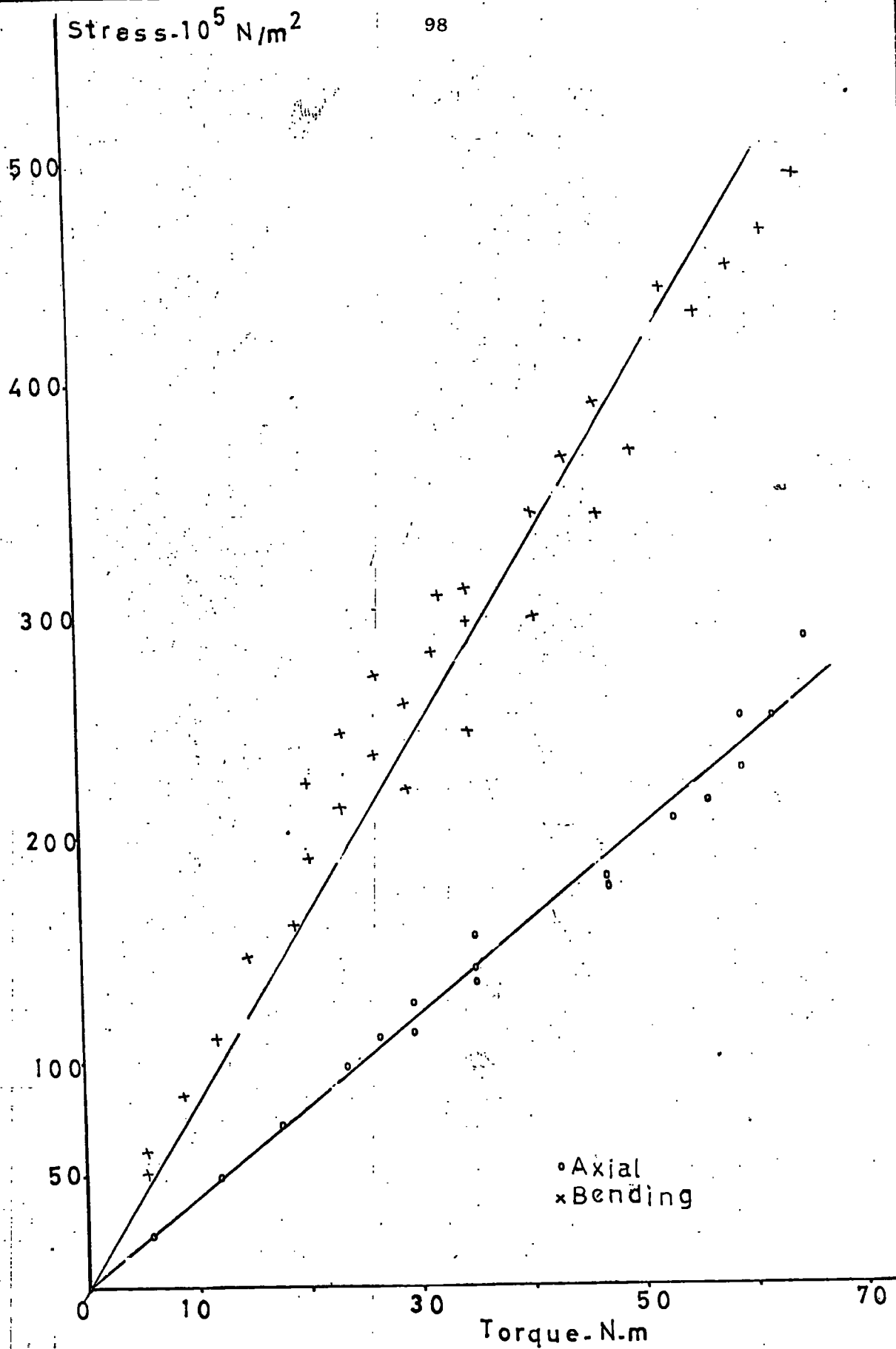


Fig. 4.5 Static bending strain test for link 3 - Variation of axial and bending (z-direction) stresses with the applied torque.

measured by using a half-bridge circuit. Strain gauges on opposing faces of link 3 are identified as gauges c and d, and the above procedure is similarly applied to determine the strain variation. Results are shown in Figures (4.6) and (4.7).

4. Tensile Test

Separate tensile tests are performed on links 3 and 5. A "Servomex Controls Ltd., tensometer, metric type-E" is used in combination with a "Peekel 4-channel 4 UD" extension box and a "Peekel type 581 DNH" Universal carrier-amplifier. The test machine is provided with a unit which automatically draws a tensile test diagram representing the relation between the load and the extension. Two strain gauges are fixed on opposing faces of the links, connected to the extension box. A half-bridge 120Ω circuit is used to measure the tensile strain. A 2500 N capacity load cell is employed. Motor speed was 600 r.p.m. and the cross-head speed was 9 mm/min. A pair of specially manufactured chucks are used for each link to grip them between the moving cross head and the base. The chucks were fitted with heat treated steel pins, having diameters as close as practical to the inner end bore diameters of the links. The chucks were designed to ensure a central application of the load. The direction of the paper movement was the same as that of the crosshead. The event marker switch is used from time to time to record the actual applied load at certain strain values registered on the carrier amplifier. The moduli of elasticity and yield point strengths are determined from the experimental data shown in Fig. 4.8 for cross-sections BB and AA of the links 3 and 5 respectively.

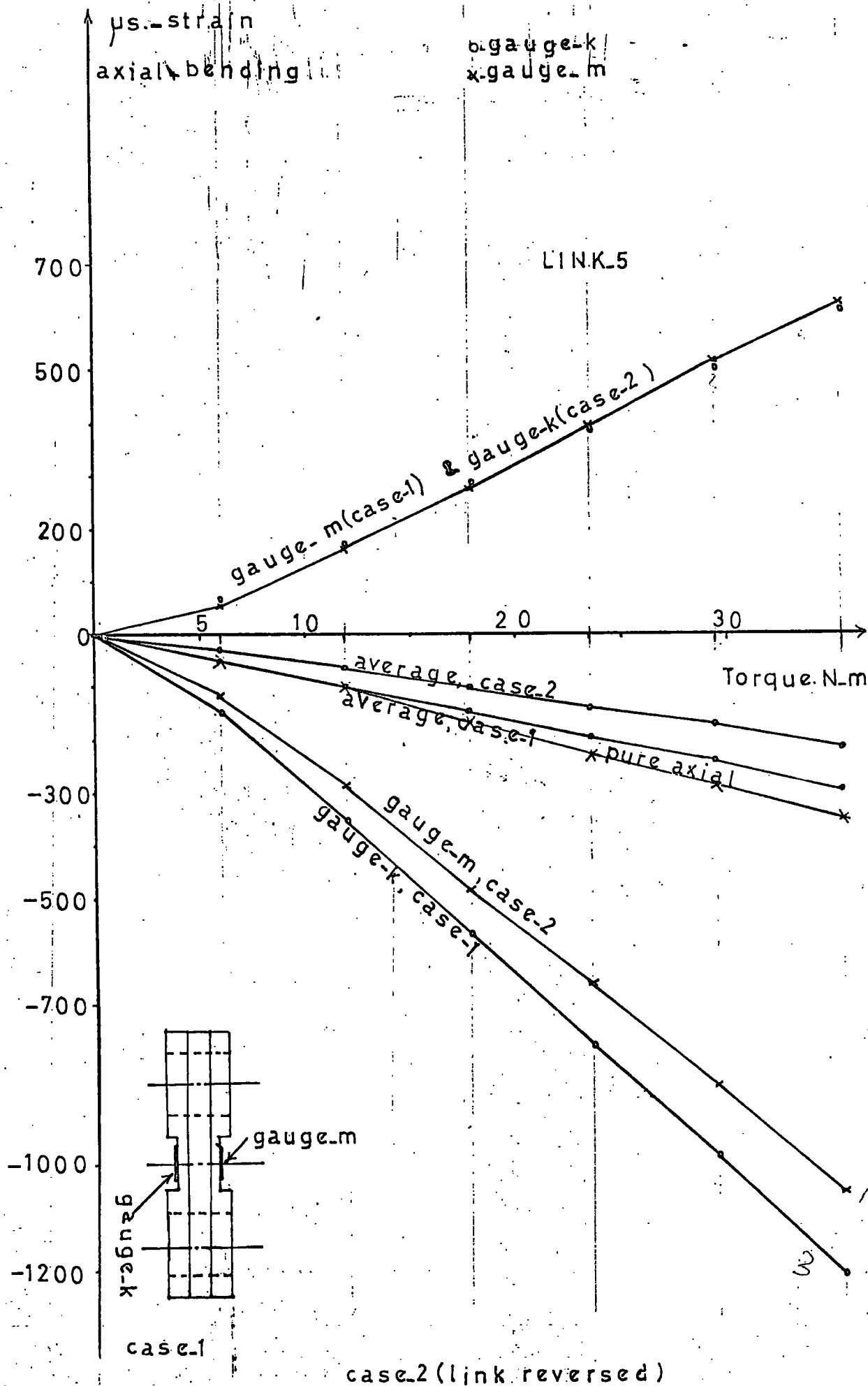


Fig. 4.67

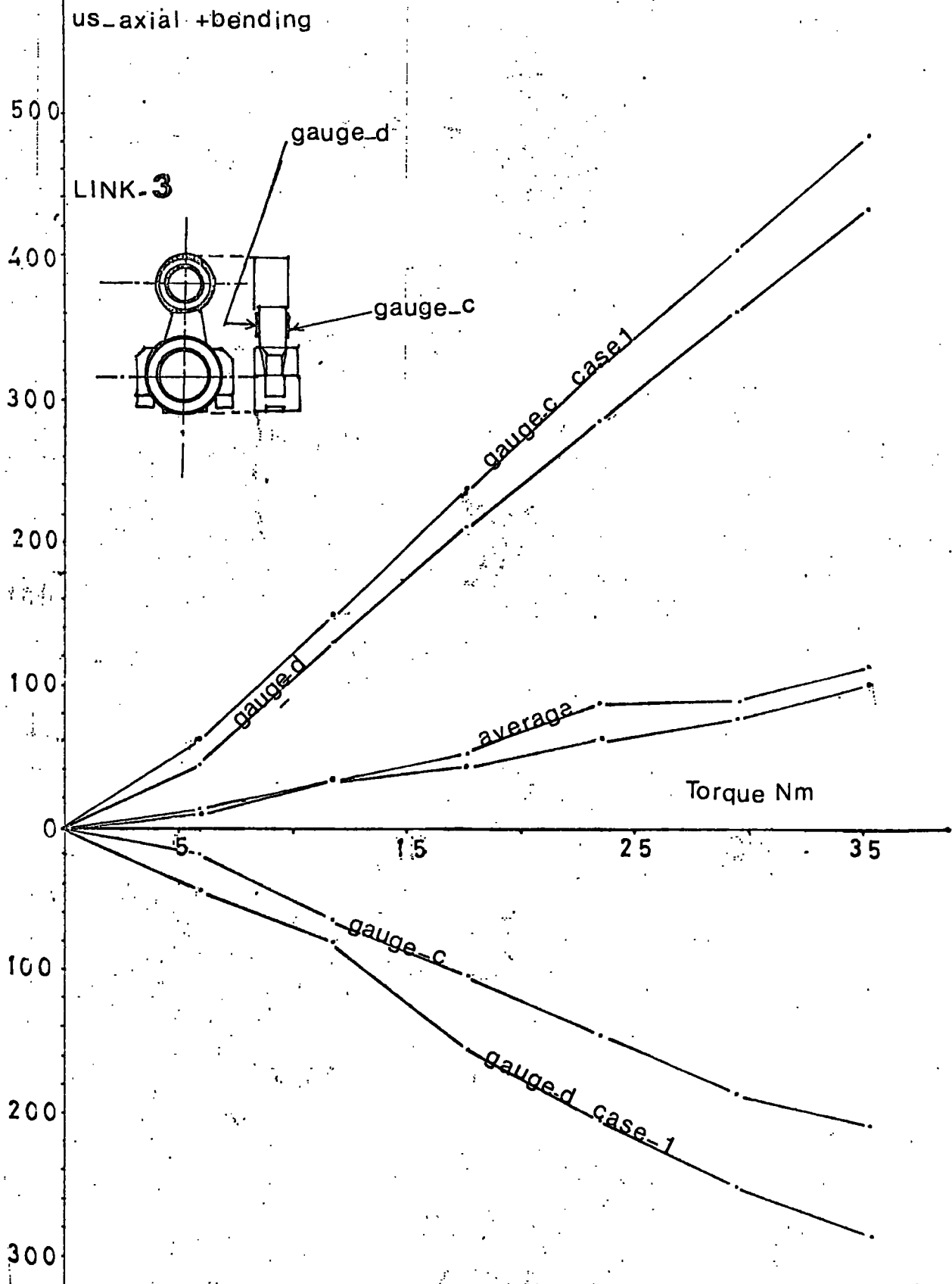


Fig. 4.7

24 NOV 1971
LIBRARY

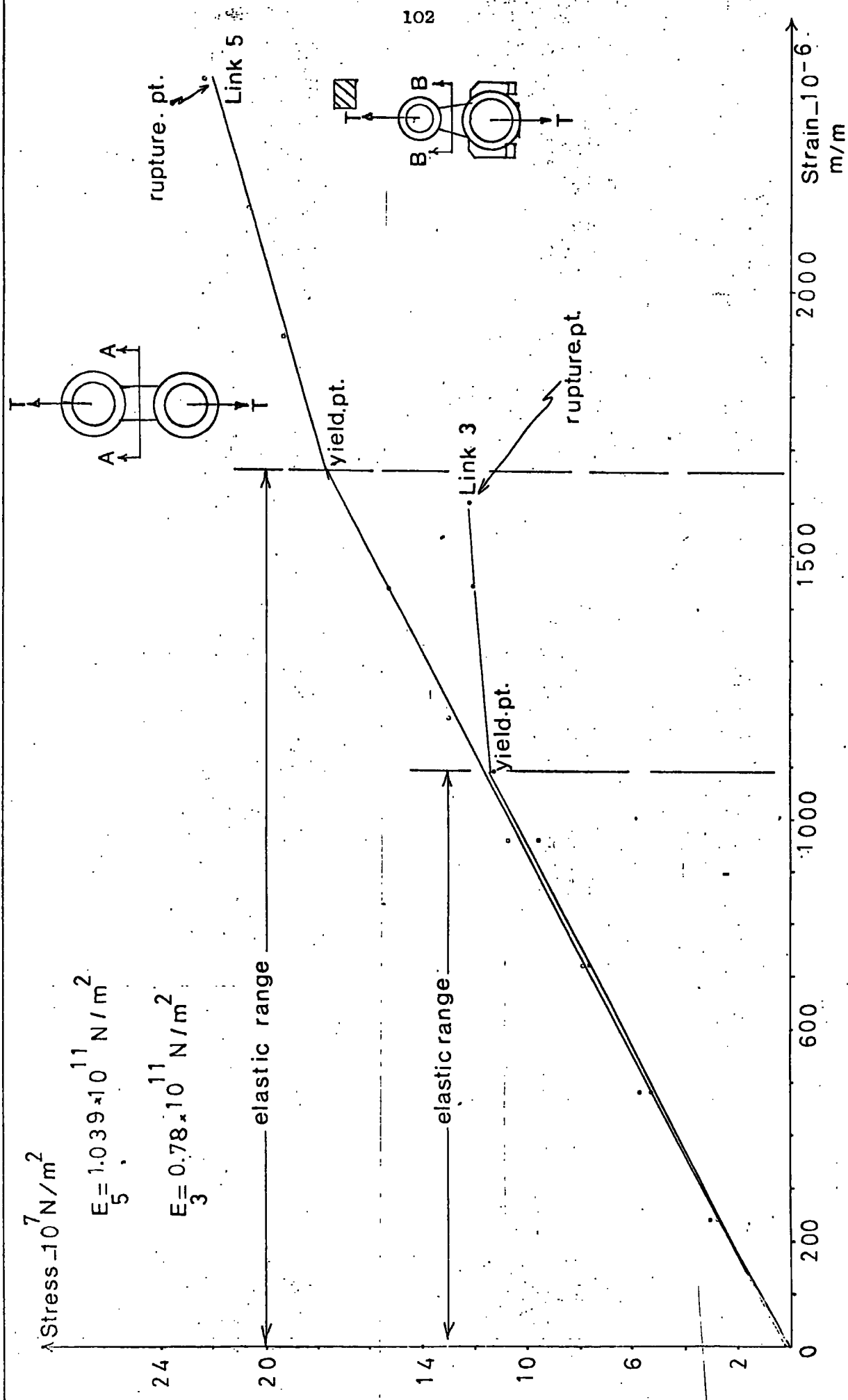


Fig. 4.8 Tensile Test for Links 3 and 5

4.5 Dynamic Strain Measurement Results

Since two active gauges are connected in a half-bridge circuit for each set of results, the reading from the bridge is twice that which would be expected if only one active gauge were used. The results are therefore divided by two to obtain the real strain and stress values shown in Table (4.2). The variation of the peak to peak stresses (both axial and bending) with the crank speed for links 3 and 5 are shown in Figures 4.9 to 4.13. Experimental sample strain patterns obtained are shown in Fig. 4.14, a - f for various crank speeds. Experimental variation of the cyclic axial stresses in both links with the crank angle ψ are presented in Figures 4.15 and 4.16.

4.6 Speed Fluctuation

Crank arm speed is assumed to remain constant during a measurement. However the following simplified theoretical calculation based on total kinetic energy of the system is made to predict an estimation;

Let

I_1 = Moment of inertia of the main drive shaft with the flywheel

I_2 = Moment of inertia of shaft O_2

I_3 = Moment of inertia of shaft O_3

From Fig. 3.6 (Torque diagram, for the crank speed = 2500 r.p.m.), Let Ω_2 be the angular velocity of the crank arm at the crank angle $\psi = 50^\circ$.

Also let Ω_4 and Ω_6 be the angular velocities of shafts O_2 and O_3 at the same crank angle. Then 2 (Total Kinetic energy) $I_1\Omega_2^2 + I_2\Omega_4^2 + I_3\Omega_6^2 = \text{constant}$
or

$$\frac{2 \text{ (K.E)}}{\Omega_2^2} I_1 + I_2 \left(\frac{\Omega_4}{\Omega_2} \right)^2 + I_3 \left(\frac{\Omega_6}{\Omega_2} \right)^2 = \text{constant} \quad (4.1)$$

The variation of Ω_2 are shown in Table 4.1 for various crank angles, $0^\circ \rightarrow 360^\circ$ by 10° intervals at an average crank speed of 2500 r.p.m. = 261.798 rad/s.

From table 4.1, coefficient of speed fluctuation is;

$$C_s = \frac{\Omega_{\max} - \Omega_{\min}}{\Omega_{\text{av}}} = \frac{267.43 - 253.95}{261.798} = 0.0515$$

speed fluctuation is also measured experimentally by using the u.v recorder and the speed pick-up unit in combination as explained in 4.1. The experimental average value of coefficient of speed fluctuation obtained was 0.082

Table 4.1

crank angle psi (degrees)	Ω_2 rad/s	crank angle psi (degrees)	Ω_2 rad/s
0	263.95	190	267.43
10	266.68	200	267.41
20	267.43	210	267.19
30	266.26	220	266.88
40	263.82	230	266.56
50	260.93	240	266.25
60	258.29	250	265.91
70	256.39	260	265.39
80	255.58	270	264.53
90	255.99	280	263.10
100	257.50	290	260.96
110	259.64	300	258.26
120	261.81	310	255.61
130	263.52	320	253.95
140	264.63	330	254.12
150	265.35	340	256.35
160	265.97	350	260.05
170	266.60	360	263.95
180	267.14		

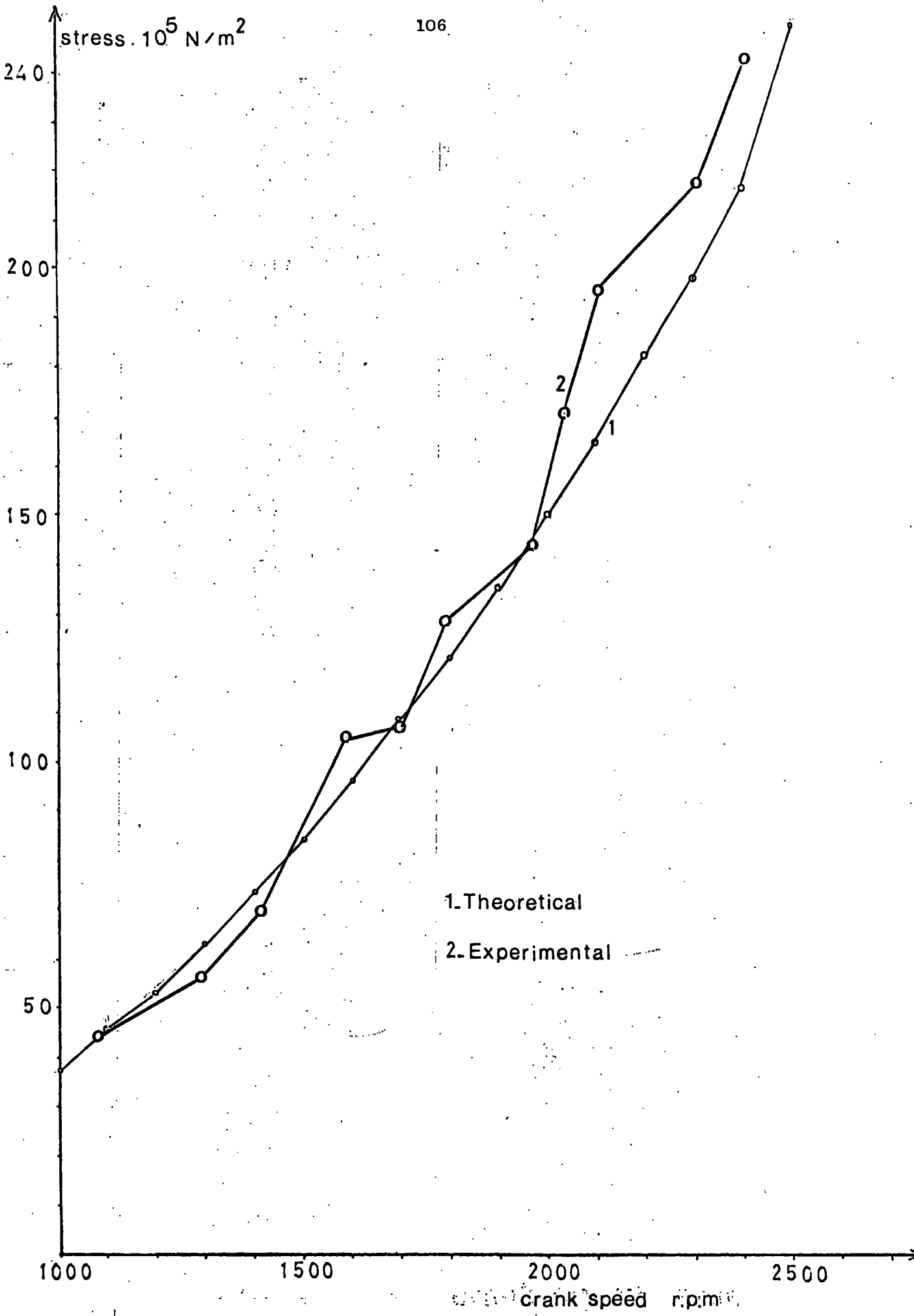


Fig. 4.9: Theoretical and experimental variation of axial stress range (peak to peak stress) in link 5 with the crank speed.

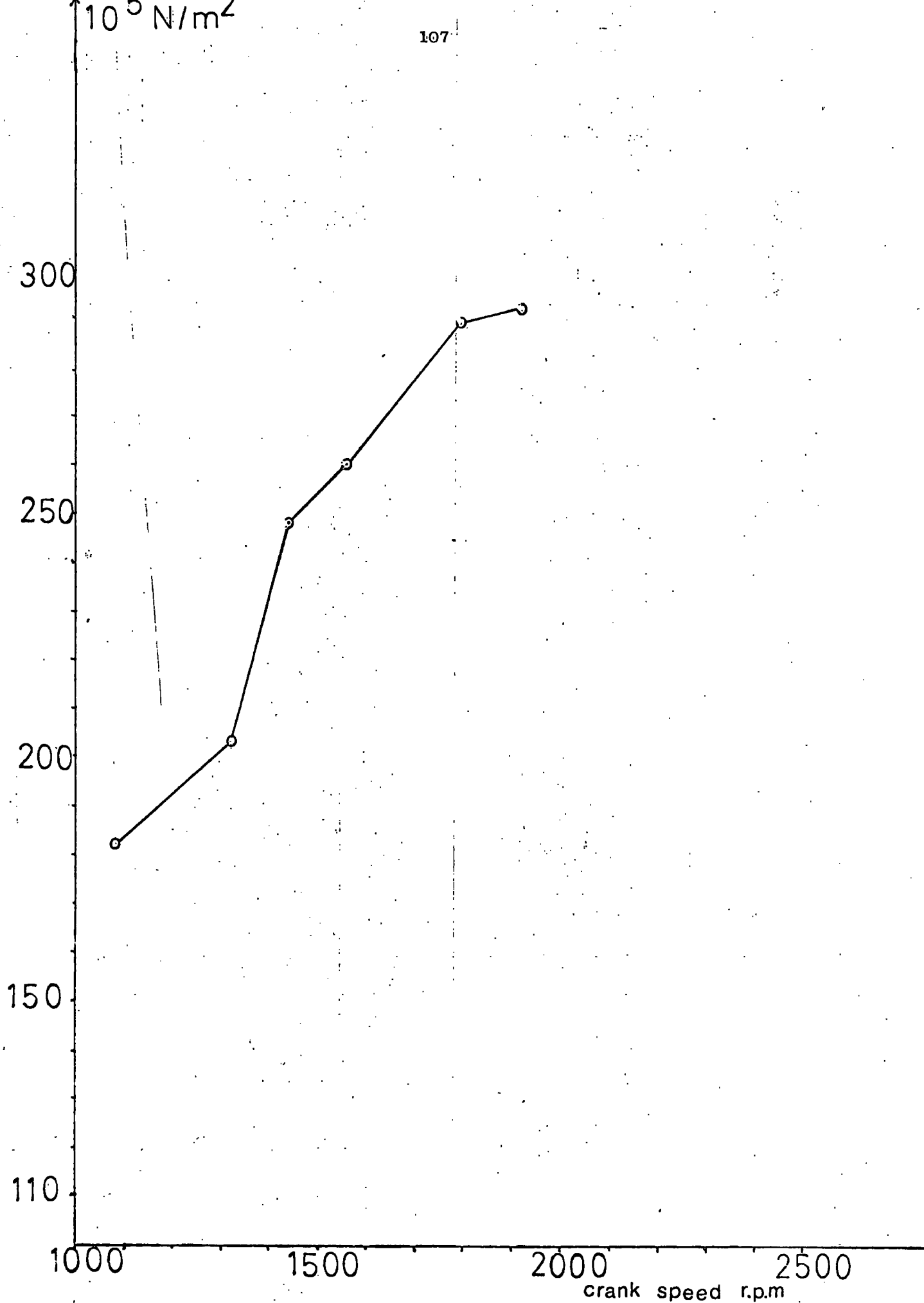
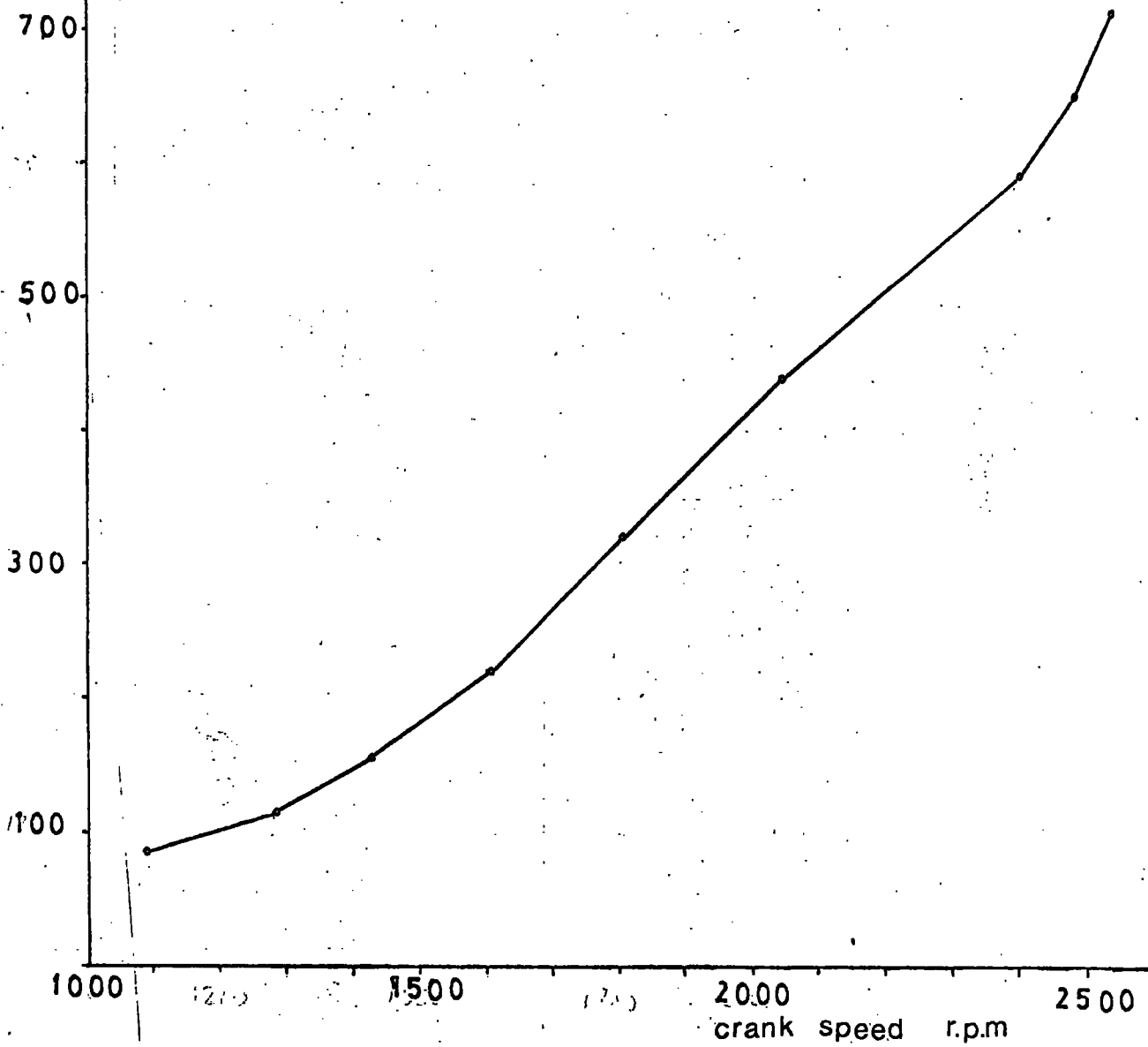


Fig. 4.10 Experimental variation of bending (z-direction) peak to peak stress (stress range) in link 3 with the crank speed.

stress $\cdot 10^5$ N/m²

Fig. 4.11 Experimental variation of bending (z-direction) peak to peak stress (stress range) in link 5 with the crank speed



10^5 N/m^2

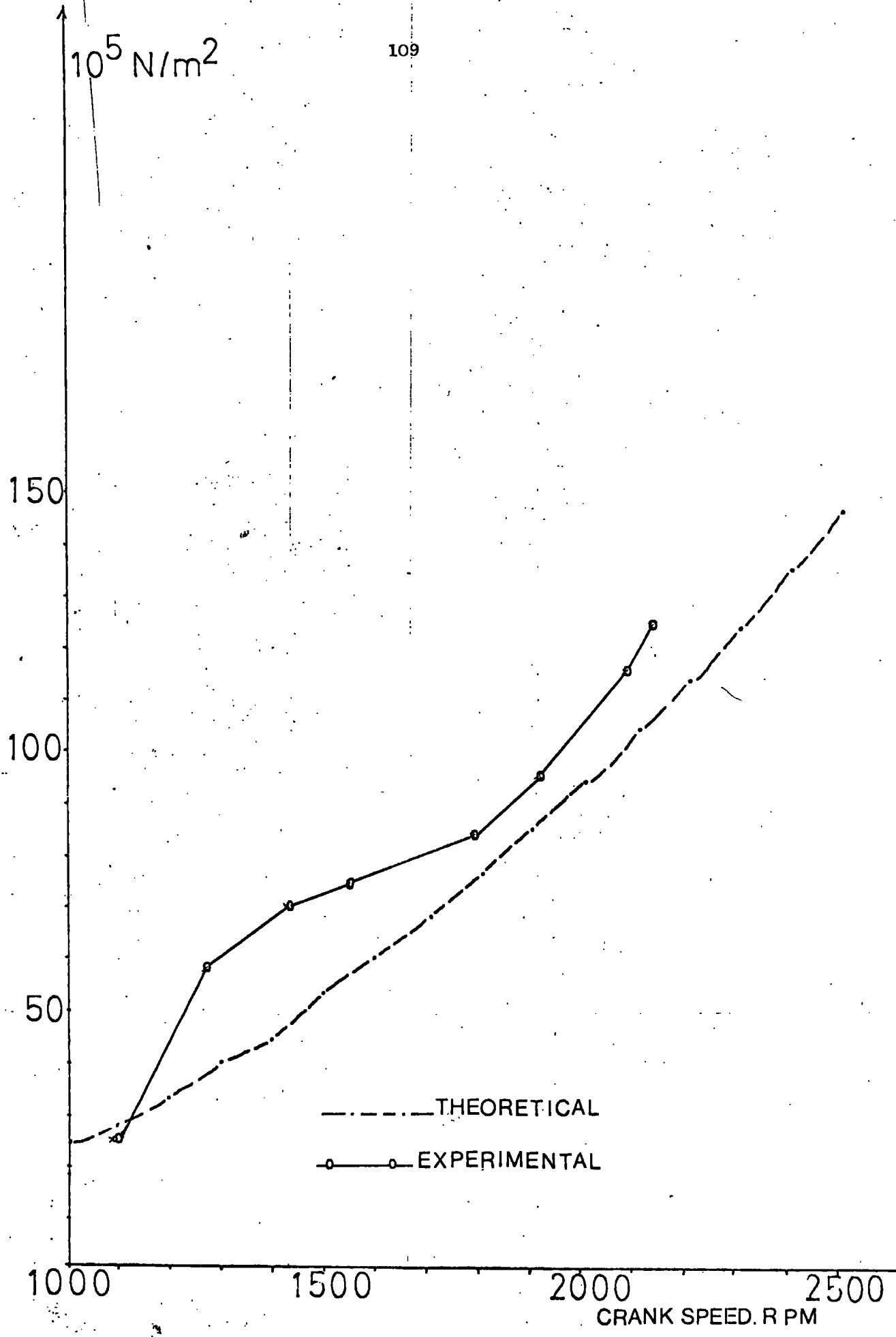


Fig. 4.12. Theoretical and experimental variation of axial peak to peak stress (Stress range) in link 3 with the crank speed

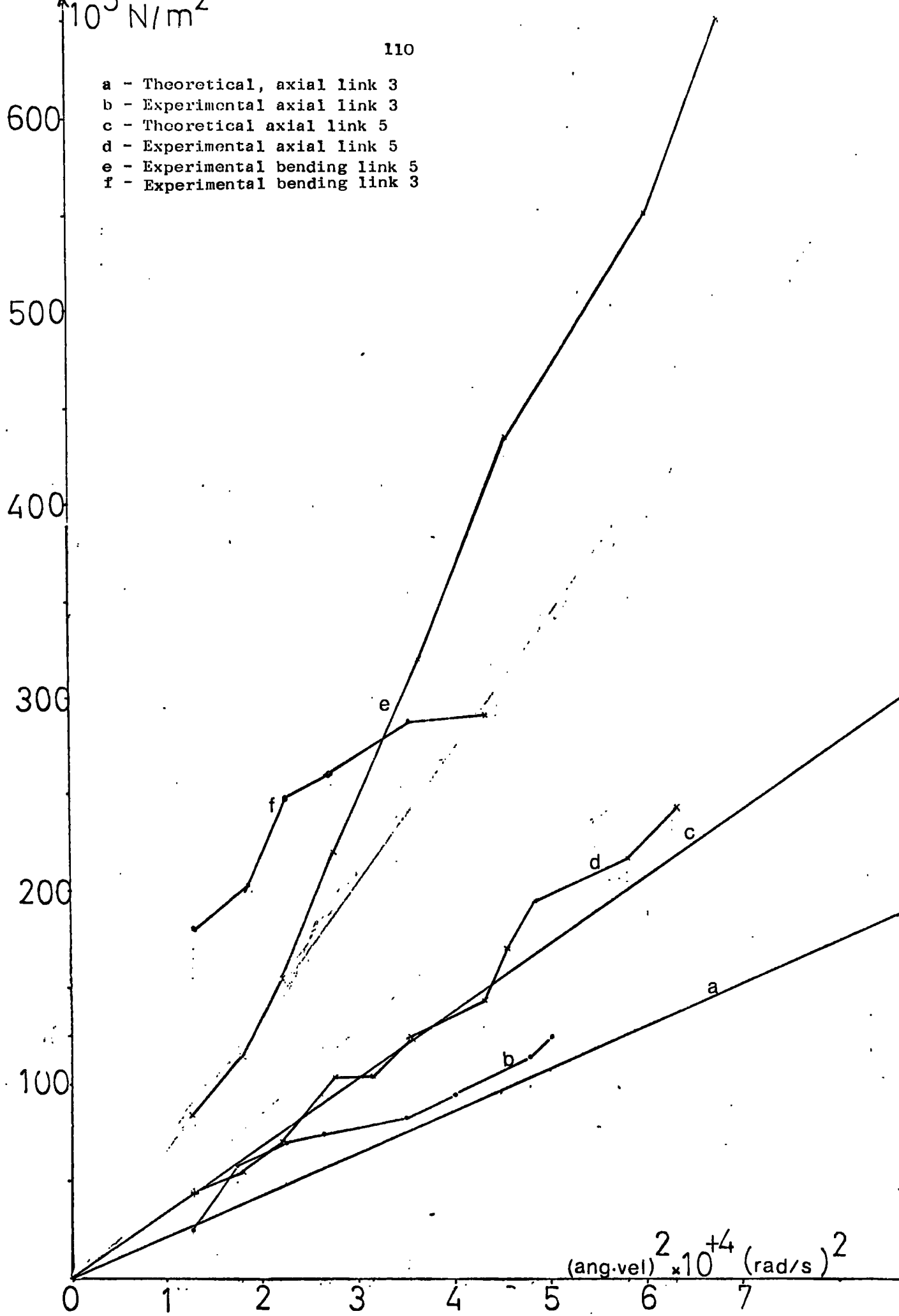
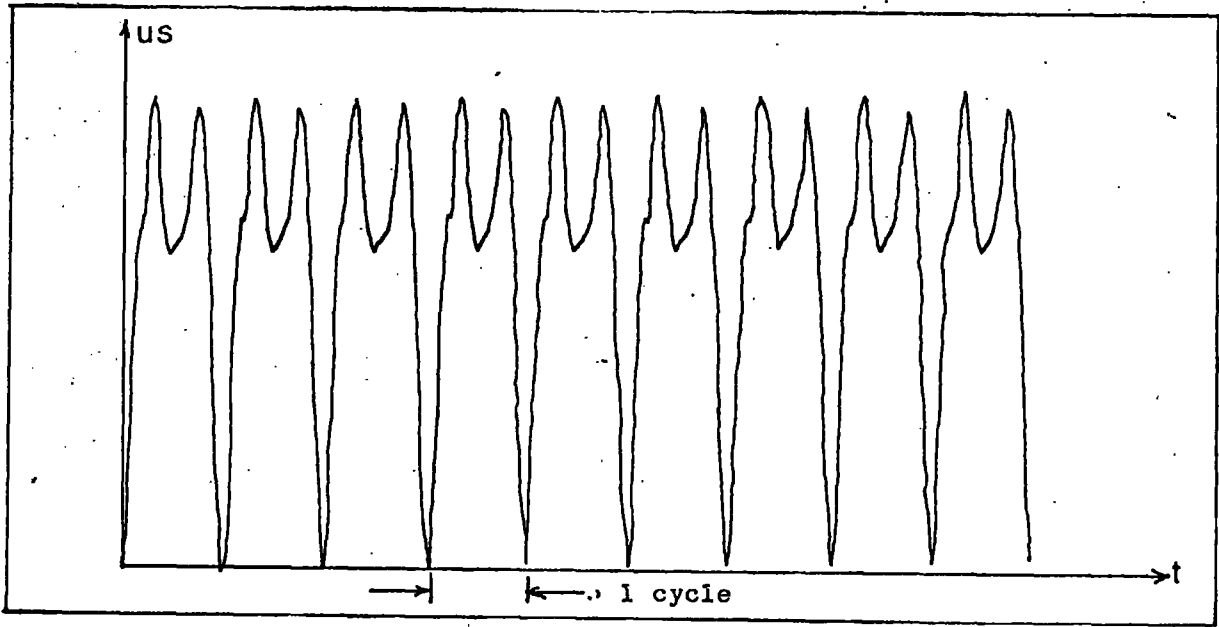
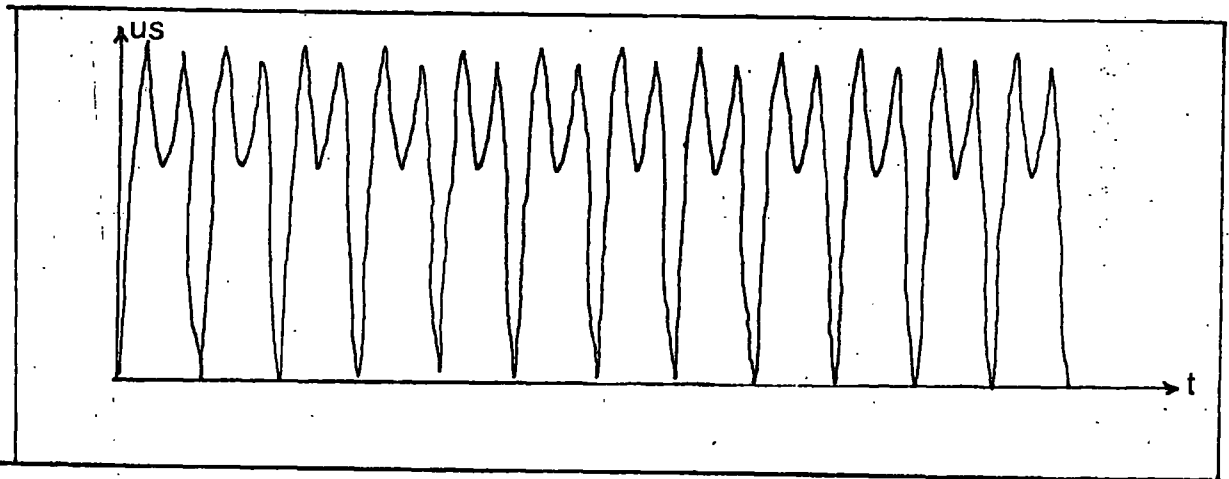


Fig. 4.13 Variation of peak to peak stresses in links 3 and 5 with the square of the crank speed

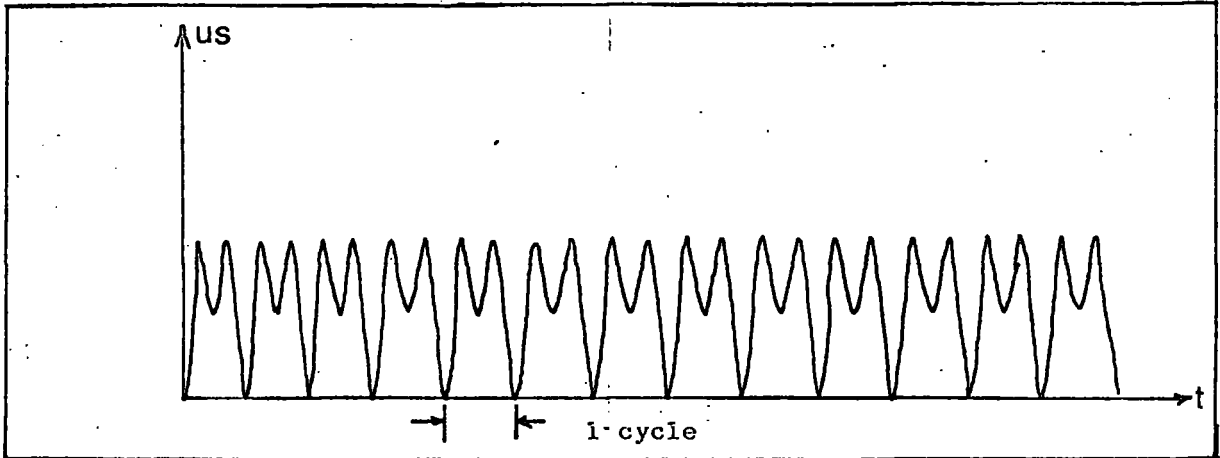
Fig. 4.14 Experimental strain patterns



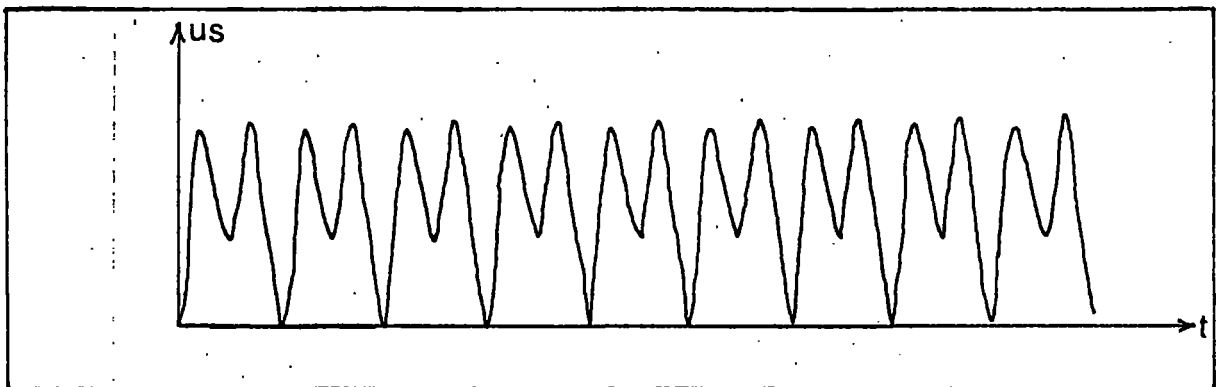
- a Record 80. Link 5. Experimental bending (z-direction) strain pattern. Crank speed = 1573 r.p.m. $\frac{1}{2}$ Bridge (120 Ω)₂ circuit. Peak to peak strain = 197.4 μ s, Peak to peak stress = 205×10^5 N/m²



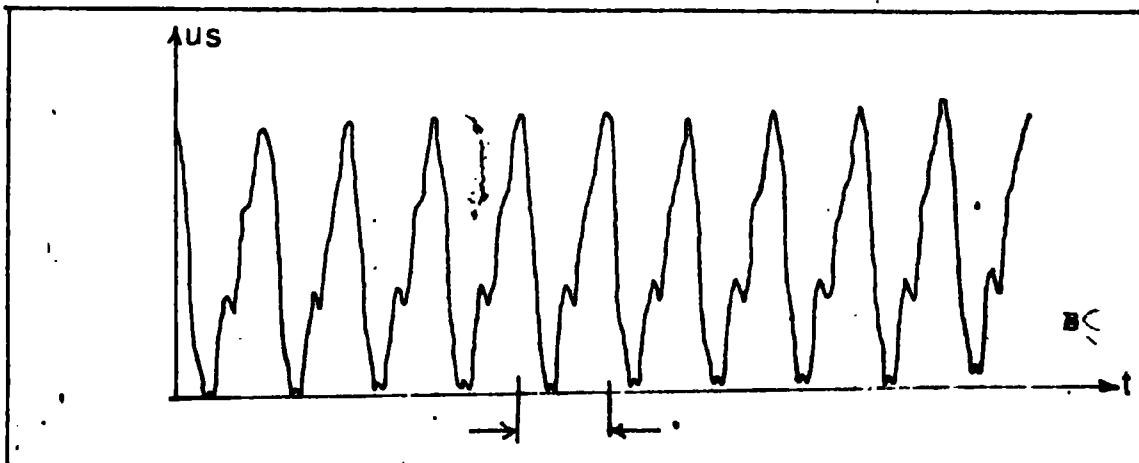
- b Record 99. Link 5. Experimental bending (z-direction) strain pattern. Crank speed = 2023 r.p.m. $\frac{1}{2}$ Bridge (120 Ω) circuit. Peak to peak strain = 417.5 μ s, Peak to peak stress = 433.8×10^5 N/m²



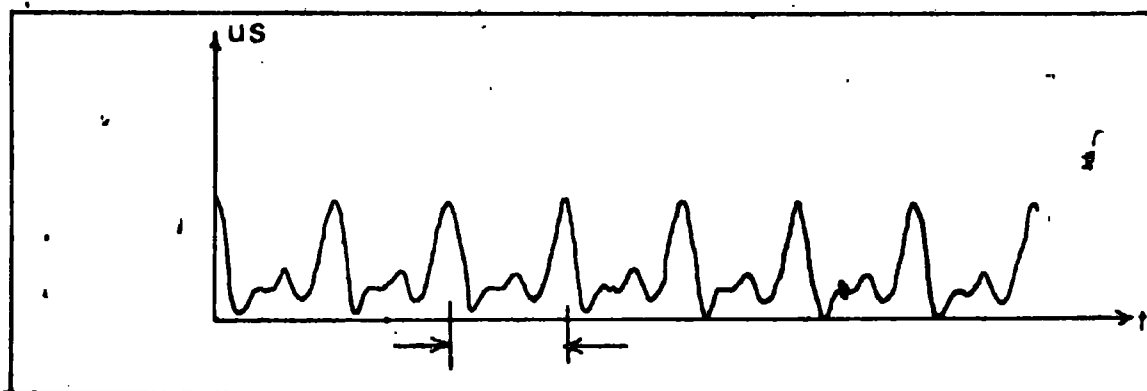
- c Record 131 Link 5 Experimental axial strain pattern. Crank speed = 2130
 $\frac{1}{2}$ Bridge (120 Ω) circuit. Peak to peak strain = 203.9 μs . Peak to peak
 stress = $211.8 \times 10^5 \text{ N/m}^2$



- d Record 16. Link 5. Experimental axial strain pattern. Crank speed = 1634 r.p.m.
 $\frac{1}{2}$ Bridge (120 Ω) circuit. Peak to peak strain = 86.7 μs , Peak to peak stress
 = $90 \times 10^5 \text{ N/m}^2$



- Record 49. Link 3. Experimental bending (z direction) strain pattern. Crank speed = 1770 r.p.m. $\frac{1}{2}$ Bridge (120) circuit. Peak to peak stress $291.2 \times 10^5 \text{ N/m}^2$



- ⌘ Record 13. Link 3. Experimental axial strain pattern. Crank speed = 1424 r.p.m. $\frac{1}{2}$ Bridge (120) circuit. Peak to peak strain = $48.5 \mu\text{s}$, peak to peak stress = $38.8 \times 10^5 \text{ N/m}^2$

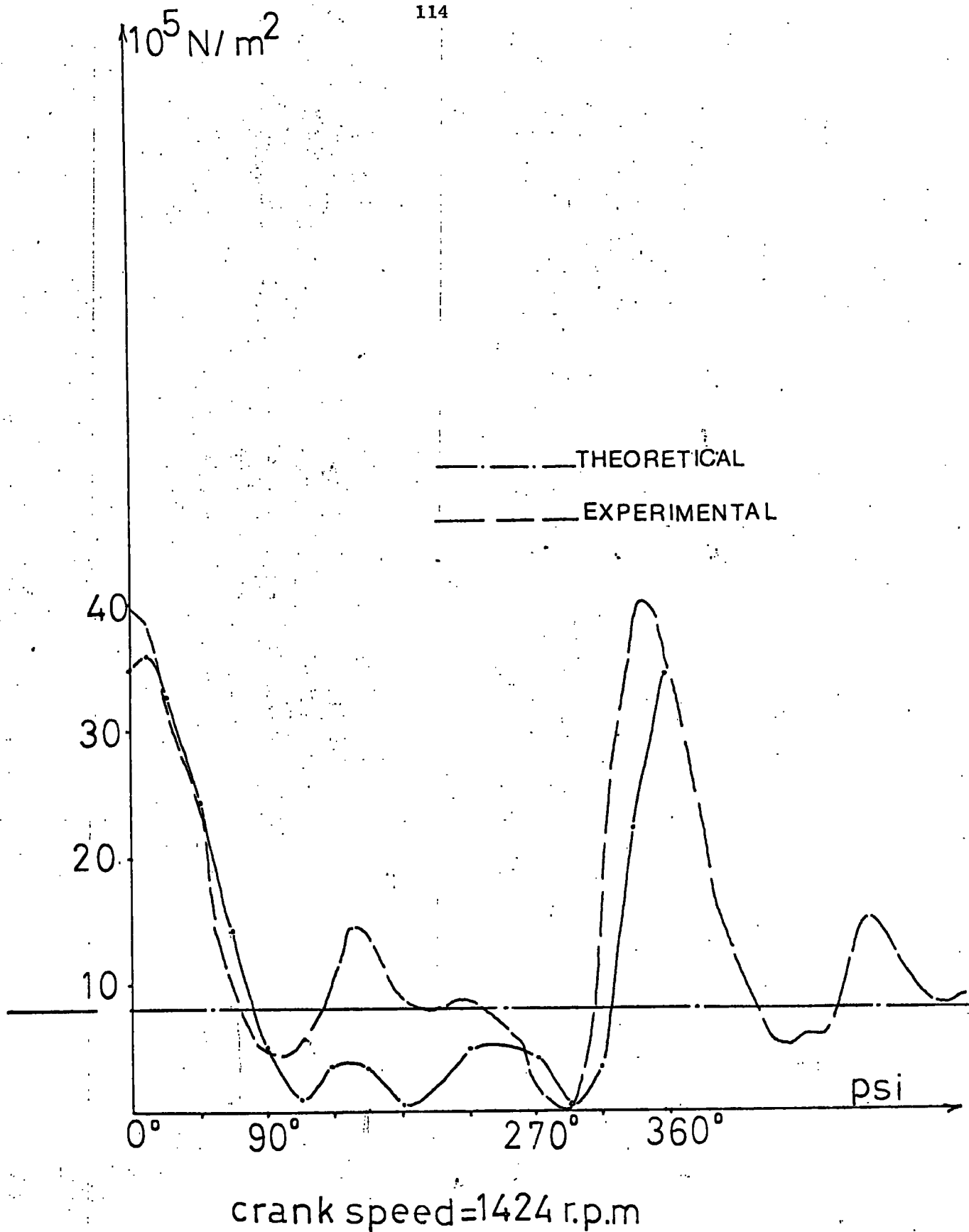


Fig. 4.15 Experimental and theoretical variation of axial stress in link 3 with the crank angle psi at a crank speed of 1424 r.p.m. (cross sectional area subject to stress = $14.95 \times 10^{-5} \text{ m}^2$)

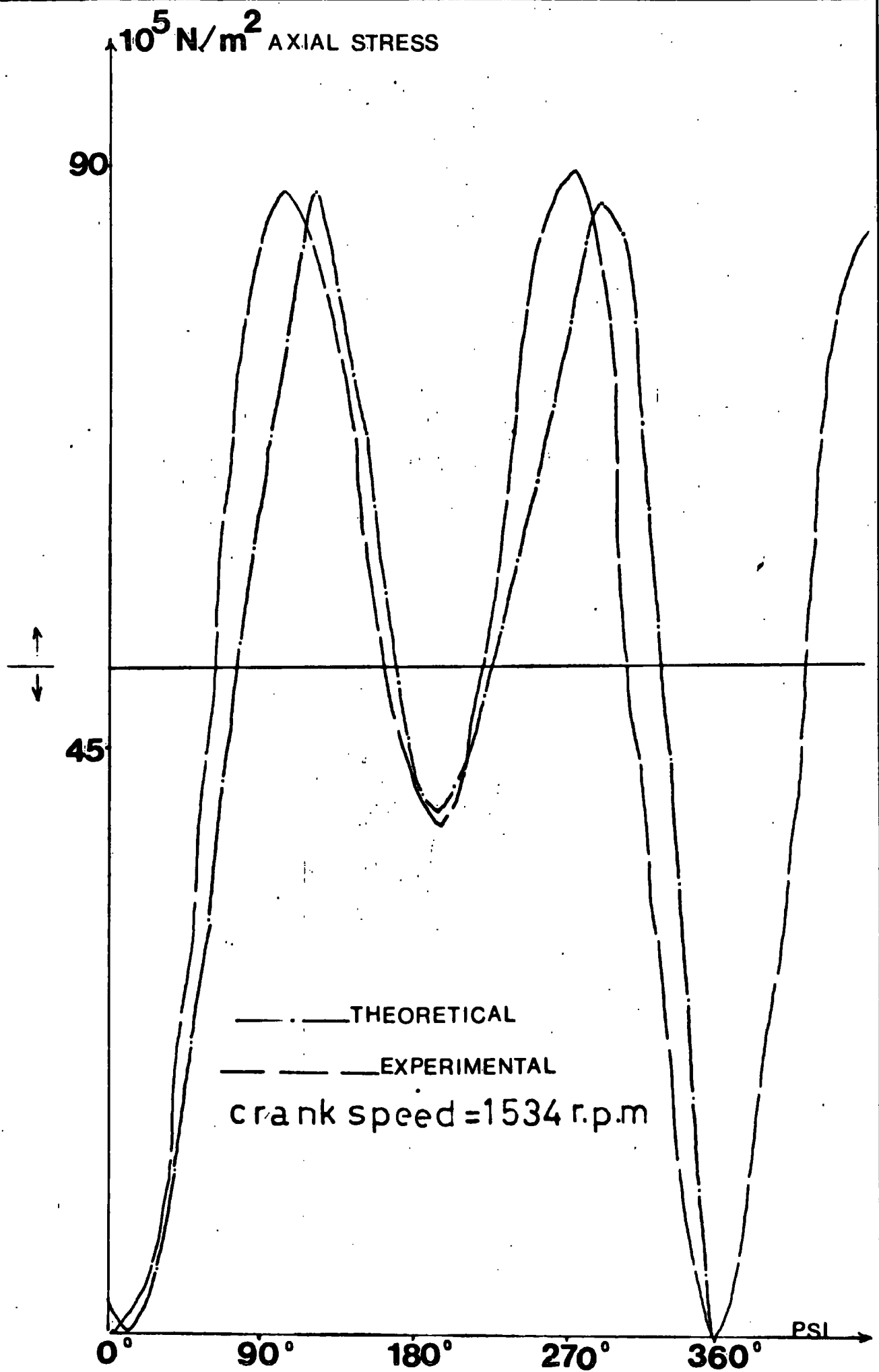


Fig. 4.16 Theoretical and experimental variation of axial stress in link 5 with the crank angle psi, at a crank speed of 1534 r.p.m.

Table 4.2

Record number	Link number	Motor scale	Nominal paper speed, mm/s.	uv. recorder speed pick-up signal, r.p.m.	Tachometer r.p.m.	From timer line 1 sec = mm.	1 cycle covers mm.	Type of strain measured	Bridge configuration	Initial range us.	range shifted to us.	Calibration us.	Calibration signal, mm.	Full scale deflection mm.	Record range mm.	Strain range us.	Stress range $\times 10^5$ N/mm ²
1-	5	220	111	1089	1080	118	6.5	Axial	Two Active arms.	300	300	100	50.5	151.5	30.5	30.2	31.4
2-	"	"	"	"	"	"	"	Bending	"	"	1000	"	"	"	26	85.8	89.1
3-	3	"	"	"	"	119	"	Axial	"	"	3000	"	50	150	31	30.9	24.7
4-	"	"	"	1037	"	121	7	"	"	3000	3000	1000	50.5	"	3.5	35	28
5-	"	"	"	1089	"	118	6.5	"	"	300	300	100	"	151.5	29.5	29.2	23.3
6-	"	"	"	"	"	"	"	Bending	"	"	3000	"	"	"	26	257.4	205.9
7-	5	200	333	1424	1440	356	15	"	"	3000	"	1000	50	150	46	153.3	159.3
8-	"	"	"	"	"	"	"	Axial	"	300	300	100	"	"	56	56	58.2
9-	"	"	111	1416	"	354	"	Bending	"	"	3000	"	"	"	15.5	155	161
10-	"	"	333	1424	"	356	"	"	"	"	1000	"	"	"	42.5	141.6	147.1
11-	3	"	"	1473	"	"	14.5	"	"	1000	"	300	46.0	153.3	95	309.8	247.8
12-	3	"	"	1424	"	"	15	"	"	"	3000	"	"	"	32	313.1	250.5
13-	3	"	"	"	"	"	"	Axial	"	300	1000	100	51.5	154.5	15	248.5	38.8

Record number	Link number	Motor scale	Nominal paper speed, mm/s.	uv. recorder speed pick-up signal, r.p.m.	Tachometer r.p.m.	From timer line 1 sec = mm.	1 cycle covers mm.	Type of strain measured	Bridge configuration	Initial range us.	range shifted to, us.	Calibration us.	Calibration signal, mm.	Full scale deflection mm.	Record range mm.	Strain range us.	Stress range $\times 10^5 N/m^2$.
14-	5	200	333	1416	1440	354	15	Axial	$\frac{1}{2}$ Two Active arms.	300	3000	100	51.5	154.5	7	67.9	70.6
15-	"	190	"	1517	1560	"	14	"	"	"	"	"	"	"	9.2	89.3	92.8
16-	"	"	"	1634	"	"	13	"	"	"	1000	"	"	"	26.8	86.7	90
17-	"	180	"	1709	1800	356	12.5	"	"	"	3000	"	"	"	12	116.5	121
18-	"	"	"	1780	"	"	12	"	"	"	"	"	"	"	"	"	"
19-	"	185	"	1770	1680	354	"	"	"	"	"	"	"	"	10	97	100.8
20-	"	175	"	2023	1980	"	10.5	"	"	"	"	"	"	"	14	136	141.3
21-	"	210	"	1256	1320	356	17	"	"	"	1000	"	"	"	14.5	46.9	48.7
22-	"	185	"	1709	1680	"	12.5	"	"	"	"	"	"	"	29.5	95.5	99.2
23-	"	220	111	1089	1080	118	6.5	"	"	"	"	"	"	"	11.5	37.2	38.6
24-	"	"	"	1108	"	120	"	"	"	"	"	"	"	"	"	"	"
25-	"	180	333	1770	1800	354	12	"	"	"	3000	"	"	"	12	116.5	121
26-	"	175	"	1942	1980	356	11	"	"	"	"	"	"	"	14	135.9	141.2

Record number	Link number	Motor scale	Nominal paper speed, mm/s.	uv. recorder speed pick-up signal, r.p.m.	Tachometer r.p.m.	From timer line 1 sec = mm.	1 cycle covers mm.	Type of strain measured	Bridge configuration	Initial range us.	range shifted to. us.	Calibration us.	Calibration signal, mm.	Full scale deflection mm.	Record range mm	Strain range us.	Stress range $\times 10^5$ N/m ² .
27-	5	170	333	2034	2040	356	10.5	Axial	2 Active arms	300	3000	100	51.5	154.5	15.5	150.5	156.4
28-	"	165	"	2023	2160	354	"	"	"	3000	"	1000	"	"	18.5	179.6	186.6
29-	"	"	"	1931	"	"	11	"	"	300	"	100	"	"	18	174.7	181.5
30-	3	190	"	1517	1560	"	14	"	"	"	"	"	"	"	10	97	77.6
31-	"	180	111	1785	1800	119	"	"	"	3000	"	1000	"	"	11.5	116.6	89.3
32-	"	175	333	1942	1920	356	11	"	"	300	1000	100	"	"	36	116.5	"
33-	"	170	"	2136	2040	"	10	"	"	"	3000	"	"	"	14.8	143.7	115
34-	"	165	"	2124	2160	354	"	"	"	3000	"	"	"	"	16	155.3	124.24
35-	5	170	"	1942	2040	356	11	"	"	300	"	"	"	"	16.2	157.3	163.4
36-	3	220	"	1062	1080	354	20	"	"	"	1000	"	"	"	15	48.5	38.8
37-	"	"	"	1089	"	"	19.5	"	"	"	"	"	"	"	6.5	21	16.8
38-	"	210	"	1214	1320	"	17.5	"	"	3000	3000	1000	"	"	7.5	72.8	58.2
39-	"	200	"	1416	1440	"	15	"	"	"	"	"	"	"	9.5	92.2	73.7

Record number	Link number	Motor scale	Nominal paper speed, mm/s.	uv. recorder speed pick-up signal, r.p.m.	Tachometer r.p.m.	From timer line 1 sec = mm.	1 cycle covers mm.	Type of strain measured	Bridge configuration	Initial range us.	range shifted to. us.	Calibration us.	Calibration signal, mm.	full scale deflection mm.	Record range mm.	Strain range us.	Stress range $\times 10^5$ N/m ² .
40-	3	190	333	1564	1560	352	13.5	Axial	$\frac{1}{2}$ Two Active arms	300	3000	100	51.5	154.5	9	87.4	69.9
41-	"	180	"	1780	1800	356	12	"	"	3000	"	1000	"	"	10	97	77.6
42-	"	175	"	1847	1980	354	11.5	"	"	"	"	"	"	"	13	126.2	101
43-	"	220	"	1062	1080	"	20	Bending	"	300	1000	100	"	"	73	236.2	188.9
44-	"	210	"	1249	1320	"	17	"	"	"	3000	"	"	"	27	262.1	209.7
45-	"	200	"	1355	1440	350	15.5	"	"	"	"	"	"	"	30.5	296.1	236.9
46-	"	190	"	1573	1560	354	13.5	"	"	"	"	"	"	"	31.5	305.8	244.6
47-	"	185	"	1709	1680	356	12.5	"	"	"	"	"	"	"	32.3	313.5	250.8
48-	"	180	"	1765	1800	353	12	"	"	"	"	"	"	"	37	359.2	287.3
49-	"	175	"	1770	1980	354	"	"	"	"	"	"	"	"	37.5	364	291.2
50-	"	190	"	1625	1560	352	13	"	"	"	"	"	"	"	35	339.8	271.8
51-	"	180	"	1770	1800	354	12	"	"	"	"	"	"	"	37.5	364	291.2
52-	"	220	"	1095	1080	356	19.5	"	"	"	1000	"	"	"	24	77.7	80.7

Record number	Link number	Motor scale	Nominal paper speed, mm/s.	uv. recorder speed pick-up signal, r.p.m.	Tachometer r.p.m.	From timer line 1 sec = mm.	1 cycle covers mm.	Type of strain measured	Bridge configuration	Initial range us.	range shifted to. us.	Calibration us.	Calibration signal, mm.	Full scale deflection mm.	Record range mm.	Strain range us.	Stress range $\times 10^5$ N/m ²
53-	5	210	333	1256	1320	356	17	Bending	2 Active arms	300	3000	100	51.5	154.5	12.5	121.3	126
54-	"	200	"	1424	1440	"	15	"	"	"	"	"	"	"	16	155.3	161.3
55-	"	195	"	1517	1500	354	14	"	"	"	"	"	"	"	18	174.7	181.5
56-	"	190	"	1582	1560	356	13.5	"	"	"	"	"	"	"	21.5	203.9	211.8
57-	"	185	"	1709	1680	356	12.5	"	"	"	"	"	"	"	26.5	257.3	267.3
58-	"	180	"	1837	1800	352	11.5	"	"	"	"	"	"	"	31	301	312.7
59-	"	190	"	1508	1560	"	14	"	"	"	"	"	"	"	22	213.6	221.9
60-	"	210	"	1214	1320	354	17.5	"	"	"	"	"	"	"	11	106.8	111
61-	"	220	"	1089	1080	"	19.5	"	"	"	1000	"	"	"	31	100.3	104.2
62-	"	"	"	1062	"	"	20	"	"	"	3000	"	"	"	8	77.6	80.6
63-	"	210	"	1287	1320	"	16.5	"	"	"	"	"	"	"	11	106.8	111
64-	"	200	"	1420	1440	355	15	"	"	"	"	"	"	"	15.5	150.5	156.3
65-	"	195	"	1465	1500	354	14.5	"	"	"	"	"	"	"	18.5	179.6	186.6

Record number	Link number	Motor scale	Nominal paper speed, mm/s.	uv. recorder speed pick-up signal, r.p.m.	Tachometer r.p.m.	From timer line 1 sec = mm.	1 cycle covers mm.	Type of strain measured	Bridge configuration	Initial range us.	range shifted to. us.	Calibration us.	Calibration signal, mm.	Full scale deflection mm.	Record range mm.	Strain range us.	Stress range $\times 10^5 \text{ N/m}^2$.
66-	5	190	333	1517	1560	354	14	Bending	$\frac{1}{2}$ Two Active arms	300	3000	100	51.5	154.5	22	213.6	221.9
67-	"	185	"	1770	1680	"	12	"	"	"	"	"	"	"	26.5	257.3	267.3
68-	"	180	"	1780	1800	356	"	"	"	"	"	"	"	"	31	301	312.7
69-	3	220	"	1077	1080	359	20	"	"	"	"	"	"	"	22.5	218.4	174.7
70-	"	210	"	1256	1320	356	17	"	"	"	"	"	"	"	25.2	244.6	195.7
71-	"	200	"	1424	1440	"	15	"	"	"	"	"	"	"	29.5	286.4	229
72-	"	195	"	1526	1500	"	14	"	"	"	"	"	"	"	32	310.7	248.5
73-	"	190	"	1643	1560	"	13	"	"	"	"	"	"	"	34	330	264
74-	"	185	"	1699	1680	354	12.5	"	"	"	"	"	"	"	"	"	"
75-	"	180	"	1780	1800	356	12	"	"	"	"	"	"	"	36	349.5	279.6
76-	5	220	"	1068	1080	"	20	"	"	"	1000	"	"	"	22.5	72.8	75.6
77-	"	210	"	1221	1320	"	17.5	"	"	"	"	"	"	"	30.5	98.7	102.5
78-	"	200	"	1416	1440	354	15	"	"	"	"	"	"	"	43	139.1	144.5

Record number	Link number	Motor scale	Nominal paper speed, mm/s.	uv. recorder speed pick-up signal, r.p.m.	Tachometer r.p.m.	From timer line 1 sec = mm.	1 cycle covers mm.	Type of strain measured	Bridge configuration	Initial range us.	range shifted to. us.	Calibration us.	Calibration signal, mm.	Full scale deflection mm.	Record range mm.	Strain range us.	Stress range $\times 10^5$ N/mm ² .
79-	5	195	333	1473	1500	356	14.5	Bending	2 Active arms	300	1000	100	51.5	154.5	49	158.6	164.8
80-	"	190	"	1573	1560	354	13.5	"	"	"	"	"	"	"	61	197.4	205
81-	"	"	"	1634	"	"	13	"	"	"	"	"	"	"	20.5	199	206.7
82-	"	185	"	1770	1680	"	12	"	"	"	"	"	"	"	25	242.7	252.1
83-	"	180	"	1847	1800	"	11.5	"	"	"	"	"	"	"	31	301	312.7
84-	"	175	"	1931	1980	"	11	"	"	"	"	"	"	"	36.5	354.3	368.1
85-	"	220	"	1068	1080	356	20	"	"	"	"	"	"	"	8	77.6	80.7
86-	"	190	"	1573	1560	354	13.5	"	"	"	"	"	"	"	22.5	213.6	221.9
87-	"	175	"	1826	1980	350	11.5	"	"	"	"	"	"	"	37.5	364	378
88-	"	220	"	1062	1080	354	20	Axial	"	"	"	"	"	"	5	48.5	50.4
89-	"	210	"	1256	1320	356	17	"	"	"	"	"	"	"	6	58.2	60.5
90-	"	200	"	1384	1440	346	15	"	"	"	"	"	"	"	8	77.7	80.7
91-	"	190	"	1634	1560	354	13	"	"	"	"	"	"	"	11	106.8	111

Record number	Link number	Motor scale	Nominal paper speed, mm/s.	uv. recorder speed pick-up signal, r.p.m.	Tachometer r.p.m.	From timer line I sec = mm.	I cycle covers mm.	Type of strain measured	Bridge configuration	Initial range us.	range shifted to. us.	Calibration us.	Calibration signal, mm.	Full scale deflection mm.	Record range mm.	Strain range us.	Stress range $\times 10^5$ N/m ² .
92-	5	185	333	1699	1680	354	12.5	Axial	Two Active arms	300	3000	100	51.5	154.5	12	116.5	121
93-	"	180	"	1770	1800	"	12	"	"	"	"	"	"	"	13	126.2	131.1
94-	"	220	"	1062	1080	"	20	Bending	"	"	"	"	"	"	7	67.9	70.5
95-	"	200	"	1370	1440	"	15.5	"	"	"	"	"	"	"	16	155.3	161.3
96-	"	190	"	1517	1560	"	14	"	"	"	"	"	"	"	21	203.9	211.8
97-	"	180	"	1699	1800	"	12.5	"	"	"	"	"	"	"	31	301	312.7
98-	"	175	"	1847	1980	"	11.5	"	"	"	"	"	"	"	37	359.2	373.2
99-	"	170	"	2023	2040	"	10.5	"	"	"	"	"	"	"	43	417.5	433.8
100-	"	220	"	1062	1080	"	20	"	"	"	"	"	"	"	9	87.4	90.8
101-	"	200	"	1416	1440	"	15	"	"	"	"	"	"	"	18.5	179.6	186.6
102-	"	190	"	1770	1560	"	13.5	"	"	"	"	"	"	"	27.5	267	277.4
103-	"	180	"	"	1800	"	12	"	"	"	"	"	"	"	36	349.5	363.1
104-	"	175	"	1847	1920	"	11.5	"	"	"	"	"	"	"	41.5	403	418.7

Record number	Link number	Motor scale	Nominal paper speed, mm/s.	uv. recorder speed pick-up signal, r.p.m.	Tachometer r.p.m.	From timer line I sec = mm.	I cycle covers mm.	Type of strain measured	Bridge configuration	Initial range us.	range shifted to. us.	Calibration us.	Calibration signal, mm.	Full scale deflection mm.	Record range mm.	Strain range us.	Stress range $\times 10^5$ N/m ² .
105-	5	170	333	2023	2040	354	10.5	Bending	$\frac{1}{2}$ Two Active Arms	300	3000	100	51.5	154.5	48	466	484.2
106-	"	165	"	2236	2160	"	9.5	"	"	"	"	"	"	"	55	534	554.8
107-	"	"	"	2124	"	"	10	"	"	"	"	"	"	"	56	543.7	564.9
108-	"	170	"	2023	2040	"	10.5	"	"	"	"	"	"	"	48.5	470.9	489.3
109-	"	175	"	1847	1980	"	11.5	"	"	"	"	"	"	"	40	388.3	403.4
110-	"	160	"	2236	2375	"	9.5	"	"	"	"	"	"	"	63	611.6	635.4
111-	"	220	"	1089	1080	"	19.5	Axial	"	"	"	"	"	"	5	48.5	50.4
112-	"	210	"	1287	1320	"	16.5	"	"	"	"	"	"	"	6	58.2	60.5
113-	"	200	"	1416	1440	"	15	"	"	"	"	"	"	"	8	77.7	80.7
114-	"	190	"	1634	1560	"	13	"	"	"	"	"	"	"	11	106.8	111
115-	"	180	"	1847	1800	"	11.5	"	"	"	"	"	"	"	13.5	131	136.1
116-	"	175	"	1931	1980	"	11	"	"	"	"	"	"	"	15	145.6	151.3
117-	"	170	"	2023	2040	"	10.5	"	"	"	"	"	"	"	17.5	170	176.6

Record number	Link number	Motor scale	Nominal paper speed, mm/s.	uv. recorder speed pick-up signal, r.p.m.	Tachometer r.p.m.	From timer line 1 sec = mm.	1 cycle covers mm.	Type of strain measured	Bridge configuration	Initial range us.	range shifted to. us.	Calibration us.	Calibration signal, mm.	Full scale deflection mm.	Record range mm.	Strain range us.	Stress range $\times 10^5$ N/m ²
118-	5	165	333	2124	2160	354	10	Axial	$\frac{1}{2}$ Two Active arms	300	3000	100	51.5	154.5	19	184.5	191.7
119-	"	160	"	2236	2375	"	9.5	"	"	"	"	"	"	"	21.5	208.7	216.8
120-	"	155	"	2360	2450	"	9	"	"	"	"	"	"	"	24	233	242
121-	"	153	"	"	2500	"	"	"	"	"	"	"	"	"	23	223.3	232
122-	"	190	111	1785	1600	119	4	Bending	"	"	"	"	52	156	21.2	203.8	211.7
123-	"	150	333	2499	2550	354	8.5	"	"	"	1000	"	51.5	154.5	19.5	631	655.7
124-	"	220	"	1068	1075	356	20	Axial	"	"	"	"	"	"	15.5	50.1	52.1
125-	"	180	"	1775	1810	355	12	"	"	"	3000	"	"	"	14.5	140.8	146.2
126-	"	"	"	1847	"	354	11.5	"	"	"	"	"	"	"	12.1	117.5	122
127-	"	190	"	1639	1600	355	13	"	"	"	"	"	"	"	11.1	107.7	112
128-	"	200	"	1370	1355	354	15.5	"	"	"	"	"	"	"	9	87.4	90.8
129-	"	190	"	1643	1600	356	13	Bending	"	"	"	"	"	"	21	203.9	211.8
130-	"	170	"	2094	2050	"	10.2	Axial	"	"	"	"	"	"	18.5	179.6	186.6

Record number	Link number	Motor scale	Nominal paper speed, mm/s.	uv. recorder speed pick-up signal, r.p.m.	Tachometer r.p.m.	From timer line 1 sec = mm.	1 cycle covers mm.	Type of strain measured	Bridge configuration	Initial range us.	range shifted to. us.	Calibration us.	Calibration signal, mm.	Full scale deflection mm.	Record range mm.	Strain range us.	Stress range $\times 10^5$ N/m ² .
131-	5	165	333	2130	2124	355	10	Axial	$\frac{1}{2}$ Two Active Arms	300	3000	100	51.5	154.5	21	203.9	211.8
132-	"	220	"	1068	1075	356	20	"	"	"	1000	"	"	"	15	48.5	50.4
133-	"	170	"	2124	2050	354	10	Bending	"	"	10000	"	"	"	12	388.3	403.5
134-	"	160	"	2373	2375	356	9	"	"	"	"	"	"	"	15.2	491.9	511
135-	"	155	"	2421	2375	355	8.8	"	"	"	"	"	"	"	17	550.1	571.6
136-	"	190	"	1643	1600	356	13	"	"	"	3000	"	"	"	21	203.9	211.8
137-	"	220	111	1190	1075	119	6	"	"	"	"	"	"	"	9.5	92.2	95.8
138-	"	210	"	1298	1230	"	5.5	"	"	"	"	"	"	"	12	116.5	121
139-	"	200	"	1440	1355	120	5	"	"	"	"	"	"	"	16	155.3	161.4
140-	"	170	333	1942	2050	356	11	"	"	"	10000	"	"	"	11.2	362.5	376.6
141-	"	180	"	1780	1810	"	12	"	"	"	"	"	"	"	9	291.3	302.6
142-	"	155	"	2373	2450	"	9	"	"	"	30000	"	"	"	6.3	611.6	635.5
143-	"	145	"	2499	-	354	8.5	"	"	"	10000	"	"	"	21.5	695.8	722.9

Record number	Link number	Strain gauges	Bridge configuration	Type of strain measured	Calibration us.	Initial range us.	Range shifted to us.	Calibration signal mm.	Full scale deflection mm.
1	3	AB	$\frac{1}{2}$ 2 Active arms	Axial	100	300	3000	54.5	163.5
2	3	XY	"	Bending	"	"	"	"	"
3	3	XY	"	"	"	"	10000	"	"
4	5	CC	"	"	"	"	30000	"	"
5	5	CC	"	"	"	"	"	"	"
6	5	CC	"	"	"	"	"	"	"
7	5	CC	"	"	"	"	"	"	"
8	5	CC	"	"	"	"	100000	"	"
9	5	CC	"	"	"	"	10000	"	"
10	5	CC	"	"	"	"	3000	"	"
11	3	XY	"	"	"	"	10000	"	"
12	3	AB	"	"	"	"	1000	"	"

Table 4.3

Record number	Link number	Strain gauges	Bridge configuration	Type of strain measured	Calibration us.	Initial range us.	Range shifted to us.	Calibration signal mm.	Full scale deflection mm.
13	5	CC	$\frac{1}{4}$ 2 Active arms	Bending	100	300	10000	54.5	163.5
14	3	XY	"	Axial	30	100	1000	49	163.3
15	3	"	"	"	100	300	"	54.5	163.5
16	3	AB	"	"	"	"	"	"	"
17	3	"	"	"	"	"	"	"	"
18	5	CC	"	"	"	"	3000	"	"
19	5	"	"	"	"	"	30000	"	"
20	5	"	"	"	"	"	"	"	"
21	5	"	"	"	"	"	10000	"	"
22	5	"	"	"	"	"	"	"	"
23	3	XY	"	"	"	"	3000	"	"
24	3	AB	"	"	"	"	300	"	"

Record No. - 1

Applied Force N	Torque Nm	Record trace deflection mm	Strain us.	Stress $\times 10^5$ N/m ²
98	29.4	10	91.7	73.4
196	58.8	20	183.5	146.8
215.6	64.7	21	192.7	154.2
235.2	70.6	22.5	206.4	165.1
254.8	76.4	24	220.2	176.2
274.4	82.3	26	238.5	190.8

Record No. - 2

Applied Force N	Torque Nm.	Record trace deflection mm	Strain us.	Stress $\times 10^5$ N/m ²
19.6	5.9	7	64.2	51.4
39.2	11.8	15	137.6	110
58.8	17.7	22	201.8	161.5
68.6	20.6	26	238.5	190.8
78.4	23.5	29	266	212.8
88.2	26.5	32	293.6	234.9
107.8	32.3	38	348.6	278.9
117.6	35.3	42	385.3	308.2

Record No. - 3

Applied Force N	Torque Nm	Record trace deflection mm	Strain us.	Stress $\times 10^5$ N/m ²
98	29.4	9	275.2	220.2
117.6	35.3	10	305.8	244.6
137.2	41.2	12	367	293.6
156.8	47	14	428.1	342.5
166.6	50	15	458.7	367
176.4	52.9	18	550.5	440.4
196	58.8	18.5	565.7	452.6
205.8	61.7	19	581	464.8
215.6	64.7	20	611.6	489.3

Record No. - 4

Applied Force N	Torque Nm.	Record trace deflection mm	Strain us.	Stress $\times 10^5$ N/m ²
49	14.7	3.5	321.1	333.6
147	44.1	13.5	1238.5	1286.8
245	73.5	23	2110	2192.4
264.6	79.4	25	2293.6	2383
284.2	85.3	27	2477	2573.6
303.8	91.1	29	2660.5	2764.3

Record No. - 5				
Applied Force N	Torque Nm	Record trace deflection mm	Strain us.	Stress $\times 10^5$ N/m ²
98	29.4	7.5	688	714.9
147	44.1	11.5	1055	1096.2
166.6	50	12.5	1146.8	1191.5
186.2	55.9	16	1467.9	1525.1
205.8	61.7	18	1651.4	1715.8

Record No. - 6				
Applied Force N	Torque Nm.	Record trace deflection mm	Strain us.	Stress $\times 10^5$ N/m ²
49	14.7	3.5	321.1	333.6
147	44.1	13	1192.6	1239.2
245	73.5	22.5	2064.2	2144.7
264.6	79.4	24.5	2247.7	2335.4
284.2	85.2	27	2477	2573.6
303.8	91.1	29	2660.5	2764.3

Record No. - 7				
Applied Force N	Torque Nm	Record trace deflection mm	Strain us.	Stress $\times 10^5$ N/m ²
49	14.7	4	366.9	381.3
147	44.1	13	1192.7	1239.2
245	73.5	22	2018.3	2097
264.6	79.4	24	2201.8	2287.7
284.2	85.2	25.5	2339.4	2430.7
303.8	91.1	26.5	2431.2	2526

Record No. - 8				
Applied Force N	Torque Nm.	Record trace deflection mm	Strain us.	Stress $\times 10^5$ N/m ²
98	29.4	3	917.4	953.2
147	44.1	3.5	1070.3	1112
166.6	50	4	1223.2	1271
186.2	55.9	4.5	1376.1	1429.8
205.8	61.7	5	1529	1588.7
225.4	67.6	5.5	1682	1747.5
245	73.5	6	1834.8	1906.4

Record No. - 9

Applied Force N	Torque Nm	Record trace deflection mm	Strain us.	Stress $\times 10^5$ N/m ²
19.6	5.9	2	61.1	63.5
39.2	11.7	4	122.3	127
58.8	17.6	8	244.6	254.2
78.4	23.5	12	367	381.3
98	29.4	17	520	540.1
117.6	35.3	22	672.8	699

Record No. - 10

Applied Force N	Torque Nm.	Record trace deflection mm	Strain us.	Stress $\times 10^5$ N/m ²
19.6	5.9	6.5	59.6	62
39.2	11.7	22	201.8	209.7
49	14.7	30.5	279.8	290.7
58.8	17.6	41	376.1	390.8

Record No. - 11				
Applied Force N	Torque Nm	Record trace deflection mm	Strain us.	Stress $\times 10^5$ N/m ²
19.6	5.9	2.5	76.5	61.1
29.4	8.8	3.5	107	85.6
49	14.7	6	183.5	146.8
68.6	20.6	9	275.2	220.2
78.4	23.5	10	305.8	244.6
88.2	26.5	11	336.4	269.1
107.8	32.3	12.5	382.2	305.8

Record No. - 12				
Applied Force N	Torque Nm.	Record trace deflection mm	Strain us.	Stress $\times 10^5$ N/m ²
19.6	5.9	3	9.17	7.3
39.2	11.7	6.5	19.9	15.9
49	14.7	8.5	26	20.8
58.8	17.6	10	30.6	24.5
78.4	23.5	13.5	41.3	33

Record No. - 13

Applied Force N	Torque Nm	Record trace deflection mm	Strain us.	Stress $\times 10^5$ N/m ²
49	14.7	8.5	259.9	270
68.6	20.6	14	428.1	444.8
88.2	26.5	19.5	596.3	619.6
107.8	32.3	25	764.5	794.3
127.4	38.2	30	917.4	953.1

Record No. - 14

Applied Force N	Torque Nm.	Record trace deflection mm	Strain us.	Stress $\times 10^5$ N/m ²
98	29.4	46	140.8	112.7
117.6	35.3	55	168.4	134.7
137.2	41.1	64	195.9	156.7
156.8	47	72.5	222	177.6

Record No. - 15				
Applied Force N	Torque Nm	Record trace deflection mm	Strain us.	Stress $\times 10^5$ N/m ²
19.6	5.9	9.5	29	23.2
39.2	11.7	20	61.1	48.9
58.8	17.6	29.5	90.2	72.1
78.4	23.5	40	122.3	97.9
88.2	26.5	45.5	139.1	111.3
98	29.4	51	155.9	124.8
117.6	35.3	64	195.7	156.6

Record No. - 16				
Applied Force N	Torque Nm.	Record trace deflection mm	Strain us.	Stress $\times 10^5$ N/m ²
98	29.4	24	73.4	58.7
117.6	35.3	31	94.8	75.8
137.2	41.2	38	116.2	93
156.8	47	46	140.6	112.5

Record No. - 17

Applied Force N	Torque Nm	Record trace deflection mm	Strain us.	Stress $\times 10^5$ N/m ²
19.6	5.9	2	6.1	4.9
39.2	11.7	6	18.3	14.7
58.8	17.6	13.5	41.3	33
78.4	23.5	21.5	65.8	52.6
98	29.4	30	91.7	73.4
117.6	35.3	40	122.3	97.9

Record No. - 18

Applied Force N	Torque Nm.	Record trace deflection mm	Strain us.	Stress $\times 10^5$ N/m ²
19.6	5.9	2.5	22.9	23.8
39.2	11.7	10.5	96.3	100
58.8	17.6	22	201.8	209.7
68.6	20.6	22	201.8	209.7
78.4	23.5	24.5	224.8	233.5
98	29.4	31.5	289	300.3

Record No. - 19

Applied Force N	Torque Nm	Record trace deflection mm	Strain us.	Stress $\times 10^5$ N/m ²
98	29.4	3	275.2	286
147	44.1	5.5	504.6	524.3
166.6	50	6	550.5	571.9
186.2	55.8	7	642.2	667.2
205.8	61.7	8	733.9	762.6
225.4	67.6	9	825.7	857.9
245	73.5	9.5	871.5	905.5

Record No. - 20

Applied Force N	Torque Nm.	Record trace deflection mm	Strain us.	Stress $\times 10^5$ N/m ²
49	14.7	2	183.5	190.6
147	44.1	6.5	596.3	619.6
245	73.5	10.5	963.3	1000.9
264.6	79.4	-	-	-

Record No. - 21

Applied Force N	Torque Nm	Record trace deflection mm	Strain us.	Stress $\times 10^5$ N/m ²
98	29.4	11	336.4	349.5
147	44.1	18	550.5	571.9
166.6	50	20	611.6	635.5
186.2	55.9	23	703.3	730.8
205.8	61.7	26	795.1	826.1
225.4	62.6	29	886.8	921.4
235.2	70.5	31	948	985
245	73.5	34	1039.7	1080.3

Record No. - 22

Applied Force N	Torque Nm.	Record trace deflection mm	Strain us.	Stress $\times 10^5$ N/m ²
49	14.7	4.5	137.6	143
68.6	20.6	7	214	222.4
88.2	26.5	10	305.8	317.7
107.8	32.3	13	397.5	413
205.8	61.7	21.5	657.5	683.1

Record No. - 23

Applied Force N	Torque Nm	Record trace deflection mm	Strain us.	Stress $\times 10^5$ N/m ²
98	29.4	10.5	96.3	77
117.6	35.3	19	174.3	139.4
137.2	41.2	21.5	197.2	157.8
156.8	47	24.5	224.8	179.8
176.4	52.9	28	256.9	205.5
186.2	55.9	29	266	212.8
196	58.8	31	284.4	227.5
205.8	61.7	34	311.9	249.5

Record No. - 24

Applied Force N	Torque Nm.	Record trace deflection mm	Strain us.	Stress $\times 10^5$ N/m ²
19.6	5.9	6	5.5	4.4
39.2	11.7	25	22.9	18.3
58.8	17.6	50	45.9	36.7
78.4	23.5	77	70.6	56.5
98	29.4	115	105.5	84.4

Record No. - 25

Applied Force N	Torque Nm	Record trace deflection mm	Strain us.	Stress $\times 10^5$ N/m ²
98	29.4	8	733.9	762
196	58.8	17.5	1605.5	1668.1
215.6	64.7	20	1834.9	1906.4
264.6	79.4	24.5	2247.7	2335.4

Record No. - 26

Applied Force N	Torque Nm.	Record trace deflection mm	Strain us.	Stress $\times 10^5$ N/m ²
98	29.4	10.5	321.1	256.9
117.6	35.3	12	367	293.6
137.2	41.1	14	428.1	342.5
147	44.1	15	458.7	367
156.8	47	16	489.3	391.4
176.4	52.9	16	489.3	391.4
186.2	55.9	17.5	535.1	428.1

Record No. - 27

Applied Force N	Torque Nm	Record trace deflection mm	Strain us.	Stress $\times 10^5$ N/m ²
98	29.4	9.5	290.5	232.4
117.6	35.3	11	336.4	269.1
127.4	38.2	11.5	351.7	281.3
137.2	41.1	12	367	293.6
156.8	47	13.5	412.8	330.3

Record No. - 28

Applied Force N	Torque Nm.	Record trace deflection mm	Strain us.	Stress $\times 10^5$ N/m ²
98	29.4	17.5	160.5	128.4
196	58.8	34	311.9	249.5
215.6	64.7	39	357.8	286.2

Chapter 5 - Discussion of Results

5.1 Determination of Axial working stress for link 5 - A theoretical approach

Load and stress variation in link 5 have been theoretically determined in chapter 3. Before comparing the experimental and theoretical stress variation in detail, the following analytical analysis is performed on the link to determine the safe working axial stress line assuming that the machine is designed for a crank speed of 4000 r.p.m. and the links are perfectly elastic, homogeneous and isotropic. The surface roughness and eccentricity in the bore axes have been neglected. The joints are taken to be ideal without any play (play in the joints introduces a mechanical error of an appreciable amount - because of hydrodynamic action of the lubricant the pin axis will not touch the end bore circle when the mechanism is in motion). From Fig. (5.1)-b, the minimum cross sectional area for link 5 is approximately $4 \times 10^{-5} \text{ m}^2$ (cross-section XX) while the maximum cross sectional area is approximately $6.32 \times 10^{-5} \text{ m}^2$ (cross-section ZZ). The ratio of maximum cross-sectional area to minimum cross-sectional area being 1.58. The actual axial loading diagram for the link is shown in Fig. (5.2a) for a crank speed of 4000 r.p.m. The stress variation for cross-section XX at the same crank speed is shown in Fig. (5.2b). The stress waveform is complex and an idealized model for the stress variation is necessary to determine the fatigue strength and the safe working stress line. Assuming a sinusoidal model, the stress variation can be expressed by the following equation:

$$\sigma = \sigma_m + \sigma_r \sin \frac{2\pi t}{T} \dots\dots\dots (5.1)$$

where σ_m = mean stress

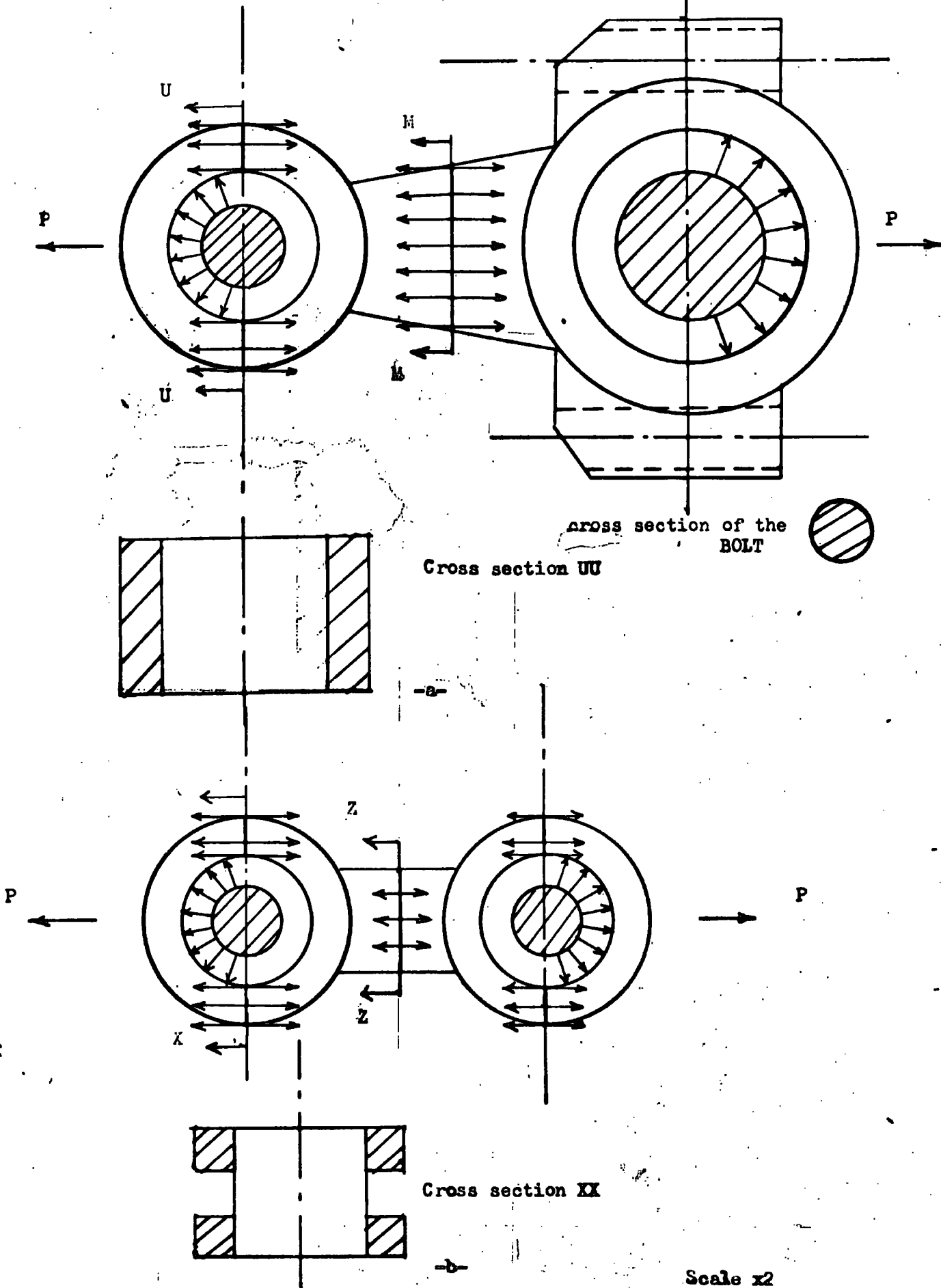
σ_r = variable stress

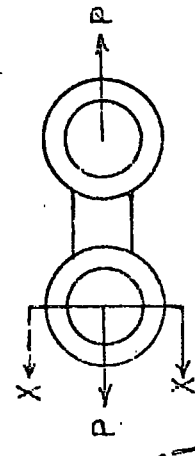
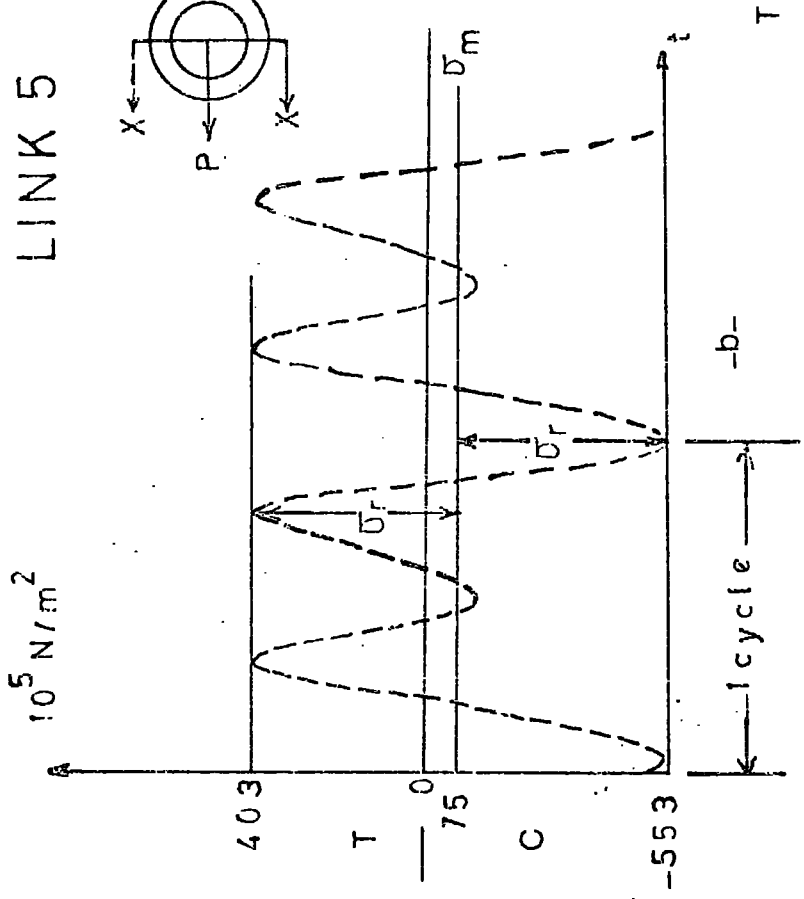
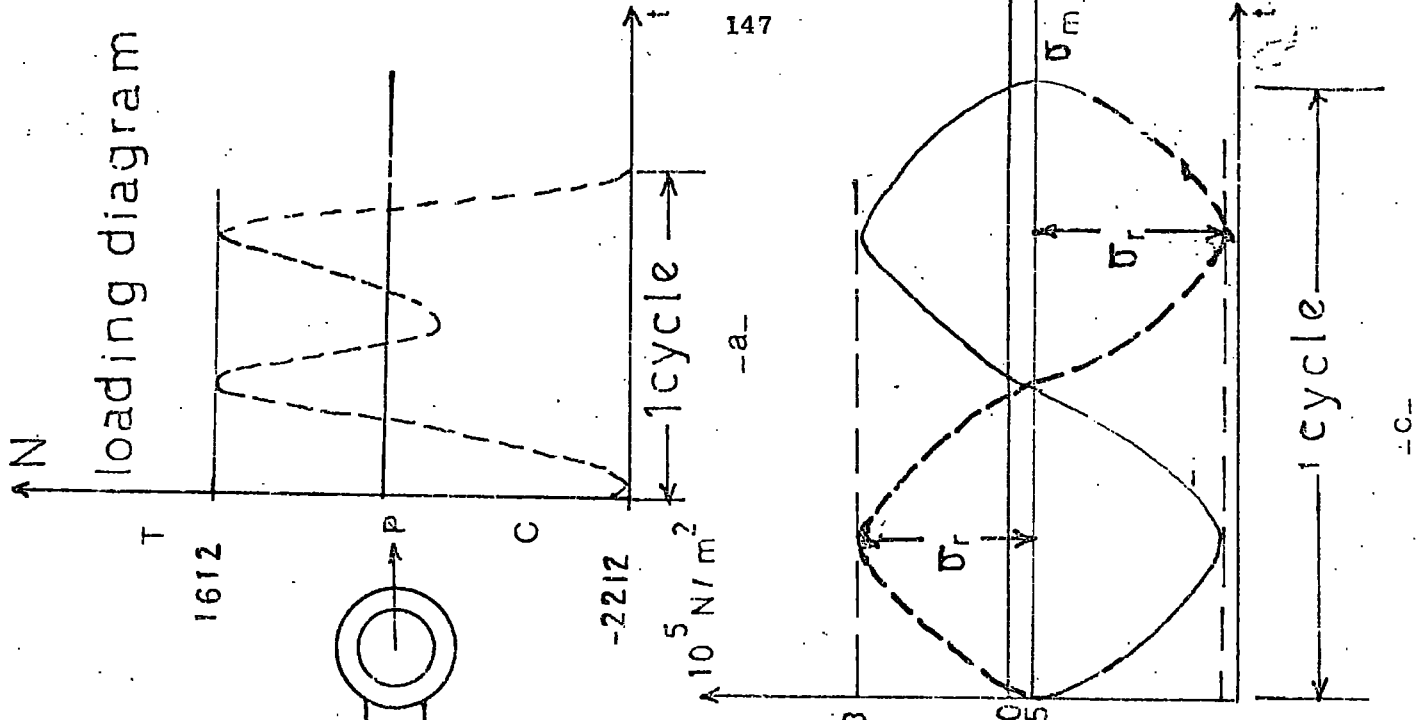
T = time for one complete cycle = 0.015 s (4000 r.p.m.)

$2\sigma_r$ = stress variation

Fig 5.1

Link 3 and Link 5 (clearances are extremely exaggerated)





crank speed 4000 r.p.m

Fig. 5.2

idealized sinusoidal model

Substituting the numerical values eq. (5.1) yields:

$$\sigma = -75 \times 10^5 \pm 478 \times 10^5 \sin \frac{2\pi t}{0.015} \quad (4000 \text{ r.p.m.})$$

which is shown in Fig. (5.3)

Stress ratio is determined as:

$$R = \frac{\sigma_{\min}}{\sigma_{\max}} = - \frac{553 \times 10^5}{103 \times 10^5} = -1.37$$

The factor of safety F.S can now be calculated as:

$$\left| \sigma_{\max} \right| = \frac{\sigma_{y.p}}{F.S}$$

$$F.S. = \frac{17.6 \times 10^7}{553 \times 10^5} \approx 3.18$$

where the yield point strength $\sigma_{y.p} = 17.6 \times 10^7$ is taken from Fig. (4.8)

There are a number of different empirical failure equations defining the relation between the variable and mean stresses. Three of the most commonly used relations are employed to calculate the endurance strength σ_e as in the following:

a - Gerber parabolic relation;

$$\left(\frac{\sigma_r}{\sigma_e} \right) + \left(\frac{\sigma_m}{\sigma_{ult}} \right)^2 = 1$$

where $\sigma_{ult} =$ ultimate tensile strength $\approx 22.4 \times 10^7 \text{ N/m}^2$ (From Fig. (4.8))

$$\sigma_e = \pm 4.78 \times 10^7 \text{ N/m}^2$$

b - Modified Goodman Relation;

$$\left(\frac{\sigma_r}{\sigma_e} \right) + \left(\frac{\sigma_m}{\sigma_{ult}} \right) = 1$$

$$\sigma_e = \pm 4.62 \times 10^7 \text{ N/m}^2$$

c - Soderberg relation

$$\left(\frac{\sigma_r}{\sigma_e} \right) + \left(\frac{\sigma_m}{\sigma_{yp}} \right) = 1$$

$$\sigma_e = \pm 4.58 \times 10^7 \text{ N/m}^2$$

The safe working axial stress line, employing Soderberg's criteria is shown in Fig. (5.3). The axial stress at a crank speed of 4000 r.p.m. can hardly be approximated by Gerber's criteria and is above the approximate lines of failure by Soderberg and modified Goodman methods, while the axial stress at a crank speed of 25000 r.p.m. is slightly under the conservative safe stress line approximated by Soderberg criteria. A good discussion of the above procedure can be found in (20) (26) and (5). It should be noted that the values calculated are only rough estimates. No standard basis for obtaining working fatigue stress relations has been universally accepted. The fatigue strength is also affected by the clearance between the pin and hole, the distribution of shear stress around the hole boundary, lubrication, pin material and pin bending effects, surface conditions, prior overloads, environmental effects, material and manufacturing effects. The calculated endurance limit stress, σ_e , is the maximum completely reversing stress that the link can sustain for an unlimited number of cycles without fatigue failure. If the completely reversed stress is higher than σ_e , the

failure can be expected to take place after some finite number of cycles. The higher the stress the fewer will be the cycles before failure can be expected.

5.2 Theoretical and experimental axial stress range variation with the crank speed in link 5

The variation of the experimental axial stress range for link 5 with the crank speed and with the square of the crank speed are presented in Figures 4.9 and 4.13 respectively. Due to gauge installation and structural failures (due to slip), causing severe mechanical damage; the maximum crank arm speed could not be increased beyond about ~~25000~~ r.p.m. although various unseccesful attempts have been made to reach 3000 r.p.m. or more. The speed fluctuation effect has been neglected (as explained in chapter 4, ± 0.08 experimental speed fluctuation coefficient has been regarded as being of no importance). The basic factors introducing error are identified as follows;

- 1 - Sensitivity and accuracy of the measuring devices employed in the experimental set-up.
- 2 - Effect of the hostile environment
- 3 - Effect of the additional moment of inertia introduced by the strain-gauges and their leads on the links
- 4 - Error in experimental determination of the cross-sectional areas and values of Young's moduli.
- 5 - Personal error in interpreting the data (u.v. Traces).

In general the experimental results are in good agreement with the calculated axial stress range values for link 5. By applying method of least squares the experimental axial stress range curve is approximated by the following straight line

$$y = 38.6 x - 7.7$$

where y = experimental axial-stress range -10^5 N/m^2

x = square of the crank speed $-10^4 (\text{rad/s})^2$

The theoretical variation is in the form;

$$y = 34.6x$$

a detailed examination of Fig. 4.9 is presented in the following table:

Table 5.1

approximate crank speed r.p.m.	A approximate Theoretical axial stress range $\times 10^5 \text{ N/m}^2$	B approximate Experimental axial stress range $\times 10^5 \text{ N/m}^2$	$\left \frac{B-A}{A} \right \times 100$
1100	45	45	0
1300	63	55	12.7
1410	73	69	5.5
1600	95	104	9.5
1700	108	106	1.9
1800	120	128	6.7
1970	143	143	0
2030	154	171	11
2110	164	194	18.3
2310	197	216	9.6
2410	216	242	12

Average value of $\left| \frac{B-A}{A} \right| \times 100 = 7.9$

The maximum deviation occurs at a crank speed of 2110 r.p.m. (18.3%, corresponding to a difference of $30 \times 10^5 \text{ N/m}^2$ between theoretical and experimental stress range). The experimental values consistently tend to be higher than calculated values after 1970 r.p.m. A comparison of theoretical and experimental variation of stress in a complete cycle (1 rev = 360°) for a crank speed of 1534 r.p.m. is shown in Fig. 4.1.6. The close resemblance

between the waveforms is significant. An approximate shift of 20° is observed at the two peak tensile stress values, between the two waveforms. The sample of the recorded axial stress waveform over one cycle shown in Fig. 4.16 is in better agreement with the calculated waveform than the experimental waveform presented and compared with the calculated waveform by Alexander and Lawrence(15), for bending strain variation in the coupler of a model four-bar planar mechanism.

5.3 Calculation of eccentricity from experimental data, for links 5 and 3

a - Link 5

From Fig. 4.4 - static bending strain test for link 5, the equation of the line approximating axial stress variation with the applied torque is:

$$\frac{\sigma_{ax}}{T} = 12.7$$

where σ_{ax} = axial stress on the cross section = $\frac{\text{Axial force}}{\text{cross-sectional area}}$

T = Torque applied to the crank arm via the lever

and the equation of the straight line approximating the bending stress variation with the applied torque is:

$$\frac{\sigma_b}{T} = 26.6$$

where σ_b = bending stress = $\frac{M_c}{I}$

where I = Moment of inertia of the cross section

c = Maximum distance from the neutral axis

M = $F_{ax} \cdot d$

where d = eccentricity

The ratio of the bending stress to axial stress is

$$K = \frac{\sigma_b}{\sigma_{ax}} = 2$$

The eccentricity d can now be calculated as:

$$K = \frac{\sigma_b}{\sigma_{ax}} = 2 = \frac{d \cdot c \cdot A}{I} \dots \dots \dots (5.2)$$

where A = cross sectional area

eq. (5.2) can be written as

$$d = \frac{KI}{cA} \dots\dots\dots (5.3)$$

assuming the cross sectional area to be a perfect rectangle;

$$I = \frac{bh^3}{12}$$

where b = base length of the rectangle

h = height of the rectangle

c = $h/2$

eq. (5.3) becomes

$$d = \frac{Kh}{6} \dots\dots\dots (5.4)$$

substituting the appropriate values:

$$d = \frac{H}{3} \approx 2.8 \text{ mm}$$

b - Link 3

Similarly from Fig 4.5 static bending strain test for link 3:

$$\frac{\sigma_{ax}}{T} = 4 \quad \text{and} \quad \frac{\sigma_b}{T} = 8.75$$

$$k = \frac{\sigma_b}{\sigma_{ax}} = 2.2$$

$$d = \frac{Kh}{6} = 0.36h = 4.3 \text{ mm}$$

In the above calculations it is assumed that the material follows Hooke's law and the magnitude of the stress is proportional to the distance from the neutral axis.

5.4 Eccentricity - dynamic case

The variation of axial and bending stresses in links 5 and 3 with the crank speed were shown in Figures 4.9, 4.11, 4.12 and 4.10 respectively. The ratio K_d of the experimental bending stress ranges to experimental axial strain ranges for both links are given in the following table, Table 5.2 a and b.

Table 5.2-a

crank speed r.p.m.	K dynamic link 5
1080	1.9
1280	2
1420	2.2
1610	2
1800	2.5
2050	2.4
2400	2.4
K dynamic average = 2.2	

Table 5.2-b

crank speed r.p.m.	k dynamic link 3
1082	7.3
1320	3.3
1440	3.5
1560	3.4
1800	3.4
2040	2.6
K dynamic average = 3.9	

Average value of K dynamic for link 5 is in good agreement with the K value for the static case while the average value of K dynamic for link 3 is about 1.77 times of the K value obtained for the static case

5.5 Determination of Axial working stress for link 3 - A theoretical approach

Applying the same assumptions and method shown in section 5.1., the working stress is determined for the minimum cross sectional area (cross section UU, Fig. 5.1) as in the following;

The loading diagram and axial cyclic stress variation are shown in Fig. 5.4 for the cross section at a crank speed of 4000 r.p.m.

$$\begin{aligned}
 A &= \text{cross sectional area} && 11 \times 10^{-5} \text{ m}^2 \\
 \sigma_{\max} &= 302 \times 10^5 \text{ N/m}^2 \\
 \sigma_{\min} &= -88 \times 10^5 \text{ N/m}^2 \\
 \sigma_m &= 107 \times 10^5 \text{ N/m}^2 \\
 \sigma_r &= 195 \times 10^5 \text{ N/m}^2 \\
 2\sigma_r &= 390 \times 10^5 \text{ N/m}^2 \\
 T &= 0.015 \text{ s}
 \end{aligned}$$

using eq. (5.1) the actual stress pattern is approximated by the following sinusoidal model:

$$\sigma = 107 \times 10^5 + 195 \times 10^5 \sin \frac{2\pi t}{0.015}$$

which is shown in Fig. (5.4)

The stress ratio is:

$$R = \frac{\sigma_{\min}}{\sigma_{\max}} = -0.3$$

From Fig (4.8)

$$\sigma_{yp} = 11.4 \times 10^7 \text{ N/m}^2$$

$$\sigma_{ult} = 12.4 \times 10^7 \text{ N/m}^2$$

The factor of safety can be calculated as

$$\left| \sigma_{\max} \right| = \frac{\sigma_{yp}}{\text{F.S}}$$

$$\text{F.S} \cong 3.77$$

Soderberg relation gives an endurance strength of $2.15 \times 10^7 \text{ N/m}^2$. σ_e calculated by modified Goodman relation is $2.13 \times 10^7 \text{ N/m}^2$. The working stress diagram is shown in Fig. (5.5). Axial stress acting on the cross section is above the Soderberg line. Cross section MM (Fig. 5.1) is also represented on the same diagram.

5.6 Theoretical and experimental axial stress range variation with the crank speed in link 3.

The variation of the experimental axial stress range for link 3 with the crank speed and with the square of the crank speed are presented in Figures 4.12 and 4.13 respectively. Crank speed could not be increased beyond about 2100 r.p.m. (due to gauge installation failures, and drift in the u.v. traces). By applying the method of least squares the experimental axial stress range curve is approximated by the straight line

$$y = 21.8x + 11.4$$

where y = experimental axial stress range -10^5 N/m^2

x = square of the crank speed $-10^4 (\text{rad/s})^2$

the theoretical variation is in the form:

$$y = 21.4x$$

a detailed examination of Fig. 4.12 is presented in the following table:

Table 5.3

approximate crank speed r.p.m.	A Approximate theoretical axial stress range 10^5 N/m^2	B Approximate experimental axial stress range 10^5 N/m^2	$\left \frac{B-A}{A} \right \times 100$
1100	27	24	11.1
1260	36	57	58.3
1430	47	70	49
1550	57	74	30
1790	75	83	10.6
1910	85	94	10.6
2080	100	114	14
2130	105	123	17.1

average value of $\left| \frac{B-A}{A} \right| \times 100 = 25$

which is about 3 times higher than that of link 5. The experiment values are generally higher than the calculated values. The maximum deviation occurs at a crank speed of 1260 r.p.m. (58.3%). A comparison of theoretical and experimental cyclic axial stress variation is shown in Fig. 4.15

5.7 Bending stresses in a direction normal to plane of the mechanism

The variation of peak to peak bending stresses with the crank speed for links 3 and 5 are shown in Figures 4.10 and 4.11 respectively.

The bending stress range curves can be approximated by the straight lines:

$$y = 37x + 150 \quad \dots\dots\dots \text{(link 3)}$$

$$y = 104x - 58 \quad \dots\dots\dots \text{(link 5)}$$

where again:

$$y = \text{bending axial stress range} - 10^5 \text{ N/m}^2$$

$$x = \text{square of crank speed} - 10 \text{ (rad/s)}^2$$

At a crank speed of 4000 r.p.m. the expected bending stress range values for the links 3 and 5 can be calculated as $800 \times 10^5 \text{ N/m}^2$ and $1767 \times 10^5 \text{ N/m}^2$ respectively. The expected axial stress ranges at the same crank speed for the links are $395 \times 10^5 \text{ N/m}^2$ (link 3) and $670 \times 10^5 \text{ N/m}^2$ (link 5) (values based on experimental data). The variable stress values are well above the endurance strength of the links. The combined effect of bending and axial stresses (method of superposition) at a crank speed of 4000 r.p.m. would indicate a state of failure.

5.8 Stress distribution in the links

The main objective of the test explained in section 4.4±3 was to determine whether the bending stresses are due to an initial permanent link deformation, an offset, or due to the pins, tolerance and/or clearance effects or other misalignments which are factors external to the links themselves. A detailed examination of Figures 4.6 and 4.7 are presented in Tables (5.4 - 7). Results of the tests for both links show that the bending stress (z-direction) are due to effects which are external to the links. The basic factors introducing error to the results are identified as follows:

- 1 - Effects of deviation in the crank angle ($90^\circ \pm 5^\circ$)
- 2 - Friction in the bearings
- 3 - Effects of elasticity of the shafts and links

The possible bending mechanisms are shown in Figures (5.6) and (5.7)

Applied torque = N.m	$\sigma_{ax} = P/A$ 10^5 N/m^2	Gauge m (Tension) axial and bending stress = $\sigma_{comp 1}$ 10^5 N/m^2	Gauge k (compression) axial + bending stress = $\sigma_{comp 2}$ 10^5 N/m^2	Net bending stress (tensile) $\sigma_{comp 1} + \sigma_{ax} =$ 10^5 N/m^2	Net bending stress (compressive) $\sigma_{comp 2} - \sigma_{ax} =$ 10^5 N/m^2	eccentricity 1 $e_1 = \frac{\sigma_{bm}}{h}$ mm	eccentricity 2 $e_2 = \frac{\sigma_{bk}}{h}$ mm	Av. eccentricity $\frac{e_1 + e_2}{2}$ mm	Bending moment 1 $e_1 \cdot P$ N.m	Bending moment 2 $e_2 \cdot P$ N.m
6	52	52	156	104	104	2.8	2.8	2.8	0.9	0.9
12	104	166	364	270	260	3.6	3.5	3.5	2.3	2.3
17.8	176	280	582	456	406	3.6	3.2	3.4	4	3.5
23.5	239	405	800	644	561	3.8	3.3	3.5	5.7	5
30	301	540	1018	841	717	3.9	3.3	3.6	7.4	6.3
35.5	364	655	1246	1019	882	3.9	3.4	3.6	9	7.8

From Fig. 4.6 - Static bending test for link 5 - Stress distribution profile
Case 1 - based on experimental data

Table 5.4

Applied Torque = N.m.	$\sigma_{ax} = P/A$ (compressive) 10^5 N/m^2	Gauge k (Tension) axial and bending stress = $\sigma_{comp 1}$ 10^5 N/m^2	Gauge m. (compression) axial + bending stress = $\sigma_{comp 2}$ 10^5 N/m^2	Net bending stress (tensile) $\sigma_{comp 1} + \sigma_{ax} =$ σ_{bk} 10^5 N/m^2	Net bending stress (compressive) $\sigma_{comp 2} - \sigma_{ax} =$ σ_{bm} 10^5 N/m^2	eccentricity 1 $e_1 = \sigma_{bk} h$ mm	eccentricity 2 $e_2 = \sigma_{bm} h$ mm	Av. eccentricity $\frac{e_1 + e_2}{2}$ mm	Bending moment 1 $e_1 \cdot P$ N.m.	Bending moment 2 $e_2 \cdot P$ N.m.
6	31	62	119	93	88	4.2	4	4.1	0.8	0.8
12	62	176	291	238	229	5.4	5.2	5.3	2.1	2
17.8	104	301	499	405	395	5.5	5.4	5.45	3.6	3.5
23.5	145	395	686	540	541	5.2	5.2	5.2	4.8	4.8
30	176	519	883	695	707	5.6	5.7	5.65	6.2	6.3
35.5	223	623	1091	846	868	5.3	5.5	5.4	7.4	7.7

From Fig. 4.6 - Static bending test for link 5 - Stress distribution profile
Case 2 - based on experimental data

Table 5.5

Applied Torque = T N.m.	$\sigma_{ax} = P/A$ (Tensile) 10^5 N/m^2	Gauge c (Tension) axial and bending stress = $\sigma_{comp 1}$ 10^5 N/m^2	Gauge d (compression) axial + bending stress = $\sigma_{comp 2}$ 10^5 N/m^2	Net bending stress (tensile) $\sigma_{comp 1} - \sigma_{ax} =$ σ_{bc} 10^5 N/m^2	Net bending stress (compressive) $\sigma_{comp 2} + \sigma_{ax} =$ σ_{bd} 10^5 N/m^2	eccentricity 1 $e_1 = \frac{\sigma_{bc}}{h}$ mm	eccentricity 2 $e_2 = \frac{\sigma_{bd}}{h}$ mm	Av. eccentricity $\frac{e_1 + e_2}{2}$ mm	Bending moment 1 $e_1 \cdot P$ N.m.	Bending moment 2 $e_2 \cdot P$ N.m.
6	7	48	35	41	42	13.6	14	13.8	1.4	1.5
12	30	120	64	90	94	7	7.3	7.15	3.1	3.3
17.8	35	192	123	157	158	10.4	10.5	10.45	5.4	5.5
23.5	48	258	163	210	211	10.2	10.2	10.2	7.3	7.3
30	62	323	198	261	260	9.8	9.8	9.8	9	9
35.5	80	387	227	307	307	8.9	8.9	8.9	10.6	10.6

163

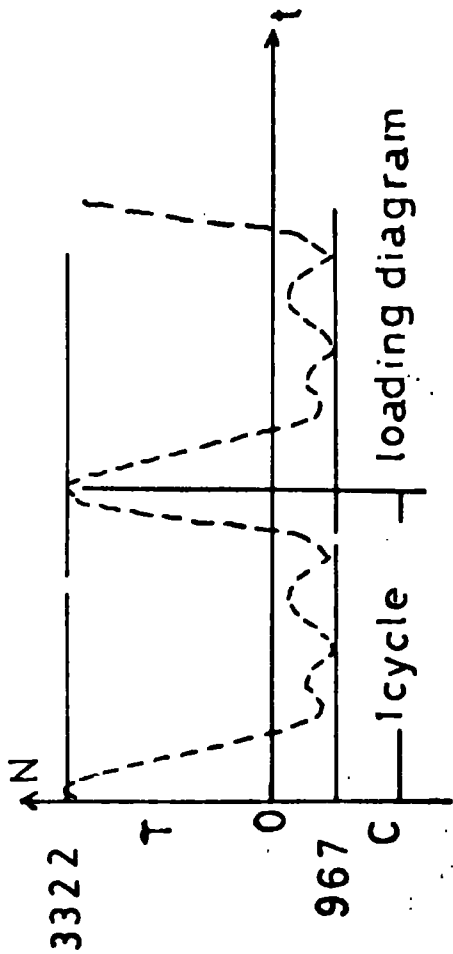
From Fig. 4.7 - static bending test for link 3 - stress distribution profile
Case 1 - based on experimental data

Table 5.6

Applied Torque, T N.m.	$\sigma_{ax} = P/A$ 10^5 N/m^2 (Tensile)	Gauge d (Tension) axial and bending stress = $\sigma_{comp 1}$ 10^5 N/m^2	Gauge c (compression) axial + bending stress = $\sigma_{comp 2}$ 10^5 N/m^2	Net bending stress (tensile) $\sigma_{comp 1} - \sigma_{ax} =$ 10^5 N/m^2	Net bending stress (compressive) $\sigma_{comp 2} + \sigma_{ax} =$ 10^5 N/m^2	eccentricity 1 $e_1 = \frac{\sigma_{bd}}{h}$ mm	eccentricity 2 $e_2 = \frac{\sigma_{bc}}{h}$ $= \frac{\sigma_{ax}}{\sigma_{bc}}$ mm	Av. eccentricity $\frac{e_1 + e_2}{2}$ mm	Bending moment 1 $e_1 \cdot P$ N.m.	Bending moment 2 $e_2 \cdot P$ N.m.
6	11	35	13	24	24	5	5	5	0.8	0.8
12	32	102	51	70	83	5.1	6	5.5	2.4	2.8
17.8	43	170	83	127	126	6.9	6.8	6.8	4.4	4.3
23.5	64	230	115	166	179	6	6.5	6.2	5.7	6.2
30	76	288	147	212	223	6.5	6.8	6.6	7.3	7.7
35.5	104	344	166	240	270	5.4	6	5.7	8.4	9.3

From Fig. 4.7 Static bending test for link 3 - Stress distribution profile
Case 2 - based on experimental data

Table 5.7



crank speed = 4000 r.p.m

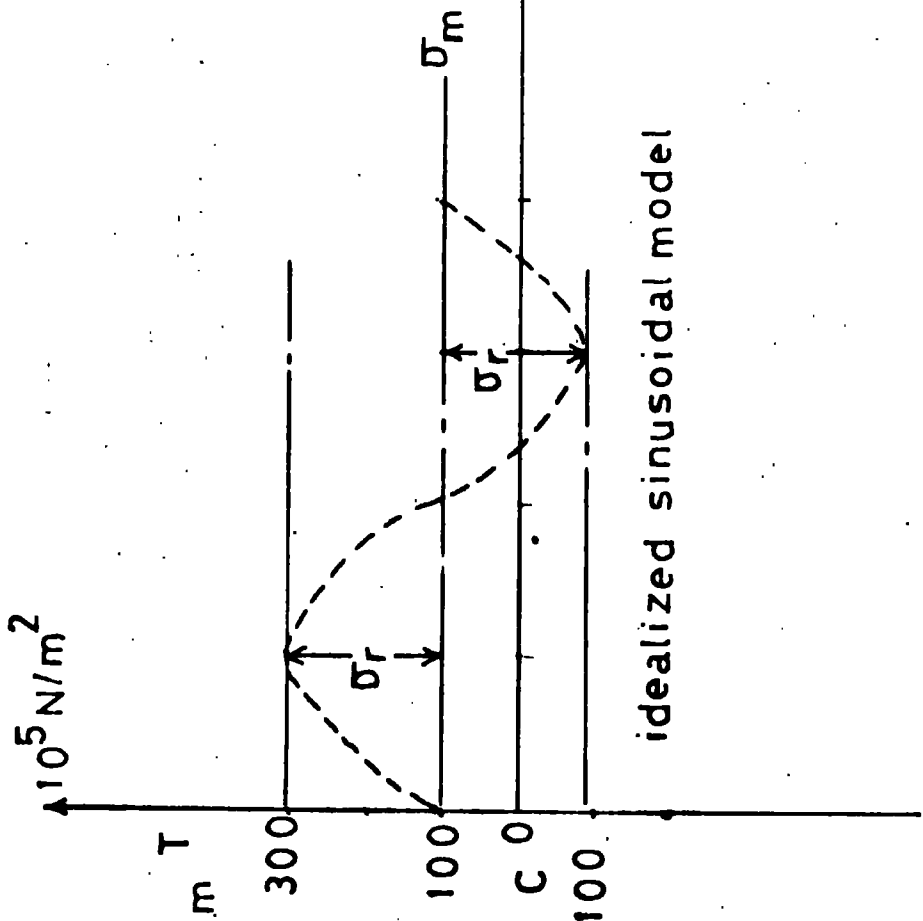
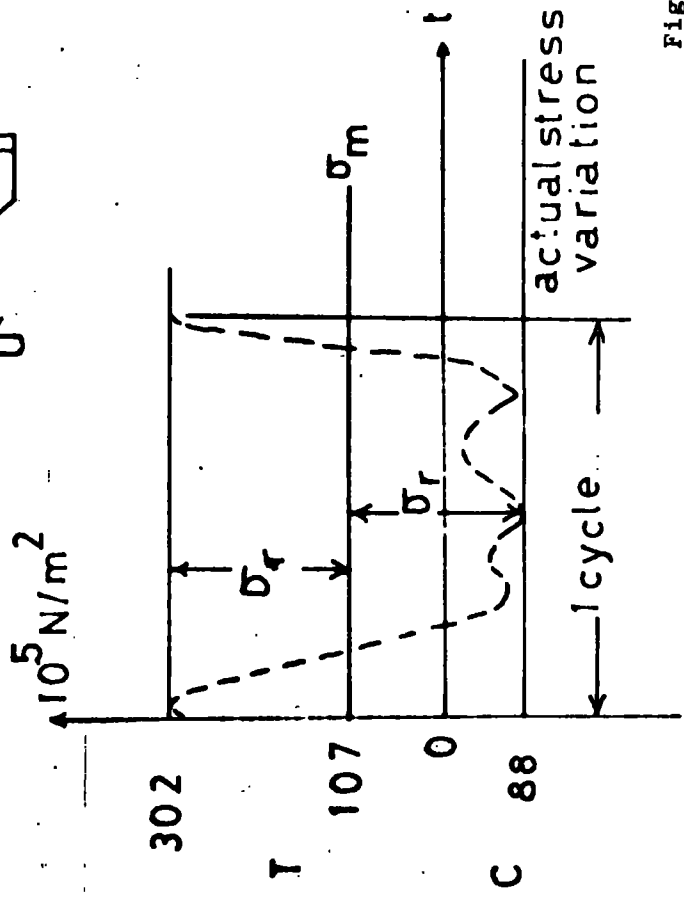
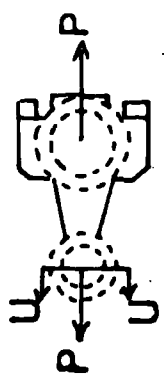


FIG. 5.4

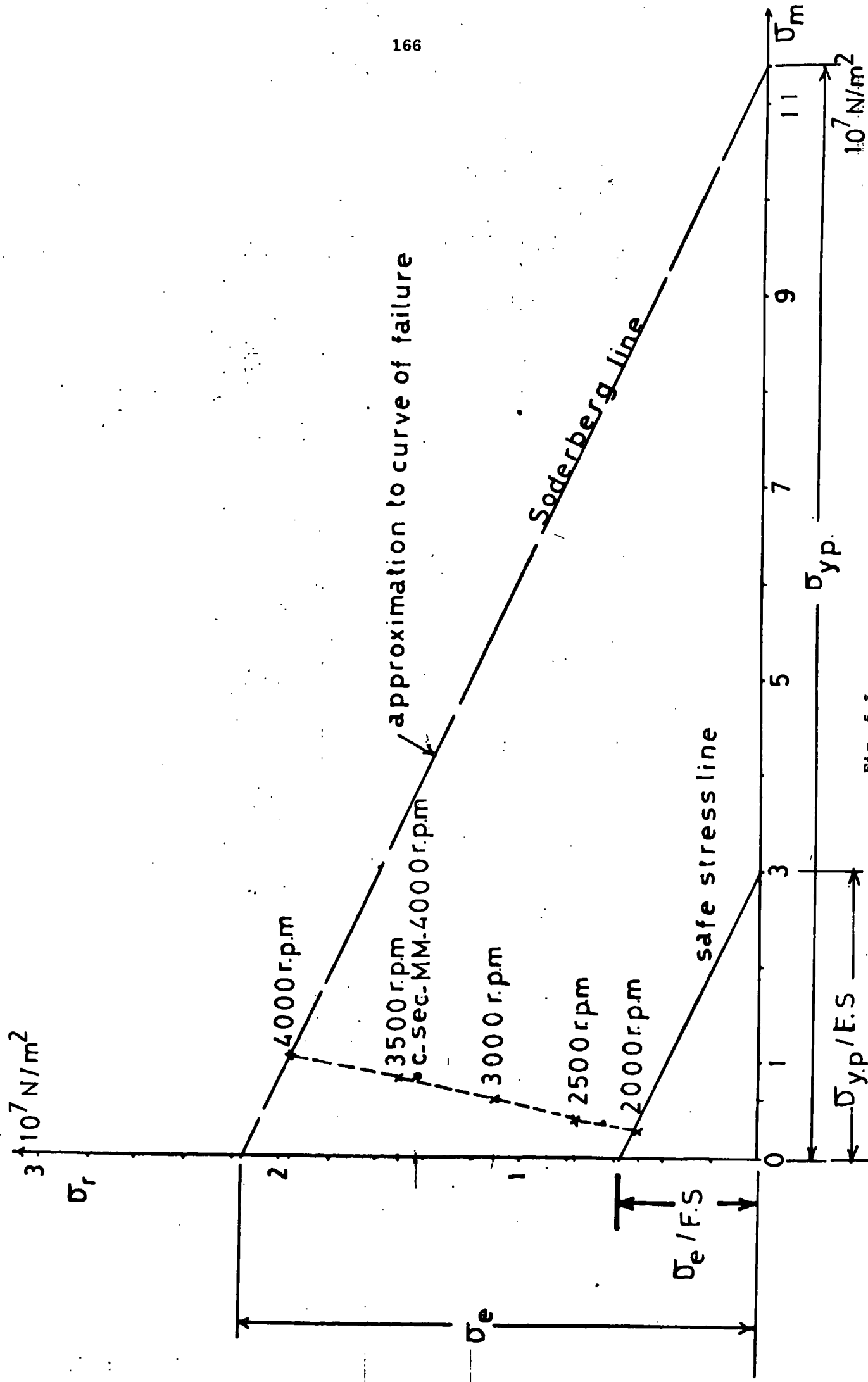
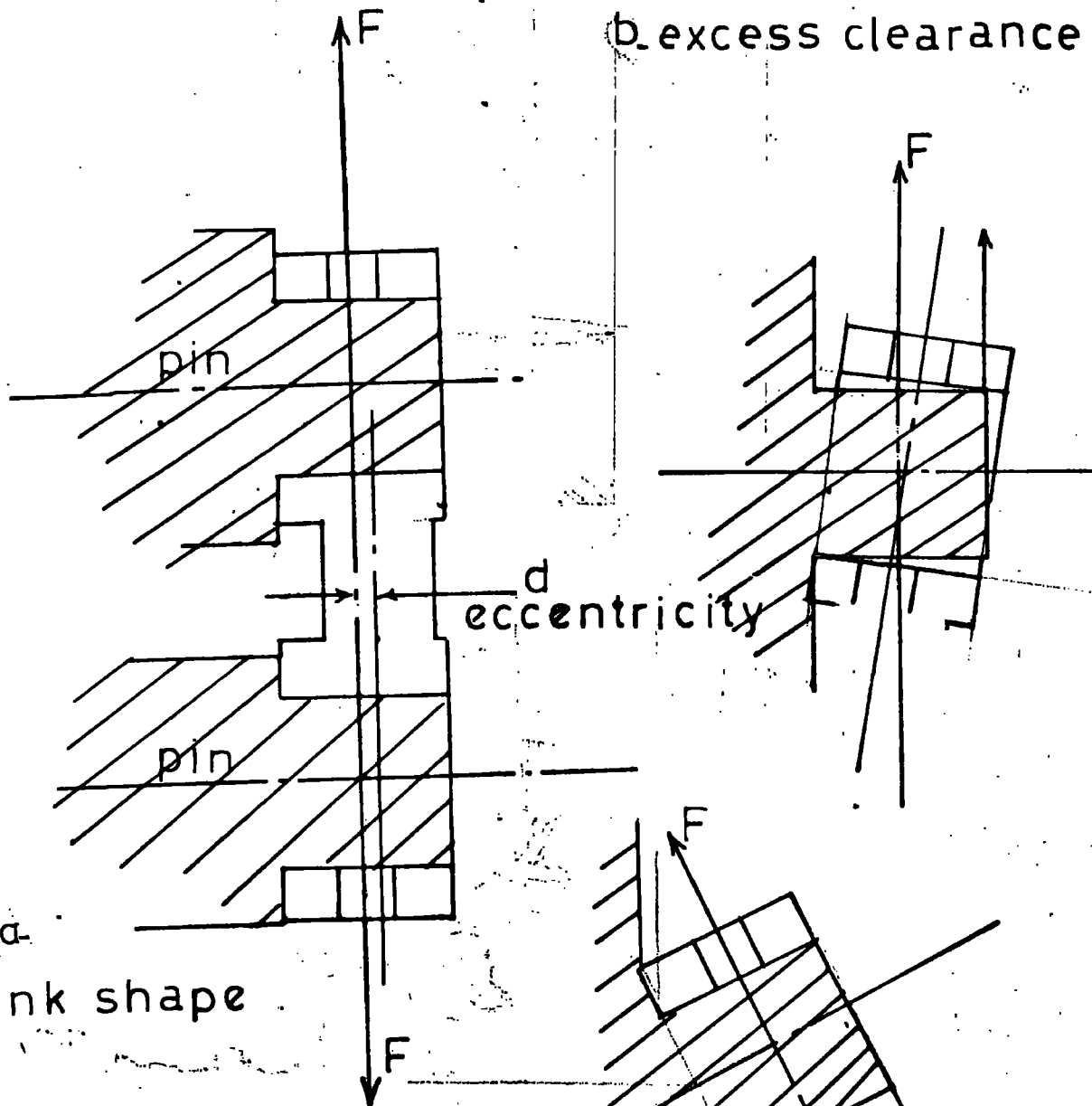


FIG. 5.5

b. excess clearance

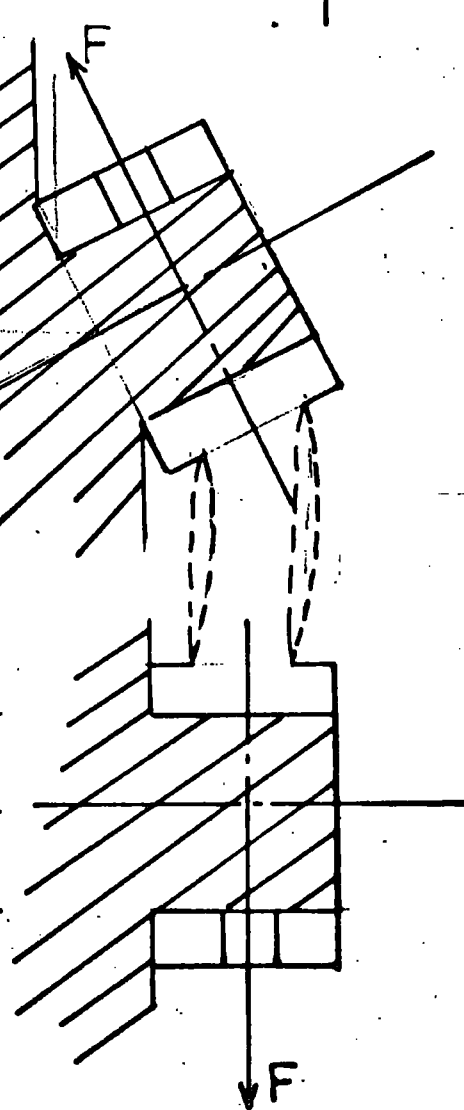


a. link shape

Fig. 5.6^b

c. single or double pin deformation

Fig. 5.7



5.9 General Considerations

During the actual weaving operation the stresses would increase due to the external resistance introduced by the threads on the combs and needle arms. The value of this expected increase is unknown. The hardness and tensile tests performed on the connecting rods showed that there is a difference between material properties of the two links although they were expected to be the same (phosphor bronze alloy). Mechanical damage (scratches inside the link bores and flange sides) is detected on both links. The effect of friction has completely been neglected in the analytical calculations. Stress waveform pattern is complex in structure for both links and is very destructive in nature from a fatigue point of view.

Chapter 6 - Conclusion

Bending stresses in a direction normal to the plane of the mechanism are present in both of the links investigated and have a dominating effect. The axial cyclic and peak to peak stress variation in both links is generally in good agreement with the calculated values. The bending stresses normal to the plane of the mechanism are due to misalignment effects which are external to the connecting rods themselves. The dominating characteristic of the dynamic bending stresses has been confirmed with static tests carried out on the mechanism. Even by neglecting the bending stress effects on the links the present design is found to be unsatisfactory at a crank speed of 4000 r.p.m. since the axial stress values are above the working axial stress line approximated by the Soderberg criteria. In the presence of bending stresses fatigue failure can be expected to occur at approximately 2000 r.p.m. However if bending stresses are negligible the present design can be used up to a crank speed of 2500 r.p.m. (See Appendix A3)

To increase the speed of the mechanism the following general basic major points are suggested:

1. A detailed deflection tolerance and clearance analysis to reduce the bending stresses due to misalignments theoretically to zero which would automatically increase the crank speed range up to 2500 r.p.m.
2. Fatigue tests on the links to determine the experimental endurance strength.
3. The stress constraints are determined. Any increase in the critical cross sections of the connecting rods will decrease the stresses, and therefore would yield a higher operating speed.
4. It was found that extreme axial stresses in a complete cycle of input crank rotation occurs at different angles of input crank

rotation for the two connecting rods. Any slight changes in link lengths and geometry to decrease the extreme angular acceleration values for links 4 and 6 will accordingly decrease the axial stresses on the two connecting rods and change the cyclic axial stress pattern.

- 5 Without changing the configuration of the mechanism, any suitable material change with a higher endurance and yield point limit will accordingly permit an increase in the crank speed.

Appendix A-1

```

> ) ) 11 03 C COMPLETE KINEMATIC, FORCE & STRESS ANALYSIS OF THE MECHANISM
> ) ) 12 05 C SERDAR OGULEN
> ) ) 13 00 C UNIVERSITY OF DURHAM, DEPT. OF ENGINEERING SCIENCE
> ) ) 14 00 C
> ) ) 15 00 C PI=3.14159265
> ) ) 16 00 C DOI I=0,360,15
> ) ) 16.5 00 C PSI=I
> ) ) 17 00 C OMEGA PSI=PSI/180.0*PI
> ) ) 17.5 OMEGA OMEGA2=(2.0*PI*2500.0)/(60.0) *
> ) ) 18 00 C XVA=OMEGA2*0.011
> ) ) 19 00 C OIE=COS(PSI)*0.011
> ) ) 10 00 C AE=SIN(PSI)*0.011
> ) ) 11 00 C XAF=AE+0.005
> ) ) 12 00 C XOF=0.048-OIE
> ) ) 13 00 C XAO2=SQR(AF**2+O2F**2)
> ) ) 14 00 C XETA=ATAN(AF/O2F)
> ) ) 15 00 C XZEK=ARCOS((0.00128-AO2**2)/(-0.044*AO2))
> ) ) 16 00 C XCAL=ARCOS((0.002248-AO2**2)/(0.001848))
> ) ) 17 00 C XALPHA=PI-(ZEK+CAL)
> ) ) 18 00 C XBETA=ALPHA-ETA
> ) ) 18.18 00 C XGAMMA=PSI-BETA
> ) ) 18.2 00 C XGAMMA2=SIN(YI)*0.011
> ) ) 19 00 C XGAMMA=PI-(ETA+ZEK+75.0/180.0*PI)
> ) ) 19.1 00 C XDO=SIN(GAMMA+75.0/180.0*PI-BETA)*0.022
> ) ) 20 00 C XDDBA=VA*((SIN(PSI)*TAN(GAMMA+165.0/180.0*PI))+COS(PSI))
> ) ) 21 00 C XDBA=(XDO)/(TAN(GAMMA+165.0/180.0*PI)-TAN(BETA+0.5*PI))
> ) ) 22 00 C XYDBA=XDBA*TAN(BETA+0.5*PI)
> ) ) 25 00 C XVBA=SQR(XDBA**2+YDBA**2)
> ) ) 26 00 C XDBB=(VA*(-SIN(PSI)))+XDBA
> ) ) 27 00 C YDBB=(VA*COS(PSI))+YDBA
> ) ) 28 00 C XVBB=SQR(XDBB**2+YDBB**2)
> ) ) 29 00 C XOMEGA3=VBA/0.042

```

```

> ) )29 .0 .0000 OMEGA3=VBA/0.042
> ) )29.1 .0 .0000 EN4=(0.5*0.0000584)*(OMEGA3**2)
> ) )3000 .0 .0000 OMEGA4=VB/0.022
> ) )30.0500 .0 .0000 EN1=(0.5*0.00002265)*(OMEGA4**2)
> ) )30.0600 .0 .0000 EN3=(0.5*0.000043502)*(OMEGA4**2)
> ) )310 .0000 .0 .0000 ABR=0.022*(OMEGA4**2)
> ) )32000 .0 .0000 ABAR=0.042*(OMEGA3**2)
> ) )330 .0000 .0 .0000 TETA=ATAN((0.032-SIN(GAMA)*0.022)/(0.042-COS(GAMA)*0.022))
> ) )3400 .0 .0000 C03=((0.032-SIN(GAMA)*0.022)/(SIN(TETA)))
> ) )350 .0000 .0000 VAN=ARCOS((0.029**2+C03**2-0.02**2)/(0.029*2*C03))
> ) )360 .0000 .0000 XLAMB=VAN+TETA
> ) )36.1 .0000 .0000 GRE=SIN(XLAMB-GAMA)*0.022
> ) )370 .0000 .0000 FI=ARCOS((0.02**2+C03**2-0.029**2)/(0.04*C03))
> ) )38 .0000 .0000 UPA=PI-TETA
> ) )38.1 .0000 .0000 YUM=PI-(UPA+XLAMB)
> ) )38.2 .0000 .0000 CD=COS(XI)*0.02
> ) )390 .0000 .0000 XDDC=VB*((COS(GAMA)+SIN(GAMA)*TAN(0.5*PI-UPA)))/
> ) )400 .0000 .0000 TAN(0.5*PI-UPA)-TAN(0.5*PI+XLAMB))
> ) )410 .0000 .0000 XDD=(VB*(-SIN(GAMA)))+XDDC
> ) )420 .0000 .0000 YDDC=XDDC*(TAN(0.5*PI+XLAMB))
> ) )430 .0000 .0000 YDD=XDD*(TAN(0.5*PI-UPA))
> ) )44 .0000 .0000 VD=SQRT(XDD**2+YDD**2)
> ) )450 .0000 .0000 VDC=SQRT(XDDC**2+YDDC**2)
> ) )460 .0000 .0000 OMEGA6=VD/0.02
> ) )46.01 .0000 .0000 EN2=(0.5*0.000306872)*(OMEGA6**2)
> ) )46.0200 .0000 .0000 EN6=(0.5*0.000022674)*(OMEGA6**2)
> ) )470 .0000 .0000 OMEGA5=VDC/0.029
> ) )47.1 .0000 .0000 EN5=(0.5*0.0000075)*(OMEGA5**2)
> ) )480 .0000 .0000 ADR=0.02*(OMEGA5**2)
> ) )49 .0000 .0000 ADCR=0.029*(OMEGA5**2)
> ) )49.2 .0000 .0000 AAR=(OMEGA2**2)*0.011
> ) )50 .0000 .0000 V1=ABR*COS(255.0/180.0*PI+GAMA)
> ) )51 .0000 .0000 Y2=ABR*SIN(255.0/180.0*PI+GAMA)

```



```

> ) )520: 0 0 0 0 V3=AAR*COS(PI+PSI)
> ) )53: 0 0 0 0 V4=AAR*SIN(PI+PSI)
> ) )54: 0 0 0 0 V5=ABAR*COS(PI+BETA)
> ) )55: 0 0 0 0 V6=ABAR*SIN(PI+BETA)
> ) )56: 0 0 0 0 V7=TAN(165.0/180.0*PI+GAMA)
> ) )57: 0 0 0 0 V8=TAN(BETA+0.5*PI)
> ) )58.1: 0 0 0 0 XDDBAT=(-V7*(V3+V5-V1)+V6+V4-V2)/(V7-V8)
> ) )58.2: 0 0 0 0 YDDBAT=XDDBAT*V8
> ) )58.3: 0 0 0 0 XDBAT=XDDBAT+V3+V5-V1
> ) )58.4: 0 0 0 0 YDBAT=YDDBAT*V7
> ) )59: 0 0 0 0 ABT=SQRT(XDDBT**2+YDDBT**2)
> ) )60: 0 0 0 0 ABAT=SQRT(XDDBAT**2+YDDBAT**2)
> ) )60.1: 0 0 0 0 ANG3=ABAT/0.042
> ) )60.11: 0 0 0 0 B1=ANG3*0.0000584
> ) )60.12: 0 0 0 0 BI=(ANG3)/(OMEGA2**2)
> ) )60.2: 0 0 0 0 ANG4=ABT/0.022
> ) )60.22: 0 0 0 0 B2=ANG4*0.000043502
> ) )60.23: 0 0 0 0 B5=ANG4*0.000092265
> ) )61: 0 0 0 0 P1=-ADR*COS(UPA)+ABR*COS(PI+GAMA)+ART*COS(1.5*PI+GAMA)
> ) )61.01: 0 0 0 0 P1+ADCR*COS(PI+XLAMB)
> ) )61.1: 0 0 0 0 P2=-ADR*SIN(-UPA)+ABR*SIN(PI+GAMA)+ABT*SIN(1.5*PI+GAMA)
> ) )61.2: 0 0 0 0 P2+ADCR*SIN(PI+XLAMB)
> ) )61.3: 0 0 0 0 P3=TAN(1.5*PI-UPA)
> ) )61.4: 0 0 0 0 P4=TAN(XLAMB-0.5*PI)
> ) )61.5: 0 0 0 0 XDDCT=(-P1+P3+P2)/(P3-P4)
> ) )61.51: 0 0 0 0 YDDCT=P4*XDDCT
> ) )61.52: 0 0 0 0 XADCT=SQRT(XDDCT**2+YDDCT**2)
> ) )61.53: 0 0 0 0 XDDDT=P1+XDDCT
> ) )61.54: 0 0 0 0 YDDDT=P2+YDDCT
> ) )61.55: 0 0 0 0 ADT=SQRT(XDDDT**2+YDDDT**2)
> ) )62.8: 0 0 0 0 ANG5=ADCT/0.029
> ) )62.801: 0 0 0 0 TIM=(ANG5)/(OMEGA2**2)
> ) )62.802: 0 0 0 0 ANG6=ADT/0.02
> ) )62.81: 0 0 0 0 B3=ANG5*0.0000075

```

```

> )62.8100 0.0000 B3=ANGC5*0.00000075
> )62.820 0.0000 B4=ANGC6*0.000022674
> )62.8300 0.0000 B6=ANGC6*0.0000306872
> )630 0.0000 AB=SQRT(ABR**2+ABT**2)
> )63.50 0.0000 PIK1=ANGC3*OMEGA3*0.0000584
> )63.51 0.0000 PIK2=0.0000075*ANGC5*OMEGA5
> )63.70 0.0000 PIK3=0.5*0.0000584*(OMEGA3**2)
> )63.80 0.0000 PIK4=0.5*0.0000075*(OMEGA5**2)
> )63.81 0.0000 RT1=OMEGA3/OMEGA2
> )63.91 0.0000 RT2=OMEGA4/OMEGA2
> )63.92 0.0000 RT3=OMEGA5/OMEGA2
> )63.93 0.0000 RT4=OMEGA6/OMEGA2
> )640 0.0000 PSI=PSI*57.2957795
> )650 0.0000 XLAMB=XLAMB*57.2957795
> )65.10 0.0000 YUM=YUM*57.2957795
> )66 0.0000 BETA=BETA*57.2957795
> )67 0.0000 UPA=UPA*57.2957795
> )67.10 0.0000 CAL=CAL*57.2957795
> )680 0.0000 GAMA=GAMA*57.2957795
> )68.10 0.0000 ZEK=ZEK*57.2957795
> )68.20 0.0000 ETA=ETA*57.2957795
> )68.3500 0.0000 PA1=0.000092265*OMEGA4*ANGC4
> )68.3510 0.0000 PA2=0.000043502*OMEGA4*ANGC4
> )68.35200 0.0000 PA3=0.0000306872*OMEGA6*ANGC6
> )68.35300 0.0000 PA4=0.000022674*OMEGA6*ANGC6
> )68.35400 0.0000 WER=B4+B6
> )68.3550 0.0000 POW=WER*OMEGA6
> )68.951 0.0000 TR=(B4+B6)/(D)
> )68.952 0.0000 STR=(TR)/(6.32)
> )68.953 0.0000 HOM1=(0.689655*B3* $\cos(2.0*\pi-UPA)$ )/( $\cos(XLAMB)$ )
> )68.954 0.0000 HOM2=-0.02* $\sin(2.0*\pi-UPA)+0.02*\tan(XLAMB)$ 
> )68.955 0.0000 F56X=(-WER-HOM1)/(HOM2)
> )68.956 0.0000 HOM3=B3+F56X*(0.029)* $\sin(XLAMB)$ 
> )68.957 0.0000 F56Y=(HOM3)/(0.029)* $\cos(XLAMB)$ 

```



```

$r -load#
#EXECUTION BEGINS
) PSI= 30.00 VBA= ) ) 3.240500 VB= ) ) 1.31081 VDC= ) ) 0.33994 VD= ) ) 1.28271
) PSI= 15.00 VBA= ) ) 2.97831 VB= ) ) 0.25167 VDC= ) ) 0.64699 VD= ) ) 0.24801
) PSI= 30.00 VBA= ) ) 2.52188 VB= ) ) 0.75752 VDC= ) ) 0.16003 VD= ) ) 0.74486
) PSI= 45.00 VBA= ) ) 2.03102 VB= ) ) 1.59194 VDC= ) ) 0.51007 VD= ) ) 1.54669
) PSI= 60.00 VBA= ) ) 1.58230 VB= ) ) 2.21668 VDC= ) ) 1.08243 VD= ) ) 2.09160
) PSI= 75.00 VBA= ) ) 1.19012 VB= ) ) 2.64496 VDC= ) ) 1.79655 VD= ) ) 2.33648
) PSI= 90.00 VBA= ) ) 0.83772 VB= ) ) 2.90031 VDC= ) ) 2.46652 VD= ) ) 2.23615
) PSI= 105.00 VBA= ) ) 0.49422 VB= ) ) 2.99685 VDC= ) ) 2.89305 VD= ) ) 1.79150
) PSI= 120.00 VBA= ) ) 0.11970 VB= ) ) 2.93125 VDC= ) ) 2.97052 VD= ) ) 1.11426
) PSI= 135.00 VBA= ) ) 0.35292 VB= ) ) 2.68153 VDC= ) ) 2.71753 VD= ) ) 0.41261
) PSI= 150.00 VBA= ) ) 0.90632 VB= ) ) 2.21863 VDC= ) ) 2.20783 VD= ) ) 0.10094
) PSI= 165.00 VBA= ) ) 1.59992 VB= ) ) 1.54521 VDC= ) ) 1.51304 VD= ) ) 0.30120
) PSI= 180.00 VBA= ) ) 2.31904 VB= ) ) 0.74672 VDC= ) ) 0.72547 VD= ) ) 0.21170
) PSI= 195.00 VBA= ) ) 2.89952 VB= ) ) 0.03069 VDC= ) ) 0.02976 VD= ) ) 0.00952
) PSI= 210.00 VBA= ) ) 3.21894 VB= ) ) 0.68693 VDC= ) ) 0.66745 VD= ) ) 0.19371
) PSI= 225.00 VBA= ) ) 3.24541 VB= ) ) 1.21350 VDC= ) ) 1.18668 VD= ) ) 0.25263
) PSI= 240.00 VBA= ) ) 2.99431 VB= ) ) 1.64895 VDC= ) ) 1.63186 VD= ) ) 0.15779
) PSI= 255.00 VBA= ) ) 2.48572 VB= ) ) 2.03290 VDC= ) ) 2.04348 VD= ) ) 0.10567
) PSI= 270.00 VBA= ) ) 1.73501 VB= ) ) 2.38646 VDC= ) ) 2.42695 VD= ) ) 0.55220
) PSI= 285.00 VBA= ) ) 0.76613 VB= ) ) 2.70337 VDC= ) ) 2.72390 VD= ) ) 1.16978
) PSI= 300.00 VBA= ) ) 0.36142 VB= ) ) 2.94059 VDC= ) ) 2.79316 VD= ) ) 1.86095
) PSI= 315.00 VBA= ) ) 1.52082 VB= ) ) 3.01082 VDC= ) ) 2.46961 VD= ) ) 2.40263
) PSI= 330.00 VBA= ) ) 2.51002 VB= ) ) 2.79739 VDC= ) ) 1.75345 VD= ) ) 2.52979
) PSI= 345.00 VBA= ) ) 3.11517 VB= ) ) 2.21750 VDC= ) ) 0.92981 VD= ) ) 2.12218
) PSI= 360.00 VBA= ) ) 3.24050 VB= ) ) 1.31082 VDC= ) ) 0.33994 VD= ) ) 1.28272
STOP ) ) 30
#EXECUTION TERMINATED
#

```

```

#r -load#
#EXECUTION BEGINS
) PSI= 70.00 ABR= 778.101590 ABT= 71019.03882 ANGCG= 46319.9453
) PSI= 15.00 ABR= 772.87890 ABT= 71063.48584 ANGCG= 48340.2656
) PSI= 30.00 ABR= 7726.08360 ABT= 77934.05835 ANGCG= 42457.1953
) PSI= 45.00 ABR= 7715.19414 ABT= 7729.81055 ANGCG= 33173.2031
) PSI= 60.00 ABR= 7723.34811 ABT= 77522.51392 ANGCG= 23750.6289
) PSI= 75.00 ABR= 77317.99104 ABT= 77338.27515 ANGCG= 15376.1406
) PSI= 90.00 ABR= 77382.35449 ABT= 77174.89513 ANGCG= 7949.7773
) PSI= 105.00 ABR= 77408.23291 ABT= 7717.66414 ANGCG= 7802.9153
) PSI= 120.00 ABR= 77300.55591 ABT= 77152.67662 ANGCG= 76939.8438
) PSI= 135.00 ABR= 77326.84521 ABT= 77352.25195 ANGCG= 16011.4492
) PSI= 150.00 ABR= 77223.74129 ABT= 77574.22046 ANGCG= 25100.9297
) PSI= 165.00 ABR= 77108.53107 ABT= 77758.14087 ANGCG= 34460.9453
) PSI= 180.00 ABR= 7725.34523 ABT= 77812.11890 ANGCG= 36914.4922
) PSI= 195.00 ABR= 7700.04282 ABT= 7725.25635 ANGCG= 32966.1953
) PSI= 210.00 ABR= 7721.44885 ABT= 77586.86938 ANGCG= 26675.8789
) PSI= 225.00 ABR= 7766.93509 ABT= 77473.47852 ANGCG= 21521.7500
) PSI= 240.00 ABR= 77123.59282 ABT= 77404.30542 ANGCG= 18377.5156
) PSI= 255.00 ABR= 77187.85001 ABT= 77367.24121 ANGCG= 16692.7812
) PSI= 270.00 ABR= 77258.87158 ABT= 77338.98071 ANGCG= 15408.2109
) PSI= 285.00 ABR= 77332.19189 ABT= 77287.84937 ANGCG= 13084.0586
) PSI= 300.00 ABR= 77393.04997 ABT= 77171.88420 ANGCG= 7812.9180
) PSI= 315.00 ABR= 77412.06688 ABT= 7751.94815 ANGCG= 2361.2795
) PSI= 330.00 ABR= 77355.70020 ABT= 77390.49927 ANGCG= 17749.9648
) PSI= 345.00 ABR= 77223.51381 ABT= 77763.05737 ANGCG= 34684.4258
) PSI= 360.00 ABR= 7778.10228 ABT= 771019.03760 ANGCG= 46319.9453
#(STOP) ) .0
#EXECUTION TERMINATED
#

```

```

$r -load#
#EXECUTION BEGINS
) PSI=30.00 OMEGA3= 77.15477 OMEGA4= 59.58249 OMEGA5= 11.72194 OMEGA6= 64.13559
) PSI=15.00 OMEGA3= 70.91211 OMEGA4= 11.43937 OMEGA5= 1.62034 OMEGA6= 12.40072
) PSI=30.00 OMEGA3= 60.04488 OMEGA4= 34.43288 OMEGA5= 5.51820 OMEGA6= 37.24315
) PSI=45.00 OMEGA3= 48.35762 OMEGA4= 72.36090 OMEGA5= 17.58873 OMEGA6= 77.33464
) PSI=60.00 OMEGA3= 37.67369 OMEGA4= 100.75807 OMEGA5= 37.32526 OMEGA6= 104.57988
) PSI=75.00 OMEGA3= 28.33611 OMEGA4= 120.22556 OMEGA5= 61.94992 OMEGA6= 116.82414
) PSI=90.00 OMEGA3= 19.94580 OMEGA4= 131.83229 OMEGA5= 85.05232 OMEGA6= 111.80748
) PSI=105.00 OMEGA3= 11.76708 OMEGA4= 136.22058 OMEGA5= 99.76045 OMEGA6= 89.57524
) PSI=120.00 OMEGA3= 2.85010 OMEGA4= 133.23869 OMEGA5= 102.43175 OMEGA6= 55.71294
) PSI=135.00 OMEGA3= 7.92662 OMEGA4= 121.88768 OMEGA5= 93.70793 OMEGA6= 20.63028
) PSI=150.00 OMEGA3= 21.57910 OMEGA4= 100.84671 OMEGA5= 75.13214 OMEGA6= 5.04721
) PSI=165.00 OMEGA3= 38.09331 OMEGA4= 70.23698 OMEGA5= 52.17387 OMEGA6= 15.06009
) PSI=180.00 OMEGA3= 55.21526 OMEGA4= 33.94196 OMEGA5= 25.01616 OMEGA6= 10.58485
) PSI=195.00 OMEGA3= 69.03607 OMEGA4= 1.39512 OMEGA5= 1.02636 OMEGA6= 0.47609
) PSI=210.00 OMEGA3= 76.64148 OMEGA4= 31.22417 OMEGA5= 23.01567 OMEGA6= 9.68526
) PSI=225.00 OMEGA3= 77.27158 OMEGA4= 55.15891 OMEGA5= 40.91989 OMEGA6= 12.63142
) PSI=240.00 OMEGA3= 71.29318 OMEGA4= 74.95238 OMEGA5= 56.27098 OMEGA6= 7.88945
) PSI=255.00 OMEGA3= 59.18387 OMEGA4= 92.40475 OMEGA5= 70.46492 OMEGA6= 5.28341
) PSI=270.00 OMEGA3= 41.30975 OMEGA4= 108.47533 OMEGA5= 83.68791 OMEGA6= 27.60994
) PSI=285.00 OMEGA3= 18.24112 OMEGA4= 122.88058 OMEGA5= 93.92773 OMEGA6= 58.48907
) PSI=300.00 OMEGA3= 8.69522 OMEGA4= 133.66330 OMEGA5= 96.31590 OMEGA6= 93.04771
) PSI=315.00 OMEGA3= 36.20990 OMEGA4= 136.85542 OMEGA5= 85.15897 OMEGA6= 120.13173
) PSI=330.00 OMEGA3= 59.76231 OMEGA4= 127.15422 OMEGA5= 60.46390 OMEGA6= 126.48959
) PSI=345.00 OMEGA3= 74.17067 OMEGA4= 100.79544 OMEGA5= 32.06226 OMEGA6= 106.10875
) PSI=360.00 OMEGA3= 77.15477 OMEGA4= 59.58275 OMEGA5= 11.72212 OMEGA6= 64.13588

) STOP) 0
#EXECUTION TERMINATED
#

```

```

$r -load#
#EXECUTION BEGINS.
; PSI=)0.0. (BETA=)) 23.80717. (GAMA=) 11.28314. (XLAMB=) 80.07616. (UPA=) 3.72884
; PSI=)15.00 (BETA=)) 19.531860 (GAMA=) 9.23006 (XLAMB=) 89.42213 (UPA=) 1.52058
; PSI=)30.00 (BETA=)) 15.76888 (GAMA=) 9.92623 (XLAMB=) 89.31837 (UPA=) 2.26468
; PSI=)45.00 (BETA=)) 12.66548 (GAMA=) 13.03031 (XLAMB=) 88.69186 (UPA=) 5.60297
; PSI=)60.00 (BETA=)) 10.20738 (GAMA=) 18.03487 (XLAMB=) 87.15282 (UPA=) 10.88072
; PSI=)75.00 (BETA=)) 8.32220 (GAMA=) 24.40552 (XLAMB=) 84.31889 (UPA=) 17.30084
; PSI=)90.00 (BETA=)) 6.94199 (GAMA=) 31.66185 (XLAMB=) 80.08264 (UPA=) 23.93680
; PSI=)105.00 (BETA=)) 6.03242 (GAMA=) 39.37505 (XLAMB=) 74.73526 (UPA=) 29.78036
; PSI=)120.00 (BETA=)) 5.60757 (GAMA=) 47.13141 (XLAMB=) 68.88387 (UPA=) 33.97580
; PSI=)135.00 (BETA=)) 5.74137 (GAMA=) 54.48360 (XLAMB=) 63.21619 (UPA=) 36.14128
; PSI=)150.00 (BETA=)) 6.57141 (GAMA=) 60.91283 (XLAMB=) 58.31439 (UPA=) 36.52240
; PSI=)165.00 (BETA=)) 8.27036 (GAMA=) 65.85439 (XLAMB=) 54.61446 (UPA=) 35.86711
; PSI=)180.00 (BETA=)) 10.94947 (GAMA=) 68.85065 (XLAMB=) 52.39787 (UPA=) 35.07826
; PSI=)195.00 (BETA=)) 14.53367 (GAMA=) 69.76382 (XLAMB=) 51.72549 (UPA=) 34.78006
; PSI=)210.00 (BETA=)) 18.74011 (GAMA=) 68.79901 (XLAMB=) 52.43596 (UPA=) 35.09433
; PSI=)225.00 (BETA=)) 23.18230 (GAMA=) 66.29965 (XLAMB=) 54.28391 (UPA=) 35.76837
; PSI=)240.00 (BETA=)) 27.46861 (GAMA=) 62.55725 (XLAMB=) 57.07643 (UPA=) 36.39465
; PSI=)255.00 (BETA=)) 31.23401 (GAMA=) 57.75487 (XLAMB=) 60.71075 (UPA=) 36.51152
; PSI=)270.00 (BETA=)) 34.14043 (GAMA=) 51.99402 (XLAMB=) 65.13399 (UPA=) 35.61368
; PSI=)285.00 (BETA=)) 35.86896 (GAMA=) 45.35529 (XLAMB=) 70.24570 (UPA=) 33.18156
; PSI=)300.00 (BETA=)) 36.15749 (GAMA=) 37.98087 (XLAMB=) 75.74832 (UPA=) 28.83652
; PSI=)315.00 (BETA=)) 34.86707 (GAMA=) 30.18243 (XLAMB=) 81.02036 (UPA=) 22.65979
; PSI=)330.00 (BETA=)) 32.08517 (GAMA=) 22.54541 (XLAMB=) 85.24081 (UPA=) 15.47143
; PSI=)345.00 (BETA=)) 28.19534 (GAMA=) 15.93368 (XLAMB=) 87.87656 (UPA=) 8.68377
; PSI=)360.00 (BETA=)) 23.80721 (GAMA=) 11.28320 (XLAMB=) 89.07616 (UPA=) 3.72891
;
; STOP ) 0
#EXECUTION TERMINATED
#

```

```

sr -load#
#EXECUTION BEGINS
PSI=0.00 ABAR= 250.01991 ABAT= 97.32770 ANGC3= 2317.32593
) PSI=15.00 ABAR= 211.19797 ABAT= 392.19482 ANGC3= 9337.96875
) PSI=30.00 ABAR= 151.42624 ABAT= 493.30322 ANGC3= 11745.31250
) PSI=45.00 ABAR= 98.21529 ABAT= 476.18530 ANGC3= 11337.74219
) PSI=50.00 ABAR= 59.61089 ABAT= 419.42163 ANGC3= 9986.22656
) PSI=75.00 ABAR= 33.72325 ABAT= 367.99414 ANGC3= 8761.76172
) PSI=90.00 ABAR= 16.70906 ABAT= 342.00513 ANGC3= 8142.97656
) PSI=105.00 ABAR= 15.81549 ABAT= 351.65967 ANGC3= 8372.84766
) PSI=120.00 ABAR= 0.34117 ABAT= 405.36035 ANGC3= 9651.43359
) PSI=135.00 ABAR= 2.63892 ABAT= 507.63647 ANGC3= 12086.58203
) PSI=150.00 ABAR= 19.55760 ABAT= 640.19067 ANGC3= 15242.63281
) PSI=165.00 ABAR= 60.94618 ABAT= 730.95532 ANGC3= 17403.69531
) PSI=180.00 ABAR= 128.04642 ABAT= 677.47510 ANGC3= 16130.35937
) PSI=195.00 ABAR= 200.17101 ABAT= 462.24561 ANGC3= 11005.84766
) PSI=210.00 ABAR= 246.70438 ABAT= 172.34203 ANGC3= 4103.37891
) PSI=225.00 ABAR= 250.77756 ABAT= 116.09473 ANGC3= 2764.16016
) PSI=240.00 ABAR= 213.47401 ABAT= 382.63623 ANGC3= 9110.38281
) PSI=255.00 ABAR= 147.11465 ABAT= 632.21533 ANGC3= 15052.74609
) PSI=270.00 ABAR= 71.67291 ABAT= 865.67188 ANGC3= 20611.23437
) PSI=285.00 ABAR= 13.97501 ABAT= 1062.77808 ANGC3= 25304.23828
) PSI=300.00 ABAR= 3.10090 ABAT= 1171.45801 ANGC3= 27891.85547
) PSI=315.00 ABAR= 55.06885 ABAT= 1112.63428 ANGC3= 26491.28906
) PSI=330.00 ABAR= 150.00441 ABAT= 827.58911 ANGC3= 19704.50000
) PSI=345.00 ABAR= 231.05397 ABAT= 365.21899 ANGC3= 8695.68750
) PSI=360.00 ABAR= 250.01991 ABAT= 97.32504 ANGC3= 2317.26294
)
) STOP ) .0
#EXECUTION TERMINATED
#

```



```

$r -load#
#EXECUTION BEGINS
) PSI= 20.00(CAL=)) 162.475890 YUM= ) 87.19501
) PSI= 15.00(CAL=)) 164.707120 YUM= ) 89.05725
) PSI= 30.00(CAL=)) 169.157300 YUM= ) 88.41690
) PSI= 45.00(CAL=)) 175.364730 YUM= ) 85.70515
) PSI= 60.00(CAL=)) 182.827410 YUM= ) 81.96642
) PSI= 75.00(CAL=)) 191.083240 YUM= ) 78.38023
) PSI= 90.00(CAL=)) 199.719820 YUM= ) 75.98050
) PSI= 105.00(CAL=)) 108.342590 YUM= ) 75.48434
) PSI= 120.00(CAL=)) 116.523790 YUM= ) 77.14032
) PSI= 135.00(CAL=)) 123.742200 YUM= ) 80.64250
) PSI= 150.00(CAL=)) 129.341370 YUM= ) 85.16516
) PSI= 165.00(CAL=)) 132.583970 YUM= ) 89.51842
) PSI= 180.00(CAL=)) 132.901150 YUM= ) 92.52380
) PSI= 195.00(CAL=)) 130.230120 YUM= ) 93.49442
) PSI= 210.00(CAL=)) 125.058840 YUM= ) 92.46967
) PSI= 225.00(CAL=)) 118.117290 YUM= ) 89.94768
) PSI= 240.00(CAL=)) 110.088590 YUM= ) 85.52887
) PSI= 255.00(CAL=)) 101.519930 YUM= ) 82.77768
) PSI= 270.00(CAL=)) 92.853520 YUM= ) 79.25232
) PSI= 285.00(CAL=)) 84.486270 YUM= ) 76.57269
) PSI= 300.00(CAL=)) 76.823290 YUM= ) 75.41512
) PSI= 315.00(CAL=)) 70.315310 YUM= ) 76.31981
) PSI= 330.00(CAL=)) 65.460140 YUM= ) 79.28772
) PSI= 345.00(CAL=)) 62.738240 YUM= ) 83.43967
) PSI= 360.00(CAL=)) 62.475890 YUM= ) 87.19490

STOP.) )0
#EXECUTION TERMINATED
#

```

```

sr -load#
#EXECUTION BEGINS
) PSI=10.00 EN2= ) 0.631140 EN3= ) 0.07722 EN4= ) 0.17382 EN5= ) 0.00052 EN6= ) 0.04663
) PSI=15.00 EN2= ) 0.02360 EN3= ) 0.00285 EN4= ) 0.14683 EN5= ) 0.00001 EN6= ) 0.00174
) PSI=30.00 EN2= ) 0.21282 EN3= ) 0.02579 EN4= ) 0.10528 EN5= ) 0.00011 EN6= ) 0.01573
) PSI=45.00 EN2= ) 0.01765 EN3= ) 0.11389 EN4= ) 0.06828 EN5= ) 0.00116 EN6= ) 0.06780
) PSI=60.00 EN2= ) 1.67812 EN3= ) 0.22082 EN4= ) 0.04144 EN5= ) 0.00522 EN6= ) 0.12399
) PSI=75.00 EN2= ) 2.09408 EN3= ) 0.31439 EN4= ) 0.02345 EN5= ) 0.01439 EN6= ) 0.15473
) PSI=90.00 EN2= ) 1.91800 EN3= ) 0.37803 EN4= ) 0.01162 EN5= ) 0.02713 EN6= ) 0.14172
) PSI=105.00 EN2= ) 1.23113 EN3= ) 0.40361 EN4= ) 0.00404 EN5= ) 0.03732 EN6= ) 0.09096
) PSI=120.00 EN2= ) 0.47625 EN3= ) 0.38614 EN4= ) 0.00024 EN5= ) 0.03935 EN6= ) 0.03519
) PSI=135.00 EN2= ) 0.06530 EN3= ) 0.32315 EN4= ) 0.00183 EN5= ) 0.03293 EN6= ) 0.00483
) PSI=150.00 EN2= ) 0.00301 EN3= ) 0.22121 EN4= ) 0.01360 EN5= ) 0.02174 EN6= ) 0.00029
) PSI=165.00 EN2= ) 0.03480 EN3= ) 0.10730 EN4= ) 0.04237 EN5= ) 0.01021 EN6= ) 0.00257
) PSI=180.00 EN2= ) 0.01710 EN3= ) 0.02506 EN4= ) 0.08902 EN5= ) 0.00235 EN6= ) 0.00127
) PSI=195.00 EN2= ) 0.00003 EN3= ) 0.00004 EN4= ) 0.13017 EN5= ) 0.00000 EN6= ) 0.00000
) PSI=210.00 EN2= ) 0.01439 EN3= ) 0.02121 EN4= ) 0.17152 EN5= ) 0.00199 EN6= ) 0.00106
) PSI=225.00 EN2= ) 0.02448 EN3= ) 0.06618 EN4= ) 0.17435 EN5= ) 0.00628 EN6= ) 0.00181
) PSI=240.00 EN2= ) 0.00955 EN3= ) 0.12219 EN4= ) 0.14842 EN5= ) 0.01187 EN6= ) 0.00071
) PSI=255.00 EN2= ) 0.00428 EN3= ) 0.18572 EN4= ) 0.10228 EN5= ) 0.01862 EN6= ) 0.00032
) PSI=270.00 EN2= ) 0.11697 EN3= ) 0.25594 EN4= ) 0.04983 EN5= ) 0.02626 EN6= ) 0.00864
) PSI=285.00 EN2= ) 0.52490 EN3= ) 0.32843 EN4= ) 0.00972 EN5= ) 0.03308 EN6= ) 0.03878
) PSI=300.00 EN2= ) 1.32843 EN3= ) 0.39860 EN4= ) 0.00216 EN5= ) 0.03479 EN6= ) 0.09815
) PSI=315.00 EN2= ) 2.21433 EN3= ) 0.40738 EN4= ) 0.03820 EN5= ) 0.02720 EN6= ) 0.16361
) PSI=330.00 EN2= ) 2.45492 EN3= ) 0.35167 EN4= ) 0.10429 EN5= ) 0.01371 EN6= ) 0.18139
) PSI=345.00 EN2= ) 1.72755 EN3= ) 0.22098 EN4= ) 0.16064 EN5= ) 0.00385 EN6= ) 0.12764
) PSI=360.00 EN2= ) 0.63115 EN3= ) 0.07722 EN4= ) 0.17382 EN5= ) 0.00052 EN6= ) 0.04663

```

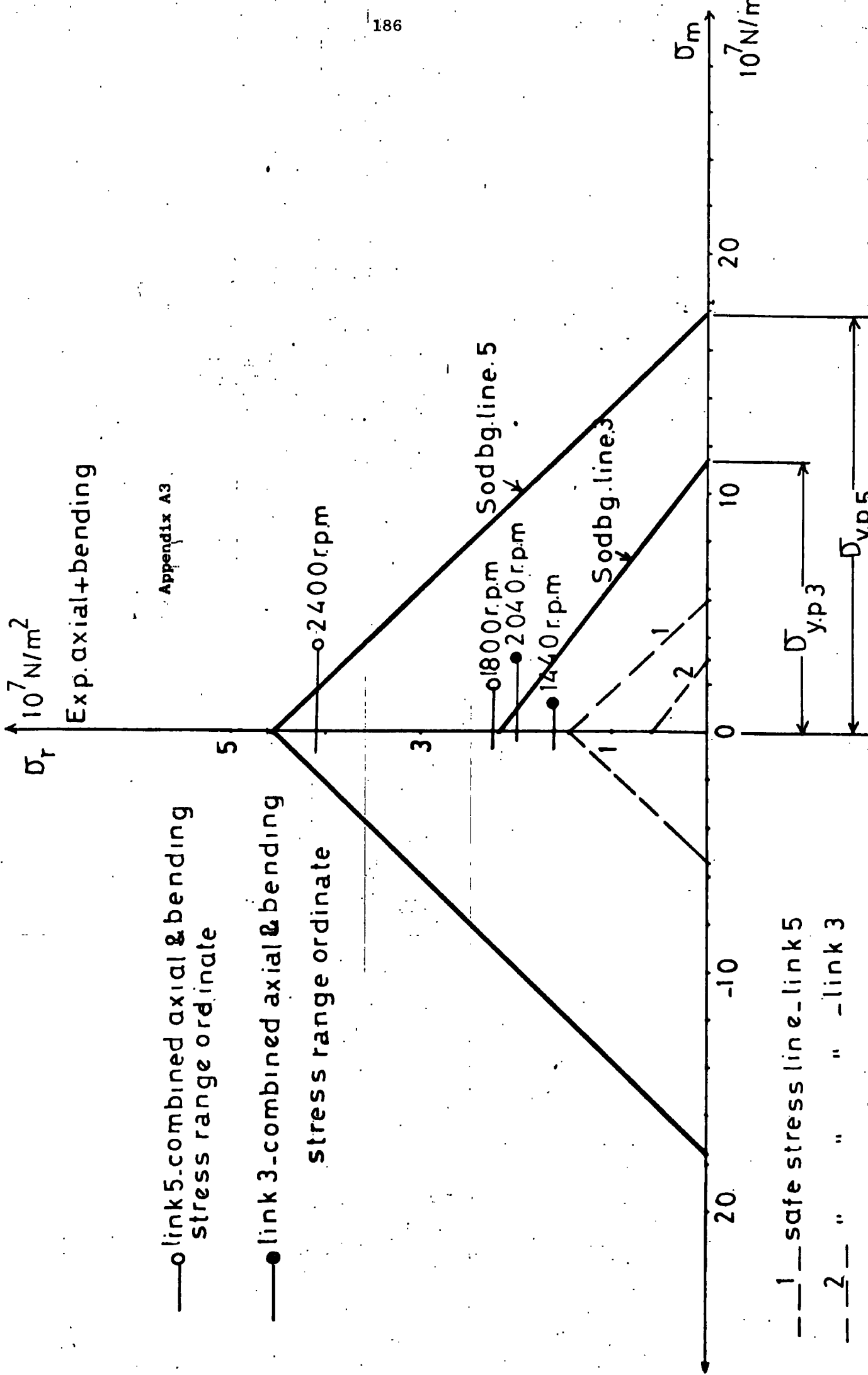
```

) STOP ) 0
#EXECUTION TERMINATED
#

```

EVOLUTION BEGINS

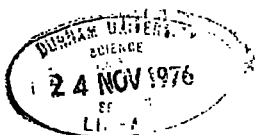
PSI=100.00	ANGC5=	8404.0859	ANGC6=	29679.0898	PSI=	0.00	ANGC5=	14550.5508	ANGC6=	49035.0078
PSI=105.00	ANGC5=	7725.5664	ANGC6=	30552.1367	PSI=	5.00	ANGC5=	11149.7656	ANGC6=	51542.2617
PSI=110.00	ANGC5=	4716.9102	ANGC6=	32998.2891	PSI=	10.00	ANGC5=	8582.5352	ANGC6=	52615.8672
PSI=115.00	ANGC5=	570.8191	ANGC6=	35337.5703	PSI=	15.00	ANGC5=	7050.7656	ANGC6=	52376.9297
PSI=120.00	ANGC5=	3399.4050	ANGC6=	36402.3164	PSI=	20.00	ANGC5=	6610.4141	ANGC6=	51001.2930
PSI=125.00	ANGC5=	7103.8398	ANGC6=	36154.7969	PSI=	25.00	ANGC5=	7193.0391	ANGC6=	48696.9492
PSI=130.00	ANGC5=	10499.7617	ANGC6=	34627.6484	PSI=	30.00	ANGC5=	8639.7617	ANGC6=	45676.2812
PSI=135.00	ANGC5=	13583.8047	ANGC6=	31914.9766	PSI=	35.00	ANGC5=	10738.0430	ANGC6=	42130.8086
PSI=140.00	ANGC5=	16376.4375	ANGC6=	28162.4375	PSI=	40.00	ANGC5=	13253.2461	ANGC6=	38212.3164
PSI=145.00	ANGC5=	18903.6211	ANGC6=	23560.4102	PSI=	45.00	ANGC5=	15950.9414	ANGC6=	34022.2773
PSI=150.00	ANGC5=	21179.1641	ANGC6=	18341.4648	PSI=	50.00	ANGC5=	18609.9141	ANGC6=	29611.8633
PSI=155.00	ANGC5=	23190.9766	ANGC6=	12778.9258	PSI=	55.00	ANGC5=	21028.6055	ANGC6=	24989.5000
PSI=160.00	ANGC5=	24895.7266	ANGC6=	7181.9648	PSI=	60.00	ANGC5=	23027.4336	ANGC6=	20135.0430
PSI=165.00	ANGC5=	26225.2812	ANGC6=	1878.9473	PSI=	65.00	ANGC5=	24451.2617	ANGC6=	15017.2344
PSI=170.00	ANGC5=	27103.6836	ANGC6=	2812.0103	PSI=	70.00	ANGC5=	25173.1367	ANGC6=	9613.4531
PSI=175.00	ANGC5=	27472.2773	ANGC6=	6624.3242	PSI=	75.00	ANGC5=	25100.6758	ANGC6=	3928.9604
PSI=180.00	ANGC5=	27312.6680	ANGC6=	9381.9844	PSI=	80.00	ANGC5=	24184.6523	ANGC6=	1985.9404
PSI=185.00	ANGC5=	26659.8672	ANGC6=	11023.2734	PSI=	85.00	ANGC5=	22427.2539	ANGC6=	8025.3125
PSI=190.00	ANGC5=	25599.7187	ANGC6=	11598.8555	PSI=	90.00	ANGC5=	19886.4141	ANGC6=	14024.6562
PSI=195.00	ANGC5=	24252.6758	ANGC6=	11246.2266	PSI=	95.00	ANGC5=	16675.1250	ANGC6=	19768.5547
PSI=200.00	ANGC5=	22750.9687	ANGC6=	10149.5859						
PSI=205.00	ANGC5=	21217.8398	ANGC6=	3501.1797						
PSI=210.00	ANGC5=	19753.2148	ANGC6=	6471.5508	PSI=305.00		ANGC5=	15547.9492	ANGC6=	22230.7344
PSI=215.00	ANGC5=	18427.9344	ANGC6=	4194.1914	PSI=310.00		ANGC5=	15916.3242	ANGC6=	22324.8750
PSI=220.00	ANGC5=	17284.4297	ANGC6=	1761.2251	PSI=315.00		ANGC5=	18780.2305	ANGC6=	18627.5742
PSI=225.00	ANGC5=	16340.0703	ANGC6=	772.7747	PSI=320.00		ANGC5=	23264.2109	ANGC6=	10882.9844
PSI=230.00	ANGC5=	15592.9727	ANGC6=	3382.5974	PSI=325.00		ANGC5=	26729.4219	ANGC6=	2192.7832
PSI=235.00	ANGC5=	15026.1367	ANGC6=	6063.8789	PSI=330.00		ANGC5=	28813.2148	ANGC6=	6985.7969
PSI=240.00	ANGC5=	14610.4844	ANGC6=	824.2969	PSI=335.00		ANGC5=	29313.0391	ANGC6=	16171.3867
PSI=245.00	ANGC5=	14306.7070	ANGC6=	11674.8555	PSI=340.00		ANGC5=	28231.9844	ANGC6=	24911.3008
PSI=250.00	ANGC5=	14065.1602	ANGC6=	14622.7773	PSI=345.00		ANGC5=	25783.6562	ANGC6=	32820.3242
PSI=255.00	ANGC5=	13824.9648	ANGC6=	17663.1836	PSI=350.00		ANGC5=	22355.2500	ANGC6=	39600.0234
PSI=260.00	ANGC5=	13512.2383	ANGC6=	20771.6406	PSI=355.00		ANGC5=	18439.1484	ANGC6=	45043.8946
PSI=265.00	ANGC5=	13038.9766	ANGC6=	23895.0312	PSI=360.00		ANGC5=	14550.6797	ANGC6=	49034.9375
PSI=270.00	ANGC5=	12302.3437	ANGC6=	26943.4922						
PSI=275.00	ANGC5=	11187.1211	ANGC6=	29782.2852						
PSI=280.00	ANGC5=	9571.8594	ANGC6=	32228.7227						
PSI=285.00	ANGC5=	7341.4023	ANGC6=	34053.2695						
PSI=290.00	ANGC5=	4406.6641	ANGC6=	34991.8437						
PSI=295.00	ANGC5=	731.15266	ANGC6=	34769.5898						
PSI=300.00	ANGC5=	3639.1833	ANGC6=	33137.8516						



REFERENCES

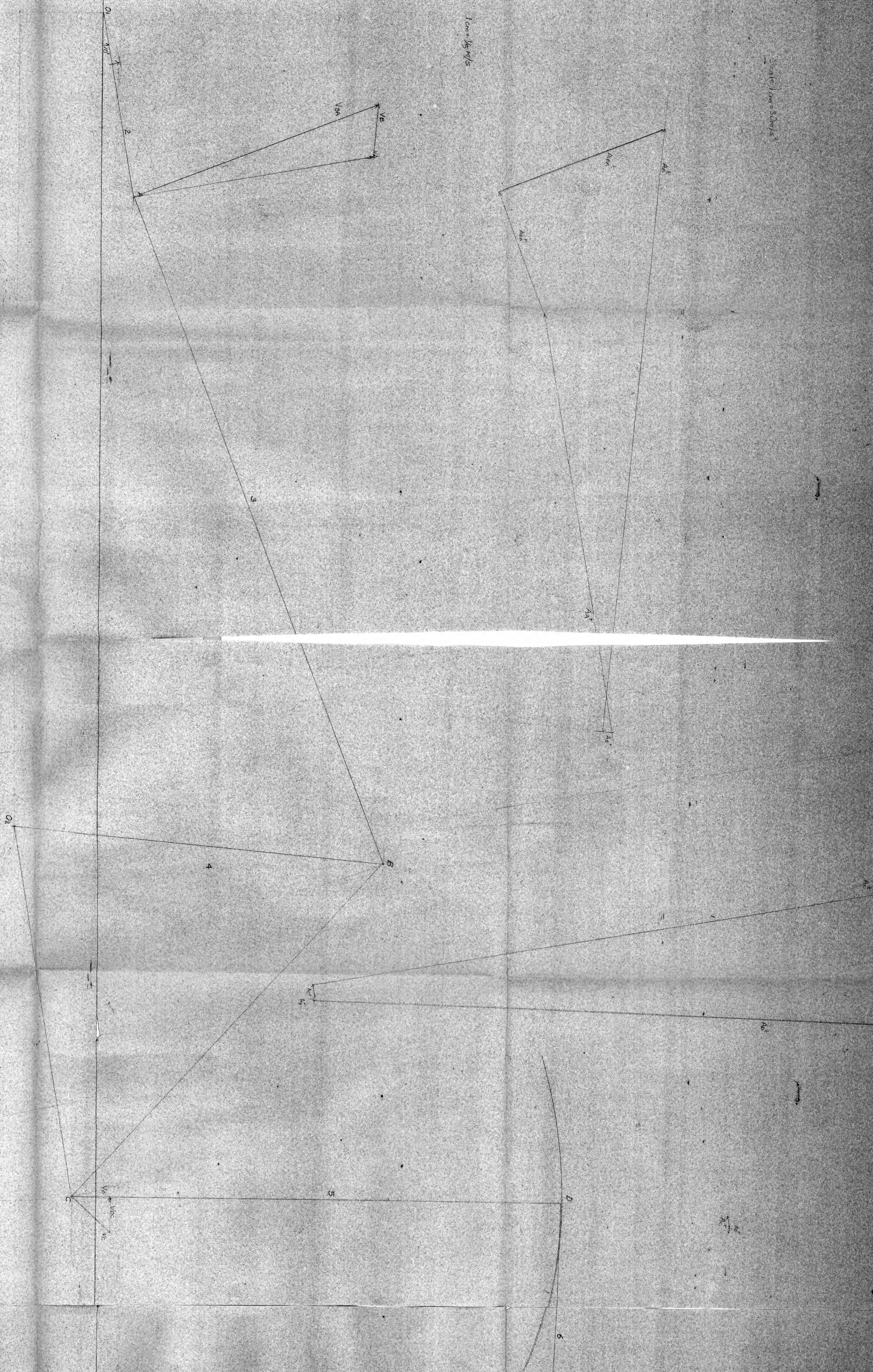
- (1) Chen, F.Y. An analytical method for synthesizing the four-bar crank-rocker mechanism. Journal of Engineering for Industry, Trans. ASME February 1969. p. 45-54
- (2) Lord, P.R. and Mohamed, M.H. An analysis of the picking mechanism of a textile loom. Journal of Engineering for Industry, Trans. ASME. May 1975. p. 385-390
- (3) Bevan, T. The Theory of Machines. Longmans, Green & Co. Ltd., 1964
- (4) Conte, F.L., George, G.R., Mayne, R.W., and Sadler, J.P. Optimum Mechanism Design combining Kinematic and Dynamic-Force considerations. Journal of Engineering for Industry, Trans. ASME. May 1975, p. 662-670
- (5) Spotts, M.F. Design of Machine Elements (4th Edition). Brentice-Hall Inc. Englewood Cliffs, N.J., U.S.A. 1971
- (6) Dove, R.C. and Adams, P.H. Experimental Stress Analysis and Motion Measurement. Charles E. Merrill Books. Inc., Ohio, U.S.A. 1964
- (7) Marin, J. Mechanical Behaviour of Engineering Materials. Prentice-Hall Inc., Englewood Cliffs, N.J., U.S.A. 1962
- (8) Green, W.G. Theory of Machines (2nd Edition) Blackie & Son Ltd., 1962
- (9) Shigley, J.E. Theory of Machines (International Student Ed.) McGraw-Hill Book Co. Inc. 1961
- (10) Tepper, F.R. and Lowen, G.G. Shaking Force Optimisation of Four-bar Linkage with Adjustable Constraints on Ground Bearing Forces. Journal of Engineering for Industry, Trans. ASME. May 1975, p 643-651
- (11) Wojcik, C.K. Synthesis of Four-bar Linkage Function generators by means of Equations of Motion. Journal of Engineering for Industry. Trans. ASME. May 1965. p. 170-176
- (12) Maxwell, R.L. Kinematics and Dynamics of Machinery. Prentice Hall, Inc. Englewood Cliffs, N.J., U.S.A. 1960
- (13) Prentis, J.M. Dynamics of Mechanical Systems. Longman Group Ltd., Great Britain 1970

- (14) Morrison, J.L.M. and Crossland, B. An introduction to the Mechanics of Machines. Longman Group Ltd., Great Britain. 1970
- (15) Alexander, R.M. and Lawrence, K.L. Experimentally Determined Dynamic Strains in an Elastic Mechanism. Journal of Engineering for Industry, Trans. ASME 1974. Paper No. 74 - DET - 33
- (16) Dubowsky, S., and Young, S.C. An Experimental and Analytical Study of Connection Forces in High-Speed Mechanisms. Journal of Engineering for Industry, Trans. ASME 1974. Paper No. 74 - DET - 72
- (17) Singer, F.L. Strength of Materials (Second Edition). Harper and Row, Publishers. 1962
- (18) Roark, R.J. Formulas for Stress and Strain. (Fourth Edition) McGraw-Hill Book Company 1965
- (19) Holister, G.S. Experimental Stress Analysis. Cambridge University Press. 1967.
- (20) Heywood, R.B. Designing Against Fatigue. Chapman and Hall Ltd., 1962
- (21) Holowenko, A.R. Dynamics of Machinery. John Wiley & Sons. Inc. 1963
- (22) Hinkle, R.T. Kinematics of Machines. Prentice-Hall, Inc. Englewood Cliffs, N.J., U.S.A. 1953
- (23) Rayevskii, N.P. The Measurement of Mechanical Parameters in Machines. Pergamon Press. Ltd., 1965
- (24) Greenwood, J.M. Stresses in the Reed and Weft Needle Arm of a Weaving Loom. Final Year Honours Project. May 1974. University of Durham. Department of Engineering Science.
- (25) Imam, I., and Sandor, G.N. High-Speed Mechanisms Design - A General Analytical Approach. Journal of Engineering for Industry. Trans. ASME. May 1975. Paper No. 74 - DET - 50
- (26) Faires, V.M. Design of Machine Elements (4th Edition). Macmillan Co. 1962, U.S.A.



Scale: 1 cm = 80 m/s

1 cm = 15 m/s



$\omega = 2500 \text{ rpm}$
 $\omega_2 = 261.66 \text{ rad/sec}$
 $\omega_3 = 73.33 \text{ rad/sec}$
 $\omega_4 = \frac{V_B}{B_1} = 28.18 \text{ rad/sec}$
 $V_C = 0.46 \text{ m/s}$
 $V_B = 0.62 \text{ m/s}$
 $V_A = 3.08 \text{ m/s}$

$A_A^t = 0$
 $A_A^r = \omega_2^2 (A_1B) = 225.84 \text{ m/s}^2$
 $A_B^r = \omega_3^2 (B_1C) = 174 \text{ m/s}^2$
 $A_C^r = \omega_4^2 (C_1D) = 1072.5 \text{ m/s}^2$

$\alpha_2 = \frac{A_A^r}{A_1B} = 7500 \text{ rad/sec}^2$
 $\alpha_3 = \frac{A_B^r}{B_1C} = 437.50 \text{ rad/sec}^2$
 $\alpha_4 = \frac{A_C^r}{C_1D} = 8431.03 \text{ rad/sec}^2$